University of Natural Resources and Life Sciences, Vienna

Cumulative Doctoral Thesis

Soil physical quality assessment for the evaluation of agricultural soil management strategies

submitted in satisfaction of the requirements for the degree of “Doktor der Bodenkultur”

by

DI Thomas Weninger

Supervised by

Priv.Doz. Dipl.-Geow. Dr. Andreas Schwen
Institute of Soil Physics and Rural Water Management
University of Natural Resources and Life Sciences, Vienna

Priv.Doz. DI Dr. Gernot Bodner
Institute of Agronomy
University of Natural Resources and Life Sciences, Vienna

Dr.habil. Kai Schwärzel
Institute of Forest Ecosystems
Thünen Institute Eberswalde, Germany

Vienna, June 2020

I hereby declare that I am the sole author of this work. No assistance other than that which is permitted has been used. Ideas and quotes taken directly or indirectly from other sources are identified as such. This written work has not yet been submitted elsewhere.

Abstract

Advances in soil management systems are supposed to improve soil physical quality and secure the potential of soil to provide crucial services such as water storage and nutrient cycling. Sophisticated methodology to assess the effects of different soil management strategies is strongly needed and promising approaches were evaluated in this thesis. The outcomes were supposed to address questions such as: How can soil physical quality issues be effectively detected? How can physical soil degradation threats be countered?

A literature review concerning options for the assessment of soil physical quality using feasible and comparable indicators is presented as introduction to the topic. The empirical work started with an evaluation of methods for the rapid, wide-range determination of soil water retention and hydraulic conductivity relations as a basis for soil physical quality assessments. The approved methods were conducted in case studies on long-term tillage experiments in Central Europe to examine mid-term alterations of soil physical quality after changing the tillage strategy. Conservation tillage increased aeration deficits in the upper soil layers and soil compaction was detected as major soil degradation risk which should be addressed by meliorating soil management strategies. Moreover, soil water repellency was quantified on fire-affected soils. The method combination employed showed high sensitivity in the sub-critical range which, according to recent findings, is relevant for wide-spread agricultural soils.

The method combinations presented here were found to effectively facilitate the data collection necessary for studies focussed on soil physical quality and connected soil degradation issues. The work in this thesis contributes valuable knowledge concerning regional soil physical conditions, and the comprehensive evaluation of methodology offers support for further improvements of soil management strategies which underlie resilient agricultural practices.

Zusammenfassung

Die Weiterentwicklung von Bodenbearbeitungssystemen kann die physikalische Bodenqualität verbessern und das Potential des Bodens erhalten, seine essenziellen Funktionen zu erfüllen. Ausgereifte Methodik für die Beurteilung von verschiedenen Bodenbearbeitungsstrategien ist notwendig und vielversprechende Ansätze dazu wurden in dieser Arbeit evaluiert. Die Ergebnisse sollten Antworten ermöglichen auf Fragen wie: Wie können Defizite in der physikalischen Bodenqualität effektiv detektiert werden? Wie kann physikalischer Bodendegradation entgegengewirkt werden?

Eine Zusammenfassung der aktuellen Literatur zur Beurteilung der physikalischen Bodenqualität mittels aussagekräftiger Indikatoren bildet die Einleitung. Als erster Schritt der empirischen Forschung wurden Methoden bewertet zur einfachen Bestimmung von Bodenwasserspeicherfähigkeit und Wasserleitfähigkeit über einen weiten Sättigungsbereich. Die gewonnenen Daten ermöglichen die Abschätzung der physikalischen Bodenqualität und die evaluierten Methoden wurden in Fallstudien auf Langzeitversuchen zu konservierender Bodenbearbeitung angewandt. Konservierende Bodenbearbeitung verstärkte Belüftungsdefizite in den oberen Bodenschichten und Verdichtung wurde als Hauptrisiko ermittelt. Darüber hinaus wurde die Hydrophobizität des Bodens auf Waldbrandböden quantifiziert. Die angewandte Methodenkombination zeigte hohe Sensitivität im sub-kritischen Bereich, der, nach jüngsten Erkenntnissen, auch in verbreiteten Ackerböden relevant ist.

Die eingesetzten Methoden erwiesen sich als gut angepasst für eine effektive Datengewinnung für zielgerichtete Forschung zur physikalischen Bodenqualität und zu den damit verbunden Risiken zur Bodendegradation. Die hier präsentierte Arbeit liefert wertvolle Erkenntnisse zum physikalischen Zustand der Böden in der Region bei und die umfangreiche Evaluierung der Methodik unterstützt die effiziente Weiterentwicklung von Bodenbearbeitungssystemen, die einer resilienten Landwirtschaft zugrunde liegen.

Inhaltsverzeichnis

0 Outline of the thesis

The assessment of soil physical quality and its temporal alteration dependent on different soil management strategies is the focus of this cumulative doctoral thesis. Following a comprehensive introduction reviewing the current research (chapters 1 and 2), three peer-reviewed first-author publications and two co-authored accepted publications comprise the core of this thesis (chapter 3). An interpretative summary of the presented studies and an illustration of the potential for advancements in future research finalizes the thesis (chapter 4).

There is a wide range of methods available for soil physical quality assessments with varied advantages and shortcomings which are subject to ongoing scientific discussion. To enable an appropriate classification and interpretation of the presented work, the introductory part of the thesis includes a concise overview of the available methods for soil physical quality assessment and the determination of hydraulic soil properties with emphasis on recent developments and current scientific discourse. A primary focus of the scientific work presented herein was on the evaluation and choice of an appropriate methodology which enabled reliable inferences to be drawn on differences in soil physical quality under various strategies for soil management or temporal alterations (Weninger et al., 2018; Weninger et al., 2019a; Weninger et al., 2019b).

The main body of this thesis has its foundation in several case studies conducted in Central Europe concerning physical soil quality and its temporal development under various soil management strategies (Kreiselmeier et al., 2019; Weninger et al., 2019a). Further research brought insight to the specific issues of soil physical characteristics, soil water repellency, and its effects on the modelling of soil water dynamics (Filipović et al., 2018; Weninger et al., 2019b).

The research for this thesis was conducted under the frame of two international cooperation projects. The first project "Development of models to predict land use-induced soil pore-space changes" was funded by the Austrian Science Fund FWF (I 2122-B16) in cooperation with the United Nations University Institute for Integrated Management of Material Fluxes and of Resources in Dresden and the TU Dresden, Germany. The second project "Impacts of soil water repellency on hydraulic characteristics under variable climate conditions: experimental and modelling approach" (HR20/2016) was funded by the Austrian Agency for International Cooperation in Education and Research (OeAD) in cooperation with the University of Zagreb.

1 Introduction

1.1 Soil Physical Quality – Definition of concept and relevance

Soil Physical Quality is the ability of a given soil to meet plant and ecosystem requirements for water, aeration, and strength over time and to resist and recover from processes that might diminish that ability.
(McKenzie et al., 2011)

Soil retains precipitation water, provides space, stability and nutrition for plants, accommodates organisms which metabolize harmful substances and fulfils a number of further functions which basically enable life on our planet. The reaction zone for the underlying processes is the network of soil pores which is physically built up of connected voids in a vast range of sizes and forms. The actual constitution of the soil pore system determines the ability of soil to fulfil the required functions and deliver demanded ecosystem services. Soil degradation, on the other hand, is considered as a major threat for sustaining civilization (e.g. Amundson et al., 2015; FAO and ITPS, 2015; Govers et al., 2017). Four out of the ten main global threats to soil functionality are of a physical nature; erosion and sealing were assessed as most severe (FAO and ITPS, 2015). Many of these threats to soil can be directly linked with soil management, for example compaction (Batey, 2011) and erosion (Pimentel, 2006) can result from the constant exposure of soil to degrading forces. Inputs of mechanical energy during management interventions, erosive weather events and the high nutrition demands of cultivated crops can all stress soil resistance.

In the light of these challenges, the term Soil Physical Quality (SPQ) was established to define the soil's capacity to provide and sustain the physical environment for enduring the required functionality. The SPQ is embedded in the broader concept of soil quality which again is a major component of environmental quality (Bünemann et al., 2018). Environmental quality refers to the functionality of the ecosystem services upon which civilization relies, it may be interpreted as the potential of natural capital stock to sustainably provide interest (Maysek et al., 2017; Spake et al., 2019). Both soil and global natural capital stocks are under increasing pressure and the extent of resource consumption has been continuously assessed to exceed the provision of interest (e.g. Wackernagel et al., 2002; Amundson et al., 2015; Steffen et al., 2015 and related discussion). In order to mitigate the subsequent resource scarcities, and to sustain or meliorate environmental quality, it is crucial that environmental management strategies consider soil physical quality as a major determinant of overall environmental functionality.

1.2 Implications for agricultural management

Within this thesis arable soils are focused upon, and the primary soil function investigated was the support for productive plant growth. Beneficial soil physical conditions for plant growth include the appropriate supply of water, nutrients and air to plant roots, high soil stability against erosion, and a harmonic water balance and micro-climate (McKenzie et al., 2011; Hartge and Horn, 2016). Plants are furthermore valuable and integrative indicators for physical soil conditions from pedon to landscape scale and allow a scientific evaluation of soil management options. Soil management has considerable potential for achieving high quality soil physical conditions (Hatfield and Sauer, 2011). It is a crucial challenge for agricultural practice and research to develop and evaluate soil management strategies which sustainably secure functionality and productivity of soils through periods of rapid change within the physical, social and economic environment.

The main aim of soil management research is the evaluation and development of sustainable soil management strategies. Tillage operations and the thoughtful planning of crop rotations are powerful instruments in changing the physical conditions soil is subjected to (Hatfield and Sauer, 2011). By changing the depth, intensity, frequency or instrumentation of tillage operations, the field or soil manager has a broad range of options which could considerably influence the soil pore system. Following tillage, abiotic environmental factors such as rain, frost, drought, and the continuous settling of soil alter the pore system throughout the seasons, decreasing pore volume and SPQ (Chandrasekhar et al., 2019). In contrast, biotic processes which support secondary soil structure foundation are regulated by decisions such as cash and cover crop selection and the respective cultivation periods (Jian et al., 2020; Page et al., 2020). Applying focussed soil management can improve soil stability by influencing the rates and intensities of such naturally fluctuating processes (e.g. Elmholt et al., 2008; Spaccini and Piccolo, 2013). Due to the vast variability in soil formation and agricultural practices at both the regional and the global level, research outcomes are seldom comparable. The SPQ-indicators (SPQIs) are appropriate proxies and offer possibilities for a somewhat standardized communication of valuable insights from case studies and monitoring systems (e.g. Huber et al., 2008; Corstanje et al., 2017). A comprehensive list of established SPQIs is presented in the sections 2.2 and 2.3.

The intention of this thesis was to present a step forward in the possibilities for SPQ assessments on agricultural soils using SPQIs. To gain an overview of the recent usage of SPQIs in studies focussed on the effects of soil management, a systematic meta-analysis was conducted in the Scopus scientific literature database. The review was restricted to the period between the year 2011 and the end of May 2020, the search terms were: ("soil physical quality" OR "physical soil quality") AND (soil management OR tillage OR crop). By these restrictions it was assured that the outcomes correspond to the goals and the concept of this thesis. The search yielded 277 publications (restricted to research articles and reviews). After screening through the abstracts and selecting only those studies investigating more than five SPQIs on arable soils and written in the English language, 85 publications were chosen for detailed review. A list of the selected publications may be found in appendix A. Figure 1-1 shows a classification based on the evaluated soil management options. The majority of studies using multiple SPQIs for evaluations of soil management strategies concentrated on the effects of different tillage treatments or different land use and farming system options. Crop rotation appears under-represented, whereas it is often combined with tillage, hence involved in the sector till+C. Thus, figure 1-1 and the corresponding literature delineate the framework of recent research into which this thesis was embedded and shows the actual relevance of the SPQI approach.

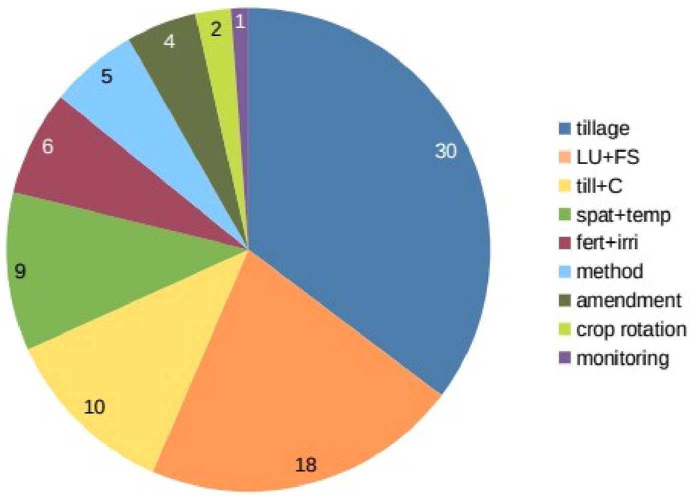

Figure 1-1: Classification of analysed publications by soil management options. Used abbreviations: LU+FS is land use and farming system, till+C is tillage combined with one or more of the other options, spat+temp is spatial and/or temporal variability of SPQ, fert+irri is fertilization and/or irrigation options, method stands for methodological developments.

2 Soil Physical Quality – Measurement and interpretation

2.1 Introduction to Soil Physical Quality Indicators

An intrinsic challenge in soil science arises from the fact that the processes or functions under analysis can hardly ever be observed directly and at the relevant scale. For the majority of research investigations, the subject – soil – needs to be severely modified or even destroyed in order to enable measurements, consequently the conditions for the acting agents and the linked processes are also altered. In soil physical research, relevant processes include water conductance and retention, aeration and the metabolism of specific soil organisms able to alter soil mechanics. These processes take place within the pore system and are highly sensitive to changes in the pore system constitution. Both soil sampling and the installation of sensors alter the pore system considerably, predominately in the region under investigation. Hence, soil science and especially soil physics often rely on the use of proxy observations such as the in- and outflow of water, solutions and gases from confined soil volumes, or the derivation of empiric quantities by lab routines which are seldom reproducible. The SPQIs are simplified outcomes of such proxy observations.

Due to the high spatial and temporal variability at all scales of soil processes, no standard way to express SPQ has been established until now (Nortcliff, 2001; Bünemann et al., 2018). Several different SPQIs were developed based on novel methodological possibilities, theoretical considerations and influenced by research discipline (Bacher et al., 2019). Overall, the aim is to integrate a preferably large amount of highly valuable information into a few simple numbers. Some of the SPQIs are standardized and broadly used while others are still in the establishing phase or rarely used due to a high resource demand or low reputation. A goal of this collection of material is to present a complete picture of the instruments available to determine SPQIs.

2.2 Methods collection

Wide-spread protocols for basic soil analysis usually include measurements of soil characteristics which indicate SPQ. The bulk density *BD* is a commonly used SPQI due to its simple determination and the high value information it conveys concerning soil compaction, porosity and feasibility for plant growth (e.g. Huber et al., 2008; Reynolds et al., 2009). Similarly to *BD*, the saturated hydraulic conductivity K_s is commonly measured for undisturbed soil cores in the laboratory (Dane and Topp, 2002). It is determined by the largest (connected) soil pores and allows inference on important hydrological soil functions such as infiltration capacity. However, results show a high variability which questions the reliability of K_s as a standardizing indicator; often a combination or substitution of K_s with more advanced techniques such as tenstion tension infiltrometer field measurements is recommended (e.g. Alagna et al., 2016; Weninger et al., 2018). Despite being a chemical characteristic by definition, the soil organic carbon content *SOC* is an effective determinant of soil physical conditions (e.g. Loveland and Webb, 2003). The *SOC* is a highly relevant indicator in many fields of research including atmospheric composition and climate as well as soil fertility and resilience, consequently *SOC* is probably the most frequently analysed soil quality parameter (Bünemann et al., 2018). For some of the SPQIs, thresholds and ranges have been suggested forming the first steps towards a standardized scale for the interpretation of SPQ and soil degradation (Tables 2-1, 2-3). However, it should be kept in mind that these values are a subject for ongoing discussion and research and should not be considered as final.

Table 2-1: Collection of SPQIs from basic soil analysis methods and, if available, ranges for SPQ interpretation.

Symbol	Unit	Description and thresholds for SPQ assessment	References for Development and Applications
BD, ρ_d	M L^{-3}	Soil bulk density 0.9 g cm^{-3} < BD < 1.2 g cm^{-3} … optimal range *BD* > 1.35 g cm^{-3} … limited plant growth	e.g. Dane and Topp (2002), Reynolds et al. (2009)
K_s	L T^{-1}	Saturated hydraulic conductivity	e.g. Dane and Topp (2002)
SOC	M M^{-3}	Soil organic carbon content (or concentration) *SOC* <≈ 2% … reduced soil stability	e.g. Loveland and Webb (2003)

A differentiation is often made between static or capacity-based, and dynamic SPQIs (Iovino et al., 2016). The latter essentially include time-dependent parameters of soil physical characteristics which the former simplifies. The discussion concerning the concept of field capacity is highly relevant in this regard and will be outlined in an extra chapter later in this manuscript. Static SPQIs are mainly derived from basic soil analysis or via a determination of the hydraulic soil property functions and include bulk density, plant available water capacity, air capacity, relative field capacity (Reynolds et al., 2008) and soil quality index S which is derived from the slope of the logarithmic soil water retention curve (Dexter, 2004a,b,c). The term Hydraulic Soil Properties (HSP) is mainly used to describe two functions representing the relationships of soil matric potential with volumetric soil water content, and with soil hydraulic conductivity, respectively. Actually these curves quantify and visualize the water retention and conductivity depending on the soil moisture state. Furthermore, Young and Laplace's capillary rise model is widely used for the approximation of pore size distribution from the water retention curve (Tuller and Or, 2005). Hence, this is an indirect approach which yields information about the pore system. As the measured process (water transport, drainage of soil) is crucially relevant in nature, this indirect approach is most effective for functional evaluations. The measurements and calculations for determining the HSP were an important subject in this thesis and are therefore described in detail in the following sub-chapter.

For the determination of dynamic SPQIs, water flow rates through a defined range of pore sizes are analysed in infiltration experiments using a tension infiltrometer (Iovino et al., 2016; Lozano et al, 2016). Similarly to interpretations in studies about FC (see excursus), the authors found advantages in the use of dynamic compared to static approaches. Additionally, time-variable characteristics of soil or pore surfaces belong to the dynamic indicators, namely the resistance of soil against water infiltration. The relevance of soil water repellency is fairly under-recognized, and the research is mostly limited to tropical or artificial soils. However, recent studies have revealed that soil water repellancy occurs within the majority of agricultural soils at a temperate climate (Müller et al., 2016). Consequently, one of the publications which contribute to the framework of this thesis focussed on soil water repellency and appropriate determination methods for its sub-critical range (Weninger et al., 2019b). Such flux-based, dynamic principles allow comprehensive insights into the interactions between different phases within the soil pore system depending on the soil moisture state. In addition to water flow, gas flux analyses led to the development of SPQIs. Air permeability which is closely linked to macropores and their connectivity, and gas diffusivity which is linked to soil matrix characteristics, are two frequently used SPQIs (Møldrup et al., 1998, Møldrup et al., 2001, Schwen et al., 2015). All these dynamic indicators allow further inference into pore system characteristics such as tortuosity and pore connectivity with a focus on specific effective pore size classes.

Further valuable information is gained by including measurements of soil mechanical properties. In an agricultural context, these determine the stability of soil and the respective soil pore system, and thus the soil's resilience against mechanical impacts such as erosion or pressure load by heavy machinery, and also the feasibility for plant roots to penetrate bulk soil (Horn and Lebert, 1994). The corresponding properties may be measured directly via aggregate stability tests, penetration resistance measurements or soil deformation experiments. Nevertheless, the scaling of the outcomes to the level of real-world conditions poses a challenge, and interpretations can often only be made relatively. The resulting SPQIs are for example indices for the stability of soil aggregates or soil structure (Mbagwu and Auerswald, 1999; Nciizah and Wakindiki, 2015); indices such as relative bulk density or degree of compaction as measures for soil densification in relation to a critical threshold (Håkansson and Lipiec, 2000); or a soil erodibility coefficient derived from shear stress estimations (Wilson et al., 2020). A more complex analysis of mechanical SPQ aims to measure the soil penetration resistance (soil penetration resistance curve; Leão, 2017; León et al., 2019) and soil volume alterations (soil shrinkage curve; Boivin et al., 2004; Dörner et al., 2009; Johannes et al., 2019), both in dependence on water content.

As another approach, visual assessment of SPQ is widely used. In research however, it is not as commonly applied as the above presented methods due to its high subjectivity. Nevertheless, for practitioners it is the most feasible, rapid and illustrative way to gain insights. Hence, increasing efforts have been made to link science to practice and develop methods which may be appropriately used by all stakeholder groups (e.g. D'Haene, 2012; Johannes et al., 2019). Mueller et al. (2009) presented a comprehensive collection of methods, the outcome of a visual SPQ-assessment is mostly a semi-quantitative score. The most established methods are the VESS (Visual Evaluation of Soil Structure, formerly VSSQA;

Franco et al., 2019) for spade sampling together with its derivation for core samples (CoreVESS; Johannes et al., 2017) and the VSA (Visual Soil Assessment; Shepherd, 2009). Various different methods were found to be responsive to the effects of soil management and temporal changes on SPQ, but discrepancies between the methods remained (Moncada et al., 2017).

Valuable SPQIs should provide sufficient sensitivity to detect trends in soil monitoring studies and allow targeted steering actions in soil management. Additionally, they need to deliver reliable results, meaning that implausible outliers or artificial outcomes caused by improper conceptualisation must be avoided (de Paul Obade and Lal, 2016; Bünemann et al., 2018). For research and monitoring practices, the demand of intellectual and material resources for a successful application also needs to be considered. Combinations of several SPQIs are often recommended to assemble a more complete picture of SPQ (Bacher et al., 2019). On the other hand, correlations between certain SPQIs occur which make measurements redundant. For example AC, PMAC and partly PAWC may be represented by RFC which combines the soil's capacity to store soil and water (Castellini et al., 2019).

Further soil characteristics which are highly relevant for SPQ and usually determined in standard soil surveying often include the grain size distribution or soil texture which builds the basis for the construction of a soil pore system and the resulting soil functionality. As soil texture cannot be changed in agricultural scales of space and time, it is not usable as a SPQI as they are intended for assessments of soil or land management. Nevertheless, textural characteristics need to be considered in all interpretations and they affect the comparability of results between different study sites. The same is valid for further soil properties which influence soil physical characteristics like pH, content of Ca or $CaCO_3$, amongst others.

2.3 SPQIs based on HSP-function analysis

The HSP in the following content refer to the relationship between the soil water head h (also used: matric head or matric potential Ψ) and volumetric soil water content θ (soil water retention curve) and soil hydraulic conductivity K (soil hydraulic conductivity curve). Certain points on these HSP-curves have been used as indicators for the distinction of soil characteristics and SPQ assessment for decades. These SPQIs relate directly to water balance components or similar functionally important quantities. The most widely used SPQIs and their relation to HSP are presented in Table 2-2 and FC as most relevant point on the soil water retention curve is discussed in a following extra chapter.

Table 2-2: Collection of SPQIs based on HSP-function analysis with explanation and, if available, ranges for SPQ interpretation.

Abbr.	Unit	Description and thresholds for SPQ assessment	References for Development and Applications
PAWC, AWC, PAW	$L^3\ L^{-3}$	Plant available water content; fraction of soil pore volume potentially filled with plant available water; $PAWC = \theta_{FC} - \theta_{PWP}$ $0 < PAWC < 0.15$ … poor quality	
AC	$L^3\ L^{-3}$	Air capacity; volume of pores filled with air at field capacity or a proportional characteristic value; $AC = \theta_S - \theta_{FC}$ or e.g. $AC = \theta_S - 0.1$ $AC < 0.1$ … limit for root growth, $0.16 < AC < 0.24$ … optimal range	da Silva et al. (1994), Reynolds et al. (2008), Koureh et al. (2020)
RFC	-	Relative field capacity; $RFC = \theta_{FC} / \theta_{PWP}$	
S, S_{inf}	-	Dexter's soil physical quality index; slope of the water retention curve (with logarithmic h-axis) at inflection point $S > 0.05$ … optimal SPQ $S < 0.035$ … physically degraded soil	Dexter (2004 a,b,c), Dexter and Czyz (2007)

AWr	-	Relative air-water energy index; balance of energy used in soil for aeration and water retention processes, energy values calculated as integrals of soil water retention curve $AW_r = \frac{\int_{\theta_{fc}}^{\theta_s} h(\theta)\, d\theta}{\int_{\theta_{pwp}}^{\theta_{fc}} h(\theta)\, d\theta}$	Armindo and Wendroth (2016, 2019)
LLWR	$L^3 L^{-3}$	Least limiting water range; advancement of *PAWC*, additional limits for plant growth based on soil aeration and root penetration resistance are implemented; interpretation corresponding to *PAWC*	da Silva et al. (1994), Leão et al. (2006), Pulido-Moncada and Munkholm (2019)
IWC		Integrative water capacity, advancement of LLWR including hydraulic conductivity and gradual limitations $IWC = \int_0^{15000\,cm} \left(\prod_{i=1}^{n} \omega_i(h) \right) C(h)\, dh$ where $C(h)$ is the slope of the water retention curve ($\lvert d\theta/dh \rvert$) or absolute differential water capacity in cm^{-1}, the index i denotes the various limiting physical soil properties (usually four: soil penetration resistance, soil aeration, high and low hydraulic conductivity), and ω the corresponding weighing function which is defined by the operator	Groenevelt et al., (2001), Asgarzadeh et al. (2014)
FPS	$L^3 L^{-3}$	Functional pore size fractions; pore size distribution measured or approximated from HSP (via the capillary rise model of Young and Laplace, see e.g. Tuller and Or, 2005) and classified into functional fractions; classification after Greenland (1981): fissures > 500 μm > transmission pores (water drainage and gas exchange) > 50 μm > storage pores (water retention) > 0.5 μm > residual pores (retention and diffusion of ions in solution) > 0.005 μm > bonding pores classification according to Cameron and Buchan (2006): Macropores P_{MAC} > 75 μm > Mesopores P_{MES} > 30 μm > Micropores P_{MIC} > 5 μm > ultramicropores P_{UM}> 0.1 μm > cryptopores P_{CRY} Several further classification schemes are frequently applied with similar borders and function assignments. Recent discussions promote dynamic approaches instead of fixed pore diameter borders (e.g. Mengistu et al., 2019).	

The basis for HSP-determination are data pairs of the respective curve, which means θ or/and K at known or given h. For the measurement of these data pairs, a range of methods is available with different demands on resources and expected reliability of results. Most of them are lab methods which are applied to undisturbed soil cores or soil aggregates. In the most wide-spread approach, negative pressure is applied to the samples by a hanging water column or suction plate for h near saturation and a pressure plate apparatus for lower h (Dane and Topp, 2002). These experiments are highly time and resource demanding, the resolution of results is limited and unsaturated hydraulic conductivity is mostly approximated by mathematical models (Mualem, 1976).

To overcome these limitations, methods for the rapid simultaneous determination of both HSP curves are gaining increasing importance, and technical progress supports the development of broadly usable methodologies. Advanced approaches include infiltration, multistep-outflow, multistep-flux or multistep-transport experiments in diverse lab or field settings where HSP parameters are determined by inverse modelling (e.g. Kumahor et al., 2015; Kotlar et al., 2019); centrifuge experiments (e.g. Caputo and Nimmo, 2005; Malengier et al., 2015); evaporation experiments (Peters and Durner, 2008); tracer methods using stable isotopes (Sprenger et al., 2015; Groh et al., 2018); or remote sensing attempts

(Mohanty, 2013) out of which the cosmic-ray (Han et al., 2016; Brunetti et al., 2019) and radar (e.g. Jadoon et al., 2008; Pan et al., 2019) technologies appear particularly promising. These methods are continuously evaluated and improved, but the primarily introduced standard methodology is still predominantly used. As an exception, the evaporation method was commercialized in an affordable and user-friendly manner, hence its dispersion is increasing. In the main experimental body of this thesis, this application builds the backbone of HSP determination methodology and showed valuable and reliable results (Weninger et al., 2018; Weninger et al., 2019a).

Another option is the calculation of HSP-parameters via pedotransfer functions based on more easily measured characteristics, e.g. bulk density, soil texture, soil organic carbon. Many of these pedotransfer functions were developed based on a large variety of data bases from all over the world. In the majority of comparative studies, this indirect approach is outperformed by direct methods (e.g. Bacher et al., 2019). Therefore and for the conciseness of this manuscript, the pedotransfer functions are excluded from further attention. They may nevertheless be a valuable opportunity for applications where a large amount of data is needed with low demand on sensitivity, for example in regional modelling. The evaluation of soil management strategies, which is the focus of this work, requires a higher sensitivity which may be reliably achieved only by using more complex determination approaches.

Usually, the HSP display non-linear correlations which may be approximated by functions determined by a small number of parameters. Two commonly used models are presented as representations for a wide range of functions which are mainly based on comparable assumptions and ideas (Table 2-3). For both, the hydraulic conductivity function was linked to the retention curve via the model of Mualem (1976). These functions have unimodal first derivatives which are equivalent to the pore size distributions. In natural soils, the pore system is often divided into a structural and a matrix domain. Hence, the size distribution is (at least) bimodal and bimodal functions are increasingly used as they show better fits to measured data (see e.g. Romano and Nasta, 2016). In practice, these bimodal functions are built by a superposition of two unimodal curves (e.g. Durner, 1994; Omuto, 2009, Romano et al., 2011). Moreover, to improve the goodness of fits, the models were complemented with terms for certain ranges of soil moisture (e.g. Peters, 2013). The usage of bimodal functions allows a specific characterization of SPQ focussed on the structural or matrix soil domain (Reynolds, 2017).

Table 2-3: examples for parametric HSP-functions.

effective saturation (-)	$S_e = \frac{\theta - \theta_r}{\theta_s - \theta_r}$ where θ is the volumetric water content (L^3 L^{-3}), θ_s the water content at water saturation (L^3 L^{-3}), θ_r the residual water content (L^3 L^{-3})
Van Genuchten (1980)	$S_e(h) = \left[1+(\alpha h)^n\right]^{-m}$ where *α* (L^{-1}) and *n* (-) and *m* (-) are shape parameters; commonly used constraint: *m* = 1/*n* - 1 $K(h) = K_s S_e^L \left[1-(1-S_e^{1/m})^m\right]^2$ where *L* (-) is a tortuosity parameter
Kosugi (1996)	$S_e(h) = \frac{1}{2}\, erfc\left(\frac{\ln h - \ln h_m}{\sigma\sqrt{2}}\right)$ where erfc denotes the complementary error function, h_m and *σ* are fitting parameters representing mean and standard deviation of the approximated log-normal distribution of *h* $K(S_e) = \left(\frac{1}{2}\, erfc\left[erfc^{-1}(2S_e)+\frac{\sigma}{\sqrt{2}}\right]\right)^{\eta}$

The parameters for these functions might be used for the modelling of soil water dynamics to obtain information about differences between different soils or soil management systems. The basis of such analyses is the prediction or reproduction of soil processes and related functions, this approach is often called functional evaluation. A direct comparison of parameter values from different study setups give very little valuable information. In contrast, the continuous definition of the respective relationships allows a prediction of characteristic points or ranges on the curve depending on known values of other parameters. The most common example is the prediction of soil water content from given soil matric potential thresholds. Compared to parametric functions, increases in computing resources support the approximation of more complex curve types like cubic splines (Othmer et al., 1991; Kastanek and Nielsen, 2001). They allow an even better representation of measured data but are not (yet) directly useable in modelling applications. The differences in goodness of model fitting between parametric and more complex also influence resulting SPQIs and the subsequent interpretations (e.g. Weninger et al., 2019a).

Excursus – The confusion about field capacity

The field capacity (FC) plays a crucial role in the formulation and determination of many of these indicators and their underlying concepts. Furthermore, it is the most relevant soil characteristic in applied science and soil management operations such as irrigation management, soil leaching, contaminant transport and groundwater recharge. Due to this relevance and as a scientific consensus about the most appropriate definition and determination procedure of FC is still lacking, a short introduction to the ongoing debate follows, even though it does not fully represent the focus of this thesis.

It may be assumed that since the advent of agricultural irrigation considerations have been made concerning the maximum amount of water which can be stored in a certain soil. The first studies which found their way to the current scientific publication system were published in the end of the 19th and beginning of the 20th century (e.g. King, 1889, as cited in Israelsen and West, 1922; Alway and McDole, 1917, as cited in Reynolds, 2018; Israelsen and West, 1922). They used a rather wide range of terms such as water-retaining capacity, field carrying capacity and water-holding capacity. An early attempt to standardize terminology and definitions was published by Viehmeyer and Hedrickson (1931). They pleaded for the usage of the term FC and defined it as the "… amount of water held in the soil after the excess gravitational water has drained away and after the rate of downward movement of water has materially decreased, which usually takes place within 2 or 3 days in pervious soils of uniform texture and structure." In this definition the dynamic nature of the concept and inherent uncertainties are evident from the phrases "materially decreased" and "within 2 or 3 days". A combination of several former attempts together with clarifying formulations were given by Reynolds (2018), where FC is the "root zone water content in an initially saturated or field-saturated soil after rate of change of water defined as content ..." or drainage flux effectively ceased (simplified, as original source gives multiple formulations for "effectively ceased"). Furthermore, four fundamental components of the FC concept are apparent from these definitions and were formulated as i) a soil water content, ii) a process characteristic being drainage flux or change of water content, iii) time for drainage from saturation, iv) the extent of the respective soil layer (Reynolds, 2018). Whenever FC is used in studies as a basis for soil scientific statements, these components should be considered and simplifications should be thoroughly justified.

Despite knowledge about the inherent imprecisions, uncertainties and concept dynamics, the majority of studies up until the present day used fixed matric potential values to determine a corresponding value at the water retention curve as field capacity. These values were rather arbitrarily chosen based on literature sources, the most commonly used are for example -50 cm, -100 cm or -330 cm (Assouline and Or, 2014). The latter more negative values are used for fine textured soils, and less negative values for coarse textured soils (e.g. Twarakavi et al., 2009; Reynolds, 2018). These values are based on so-called static approaches and lab experiments where the corresponding pressure heads are applied to soil samples. Hence, the components drainage time and vertical dimension are somewhat neglected in the determination process which leads to outcomes that seldom represent natural circumstances (Reynolds, 2018).

In contrast, so-called dynamic approaches to FC were frequently presented but did not gain wider attention, mainly due to their higher complexity in comparison with the convenient static approach (Twarakavi et al., 2009). The formulation of Viehmeyer and Hendrickson (1931), as given above, already included the basic idea of a dynamic concept for FC in their distinct appreciation for drainage time and the criterion of negligibly small internal drainage flux. Based on this, several studies aimed to progress the dynamic conceptualization. The most relevant steps in the debate were comprehensively discussed by Assouline and Or (2014) and Reynolds (2018). A detailed repetition of the delineations given therein would be beyond the scope of this thesis. However, it can be stated that it was universally agreed within the debate that a threshold for negligibility of flux needs to be defined. This threshold could be a fraction of saturated hydraulic conductivity, of the water content in the studied soil layer or a prescribed drainage time. The threshold values were chosen arbitrarily (e.g. in the range of 0.009 – 0.9 mm d−1; Meyer and Gee, 1999) and the detection of the corresponding soil water state in natural soil and even in lab experiments is highly challenging. Such measurements require extensive instrumentation and are nevertheless susceptible to bias caused by arbitrary decisions (Nemes et al., 2011; Turek et al., 2019). Hence, robust research on dynamic FC determination was effectively impossible for a long time, and respectively restricted to theoretical considerations.

With the emergence of numerical simulation models and the required computational power, an ongoing increase in attention was caused by new possibilities for the progression of the dynamic FC concept. This manifested in a growing number of publications containing formal advances and applied studies based on extensive simulation studies (e.g. Zacharias and Bohne, 2008; Twarakavi et al., 2009; Assouline and Or, 2014; de Jong van Lier and Wendroth, 2016; Reynolds, 2018). Turek et al. (2019) presented a comparison of five dynamic approaches with four static criteria and one PTF for the determination of FC. They conducted a functional evaluation study with soil and weather data for six temperate and tropical sites and found considerable differences in SPQIs and simulated crop yield. This highlighted a strong need for further research towards more representative ways of calculating FC.

3 Outline of research articles and major findings

In this chapter the prevailing theme of the thesis is highlighted by means of selected research articles, summarized in a concise form. In the text, parts of the respective abstracts are combined with a brief discussion, hence repetitions of phrases stated in the abstracts are inevitably included and are not marked as direct quotes to allow better readability. The corresponding publications are presented in grey coloured infoboxes including the citation, the highlights, and a selected graphical outcome with an extended figure caption. Extensive descriptions of the materials, methods and results as well as a detailed discussion and interpretation along with the corresponding literature references are found in the original peer-reviewed articles. Complete copies of the publications are attached in Appendix B.

As pointed out above (subchapter 2.3), an assessment of SPQ or of temporal alterations in soil physical properties is often based on HSP determination. The methodology for this thesis was also based on measuring and analysing HSP. Many soil hydrological studies answer their research questions using a certain method for HSP determination which is assessed to be most appropriate for the respective application. This practice is frequently questioned, especially because the single methods cover only a limited range of soil moisture conditions (e.g. Siltecho et al., 2015; da Silva et al., 2020). The establishment of advanced methods allowing for higher flexibility is progressing slowly. Nevertheless, recent technical developments facilitate the efficient and cheap collection of soil water characteristics data, although the quantitative benefit of methodological advances has not been adequately tested yet in extended measurement campaigns.

In the first study presented, we combined four methods to measure water retention and hydraulic conductivity at different moisture ranges: evaporation method, dewpoint psychrometry, hood infiltrometer experiments, and the falling head method for saturated conductivity (Weninger et al., 2018; infobox 1). The sampling and experiments took place at two experimental sites in eastern Austria. The effects of including these particular methods in the measurement strategy were examined by visual evaluation and a 1D-modelling sensitivity study including the near-natural scenarios of drainage, infiltration and drought.

The step-wise evaluation approach helped to obtain results which are highly robust in comparison to single-method observations. The evaporation method was considered essential due to its broad measurement range for both water retention and hydraulic conductivity. In addition to this, the largest effect on simulated water balance components was induced by the inclusion of separate conductivity measurements near saturation. Water content following three days of drainage was 15 percent higher and the transpiration rate during a drought period was 22 percent higher without near-saturated conductivity measurements. Based on relative

Combination of Measurement Methods for a Wide-Range Description of Hydraulic Soil Properties

1

Weninger, T., Bodner, G., Kreiselmeier, J., Chandrasekhar, P., Julich, S., Feger, K.-H., Schwärzel, K., Schwen, A., 2018. Water 10 (8), 1021.

Highlights

•Combination of measurement methods enables to measure the full range hydraulic soil properties, from dry to saturated

•Measurements of near-saturated hydraulic conductivity are crucial for assessments of hydraulic soil properties

Selected graphical outcome

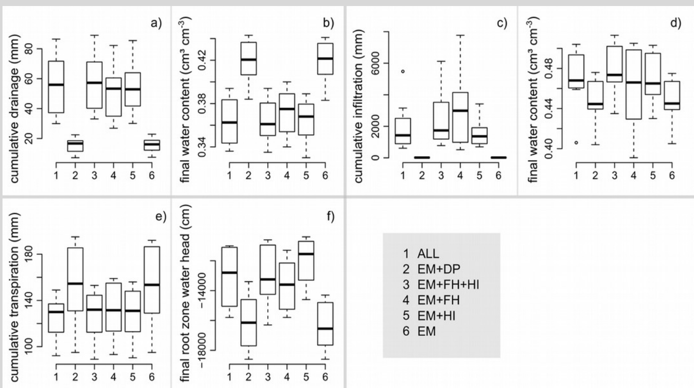

Figure 4-1. Final state results from a modelling study in HYDRUS-1D, consisting of 3 parts: a 72-h-drainage experiment starting with a fully saturated soil column and free drainage at the bottom (a, b), followed by an infiltration period of 24 h with saturated soil surface and free drainage at the bottom (c, d). The third simulated process was drought over 45 days from an initial soil water head of h = -100 cm with constant potential evapotranspiration of 9.5 mm (e, f). Different boxes stand for varying method combinations of EM … evaporation method using HYPROP for water retention and hydraulic conductivity in medium soil moisture range, DP … dewpoint potentiometry for retention in dry soil range, FH … falling head method for saturated hydraulic conductivity, and HI for hood infiltrometer field measurements of near-saturated hydraulic conductivity. Most impressive are the consistent differences between 2+6, without measurements of near-saturated or saturated hydraulic conductivity, and the other combinations.

comparisons between different combinations, we suggested combining evaporation method and hood infiltrometer experiments as the basis for representative predictions of soil water dynamics. This study formed part of the framework from which this thesis developed, specifically from the initial attempts to evaluate the available methodological resources and develop a comprehensive base of information concerning the usefulness and opportunities certain methods present for HSP determination.

Subsequently, the evaluated set of measurement methods was applied to three field sites in eastern Austria and eastern Germany. A detailed description of climatic conditions and basic soil properties is given in Weninger et al. (2019a). At all three sites, long-term tillage experiments were established with the four different treatments: conventional mouldboard tillage; chiselling + rotary harrow; rotary harrow; and no till. These treatments differed in mechanical intensity and depth. The conversion from the former tillage system (conventional tillage) took place 6, 10 and 23 years before first sampling, respectively. Hence it was possible to estimate rates of mid-term alterations in soil physical conditions, especially SPQ and HSP. The sampling design included frequent field campaigns throughout two vegetation periods (2016 and 2017), and due to this the seasonal variability of the observed indicators and properties was analysed.

In the second study, the effects of changes in tillage intensity on SPQ and pore size distribution since the establishment of the trials were quantified (Weninger et al., 2019a; infobox 2). Extensive field campaigns were conducted on randomized block designs to minimize the probability of bias due to spatial variability. Pore size distributions were calculated from soil water retention curves based on the high-resolution measurements. Subsequently, fractions of functional pore size classes and selected SPQIs were determined and compared between treatments. In addition, we evaluated the performance of two calculation approaches for pore size distribution: (1) fitting of a smoothing cubic spline; and (2) a bimodal van Genuchten function. The parametric function yielded a higher proportion of storage pores by approximately 3–5%. The combination of multiple measurement and evaluation methods enabled detailed comparison of soil physical characteristics between different tillage treatments.

The resulting sets of HSP and SPQIs were used to derive statements about soil quality development under agricultural practices. No-till soils showed a distinct lack of transmissive pores and higher bulk density, but similar plant-available water capacity, compared to the other treatments. Under all soil management systems, aeration deficits were observed, emphasising the vulnerability of silt-dominated arable soils with a low organic matter content to compaction. The targeted temporal and spatial scales are the most relevant scales for effective

Effects of tillage intensity on pore system and physical quality of silt-textured soils detected by multiple methods

2

Weninger, T., Kreiselmeier, J., Chandrasekhar, P., Julich, S., Feger, K.-H., Schwärzel, K., Bodner, G., Schwen, A., 2019. Soil Research 57, 703-711.

Highlights

•Compaction and aeration deficits were found in silt-dominated soils under four tillage treatments with different intensity
•No-till soils showed highest bulk density and lack of macropores but high plant available water capacity
•Two different approaches for determination of soil pore size distribution yielded significantly different results

Selected graphical outcome

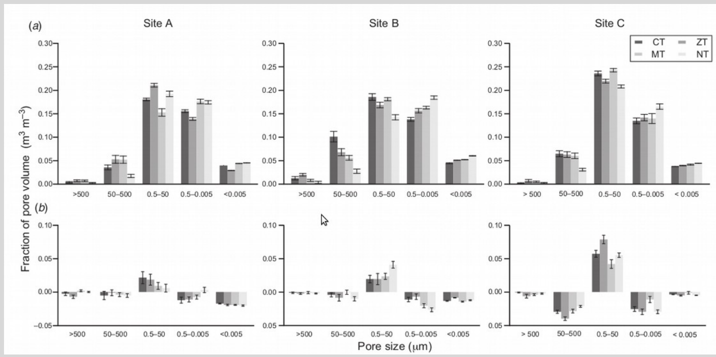

Figure 4-2. Differences in functional pore size classification between different tillage treatments on three sites. Sites are Lüttewitz, Germany (A), Hollabrunn, Austria (B), and Obersiebenbrunn, Austria (C). Treatments in sequence of reduced tillage intensity are conventional tillage using moldboard plough (CT), reduced tillage with chisel plow and rotary harrow (ZT), minimal tillage using rotary harrow (MT), and no-till direct seeding (NT). Borders of pore size classes were chosen considering soil hydrological function where pores with diameter >500 μm are fissures, from 50 to 500 μm are transmissive pores (both conducting water rapidly), from 0.5 to 50 μm are storage pores, from 0.005 to 0.5 are bonding pores, and pores with diameter <0.005 μm are residual pores (both latter hold water too tight for plant water uptake). Row b) shows differences in pore size classification when measured values are analysed by fitting of a parametric function (van Genuchten, 1980) in comparison to cubic spline fitting as presented in a) (values in row b = results from cubic spline – results from parametric function). A slight shift towards higher content of finer pores by reducing tillage intensity is observable.

management-induced improvement of soil quality. Consequently, the outcomes have high potential to induce beneficial developments. The analysed soils are remarkably vulnerable to several types of soil degeneration but are also most valuable for agricultural production in Austria. Hence, optimization of soil management practices focusing on soil protection is a crucial issue for soil science and this study adds a valuable contribution to the collection of scientific knowledge linking soil science and agriculture.

Quantification of soil pore dynamics during a winter wheat cropping cycle under different tillage treatments

3

Kreiselmeier, J., Chandrasekhar, P., Weninger, T., Schwen, A., Julich, S., Feger, K.-H., Schwärzel, K., 2019. Soil and Tillage Research 192, 222-232.

Highlights

- Pore size distribution was monitored over one cropping cycle on no-till/till soils
- There was distinct temporal variation in the structural pore domain of tilled soils
- No-till soil was temporally more stable
- Overall soil physical/hydraulic properties were not significantly different

Selected graphical outcome

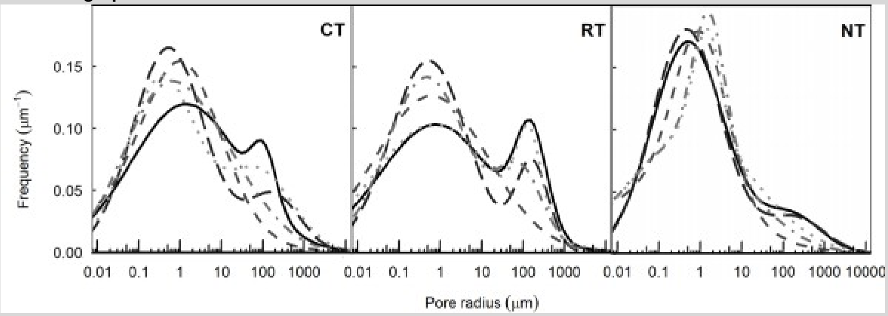

Figure 4-3. Evolution of pore size distributions under different tillage treatments throughout a vegetation period. Tillage treatments are: conventional tillage (CT), reduced mulch tillage (RT) and no tillage (NT). Different lines represent days after seeding of winter wheat.

In another study, the seasonal development of HSP was analysed (Kreiselmeier et al., 2019; infobox 3). The HSP were parametrized using a bimodal Kosugi retention function (Tab. 2-2) in combination with the conductivity model of Mualem (1976). The bimodal version once more allowed a detailed analysis of both textural and structural pores. Fractions of functional pore size classes were calculated via the bimodal water retention curve. The conventional and reduced tillage treatments showed a shift to smaller pore sizes, similarly to the results in Weninger et al. (2019a), but on a seasonal time scale.

In an attempt to broaden the view on SPQ and its assessment, a further focus was set on soil water repellency (SWR). This soil property has often been considered as a soil physical characteristic of a very narrow selection of soil types, for example in tropical ecosystems or volcanic soils. Widely used methods for detection of SWR give semi-quantitative or binary results which are not representative for natural soil physical processes and only sensitive to severe SWR. In the presented study, we determined SWR through the combination of multiple field and lab methods (Weninger et al., 2019b; infobox 4). The focus was on the sub-critical range of SWR which is increasingly recognized to play an important role in most agricultural and forest soils. Field infiltration measurements were performed with a tension disc infiltrometer and a minidisc tension infiltrometer using water and ethanol as infiltrating liquids. The

Estimating the extent of fire induced soil water repellency in Mediterranean environment

4

Weninger, T., Filipović, V., Mesić, M., Clothier, B., Filipović, L., 2019. Geoderma 338, 187-196.

Highlights

- Fire affected plots revealed SWR with significant change in infiltration patterns
- SWR decreased with increasing depth and decreasing organic matter content
- The combination of applied methods is useful in determination of sub-critical SWR
- Hydraulic conductivities decreased with increasing repellency indexes (RI)
- All methods confirm SWR at burnt sites, but with some discrepancies between them

Selected graphical outcome

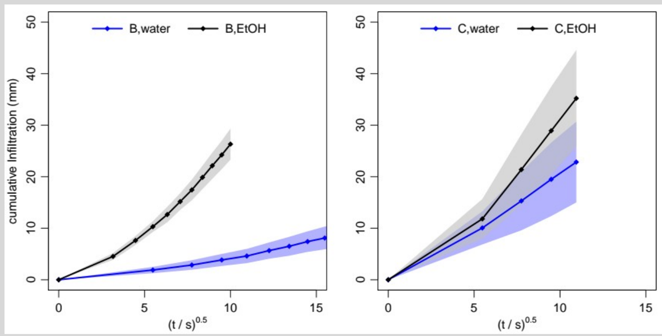

Figure 4-4. Semi-quantitative comparison of cumulative infiltration (mm) vs. square root of time ($s^{0.5}$) for mini disc infiltration measurements on burnt soil (B) and control plot (C) performed with water and ethanol (EtOH) as infiltrating liquids. Shaded areas are the 95%-confidence intervals, sample size for B is 9, for C is 6. The considerable differences between infiltration curves with water (blue) in the two plots show the presence and persistence of soil water repellency.

comparison of the infiltration behaviour of these two fluids is often used due to the physical property of ethanol as fully wetting fluid (i.e. no repellency observable) in contrast to water which is affected by repellent surfaces.

The study sites were located in Croatia and sampled shortly after a wildfire. Wildfires are known to cause SWR, hence the sites were appropriate for methodological advances. Experiments were conducted on two locations: burnt and control (unaffected by fire). Additionally to the infiltration experiments, the most common lab methods (water drop penetration time tests, and molarity of ethanol droplet time test) were carried out on disturbed and undisturbed soil samples from various depths. Previously, these lab methods have only been used for the detection of critical SWR, which refers to the formation of a drop on the soil surface which remains stable for more than five seconds.

In common agricultural soils, it is expected that sub-critical SWR plays a more relevant role by decreasing infiltration rates, confirming data is however widely lacking. By a slight modification of the standard procedure for sample preparation, we enhanced the possibilities of detecting sub-critical SWR using these lab methods. Additionally, in the interpretation of the field methods, recently published calculation procedures with a focus on sub-critical SWR were used. All methods revealed significant differences between the burnt and control plots, at least at the soil surface. Infiltration capacity and hydraulic conductivity were reduced and the repellency index was increased at the fire affected sites. The SWR decreased with depth which can be associated with decreasing organic matter and fire burning effect. The two lab methods in combination with mini disc tension infiltrometer measurements were found to be useful for the determination of sub-critical SWR.

The effect of SWR on the HSP and their determination was analysed in a further study (Filipović et al., 2018; infobox 5). Sequential modelling using HYDRUS (2D/3D) was performed based on data from an experimental field site in eastern Austria with artificially imposed drought scenarios (moderately and severely stressed) and a control plot. First, inverse modelling was performed for HSP estimation based on infiltration experiments using water and ethanol as inflitration liquids, followed by model validation on one selected irrigation event. Finally, hillslope modelling was performed to assess water balance for a period of one year. Results supported the expectation that prolonged dry periods can increase SWR. Inverse modelling was successfully performed for infiltrating liquids, water and ethanol, with R^2 and model efficiency values both above 0.9. The HSP derived from the ethanol measurements showed large differences in van Genuchten-Mualem (VGM) parameters for the moderate and severe plots compared to water infiltration experiments. The differences in SWR caused a remarkable decrease in saturated hydraulic conductivity at the drought-affected plots. After validation of HSP on water content measurements during a selected irrigation event, one year simulations (2014) showed that water repellency increases surface run-off for non-structured soils on hillslopes. Based on the presented approach, the resulting HSP could be used for an advanced SPQ assessment where the effects of SWR are considered.

Increasing knowledge in this field is especially important as the impact of SWR on SPQ and soil functionality is not yet fully understood. It decreases infiltration capacity in an undesirable manner on the one hand, and yet displays a positive effect in stabilizing soil aggregates

Inverse estimation of soil hydraulic properties and water repellency following artificially induced drought stress

5

Filipović, V., Weninger, T., Filipović, L., Schwen, A., Bristow, K.L., Zechmeister-Boltenstern, S., Leitner. S., 2018. Journal of Hydrology and Hydromechanics 66 (2), 170-180.

Highlights

• Soil water repellency changed hydraulic soil properties and caused differences in soil water simulation results

Selected graphical outcome

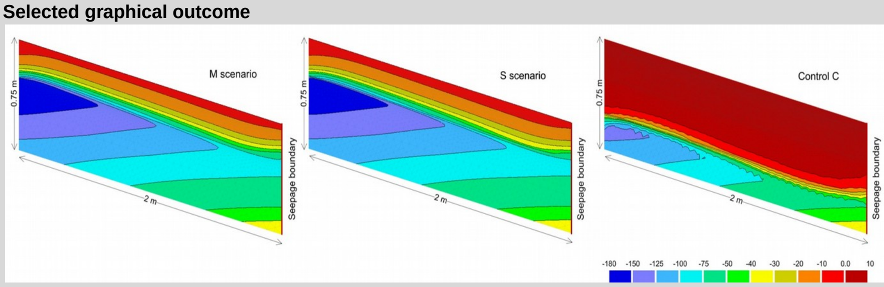

Figure 4-5: Simulation results: Pressure head distribution for moderately stressed (M), severely stressed (S) and control (C) scenarios after 150 mm of the irrigation event on the previous day. Differences are caused by hydraulic soil properties of differently water repellent soil as detected in previous steps in the study.

by reducing dispersion by water on the other. In addition to wildfires, very dry soils and a high content of soil organic carbon are known to increase SWR. Global climate change is projected to result in prolonged and intense droughts, hence the relevance of SWR is expected to rise. In our studies, we obtained comparable quantitative results through combined methods and present methodological advancements which aid developments in valuable research for specific aspects of SWR. Further research is needed to develop a framework for quantitative SWR classification, as well as subsequent estimation of the relevance of SWR for critical hydrological processes such as infiltration, run-off, and preferential flow.

A common characteristic of the studies discussed above is the determination of soil physical properties in high detail and high resolution, be it temporal or on the soil moisture scale from dry to wet. Advanced and approved methodology was used for measurements and subsequent calculation procedures. The resulting collection of methods and the case studies presented comprise a rare resource in their extent and resolution. The findings offer several opportunities for further research, two consecutive approaches were followed in the course of this project and are presented briefly. A detailed description of the resulting studies would be beyond the scope of this thesis.

One consecutive focus was the modelling of temporal alterations of HSP. In most standard applications for the modelling of soil water dynamics, HSP should be defined as basic soil parameters. This is usually achieved through a static approach, meaning that temporal HSP alterations are neglected. A review of critical literature and corresponding data led to the statement that this simplification could significantly bias the results and interpretations of modelling studies (Chandrasekhar et al., 2018). Data from our field experiments and the available literature was used to evaluate a mathematical model for the seasonal alterations of HSP (Chandrasekhar et al., 2019a). Based on this, an open source code script was developed, enabling the modelling of temporal HSP-alterations and available for implementation into advanced simulation software applications (Chandrasekhar et al., 2019b).

The second line of consecutive research concentrates on the interpretation of results from the usage of agricultural practices. This intention was partly covered by Weninger et al. (2019a), Kreiselmeier et al. (2019) and Kreiselmeier et al. (2020) where the effects of different tillage systems on soil pore systems were analysed. The results and conclusions of these studies include a detailed analysis of practically relevant alterations of soil characteristics and the intrinsic risk of soil degradation. A further step towards practical implementation was made in a study by Bodner et al. (2019) where long-term yield data from the experimental fields in eastern Austria were included in the analyses. Through a comparison of similar results from other regions it was shown that positive effects of conservation tillage on yield were less probable in the temperate humid climate of the study sites than in dryer regions. The susceptibility to yield losses due to compaction, aeration deficits and affected soil temperature balance was interpreted to be a limiting factor and implies challenges in developing appropriate soil management strategies with reduced tillage intensity.

4 Conclusions and Outlook

This thesis presents a sequence of steps towards a more detailed and robust assessment of soil physical quality than is commonly applied. The methodological advancements were described and evaluated in several case studies. Sophisticated methods for soil physical quality assessment are needed for the comprehensive evaluation of different soil management strategies, which are under continuous development in order to enhance and sustain the functionality of agricultural soils. The novelty of the assessment approaches evaluated here was in the vertical and horizontal method combinations which led to an exceptionally high grade of detail and high feasibility of the case study results. These properties of the results assure a high informative value and enable their effective communication, and subsequently the implementation of findings, within agricultural practices.

The effects of different soil tillage strategies on the soil's physical constitution were investigated in the case studies. Distinct differences between tillage treatments were found in soil physical quality and hydraulic soil properties on long-term tillage experimental sites. Consequently, inferences could be drawn for temporal alteration rates of the analysed properties based on these results. Under the present climatic and geographical conditions, the expected improvements in soil physical quality after changing the soil tillage strategy were found to occur at too slow of a pace to be sufficiently effective at the observed mid-term time scale. In addition, soil physical quality indicators were determined and a comparison with established thresholds enabled an assessment of soil degradation risks. At the study sites, soil compaction and lacking aeration were detected as the main threats for soil functionality. The conclusion for the design of future soil management systems was that melioration strategies should particularly aim to establish a stable macropore network.

The interpretations presented here are limited to the geographical, agricultural and pedological conditions of the study sites, however these conditions are representative for great parts of Central Europe. Therefore, not only the soil management approaches investigated, but also the knowledge about useful methods to estimate soil quality and functionality and their reliability and shortcomings, could be applicable for wider regions. As the soil physical characteristics under analysis are highly variable in space and time, a continuous extension of the available reservoir of data is highly beneficial for agricultural soil science and practice. New ideas for sustainable soil and crop management are usually developed by innovative practitioners for given conditions. However, a crucial evaluation of the success and general usability of these ideas is facilitated by the ideas and findings presented herein. Nevertheless, the potential for advances in both soil management strategies and in their evaluation methodology is large and continuous research is needed in this direction, especially as predicted future climate scenarios and demographic developments imply rising demands on soil functionality.

5 Declaration of Authorship

Core publications (discussed in chapter 4)

Weninger, T., Bodner, G., Kreiselmeier, J., Chandrasekhar, P., Julich, S., Feger, K.-H., Schwärzel, K., Schwen, A., 2018. Combination of Measurement Methods for a Wide-Range Description of Hydraulic Soil Properties. Water 10 (8), 1021.
Contribution: field and lab measurements, data analysis, modelling, manuscript design and writing, corresponding and first author

Weninger, T., Kreiselmeier, J., Chandrasekhar, P., Julich, S., Feger, K.-H., Schwärzel, K., Bodner, G., Schwen, A., 2019. Effects of tillage intensity on pore system and physical quality of silt-textured soils detected by multiple methods. Soil Research 57, 703-711.
Contribution: field and lab measurements, data analysis, manuscript design and writing, corresponding and first author

Kreiselmeier, J., Chandrasekhar, P., Weninger, T., Schwen, A., Julich, S., Feger, K.-H., Schwärzel, K., 2019. Quantification of soil pore dynamics during a winter wheat cropping cycle under different tillage treatments. Soil and Tillage Research 192, 222-232.
Contribution: synchronization of field and lab experiments, manuscript editing

Weninger, T., Filipović, V., Mešić, M., Clothier, B., Filipović, L., 2019. Estimating the extent of fire induced soil water repellency in Mediterranean environment. Geoderma 338, 187-196.
Contribution: field and lab measurements, data analysis, manuscript writing, corresponding and first author

Filipović, V., Weninger, T., Filipović, L., Schwen, A., Bristow, K.L., Zechmeister-Boltenstern, S., Leitner. S., 2018. Inverse estimation of soil hydraulic properties and water repellency following artificially induced drought stress. Journal of Hydrology and Hydromechanics 66 (2), 170-180.
Contribution: manuscript editing and partly writing, data collection

Further related publications

Bodner, G., Weninger, T., Rosner, J., Summerer, H., Schwen, A., 2019. Ertragsmöglichkeiten und bodenphysikalische Herausforderungen reduzierter Bodenbearbeitung. ALVA (Hrsg.), ALVA - Jahrestagung 2019, 59-61; ISBN: ISSN 1606-612X..
Contribution: field and lab experiments, data analysis and presentation, manuscript editing

Chandrasekhar, P., Kreiselmeier, J., Schwen, A., Weninger, T., Julich, S., Feger, K.-H., Schwärzel, K., 2018. Why We Should Include Soil Structural Dynamics of Agricultural Soils in Hydrological Models. Water 10 (12), 1862.
Contribution: literature research, data collection, manuscript editing

Chandrasekhar, P., Kreiselmeier, J., Schwen, A., Weninger, T., Julich, S., Feger, K.-H., Schwärzel, K., 2019. SporDyn: A Python code for modeling the evolution of soil pore size distribution after tillage. MethodsX 6, 2118-2126.
Contribution: data collection, control and preparation

Chandrasekhar, P., Kreiselmeier, J., Schwen, A., Weninger, T., Julich, S., Feger, K.-H., Schwärzel, K., 2019. Modeling the evolution of soil structural pore space in agricultural soils following tillage. Geoderma 353, 401-414.
Contribution: data collection and preparation, manuscript editing

Filipović, L., Mešić, M., Weninger, T., Schwen, A., Novosel, A., Maretić, M., Filipović, V., 2019. Effect of fire-induced water repellency on soil hydraulic properties and water flow. Agriculturae Conspectus Scientificus 84 (2), 143-150.
Contribution: field and lab experiments, data analysis, manuscript editing

Kreiselmeier, J., Chandrasekhar, P., Weninger, T., Schwen, A., Julich, S., Feger, K.-H., Schwärzel, K., 2020. Temporal variations of the hydraulic conductivity characteristic under conventional and conservation tillage. Geoderma 362, 114127.
Contribution: synchronization of field and lab experiments, manuscript editing

6 Acknowledgements

My special thanks go to all the colleagues at the Institute of Soil Physics and Rural Water Management and the project team from UNU and TU Dresden which supportingly took part of the work and shared some inspiring time.

Appreciated key roles for the completion of the thesis were played by Andreas Schwen and Kai Schwärzel who designed the project, raised funding and provided valuable scientific support; Gernot Bodner and Johannes Tintner as motivators and communicators of the fascination of plant and soil science; Peter Strauss, Vesna Zupanc, Lana and Vilim Filipović with their resistant belief in my scientific abilities; and many others more who will receive my thanks personally.

As most valuable part, I am thankful for all the discussions besides the everyday working routines about soil, science, roots, agriculture and many other topics which made the long time for the genesis of this thesis to a time of valuable personal formation.

7 References

Alagna, V., Bagarello, V., Di Prima, S., Iovino, M., 2016. Determining hydraulic properties of a loam soil by alternative infiltrometer techniques. Hydrological Processes 30, 263–275.

Amundson, R., Berhe, A.A., Hopmans, J.W., Olson, C., Sztein, A.E., and Sparks, D.L. 2015. Soil and human security in the 21st century. Science 348:1261071.

Armindo, R. A., Wendroth, O., 2016. Physical soil structure evaluation based on hydraulic energy functions. Soil Science Society of America Journal, 80(5), 1167–1180.

Armindo, R.A., Wendroth, O., 2019. Alternative approach to calculate soil hydraulic-energy-indices and -functions. Geoderma 355, 113903.

Asgarzadeh, H., Mosaddeghi, M.R., Dexter, A.R., Mahboubi, A.A., Neyshabouri, M.R., 2014. Determination of soil available water for plants: consistency between laboratory and field measurements. Geoderma 226–227, 8–20.

Assouline, S., Or, D., 2014. The concept of field capacity revisited: Defining intrinsic static and dynamic criteria for soil internal drainage dynamics. Water Resources Research 50 (6), 4787–4802.

Bacher, M.G., Schmidt, O., Bondi, G., Creamer, R., Fenton, O., 2019. Comparison of Soil Physical Quality Indicators Using Direct and Indirect Data Inputs Derived from a Combination of In-Situ and Ex-Situ Methods. Soil Science Society of America Journal 83, 5–17.

Batey, T., 2009. Soil compaction and soil management – a review. Soil Use and Management 25, 335–345.

Boivin, P., Garnier, P., Tessier, D., 2004. Relationship between clay content, clay type and shrinkage properties of soil samples. Soil Science Society of America Journal 68, 1145–1153.

Brunetti, G., Šimůnek, J., Bogena, H., Baatz, R., Huisman, J.A., Dahlke, H., Vereecken, H., 2019. On the Information Content of Cosmic-Ray Neutron Data in the Inverse Estimation of Soil Hydraulic Properties. Vadose Zone Journal 18 (1), 180123.

Bünemann, E.K., Bongiorno, G., Bai, Z., Creamer, R.E., De Deyn, G., de Goede, R., Fleskens, L., Geissen, V., Kuyper, T.W., Mäder, P., Pulleman, M., Sukkel, W., van Groenigen, J.W., Brussaard, L., 2018. Soil quality – A critical review. Soil Biology and Biochemistry 120, 105–125.

Cameron, K. C. and Buchan, G. D. 2006. Porosity and pore size distribution. In Lal, R. (ed.). Encyclopedia of Soil Science. CRC Press, Boca Raton, FL, USA, pp. 1350–1353.

Caputo, M.C., Nimmo, J.R., 2005. Quasi-Steady Centri-fuge Method for Unsaturated Hydraulic Properties. Water Resources Research 41, 1–5.

Castellini, M., Stellacci, A.M., Barca, E., Iovino, M., 2019. Application of Multivariate Analysis Techniques for Selecting Soil Physical Quality Indicators: A Case Study in Long-Term Field Experiments in Apulia (Southern Italy). Soil Science Society of America Journal 83 (3), 707–720.

Chandrasekhar, P., Kreiselmeier, J., Schwen, A., Weninger, T., Julich, S., Feger, K.-H., Schwärzel, K., 2018. Why We Should Include Soil Structural Dynamics of Agricultural Soils in Hydrological Models. Water 10 (12), 1862.

Chandrasekhar, P., Kreiselmeier, J., Schwen, A., Weninger, T., Julich, S., Feger, K.-H., Schwärzel, K., 2019. SporDyn: A Python code for modeling the evolution of soil pore size distribution after tillage. MethodsX 6, 2118–2126.

Chandrasekhar, P., Kreiselmeier, J., Schwen, A., Weninger, T., Julich, S., Feger, K.-H., Schwärzel, K., 2019. Modeling the evolution of soil structural pore space in agricultural soils following tillage. Geoderma 353, 401–414.

Corstanje, R., Mercer, T.G., Rickson, J.R., Deeks, L.K., Newell-Price, P., Holman, I., Kechavarsi, C., Waine, T.W., 2017. Physical soil quality indicators for monitoring British soils. Solid Earth 8, 1003-1016.

da Silva, A.P., Kay, B.D., Perfect, E., 1994. Characterization of the least limiting water range of soils. Soil Science Society of America Journal 58, 1775 – 1781.

da Silva, A.J.P., Pinheiro, E.A.R., de Jong van Lier, Q., 2020. Determination of soil hydraulic properties and its implications for mechanistic simulations and irrigation management. Irrigation Science 38 (3), 223-234.

D'Haene, K., 2012. An indicator for soil physical quality in integrated sustainability assessment models. Archives of Agronomy and Soil Science 58 (sup1), S66-S70.

Dane, J.H., Topp, G.C. (Eds.), 2002. Methods of soil analysis. Part 4: Physical Methods. SSSA Book Series No. 5. Soil Science Society of America, Madison, WI, USA.

de Jong van Lier, Q., Wendroth, O., 2016. Reexamination of the Field Capacity Concept in a Brazilian Oxisol. Soil Science Society of America Journal, 80, 264 – 274.

de Paul Obade, V., Lal, R., 2016. A standardized soil quality index for diverse field conditions. Science of the Total Environment 541, 424-434.

Dexter, A.R., 2004a. Soil physical quality. Part 1 theory, effects of soil texture, density, and organic matter, and effects on root growth. Geoderma, 120, 210 – 214.

Dexter, A.R., 2004b. Soil physical quality. Part 11. Friability, till-age, tilth and hard-setting. Geoderma 120, 215 – 225.

Dexter, A.R., 2004c. Soil physical quality: Part III: Unsaturated hydraulic conductivity and general conclusions about S-theory. Geoderma 120, 227-239.

Dexter, A.R., Czyz, E.A., 2007. Applications of S-Theory in the study of soil physical degradation and its consequences. Land Degradation and Development 18, 369-381.

Dörner, J., Dec, D., Peng, X., Horn, R., 2009. Change of shrinkage behavior of an Andisol in southern Chile: Effects of land use and wetting/drying cycles. Soil and Tillage Research 106 (1), 45-53.

Durner, W., 1994. Hydraulic conductivity estimation for soils with heterogeneous pore structure, Water Resources Research 30, 211 – 223.

Elmholt, S., Schjønning, P., Munkholm, L.J., Debosz, K., 2008. Soil management effects on aggregate stability and biological binding. Geoderma 144 (3-4), 455-467.

FAO and ITPS, 2015. Status of the World's Soil Resources (SWSR)—Main Report. Food and Agriculture Organization of the United Nations and Intergovernmental Technical Panel on Soils, Rome, Italy.

Filipović, V., Weninger, T., Filipović, L., Schwen, A., Bristow, K.L., Zechmeister-Boltenstern, S., Leitner. S., 2018. Inverse estimation of soil hydraulic properties and water repellency following artificially induced drought stress. Journal of Hydrology and Hydromechanics 66 (2), 170-180.

Filipović, L., Mešić, M., Weninger, T., Schwen, A., Novosel, A., Maretić, M., Filipović, V., 2019. Effect of fire-induced water repellency on soil hydraulic properties and water flow. Agriculturae Conspectus Scientificus 84 (2), 143-150.

Franco, H.H.S., Guimarães, R.M.L., Tormena, C.A., Cherubin, M.R., Favilla, H.S., 2019. Global applications of the Visual Evaluation of Soil Structure method:A systematic review and meta-analysis. Soil and Tillage Research 190, 61-69.

Govers, G., Merckx, R., van Wesemael, B., Van Oost, K., 2017. Soil conservation in the 21st century: why we need smart agricultural intensification. SOIL 3, 45-59.

Greenland, D.J., 1981. Soil management and soil degradation. Journal of Soil Science 32, 301 – 322.

Groenevelt, P.H., Grant, C.D., Semetsa, S., 2001. A new procedure to determine soil water availability. Australian Journal of Soil Research 39 (3), 577 – 598.

Groh, J., Stumpp, C., Lücke, A., Pütz, T., Vanderborght, J., Vereecken, H., 2018. Inverse Estimation of Soil Hydraulic and Transport Parameters of Layered Soils from Water Stable Isotope and Lysimeter Data. Vadose Zone Journal 17 (1), 170168.

Håkansson, I., Lipiec, J., 2000. A review of the usefulness of relative bulk density values in studies of soil structure and compaction. Soil and Tillage Research 53 (2), 71–85.

Han, X., Hendricks Franssen, H.-J., Jiménez Bello, M.Á., Rosolem, R., Bogena, H, Alzamora, F.M., Chanzy, A., Vereecken, H., 2016. Simulataneous soil moisture and properties estimation for a drip irrigated field by assimilating cosmic-ray neutron intensity. Journal of Hydrology 539, 611–624.

Hartge, K.-H., Horn, R., 2016. Essential Soil Physics – An introduction to soil processes, functions, structure and mechanics. 1st edition, based on the 4th, completely revised and extended German edition. Ed.: Horton, R., Horn, R., Bachmann, J., Peth, S. Schweizerbart Science Publishers, Stuttgart, Germany.

Hatfield, J.L., Sauer, T.J. (Eds.), 2011. Soil Management: Building a Stable Base for Agriculture. ASA, CSSA, and SSSA Books Series. American Society of Agronomy, Soil Science Society of America, Madison, WI, USA.

Horn, R., Lebert, M., 1994. Soil compactability and compressibility. In: Soane BD, Van Ouwerkerk C, editors. Soil compaction in crop production. Elsevier, Amsterdam, Nedtherlands, 45 – 69.

Huber, S., Prokop, G., Arrouays, D., Banko, G., Bispo, A., Jones, R.J.A., Kibblewhite, M.G., Lexer, W., Möller, A., Rickson, R.J., Shishkov, T., Stephens, M., Toth, G., Van den Akker, J.J.H., Varallyay, G., Verheijen, F.G.A., Jones, A.R., 2008. Environmental Assessment of Soil for Monitoring: Volume I Indicators & Criteria. EUR 23490 EN/1. Office for the Official Publications of the European Communities, Luxembourg, pp.339.

Iovino, M., Castellini, M., Bagarello, V., Giordano., G., 2016. Using static and dynamic indicators to evaluate soil physical quality in a sicilian area. Land Degradation and Development 27, 200–210.

Israelsen, O. W., West, F. L., 1922. Water-Holding Capacity of Irrigated Soils. UAES Bulletin No. 183.

Jadoon, K.Z., Slob, E., Vanclooster, M., Vereecken, H., Lambot, S., 2008. Uniqueness and stability analysis of hydrogeophysical inversion for time-lapse ground-penetrating radar estimates of shallow soil hydraulic properties. Water Resources Research 44 (9), W09421.

Jian, J., Lester, B.J., Du, X., Reiter, M.S., Stewart, R.D., 2020. A calculator to quantify cover crop effects on soil health and productivity. Soil and Tillage Research 199, 104575.

Johannes, A., Weisskopf, P., Schulin, R., Boivin, P., 2017. To what extent do physical measurements match with visual evaluation of soil structure? Soil and Tillage Research 173, 24–32.

Johannes, A., Weisskopf, P., Schulin, R., Boivin, P., 2019. Soil structure quality indicators and their limit values. Ecological Indicators 104, 686–694.

Kastanek, F.J., Nielsen, D.R., 2001. Description of soil water characteristics using cubic spline interpolation. Soil Science Society of America Journal 65, 279 – 283.

Kosugi, K. (1996), Log-normal distribution model for unsaturated soil hydraulic properties, Water Resources Research 32, 2697 – 2703.

Kotlar, A.M., Varvaris, I., de Jong van Lier, Q., de Jonge, L.W., Møldrup, P., Iversen, B.V., 2019. Soil Hydraulic Properties Determined by Inverse Modeling of Drip Infiltrometer Experiments Extended with Pedotransfer Functions. Vadose Zone Journal 18 (1), 1-11.

Koureh, H.K., Asgarzadeh, H., Mosaddeghi, M.R., Khodaverdiloo, H., 2020. Critical Values of Soil Physical Quality Indicators Based on Vegetative Growth Characteristics of Spring Wheat (*Triticum aestivum* L.). Journal of Soil Science and Plant Nutrition 20, 493–506.

Kreiselmeier, J., Chandrasekhar, P., Weninger, T., Schwen, A., Julich, S., Feger, K.-H., Schwärzel, K., 2019. Quantification of soil pore dynamics during a winter wheat cropping cycle under different tillage treatments. Soil and Tillage Research 192, 222-232.

Kreiselmeier, J., Chandrasekhar, P., Weninger, T., Schwen, A., Julich, S., Feger, K.-H., Schwärzel, K., 2020. Temporal variations of the hydraulic conductivity characteristic under conventional and conservation tillage. Geoderma 362, 114127.

Kumahor, S.K., De Rooij, G.H., Schlüter, S., Vogel, H.J., 2015. Water Flow and Solute Transport in Unsaturated Sand—A Comprehensive Experimental Approach. Vadose Zone Journal 14 (2), 1-9.

Leão, T.P., da Silva, A.P., Macedo, M.C.M., Imhoff, S., Euclides, V.P.B., 2006. Least limiting water range: A potential indicator of changes in near-surface soil physical quality after the conversion of Brazilian Savanna into pasture. Soil and Tillage Research 88 (1-2), 279-285.

Leão, T.P., 2017. Water retention and penetration resistance equations for the least limiting water range. Scientia Agricola 76 (2), 172-178.

León, H.N., Almeida, B.G., Almeida, C.D.G.C., Freire, F.J., Souza, E.R., Oliveira, E.C.A., Silva, E.P., 2019. Medium-term influence of conventional tillage on the physical quality of a Typic Fragiudult with hardsetting behaviour cultivated with sugarcane under rainfed conditions. Catena 175, 37-46.

Loveland, P., Webb, J., 2003. Is there a critical level of organic matter in the agricultural soil of temperate regions: a review. Soil and Tillage Research 70, 1-18.

Lozano, L.A., Soracco, C.G., Villareal, R., Ressia, J.M., Sarli, G.O., Filgueira, R.R., 2016. Soil Physical Quality and Soybean Yield as Affected by Chiseling and Subsoiling of a No-Till Soil. Revista Brasileira de Ciência do Solo, v40:e0150160.

Malengier, B., Di Emidio, G., Peiffer, H., Ciocci, M.-C., Kišon, P., 2015. Unsaturated Permeability and Retention Curve Determination From In-Flight Weight Measurements in a Bench-Scale Centrifuge. Geotechnical Testing Journal 38 (2), 243–254.

Maseyk, F.J.F., Mackay, A.D., Possingham, H.P., Dominati, E.J., Buckley, Y.M., 2017. Managing natural capital stocks for the provision of ecosystem services. Conservation Letters 10, 211–220.

Mbagwu, J.S.C., Auerswald, K., 1999. Relationship of percolation stability of soil aggregates to land use, selected properties, structural indices and simulated rainfall erosion. Soil and Tillage Research 50 (3-4), 197-206.

McKenzie, B.M., Tisdall, J.M., Vance, W.H., 2011. Soil Physical Quality. In: Gliński, J., Horabik, J., Lipiec, J. (Eds.). Encyclopedia of Agrophysics. Encyclopedia of Earth Sciences Series. Springer, Dordrecht, Netherlands.

Mengistu, A.G., Mavimbela, S.S.W., van Rensburg, L.D., 2019. Characterisation of the soil pore system in relation to its hydraulic functions in two South African soil groups. South African Journal of Plant and Soil 36 (2), 107-116.

Meyer, P.D., Gee, G.W., 1999. Flux-based estimation of field capacity. Journal of Geotechnical and Geoenvironmental Engineering 125, 595–599.

Mohanty, B.P., 2013. Soil Hydraulic Property Estimation Using Remote Sensing: A Review. Vadose Zone Journal 12 (4), 1-9.

Møldrup, P., Poulsen, T.G., Schjønning, P., Olesen, T., Yamaguchi, T., 1998. Gas permeability in undisturbed soils: measurements and predictive models. Soil Science 163 (3), 180-189.

Møldrup, P., Olesen, T., Komatsu, T., Schjønning, P., Rolston, D.E., 2001. Tortuosity, Diffusivity, and Permeability in the Soil Liquid and Gaseous Phases. Soil Science Society of America Journal 65 (3), 613-623.

Moncada, M.P., Penning, L.H., Timm, L.C., Gabriels, D., Cornelis, W.M., 2017. Visual examination of changes in soil structural quality due to land use. Soil and Tillage Research 173, 83-91.

Mualem, Y., 1976. A new model for predicting the hydraulic conductivity of unsaturated porous media. Water Resources Research, 12, 513–522.

Mueller, L., Kay, B.D., Hu, C., Li, Y., Schindler, U., Behrendt, A., Shepherd, T.G., Ball, B.C., 2009. Visual assessment of soil structure: Evaluation of methodologies on sites in Canada, China and Germany. Part I: Comparing visual methods and linking them with soil physical data and grain yield of cereals. Soil and Tillage Research 103, 178-187.

Müller, K., Carrick, S., Meenken, E., Clemens, G., Hunter, D., Rhodes, P., Thomas, S., 2016. Is subcritical water repellency an issue for efficient irrigation in arable soils? Soil and Tillage Research 161, 53–62.

Nciizah, A.D., Wakindiki, I.I.C., 2015. Physical indicators of soil erosion, aggregate stability and erodibility. Archives of Agronomy and Soil Science 61 (6), 827-842.

Nemes, A., Pachepsky, Y.A., Timlin, D.J., 2011. Toward improving global estimates of field soil water capacity. Soil Science Society of America Journal, 75, 807–812.

Nortcliff, S., 2001. Standardization of soil quality attributes. Agriculture, Ecosystems and Environment 88 (2), 161-168.

Omuto, C.T., 2009. Biexponential model for water retention characteristics. Geoderma 149, 235-242.

Othmer, H., Diekkrüger, B., Kutilek, M., 1991. Bimodal porosity and unsaturated hydraulic conductivity. Soil Science 152, 139–150.

Page, K.L., Dang, Y.P., Dalal, R.C., 2020. The Ability of Conservation Agriculture to Conserve Soil Organic Carbon and the Subsequent Impact on Soil Physical, Chemical, and Biological Properties and Yield. Frontiers in Sustainable Food Systems 4, 31.

Pan, X., Jaumann, S., Zhang, J., Roth, K., 2019. Efficient estimation of effective hydraulic properties of stratal undulating surface layer using time-lapse multi-channel GPR. Hydrology and Earth System Sciences 23, 3653-3663.

Peters, A., Durner, W., 2008. Simplified evaporation method for determining soil hydraulic properties. Journal of Hydrology 356, 147–162.

Peters, A., 2013. Simple consistent models for water retention and hydraulic conductivity in the complete moisture range. Water Resources Research 49, 6765-6780.

Pimentel, D., 2006. Soil erosion: A food and environmental threat. Environment, Development and Sustainability 8 (1), 119-137.

Pulido-Moncada, M., Munkholm, L.J., 2019. Limiting Water Range: A Case Study for Compacted Subsoils. Soil Science Society of America Journal 83, 982-992.

Reynolds, W.D., Drury, C.F., Yang, X.M., Tan, C.S., 2008. Optimal soil physical quality inferred through structural regression and parameter interactions. Geoderma 146, 466–474.

Reynolds, W.D., Drury, C.F., Tan,C.S., Fox, C.A., Yang, X.M., 2009. Use of indicators and pore volume-function characteristics to quantify soil physical quality. Geoderma 152, 252–263.

Reynolds, W.D., 2017. Use of bimodal hydraulic property relationships to characterize soil physical quality. Geoderma 294, 38-49.

Reynolds, W.D., 2018. An analytic description of field capacity and its application in crop production. Geoderma 326, 56-67.

Romano, N., Nasta, P., Severino, G., Hopmans, J.W., 2011. Using bimodal log-normal functions to describe soil hydraulic properties. Soil Science Society of America Journal 75, 468–480.

Romano, N., Nasta, P., 2016. How effective is bimodal soil hydraulic characterization? Functional evaluations for predictions of soil water balance. European Journal of Soil Science 67, 523-535.

Schwen, A., Jeitler, E., Böttcher, J., 2015. Spatial and temporal variability of soil gas diffusivity, its scaling and relevance for soil respiration under different tillage. Geoderma 259-260, 323-336.

Shepherd, T. G., 2009. Visual Soil Assessment. Volume 1. Field Guide for Pastoral Grazing and Cropping on Flat to Rolling Country, 2nd edition. Horizons Regional Council, Palmerston North, New Zealand.

Siltecho, S., Hammecker, C., Sriboonlue, V., Clermont-Dauphin, C., Trelo-ges, V., Antonino, A.C.D., Angulo-Jaramillo, R., 2015. Use of field and laboratory methods for estimating unsaturated hydraulic properties under different land uses. Hydrology and Earth System Sciences 19, 1193-1207.

Spaccini, R., Piccolo, A., 2013. Effects of field managements for soil organic matter stabilization on water-stable aggregate distribution and aggregate stability in three agricultural soils. Jounal of Geochemical Exploration 129, 45-51.

Spake, R., Bellamy, C., Graham L.J., Watts, K., Wilson, T., Norton, L.R., Wood C.M., Schmucki, R., Bullock, J.M., Eigenbrod, F., 2019. An analytical framework for spatially targeted management of natural capital. Nature sustainability 2 (2), 90-97.

Sprenger, M., Volkmann, T.H.M., Blume, T., Weiler, M., 2015. Estimating flow and transport parameters in the unsaturated zone with pore water stable isotopes. Hydrology and Earth System Sciences, 19, 2617–2635.

Steffen, W., Richardson, K., Rockström, J., Cornell, S.E., Fetzer, I., Bennett, E.M., Biggs, R., Carpenter, S.R., De Vries, W., De Wit, C.A., Folke, C., Gerten, D., Heinke, J., Mace, G.M., Persson, L.M., Ramanathan, V., Reyers, B., Sörlin, S., 2015. Planetary boundaries: Guiding human development on a changing planet. Science 347 (6223), 1259855.

Tuller, M., Or, D., 2005. Water Retention and Characteristic Curve. In: Hillel, D. (Ed.). Encyclopedia of Soils in the Environment. Elsevier, Oxford, UK and St. Lous, MO, USA, p. 278-289.

Turek, M.E., Armindo, R.A., Wendroth, O., Dos Santos, I., 2019. Criteria for the estimation of field capacity and their implications for the bucket type model. European Journal of Soil Science 70, 278-290.

Twarakavi, N.K.C., Sakai, M., Šimůnek, J., 2009. An objective analysis of the dynamic nature of field capacity. Water Resources Research 45, W10410.

van Genuchten, M.T., 1980. A closed-form equation for predicting the hydraulic conductivity of unsaturated soils, Soil Science Society of America Journal, 44, 892 – 898.

Veihmeyer, F.J., Hendrickson, A.H., 1931. The moisture equivalent as a measure of the field capacity of soils. Soil Science 32, 181–193.

Wackernagel, M., Schulz, N.B., Deumling, D., Linares, A.C., Jenkins, M., Kapos, V., Monfreda, C., Loh, J., Myers, N., Norgaard, R.B., Randers, J., 2002. Tracking the ecological overshoot of the human economy. Proceedings of the National Academy of Sciences of the United States of America, 99, 9266–9271.

Weninger, T., Bodner, G., Kreiselmeier, J., Chandrasekhar, P., Julich, S., Feger, K.-H., Schwärzel, K., Schwen, A., 2018. Combination of Measurement Methods for a Wide-Range Description of Hydraulic Soil Properties. Water 10, 1021.

Weninger, T., Kreiselmeier, J., Chandrasekhar, P., Julich, S., Feger, K.-H., Schwärzel, K., Bodner, G., Schwen, A., 2019a. Effects of tillage intensity on pore system and physical quality of silt-textured soils detected by multiple methods. Soil Research 57, 703–711.

Weninger, T., Filipović, V., Mešić, M., Clothier, B., Filipović, L., 2019b. Estimating the extent of fire induced soil water repellency in Mediterranean environment. Geoderma 338, 187–196.

Wilson, G.V., Zhang, T., Wells, R.R., Liu, B., 2020. Consolidation effects on relationships among soil erosion properties and soil physical quality indicators. Soil and Tillage Research 198, 104550.

Zacharias, S., Bohne, K., 2008. Attempt of a flux-based evaluation of field capacity. Journal of Plant Nutrition and Soil Science 171, 399–408.

Appendix

A: Reference list for review in 2.2

Anghinoni, G., Tormena, C. A., Lal, R., Moreira, W. H., Júnior, E. B., & Ferreira, C. J. B. (2017). Within cropping season changes in soil physical properties under no-till in southern brazil. Soil and Tillage Research, 166, 108-112. doi:10.1016/j.still.2016.10.015

Anghinoni, G., Tormena, C. A., Lal, R., Zancanaro, L., & Kappes, C. (2019). Enhancing soil physical quality and cotton yields through diversification of agricultural practices in central brazil. Land Degradation and Development, 30(7), 788-798. doi:10.1002/ldr.3267

Are, K. S., Adelana, A. O., Fademi, I. O., & Aina, O. A. (2017). Improving physical properties of degraded soil: Potential of poultry manure and biochar. Agriculture and Natural Resources, 51(6), 454-462. doi:10.1016/j.anres.2018.03.009

Armindo, R. A., & Wendroth, O. (2016). Physical soil structure evaluation based on hydraulic energy functions. Soil Science Society of America Journal, 80(5), 1167-1180. doi:10.2136/sssaj2016.03.0058

Auler, A. C., Miara, S., Pires, L. F., da Fonseca, A. F., & Barth, G. (2014). Soil physico-hydrical properties resulting from the management in integrated production systems. Revista Ciencia Agronomica, 45(5), 976-989. Retrieved from www.scopus.com

Babalola, O. A., Adesodun, J. K., Olasantan, F. O., & Adekunle, A. F. (2012). Responses of some soil biological, chemical and physical properties to short-term compost amendment. International Journal of Soil Science, 7(1), 28-38. doi:10.3923/ijss.2012.28.38

Bacher, M. G., Schmidt, O., Bondi, G., Creamer, R., & Fenton, O. (2019). Comparison of soil physical quality indicators using direct and indirect data inputs derived from a combination of in-situ and ex-situ methods. Soil Science Society of America Journal, 83(1), 5-17. doi:10.2136/sssaj2018.06.0218

Bamberg, A. L., Cornelis, W. M., Timm, L. C., Gabriels, D., Pauletto, E. A., & Pinto, L. F. S. (2011). Temporal changes of soil physical and hydraulic properties in strawberry fields. Soil use and Management, 27(3), 385-394. doi:10.1111/j.1475-2743.2011.00355.x

Bergamin, A. C., Vitorino, A. C. T., Souza, F. R., Venturoso, L. R., Bergamin, L. P. P., & Campos, M. C. C. (2015). Relationship of soil physical quality parameters and maize yield in a brazilian oxisol. Chilean Journal of Agricultural Research, 75(3), 357-365. doi:10.4067/S0718-58392015000400013

Bhaduri, D., Purakayastha, T. J., Chakraborty, D., Chakraborty, K., & Singh, M. (2018). Integrated tillage-water-nutrient management effects on selected soil physical properties in a rice-wheat system in the indian subcontinent. Archives of Agronomy and Soil Science, 64(1), 132-145. doi:10.1080/03650340.2017.1332407

Blum, J., Giarola, N. F. B., da Silva, A. P., Filho, O. G., Silva, S. G. C., Eberhardt, D. N., & Araújo, S. R. (2014). Assessment of soil physical attributes at sowing row and inter-row under no-till system. Revista Ciencia Agronomica, 45(5), 888-895. Retrieved from www.scopus.com

Castellini, M., Niedda, M., Pirastru, M., & Ventrella, D. (2014). Temporal changes of soil physical quality under two residue management systems. Soil use and Management, 30(3), 423-434. doi:10.1111/sum.12137

Castellini, M., Pirastru, M., Niedda, M., & Ventrella, D. (2013). Comparing physical quality of tilled and no-tilled soils in an almond orchard in southern italy. Italian Journal of Agronomy, 8(3), 149-157. doi:10.4081/ija.2013.e20

Castellini, M., Stellacci, A. M., Barca, E., & Iovino, M. (2019). Application of Multivariate Analysis Techniques for Selecting Soil Physical Quality Indicators: A Case Study in Long-Term Field Experiments in Apulia (Southern Italy). Soil Science Society of America Journal, 83(3), 707-720. doi:10.2136/sssaj2018.06.0223

Castioni, G. A., Cherubin, M. R., Menandro, L. M. S., Sanches, G. M., Bordonal, R. D. O., Barbosa, L. C., . . . Carvalho, J. L. N. (2018). Soil physical quality response to sugarcane straw removal in brazil: A multi-approach assessment. Soil and Tillage Research, 184, 301-309. doi:10.1016/j.still.2018.08.007

Cavalcanti, R. Q., Rolim, M. M., de Lima, R. P., Tavares, U. E., Pedrosa, E. M. R., & Cherubin, M. R. (2020). Soil physical changes induced by sugarcane cultivation in the atlantic forest biome, northeastern brazil. Geoderma, 370 doi:10.1016/j.geoderma.2020.114353

Chatterjee, S., Bandyopadhyay, K. K., Pradhan, S., Singh, R., & Datta, S. P. (2016). Influence of irrigation, crop residue mulch and nitrogen management practices on soil physical quality. Journal of the Indian Society of Soil Science, 64(4), 351-367. doi:10.5958/0974-0228.2016.00048.7

Chen, X. W., Liang, A. Z., Jia, S. X., Zhang, X. P., & Wei, S. C. (2014). Impact of tillage on physical characteristics in a mollisol of northeast china. Plant, Soil and Environment, 60(7), 309-313. Retrieved from www.scopus.com

Cherubin, M. R., Chavarro-Bermeo, J. P., & Silva-Olaya, A. M. (2019). Agroforestry systems improve soil physical quality in northwestern colombian amazon. Agroforestry Systems, 93(5), 1741-1753. doi:10.1007/s10457-018-0282-y

Cherubin, M. R., Karlen, D. L., Franco, A. L. C., Tormena, C. A., Cerri, C. E. P., Davies, C. A., & Cerri, C. C. (2016). Soil physical quality response to sugarcane expansion in brazil. Geoderma, 267, 156-168. doi:10.1016/j.geoderma.2016.01.004

Corstanje, R., Mercer, T. G., Rickson, J. R., Deeks, L. K., Newell-Price, P., Holman, I., . . . Waine, T. W. (2017). Physical soil quality indicators for monitoring british soils. Solid Earth, 8(5), 1003-1016. doi:10.5194/se-8-1003-2017

Costa, J. L., Aparicio, V., & Cerdà, A. (2015). Soil physical quality changes under different management systems after 10 years in the argentine humid pampa. Solid Earth, 6(1), 361-371. doi:10.5194/se-6-361-2015

Crittenden, S. J., & de Goede, R. G. M. (2016). Integrating soil physical and biological properties in contrasting tillage systems in organic and conventional farming. European Journal of Soil Biology, 77, 26-33. doi:10.1016/j.ejsobi.2016.09.003

Crittenden, S. J., Poot, N., Heinen, M., van Balen, D. J. M., & Pulleman, M. M. (2015). Soil physical quality in contrasting tillage systems in organic and conventional farming. Soil and Tillage Research, 154, 136-144. doi:10.1016/j.still.2015.06.018

D'Haene, K. (2012). An indicator for soil physical quality in integrated sustainability assessment models. Archives of Agronomy and Soil Science, 58(SUPPL.), S66-S70. doi:10.1080/03650340.2012.693602

de Almeida, C. X., Jorge, R. F., Centurion, J. F., Borges, E. N., Rossetti, K. V., & Pereira, F. S. (2014). Physical quality of an oxisol under no-tillage and conventional tillage. [Qualidade física de um latossolo vermelho, sob sistema de semeadura direta e cultivo convencional] Bioscience Journal, 30(5), 1395-1411. Retrieved from www.scopus.com

De Melo, M. L. A., Guimarães, E. V., Silva, B. M., Da Costa, E. L., & Caixeta, S. P. (2017). Soil physical quality after nitrogen fertilizers use in irrigated pasture of tifton 85. Scientia Agraria, 18(4), 194-203. doi:10.5380/rsa.v18i4.53207

DI PRIMA, S., RODRIGO-COMINO, J., NOVARA, A., IOVINO, M., PIRASTRU, M., KEESSTRA, S., & CERDÀ, A. (2018). Soil physical quality of citrus orchards under tillage, herbicide, and organic managements. Pedosphere, 28(3), 463-477. doi:10.1016/S1002-0160(18)60025-6

Dörner, J., Zúñiga, F., & López, I. (2013). Short-term effects of different pasture improvement treatments on the physical quality of an andisol. Journal of Soil Science and Plant Nutrition, 13(2), 381-399. doi:10.4067/S0718-95162013005000031

dos Reis, A. M. H., Armindo, R., & Pires, L. (2019). Physical assessment of a haplohumox soil under integrated crop-livestock system. Soil and Tillage Research, 194 doi:10.1016/j.still.2019.104294

Emami, H., Neyshabouri, M. R., & Shorafa, M. (2012). Relationships between some soil quality indicators in different agricultural soils from varamin, iran. Journal of Agricultural Science and Technology, 14(4), 951-959. Retrieved from www.scopus.com

Fernández, R., Frasier, I., Noellemeyer, E., & Quiroga, A. (2017). Soil quality and productivity under zero tillage and grazing on mollisols in argentina – A long-term study. Geoderma Regional, 11, 44-52. doi:10.1016/j.geodrs.2017.09.002

Filho, O. J. V., de Souza, Z. M., de Souza, G. S., da Silva, R. B., Torres, J. L. R., de Lima, M. E., & Tavares, R. L. M. (2017). Physical attributes and limiting water range as soil quality indicators after mechanical harvesting of sugarcane. Australian Journal of Crop Science, 11(2), 169-176. doi:10.21475/ajcs.17.11.02.p215

Garba, M., Logah, V., Wildemeersch, J., Mahaman, S., Yadji, G., Quansah, C., . . . Abaidoo, R. C. (2016). Improvement in physical quality of a sahelian arenosol and implications on millet yield. Archives of Agronomy and Soil Science, 62(7), 947-962. doi:10.1080/03650340.2015.1104414

Guenette, K. G., Hernandez-Ramirez, G., Gamache, P., Andreiuk, R., & Fausak, L. (2019). Soil structure dynamics in annual croplands under controlled traffic management. Canadian Journal of Soil Science, 99(2), 146-160. doi:10.1139/cjss-2018-0117

Guimarães, R. M. L., Ball, B. C., Tormena, C. A., Giarola, N. F. B., & da Silva, T. P. (2013). Relating visual evaluation of soil structure to other physical properties in soils of contrasting texture and management. Soil and Tillage Research, 127, 92-99. doi:10.1016/j.still.2012.01.020

Hamidi Nehrani, S., Askari, M. S., Saadat, S., Delavar, M. A., Taheri, M., & Holden, N. M. (2020). Quantification of soil quality under semi-arid agriculture in the northwest of iran. Ecological Indicators, 108 doi:10.1016/j.ecolind.2019.105770

Harasim, E., Antonkiewicz, J., & Kwiatkowski, C. A. (2020). The effects of catch crops and tillage systems on selected physical properties and enzymatic activity of loess soil in a spring wheat monoculture. Agronomy, 10(3) doi:10.3390/agronomy10030334

Herencia, J. F., García-Galavís, P. A., & Maqueda, C. (2011). Long-term effect of organic and mineral fertilization on soil physical properties under greenhouse and outdoor management practices. Pedosphere, 21(4), 443-453. doi:10.1016/S1002-0160(11)60146-X

Hu, W., Tabley, F., Beare, M., Tregurtha, C., Gillespie, R., Qiu, W., & Gosden, P. (2018). Short-term dynamics of soil physical properties as affected by compaction and tillage in a silt loam soil. Vadose Zone Journal, 17(1) doi:10.2136/vzj2018.02.0041

Iqbal, M., van Es, H. M., Anwar-ul-Hassan, Schindelbeck, R. R., & Moebius-Clune, B. N. (2014). Soil health indicators as affected by long-term application of farm manure and cropping patterns under semi-arid climates. International Journal of Agriculture and Biology, 16(2), 242-250. Retrieved from www.scopus.com

Jat, M. L., Gathala, M. K., Saharawat, Y. S., Tetarwal, J. P., Gupta, R., & Yadvinder-Singh. (2013). Double no-till and permanent raised beds in maize-wheat rotation of north-western indo-gangetic plains of india: Effects on crop yields, water productivity, profitability and soil physical properties. Field Crops Research, 149, 291-299. doi:10.1016/j.fcr.2013.04.024

Jin, V. L., Potter, K. N., Johnson, M. -. V., Harmel, R. D., & Arnold, J. G. (2015). Surface-applied biosolids enhance soil organic carbon and nitrogen stocks but have contrasting effects on soil physical quality. Applied and Environmental Soil Science, 2015 doi:10.1155/2015/715916

Jirků, V., Kodešová, R., Nikodem, A., Mühlhanselová, M., & Žigová, A. (2013). Temporal variability of structure and hydraulic properties of topsoil of three soil types. Geoderma, 204-205, 43-58. doi:10.1016/j.geoderma.2013.03.024

Kahlon, M. S., Lal, R., & Ann-Varughese, M. (2013). Twenty two years of tillage and mulching impacts on soil physical characteristics and carbon sequestration in central ohio. Soil and Tillage Research, 126, 151-158. doi:10.1016/j.still.2012.08.001

León, H. N., Almeida, B. G., Almeida, C. D. G. C., Freire, F. J., Souza, E. R., Oliveira, E. C. A., & Silva, E. P. (2019). Medium-term influence of conventional tillage on the physical quality of a typic fragiudult with hardsetting behavior cultivated with sugarcane under rainfed conditions. Catena, 175, 37-46. doi:10.1016/j.catena.2018.12.005

Li, L., Chan, K. Y., Niu, Y., Li, G., Oates, A., Dexter, A., & Huang, G. (2011). Soil physical qualities in an oxic paleustalf under different tillage and stubble management practices and application of S theory. Soil and Tillage Research, 113(2), 82-88. doi:10.1016/j.still.2011.02.007

Lozano, L. A., Soracco, C. G., Villarreal, R., Ressia, J. M., Sarli, G. O., & Filgueira, R. R. (2016). Soil physical quality and soybean yield as affected by chiseling and subsoiling of a no-till soil. Revista Brasileira De Ciencia do Solo, 40 doi:10.1590/18069657rbcs20150160

Martinkoski, L., Vogel, G. F., Jadoski, S. O., & Watzlawick, L. F. (2017). Soil physical quality under silvopastoral management and secondary forest. [Qualidade física do solo sob manejo silvipastoril e floresta secundária] Floresta e Ambiente, 24 doi:10.1590/2179-8087.028216

Mirko, C., Maria, S. A., Matteo, T., & Emanuele, B. (2019). Spatial variability of soil physical and hydraulic properties in a durum wheat field: An assessment by the BEST-procedure. Water (Switzerland), 11(7) doi:10.3390/w11071434

Moreira, W. H., Tormena, C. A., Karlen, D. L., Silva, Á. P. D., Keller, T., & Betioli, E. (2016). Seasonal changes in soil physical properties under long-term no-tillage. Soil and Tillage Research, 160, 53-64. doi:10.1016/j.still.2016.02.007

Mota, J. C. A., Alves, C. V. O., Freire, A. G., & de Assis Júnior, R. N. (2014). Uni and multivariate analyses of soil physical quality indicators of a cambisol from apodi plateau - CE, brazil. Soil and Tillage Research, 140, 66-73. doi:10.1016/j.still.2014.02.004

Nascimento, D. M. D., Cavalieri-Polizeli, K. M. V., Silva, A. H. D., Favaretto, N., & Parron, L. M. (2019). Soil physical quality under long-term integrated agricultural production systems. Soil and Tillage Research, 186, 292-299. doi:10.1016/j.still.2018.08.016

Nouri, A., Lee, J., Yin, X., Tyler, D. D., & Saxton, A. M. (2019). Thirty-four years of no-tillage and cover crops improve soil quality and increase cotton yield in alfisols, southeastern USA. Geoderma, 337, 998-1008. doi:10.1016/j.geoderma.2018.10.016

Oliveira, F. C. C., Ferreira, G. W. D., Souza, J. L. S., Vieira, M. E. O., & Pedrotti, A. (2020). Soil physical properties and soil organic carbon content in northeast brazil: Long-term. Scientia Agricola, 77(4) doi:10.1590/1678-992x-2018-0166

Ordóñez, I., López, I. F., Kemp, P. D., Descalzi, C. A., Horn, R., Zúñiga, F., . . . Dörner, J. (2018). Effect of pasture improvement managements on physical properties and water content dynamics of a volcanic ash soil in southern chile. Soil and Tillage Research, 178, 55-64. doi:10.1016/j.still.2017.11.013

Ortiz, P. F. S., Rolim, M. M., de Lima, J. L. P., Pedrosa, E. M. R., Dantas, M. S. M., & Tavares, U. E. (2017). Physical qualities of an ultisol under sugarcane and atlantic forest in brazil. Geoderma Regional, 11, 62-70. doi:10.1016/j.geodrs.2017.10.001

Papadopoulos, A., Bird, N. R. A., Whitmore, A. P., & Mooney, S. J. (2014). Does organic management lead to enhanced soil physical quality? Geoderma, 213, 435-443. doi:10.1016/j.geoderma.2013.08.033

Pereira, V. P., Ortiz-Escobar, M. E., Rocha, G. C., Assis Jr., R. N. A., & Oliveira, T. S. (2012). Evaluation of soil physical quality of irrigated agroecosystems in a semi-arid region of north-eastern brazil. Soil Research, 50(6), 455-464. doi:10.1071/SR12083

Rabbi, S. M. F., Roy, B. R., Miah, M. M., Amin, M. S., & Khandakar, T. (2014). Spatial variability of physical soil quality index of an agricultural field. Applied and Environmental Soil Science, 2014 doi:10.1155/2014/379012

Reichert, J. M., Rodrigues, M. F., Bervald, C. M. P., & Kato, O. R. (2016). Fire-free fallow management by mechanized chopping of biomass for sustainable agriculture in eastern amazon: Effects on soil compactness, porosity, and water retention and availability. Land Degradation and Development, 27(5), 1403-1412. doi:10.1002/ldr.2395

Reis, D. A., de Lima, C. L. R., & Bamberg, A. L. (2019). Developing a soil physical quality index (SPQi) for lowlands under different deployment times of no-tillage. Scientia Agricola, 76(2), 157-164. doi:10.1590/1678-992x-2017-0196

Reynolds, W. D., Drury, C. F., Tan, C. S., & Yang, X. M. (2015). Temporal effects of food waste compost on soil physical quality and productivity. [Effets temporels d'un compost de résidus d'aliments sur la qualité physique et la productivité du sol] Canadian Journal of Soil Science, 95(3), 251-268. doi:10.4141/CJSS-2014-114

Reynolds, W. D., Drury, C. F., Yang, X. M., Tan, C. S., & Yang, J. Y. (2014). Impacts of 48 years of consistent cropping, fertilization and land management on the physical quality of a clay loam soil. Canadian Journal of Soil Science, 94(3), 403-419. doi:10.4141/CJSS2013-097

Rodrigues Torres, J. L., e Silva, V. R., de Assis, R. L., de Souza, Z. M., da Silva Vieira, D. M., & Tamburús, A. Y. (2016). Soil physical quality after the fifth and sixth harvest of sugarcane in brazilian cerrado. Australian Journal of Crop Science, 10(9), 1306-1311. doi:10.21475/ajcs.2016.10.09.p7776

Rücknagel, J., Rademacher, A., Götze, P., Hofmann, B., & Christen, O. (2017). Uniaxial compression behaviour and soil physical quality of topsoils under conventional and conservation tillage. Geoderma, 286, 1-7. doi:10.1016/j.geoderma.2016.10.015

Sağlam, M., Selvi, K. Ç., Dengiz, O., & Gürsoy, F. E. (2015). Affects of different tillage managements on soil physical quality in a clayey soil. Environmental Monitoring and Assessment, 187(1) doi:10.1007/s10661-014-4185-8

Santi, A. L., Amado, T. J. C., Cherubin, M. R., Martin, T. N., Pires, J. L., Flora, L. P. D., & Basso, C. J. (2012). Principal component analysis of soil chemical and physical attributes limiting grain yield. [Análise de componentes principais de atributos químicos e físicos do solo limitantes á produtividade de graos] Pesquisa Agropecuaria Brasileira, 47(9), 1346-1357. doi:10.1590/S0100-204X2012000900020

Schossler, T. R., Marchão, R. L., Dos Santos, I. L., Santos, D. P., Nóbrega, J. C. A., & Santos, G. G. (2018). Soil physical quality in agricultural systems on the cerrado of piauí state, brazil. Anais Da Academia Brasileira De Ciencias, 90(4), 3975-3989. doi:10.1590/0001-3765201820180681

Silva, G. L., Lima, H. V., Campanha, M. M., Gilkes, R. J., & Oliveira, T. S. (2011). Soil physical quality of luvisols under agroforestry, natural vegetation and conventional crop management systems in the brazilian semi-arid region. Geoderma, 167-168, 61-70. doi:10.1016/j.geoderma.2011.09.009

Singh, M. J., Khera, K. L., & Santra, P. (2012). Selection of soil physical quality indicators in relation to soil erodibility. Archives of Agronomy and Soil Science, 58(6), 657-672. doi:10.1080/03650340.2010.537324

Soracco, C. G., Lozano, L. A., Villarreal, R., Melani, E., & Sarli, G. O. (2018). Temporal variation of soil physical quality under conventional and no-till systems. Revista Brasileira De Ciencia do Solo, 42 doi:10.1590/18069657rbcs20170408

Stavi, I., & Lal, R. (2011). Variability of soil physical quality in uneroded, eroded, and depositional cropland sites. Geomorphology, 125(1), 85-91. doi:10.1016/j.geomorph.2010.09.006

Stone, L. F., Didonet, A. D., Alcântara, F., & Ferreira, E. P. B. (2015). Physical quality of an acric red latosol under agroforestry systems. [Qualidade física de um Latossolo Vermelho ácrico sob sistemas silviagrícolas] Revista Brasileira De Engenharia Agricola e Ambiental, 19(10), 953-960. doi:10.1590/1807-1929/agriambi.v19n10p953-960

Tran Ba, L., Le Van, K., Van Elsacker, S., & Cornelis, W. M. (2016). Effect of cropping system on physical properties of clay soil under intensive rice cultivation. Land Degradation and Development, 27(4), 973-982. doi:10.1002/ldr.2321

Tuzzin de Moraes, M., Debiasi, H., Carlesso, R., Cezar Franchini, J., Rodrigues da Silva, V., & Bonini da Luz, F. (2016). Soil physical quality on tillage and cropping systems after two decades in the subtropical region of brazil. Soil and Tillage Research, 155, 351-362. doi:10.1016/j.still.2015.07.015

Valle, S. R., Dörner, J., Zúñiga, F., & Dec, D. (2018). Seasonal dynamics of the physical quality of volcanic ash soils under different land uses in southern chile. Soil and Tillage Research, 182, 25-34. doi:10.1016/j.still.2018.04.018

Verhulst, N., Kienle, F., Sayre, K. D., Deckers, J., Raes, D., Limon-Ortega, A., . . . Govaerts, B. (2011). Soil quality as affected by tillage-residue management in a wheat-maize irrigated bed planting system. Plant and Soil, 340(1), 453-466. doi:10.1007/s11104-010-0618-5

Veum, K. S., Goyne, K. W., Kremer, R. J., Miles, R. J., & Sudduth, K. A. (2014). Biological indicators of soil quality and soil organic matter characteristics in an agricultural management continuum. Biogeochemistry, 117(1), 81-99. doi:10.1007/s10533-013-9868-7

Watanabe, R., Tormena, C. A., Guimarães, M. F., Tavares Filho, J., Ralisch, R., Franchini, J., & Debiasi, H. (2018). Is structural quality as assessed by the "profil cultural" method related to quantitative indicators of soil physical quality? Revista Brasileira De Ciencia do Solo, 42 doi:10.1590/18069657rbcs20160393

Weninger, T., Kreiselmeier, J., Chandrasekhar, P., Julich, S., Feger, K. -., Schwärzel, K., . . . Schwen, A. (2019). Effects of tillage intensity on pore system and physical quality of silt-textured soils detected by multiple methods. Soil Research, 57(7), 703-711. doi:10.1071/SR18347

Williams, D. M., Blanco-Canqui, H., Francis, C. A., & Galusha, T. D. (2017). Organic farming and soil physical properties: An assessment after 40 years. Agronomy Journal, 109(2), 600-609. doi:10.2134/agronj2016.06.0372

Wilson, G. V., Zhang, T., Wells, R. R., & Liu, B. (2020). Consolidation effects on relationships among soil erosion properties and soil physical quality indicators. Soil and Tillage Research, 198 doi:10.1016/j.still.2019.104550

Zong, Y., & Lu, S. (2020). Does long-term inorganic and organic fertilization affect soil structural and mechanical physical quality of paddy soil? Archives of Agronomy and Soil Science, 66(5), 625-637. doi:10.1080/03650340.2019.1630823

Zúñiga, F., Ivelic-Sáez, J., López, I., Huygens, D., & Dörner, F. J. (2015). Temporal dynamics of the physical quality of an andisol under a grazing system subjected to different pasture improvement strategies. Soil and Tillage Research, 145, 233-241. doi:10.1016/j.still.2014.09.014

B: peer reviewed publications, full text

water

MDPI

Article

Combination of Measurement Methods for a Wide-Range Description of Hydraulic Soil Properties

Thomas Weninger [1,*], Gernot Bodner [2], Janis Kreiselmeier [3,4], Parvathy Chandrasekhar [3,4], Stefan Julich [4], Karl-Heinz Feger [4], Kai Schwärzel [3] and Andreas Schwen [1]

1 Institute of Hydraulics and Rural Water Management, University of Natural Resources and Life Sciences, Muthgasse 18, 1190 Vienna, Austria; andreas.schwen@boku.ac.at
2 Division of Agronomy, Department of Crop Sciences, University of Natural Resources and Life Sciences, Vienna, Konrad Lorenz-Straße 24, 3430 Tulln, Austria; gernot.bodner@boku.ac.at
3 Institute for Integrated Management of Material Fluxes and of Resources (UNU-FLORES), United Nations University, 01067 Dresden, Germany; kreiselmeier@unu.edu (J.K.); chandrasekhar@unu.edu (P.C.); schwaerzel@unu.edu (K.S.)
4 Institute of Soil Science and Site Ecology, Faculty of Environmental Sciences, TU Dresden, 01737 Tharandt, Germany; stefan.julich@tu-dresden.de (S.J.); karl-heinz.feger@tu-dresden.de (K.-H.F.)
* Correspondence: thomas.weninger@boku.ac.at; Tel.: +43-1-47654-81513

Received: 25 June 2018; Accepted: 30 July 2018; Published: 2 August 2018

check for updates

Abstract: Established measurement methods for hydraulic soil properties cover a limited soil moisture range. Simulations of soil water dynamics based on such observations are therefore rarely representative for all conditions from saturation to drought. Recent technical developments facilitate efficient and cheap collecting of soil water characteristics data, but the quantitative benefit of extended measurement campaigns has not been adequately tested yet. In this study, a combination of four methods to measure water retention and hydraulic conductivity at different moisture ranges was applied. Evaporation method, dewpoint psychrometry, hood infiltrometer experiments, and falling head method for saturated conductivity were conducted at two experimental sites in eastern Austria. Effects of including the particular methods in the measurement strategy were examined by visual evaluation and a 1D-modelling sensitivity study including drainage, infiltration and drought conditions. The evaporation method was considered essential due to its broad measurement range both for water retention and hydraulic conductivity. In addition to that, the highest effect on simulated water balance components was induced by the inclusion of separate conductivity measurements near saturation. Water content after three days of drainage was 15 percent higher and the transpiration rate in a drought period was 22 percent higher without near-saturated conductivity measurements. Based on relative comparisons between different combinations, we suggested combining evaporation method and hood infiltrometer experiments as the basis for representative predictions of soil water dynamics.

Keywords: hydraulic soil properties; soil water simulations; measurement method evaluation; functional evaluation

1. Introduction

Numerical simulations of soil water dynamics are supposed to comprise a wide range of soil moisture conditions; matching simulation data with reality is a fundamental issue of soil science [1,2]. The components which control a model's ability to represent reality over the full moisture range are the hydraulic soil properties (HSP). In most modelling applications, HSP are formalized in two mathematical functions: (i) the water retention function $\theta(h)$, the relation of volumetric soil water content θ and soil water head h; and (ii) the hydraulic conductivity function $K(h)$, where K is the hydraulic conductivity of soil [1,3]. These functions are defined by parameters which may be derived indirectly by empirical pedotransfer functions (PTF) [4,5] or from direct measurements of $\theta(h)$ and $K(h)$ [6].

In contrast to PTF, direct measurements of HSP allow for site-specific capture of soil physical characteristics with high spatial and temporal resolution. Most of the established direct measurement methods yield data only for the retention function or for a limited range of soil moisture [7,8]. Furthermore, HSP-parameters are often obtained from fits to the retention curve and the corresponding conductivity curve is scaled by a single measured value, the saturated conductivity (e.g., [9]). Consequently, shape information of $K(h)$ is neglected. Extensive overviews of options to determine HSP were presented before [6]. One of the most established methods is a multi-step outflow experiment, where a sequence of positive pressure values is applied to a soil sample and water content and outflow is recorded. Depending on the actual setup, measurements near saturation (h = 0 to -10 cm) and at dry conditions ($h < -1000$ cm) are hardly possible or very time consuming. The same principle is applied in hanging water column, pressure cell or sand box experiments. Their setup is simpler, but the ranges of measurements are even narrower [6]. Multi-step outflow experiments are also done in centrifuges. A sequence of water heads is applied via rotation and centrifugal force and water content and outflow rates are measured [10,11]. This approach has been continuously developed to eliminate practical issues like consolidation of undisturbed samples [12]. In addition, the evaporation method [13] is widely used, which allows high-resolution observation of HSP from saturation (only retention curve) to around $h = -1000$ cm and in an extended version up to $h = -8800$ cm [14]. In the field, the instantaneous profile approach describes various types of soil profiles equipped with sensors for water content and soil water head in at least two depths [15]. The importance of this method is small due to its high demands on equipment and logistics.

A major part of actual studies calls for a sounder data basis for the parametrization of HSP, especially concerning the range of represented soil moisture and the sampled soil volume (e.g., [16,17]). Additionally, simultaneous determination of $\theta(h)$ and $K(h)$ is desired to use the full capacity of wide-range measurements of both HSP-functions [7]. For such simultaneous determination, two general approaches are used: (i) recordings of a water flow process and subsequent inverse modelling; and (ii) fitting of HSP-functions to measured data of $\theta(h)$ and $K(h)$. Exemplary observation setups for (i) are: one- or multistep outflow lab experiments (e.g., [18,19]), evaporation experiments [20], infiltration experiments in the field [17,21,22], or field monitoring of soil water state [23,24]. Inverse modelling rapidly gives reliable results and is the most established method to obtain HSP. Nevertheless, reference observations are needed which require considerable time or equipment resources, especially in field-based studies.

In contrast to inverse simulation, wide-moisture-range measurement of data for both HSP-functions with subsequent direct fitting is rarely done. Multi-step flux experiments are advancements of multi-step outflow methods and allow to measure HSP directly in disturbed samples [25,26]. Peters and Durner [27] used virtual evaporation experiments as the data basis for simultaneous HSP-fitting, interpreted their results as reliable and pointed out the need for additional information in $K(h)$ near saturation. The intention of their study was to test models, not to evaluate measurement methods. In a comparative study, Mermoud and Xu [28] obtained HSP-parameters from direct field and lab measurements as well as by using four PTF. By modelling they examined which results are most appropriate to reproduce field-observed water content. They found best agreement with HSP from field measurements, less quality with lab experiments and poor results with PTF. Their field experiments were intensively equipped and laborious and the data analysis was done for each method separately. A combination of methods in the parametrization procedure might allow a reduction of effort in field measurements. Siltecho et al. [29] also compared different approaches including rapid and cheap field and lab measurements, PTF and inverse modelling. No method was found to be superior and they suggested the use of the cheapest and easiest method to obtain starting values for a more elaborate inverse parametrization or model calibration.

To establish statements about the appropriateness of different HSP-parametrization approaches, measures for the goodness of fits are usually used [30]. They allow a statement about the alignment of reference values to a simplifying model. Nevertheless, information about the representation of natural water dynamics or the effects of changing options in the measuring-fitting procedure may be only gained by subsequent modelling. Such functional approaches were applied to evaluate effectivity of uni- or bimodal soil hydraulic characterization [31], to compare the ability of different models to account for dry periods [32] or to evaluate different PTF [33].

In summary, the potential of combining methods, preferably field and lab experiments, to yield a comprehensive data basis for the parametrization of HSP was repeatedly pointed out. Nevertheless, there are few studies which conclusively suggest an optimum strategy for HSP measurements due to high experimental efforts with uncertain benefit. There is a need to develop and evaluate methods to measure data over a wide range of soil moisture states. Especially for studies on field- or catchment scale, rapid and cheap technologies are required which allow a high number of replications to capture a possibly representative soil volume. The aim of this study was to show if combining multiple methods for acquisition of HSP-data is an efficient strategy to subsequently obtain reliable results in modelling applications.

2. Materials and Methods

2.1. Summary of Methodology

Four rapid methods were applied to measure HSP: (i) the evaporation method (EM) [14]; (ii) a dew point hygrometer [34]; (iii) the falling head method for saturated hydraulic conductivity [35], and (iv) the hood infiltrometer (HI), a type of tension infiltrometer [36]. The widely used bimodal HSP-functions of Priesack and Durner [37], based on van Genuchten [38] and Mualem [39], were fitted simultaneously to different combinations of measured data. To evaluate the measurements, we used a functional approach [31] and conducted a numerical sensitivity study including drainage, infiltration, and drying conditions. This allowed to estimate quantitatively how different measurement methods alter soil water balance. Additionally, we discussed characteristics of used methods concerning application issues and reliability.

2.2. Sampling Sites and Procedure

Experiments and soil sampling were carried out at two long-term tillage experiments in north-eastern Austria (Table 1). In each soil unit (defined by same site and tillage treatment), measurements and sampling were replicated 11 times (Table 2, values 10 and 12 resulted from a mapping error). Sampling positions were predetermined on a 6 × 12 m raster and placed in inter-row space avoiding machine tracks. The measurements were carried out in early summer when soil water status was neither around saturation nor drying cracks were present on the soil surface (i.e., vol. water content θ = 0.20 to 0.35 cm^3 cm^{-3}). At sampling time, plant cover was established over the whole field area, minimizing structural degradation like crusting, shrinking or splash erosion. Fraction of stable soil aggregates (measured after Kemper and Koch [40]) ranged from 0.15 to 0.5 with a median at 0.31 depending on site and tillage treatment. Similarly, macro-porous soil structure development was considerably variable as visual estimation showed. This plurality was appreciated to account for a majority of possible conditions of agricultural soils in the study region.

2.3. Field and Lab Measurement Methods

To measure hydraulic soil properties, four methods were applied sequentially to the same soil sample. The field measurement procedure included the following steps:

(i) hood infiltrometer experiment, see Section 2.3—HI;
(ii) percolation and drying time, at least 2 h, to minimize soil smearing during subsequent sampling;

(iii) soil core sampling, one ring placed at the centre of the infiltration area from (i), carefully pushed in without hammering to avoid sample disturbance or tilting, steel rings with inner diameter $d_{in} = 84$ mm and height $h = 50$ mm, another ring in a distance of approximately one meter for measurement of initial water content and as backup sample;
(iv) collecting disturbed soil samples (ca. 500 cm^3) from the immediate surroundings of the core.

Table 1. Study site description. Grain size distribution classified as: 2 mm $\geq$ sand > 0.063 mm $\geq$ silt > 0.002 mm $\geq$ clay [41]. Coordinates refer to the Universal Transverse Mercator system (UTM), zone 33N.

	Site A	**Site B**
location name	Obersiebenbrunn	Hollabrunn
crop	winter wheat	sunflower
sand	34%	24%
silt	50%	55%
clay	16%	21%
soil type	Chernozem	Chernozem
mean annual precipitation	520 mm	519 mm
soil organic carbon	1–2%	1–2%
coordinates field site	E 625720, N 5347520	E 578580, N 5379390
coordinates weather station	E 625992, N 5347056	E 578953, N 5380331
measurement dates 2016	02, 05, and 06 May	13, 14, and 16 June

Table 2. Number of replicates per analysed unit. T1 to T4 are different tillage treatments (not in the focus of this study, hence not explained).

Treatments	**Sites**	
	Site A	**Site B**
T1	11	11
T2	11	11
T3	11	12
T4	11	10

The methods are listed below and each of them yields data at a certain range of soil moisture state (Figure 1). During all measurements, soil water head decreased to more negative, which means we nominally measured drainage conditions to avoid bias due to hysteresis. Still, the infiltration observed with the HI may also be considered as wetting process. Consequently, measurements of HI and EM (draining process) could not be combined. Nevertheless, hysteresis in tension infiltrometer measurements is present, but does not impact quantitative outcomes in application cases [42,43]. As the HI additionally yields data for a very narrow range of h near saturation, where hysteresis in HSP is minimal, hysteresis was negligible in this study setup. To determine bulk density for calculation of volumetric water content θ, sample rings were dried after the experiments at 105 °C for 24 h. As the samples were taken a few hours after infiltration experiments, bulk density corresponds to conditions near field capacity.

HI Hood Infiltrometer

The hood infiltrometer [36] is a type of tension infiltrometer which lets water infiltrate into the soil directly from an open-bottomed, semi-spheric hood without any artificial contact layer. Via a connected Mariotte bottle system, tension is established which has to be overcome by the soil matrix to initiate infiltration. The achievable minimum water head is restricted by entrance of air from soil into the water-filled hood, which usually occurred at around $h = -3$ cm in this study (range ca. -1.5 to -7 cm).

To prepare the measurement, a level area in the micro-relief was chosen where loose plant and soil clod material was carefully removed. After installing the infiltrometer hood, the first tension step was set at approximately $h = -0.5$ cm and infiltration started for a few minutes without measuring to initially wet the soil body. Tension was kept constant until a steady infiltration rate for at least 3 min was reached (reading time steps were 15 to 60 s). Subsequently, two further pressure steps were measured, one around $h = -2$ cm and the last one slightly less negative than air entry pressure. As a result, three data points for near-saturated hydraulic conductivity are derived from the infiltration rate. Calculation of $K(h_i)$ from readings of water outflow Q_i (in cm^3 s^{-1}) and water head h_i followed the suggested procedure in Schwärzel and Punzel [36].

FH Falling Head Method

Saturated hydraulic conductivity K_s was measured directly in undisturbed soil core samples by the falling head method with rising water level [44], modified after Klute and Dirksen [35]. As a simplification for further analysis, the corresponding water head for K_s was nominally set to $h = -0.01$ cm (pF = −2).

EM Evaporation Method

Undisturbed soil cores were placed on a digital measuring device (HYPROP® METER Group AG, Munich, Germany; cf. Schindler et al. [14] for details). Two tensiometers measure the water head h in different depths and water content θ is determined by weighing. Additionally, the measurement range was extended to the tensiometer's air-entry point at $h = -8800$ cm [14]. Measured data were transformed to data points at the retention curve $\theta(h)$ (range: $h = 0$ to -8800 cm) and the hydraulic conductivity curve $K(h)$ (range: h = ca. −20 to −8800 cm). The experiments were run in a lab at a temperature of 21–23 °C and air humidity of 20–40%.

DP Dew Point Method

A dew point hygrometer (WP4C PotentiaMeter® METER Group AG, Munich, Germany) was used to measure water retention $\theta(h)$ under dry conditions (pF = 3.5–6.2). Here, the liquid water phase in the soil sample and the vapour phase in surrounding air is equilibrated in a sealed chamber. Finally, water potentials of vapour and liquid phase are equal and the former is measured via the dew point on a cooled mirror inside of the chamber. A detailed description of the measurement principle is given elsewhere [34,45]. Water content for each reading is measured gravimetrically and transformed to volumetric θ via the average bulk density of the corresponding EM-cores. Before DP-measurements, samples of the same treatments were mixed and two replicates of the mixed samples were analysed. 3–4 g of air-dry soil was put into circular steel cups (d = 37 mm) and wetted using deionized water to around $\theta = 0.2$ cm^3 cm^{-3}. During air drying the sample, up to seven measurements in precise mode—repeated readings until they remain within a defined level of tolerance—were taken of each sample with the intention to obtain values evenly distributed between pF = 3.5 and 6.2.

For further analysis, six combinations of measurement methods were defined and compared. Only EM was included in all combinations. It serves as the backbone method due to its wide measuring range at both HSP-curves. Data from all other methods were variably omitted and the following combinations were analysed: ALL, EM + FH + HI, EM + FH, EM + HI, EM + DP, EM.

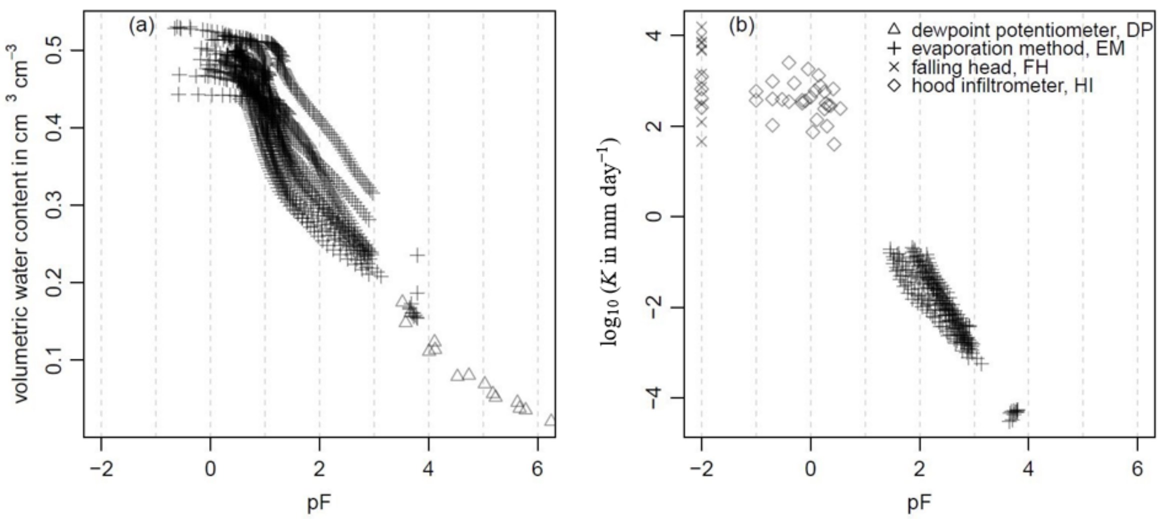

Figure 1. Example of measurements for hydraulic soil properties to illustrate ranges of different methods; 11 replicates measured in one treatment (site B, T1). Subplot (**a**) is the water retention curve $\theta(h)$, (**b**) is the hydraulic conductivity curve $K(h)$. For both, h is transformed to pF by pF = $\log_{10}|h|$.

2.4. Fitting of Functions for Hydraulic Soil Properties

For the formalization of HSP, we used the van Genuchten-Mualem model (VGM) [38,39] in its bimodal version (Equations (1)–(3) [37]). This model was chosen because of its high acceptance and its compatibility to the later used modelling software HYDRUS-1D (PC-Progress, Prague, Czech Republic) [46]. The bimodal version superimposes two subcurves to be able to account for two different flow domains in soil, usually macropore system and soil matrix. In this case, a pre-study comparing goodness of fit for uni- and bimodal model did not show significant differences. Nevertheless, the bimodal model was used to enable usage of the approach also for highly structured soils.

Introduced variables and parameters in VGM are: θ_s is the volumetric water content at saturation (cm^3 cm^{-3}), S_e is the degree of saturation ($S_e = \theta/\theta_s$, dimensionless), α (cm^{-1}, commonly denoted as reciprocal of the air-entry point of soil), n, and τ (both dimensionless, parameter defining the slope of the retention curve and tortuosity parameter, respectively) are fitting parameters of VGM, J is the number of subcurves in the used model (i.e., $J = 1$ for uni-modal and $J = 2$ for bi-modal functions), w is a dimensionless weighing factor for the respective subcurve j. Herein, the index j = 1 always relates to the subcurve for the flow domain comprising the coarser pores (i.e., $\alpha_1 > \alpha_2$). Furthermore, we used a simplified form with residual water content $\theta_r = 0$ and $m = 1 - 1/n$.

$$\theta(h) = (\theta_s - \theta_r)S_e(h) \tag{1}$$

$$S_e(h) = \sum_{j=1}^{J} w_j \left[1 + (\alpha_j h)^{n_j}\right]^{-m_j} \tag{2}$$

$$K(h) = K_s \left(\sum_{j=1}^{J} w_j \left[1 + (\alpha_j h)^{n_j}\right]^{-m_j}\right)^{\tau} \left(\frac{\sum_{j=1}^{J} w_j \alpha_j \{1 - (\alpha_j h)^{n_j} \left[1 + (\alpha_j h)^{n_j}\right]^{-m_j}\}}{\sum_{j=1}^{J} w_j \alpha_j}\right)^2 \tag{3}$$

The functions $\theta(h)$ and $K(h)$ (Equations (1)–(3)) were fitted simultaneously to measured data by use of the artificial bee colony global optimization algorithm ([47], implemented in [48]) minimizing the objective function given in Equation (4). There, Φ is the evaluation criterion to be minimized, r and k are the number of observations in the respective data class, $\boldsymbol{b}$ is the parameter vector, hence $\hat{\theta}_i(\boldsymbol{b})$ and $\hat{K}_i(\boldsymbol{b})$ are model predicted values and $\bar{\theta}_i$ and $\bar{K}_i$ are measurements. The weighting factor of 0.5 for the conductivity curve in Equation (4) was based on a pre-study (unpublished) using a representative part of the dataset. Additionally, ranges for the parameters were predestined according to literature [9,49,50] and visual plausibility evaluations (Table 3). For the physically related parameters θ_s and K_s, information from measurements was also used.

$$\Phi(\boldsymbol{b}) = \sum_{i=1}^{r} \left[\bar{\theta}_i - \hat{\theta}_i(\boldsymbol{b})\right]^2 + 0.5 \sum_{i=1}^{k} \left[\log_{10}(\bar{K}_i) - \log_{10}(\hat{K}_i)(\boldsymbol{b})\right]^2 \quad (4)$$

Table 3. Boundaries for parameters of bimodal van Genuchten-Mualem model. Parameters are: α_j in cm^{-1}, n_j and τ, both dimensionless, are fitting parameters; θ_s, in cm^3 cm^{-3}, is saturated water content; w_2, dimensionless, is the weight of the second sub-function; and K_s in cm day^{-1} is saturated hydraulic conductivity.

Parameter	θ_s	α_1	n_1	α_2	n_2	w_2	K_s	τ
upper boundary	1	0.5	15	0.5	15	1	10^5	10
lower boundary	0.1	10^{-5}	1.01	10^{-5}	1.01	0	1	−2

2.5. Numerical Simulations

A three-part sensitivity study using HYDRUS-1D [46] was run to assess the effects of different method combinations on soil water balance components. The setup was adopted from Romano and Nasta [31] and includes a drainage, an infiltration, and a drying process. Accordingly, simulations were conducted without accounting for hysteresis considering the arguments given in Section 2.3. Nevertheless, for the infiltration experiment, HSP during wetting are decisive and hysteresis would have an effect. Consequently, the infiltration experiment will be interpreted with caution to potential bias due to neglected hysteresis.

For all simulations, we defined a soil column of 200 cm depth but analysis comprised only the soil region from z = 0–50 cm. The soil material was constant all over depth and its HSP were determined by the different combinations of measurements following the procedure in Section 2.4. Separate model runs were conducted for each sample and measurement combination (528 runs, see Section 2.6). The drainage process started at fully saturated state (h = 0 cm) and ran for 72 h with zero flux as top boundary condition and free drainage at the bottom. The vertical distribution of water head after the drainage simulation was taken as initial condition for the infiltration experiment. Therein, boundary conditions were set to a constant water head of h = 0 cm at the top and free drainage at bottom. The infiltration simulation was run for 24 h.

The drying process started with a global initial water head of h = −100 cm and was simulated for 45 days. Boundary conditions were free drainage at the bottom and an atmospheric top with zero precipitation and constant rates of potential evaporation (2 mm day^{-1}) and potential transpiration (7.5 mm day^{-1}). These rates represent high but plausible summer values for the sampling regions. We defined a grass vegetation cover with a constant height of 12 cm and rooting depth of 50 cm (water uptake was equally distributed from z = 0–50 cm). Hence, the difference between actual and potential transpiration was exclusively determined by HSP. The water stress response function after Feddes [51] was applied with standard parameters for grass [46].

2.6. Data Processing and Statistics

The measurement procedure was applied at 88 soil sampling units (Table 2). In the calculations, each was described with six combinations of measurement methods, what leads to 528 data sets. The fitting procedure (Section 2.4) was applied to each data set resulting in a set of parameters as input for a separate model run. Results of the modelling study were normalized by the corresponding value of ALL to eliminate the influence of treatment and site as disturbing factors. More in detail, the presented numbers (Section 3.2) were calculated in three steps: (i) averaging replicate results for identical site, treatment and method combination (from 528 to 48 values); (ii) divide these by the result from ALL on the same site and same tillage treatment (48 absolute to 48 relative values); (iii) calculate average of relative values for each combination of measurement methods (48 to 6).

For all data processing we used the statistical software environment R, version 3.3.1 [52]. Differences between results for data units were detected by ANOVA, Tukey's HSD-test [53] was used as post-hoc test to define coherent groups [54]. Data sets for $\theta(h)$ and $K(h)$ will be provided as supplementary material.

3. Results

3.1. Fitting of HSP-Functions

Goodness of fits may be estimated visually in Figure 2. The values for θ_{sim} and K_{sim} were calculated for all measured values of h (combination ALL) using Equations (1)–(3). Irregular patterns occurred in both combinations without measurements for (near-)saturated conductivity: EM and EM + DP (subsequently denoted as NoCon). In contrast, all other combinations (subsequently denoted as YesCon) gave a good overall picture without a systematic pattern of deviations. The methods FH and HI represented the near-saturated conductivity curve, where FH induces higher variability (Figures 1 and 2).

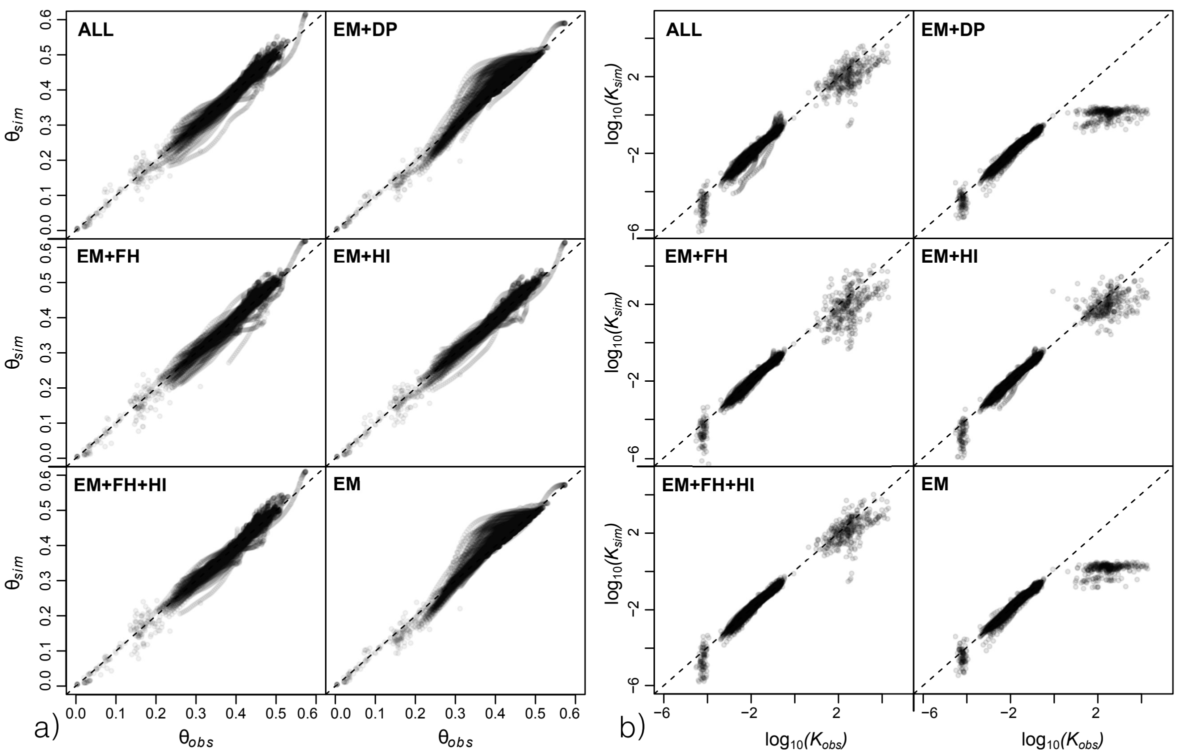

Figure 2. (**a**) comparison of volumetric water content $\theta(h)$ (cm^3 cm^{-3}) observed (θ_{obs}) and calculated (θ_{sim}) with fitted parameters; (**b**) comparison of hydraulic soil conductivity $K(h)$ ($\log_{10}$ (m day^{-1})) observed (K_{obs}) and calculated (K_{sim}) with fitted parameters; points are printed in semi-transparent black colour, hence dark parts show high point density; 88 samples included in each subplot.

Table 4 shows a summary of fitted parameters. Most of them were clearly different between NoCon and YesCon. Lower values of K_s and θ_s of NoCon indicated a smaller fraction of observed macropores and lower α_1 a shift of the first (coarser) mode of the bimodal pore size distribution to smaller sizes. Only n_2, the shape parameter of the second subcurve (representing the finer part of the pore size distribution) and w_2, the extent of bimodality, were not significantly different ($\alpha = 0.05$) between methods.

Table 4. Fitted parameters of bimodal van Genuchten-Mualem model and evaluation criterion root mean square error (RMSE).

		ALL	EM + FH + HI	EM + FH	EM + HI	EM + DP	EM
$\log_{10}(K_s/\text{cm day}^{-1})$	mean (sd)	2.50 (0.61)	2.55 (0.62)	2.39 (0.90)	2.35 (0.59)	0.10 (0.26)	0.11 (0.28)
	min–max	0.99–3.61	1.12–4.08	0.00–4.11	1.14–3.75	−0.75–0.44	−0.86–0.46
$\theta_s/\text{cm}^3\ \text{cm}^{-3}$	mean (sd)	0.48 (0.04)	0.48 (0.04)	0.48 (0.04)	0.48 (0.04)	0.45 (0.03)	0.45 (0.03)
	min–max	0.41–0.62	0.41–0.61	0.40–0.62	0.42–0.62	0.39–0.59	0.39–0.57
$\log_{10}(\alpha_1/\text{cm}^{-1})$	mean (sd)	−0.9 (0.5)	−0.9 (0.4)	−0.9 (0.5)	−1.0 (0.5)	−1.8 (0.4)	−1.8 (0.4)
	min–max	−1.8–−0.3	−1.9–−0.3	−2.1–−0.3	−2.0–−0.3	−2.5–−1.0	−2.6–−1.1
n_1	mean (sd)	1.60 (0.56)	1.66 (0.56)	1.59 (0.67)	1.82 (1.10)	2.40 (1.53)	2.38 (1.50)
	min–max	1.01–4.10	1.01–3.98	1.08–5.24	1.08–10.00	1.25–10.00	1.43–10.00
τ	mean (sd)	0.2 (2.2)	0.2 (2.1)	−0.4 (2.0)	0.5 (2.2)	−2.2 (1.1)	−2.2 (1.1)
	min–max	−3.0–5.9	−3.0–6.0	−3.0–6.0	−3.0–6.0	−3.0–1.3	−3.0–2.2
$\log_{10}(\alpha_2/\text{cm}^{-1})$	mean (sd)	−3.5 (0.8)	−3.4 (0.8)	−3.5 (0.9)	−3.5 (0.8)	−3.9 (1.1)	−3.9 (1.1)
	min–max	−5.0–−1.9	−5.0–−1.0	−5.0–−1.2	−5.0–−2.3	−5.0–−2.2	−5.0–−2.1
n_2	mean (sd)	1.70 (1.02)	1.70 (1.13)	1.82 (1.41)	1.55 (0.28)	1.60 (0.29)	1.59 (0.29)
	min–max	1.16–8.27	1.20–9.06	1.14–10.00	1.18–2.73	1.21–2.03	1.01–2.01
w_2	mean (sd)	0.53 (0.21)	0.57 (0.20)	0.51 (0.21)	0.55 (0.20)	0.50 (0.28)	0.51 (0.29)
	min–max	0.19–0.93	0.11–0.93	0.06–0.89	0.18–0.87	0.07–0.93	0.00–0.95
RMSE	mean (sd)	1.26 (0.77)	1.12 (0.50)	1.19 (0.62)	1.12 (0.66)	1.10 (0.61)	1.10 (0.49)
	min–max	0.29–5.05	0.30–2.43	0.30–2.98	0.27–2.84	0.23–2.95	0.33–2.31

3.2. Numerical Simulations

Figure 3 shows summary boxplots of simulated water balance components. The influence of different sites and tillage treatments on absolute results and variability was not eliminated or pointed out. Hence, these illustrations only serve as an impression about orders of magnitude of modelling results and the differences between methods. To enable statistically sound comparison, results were normalized to the combination of all measurement methods (Section 2.6). The ranges of water head in the numerical experiments ranged from $h = 0$ to -150 cm in the drainage experiment, during infiltration it went up to between $h = 0$ and -5 cm, and in the drying period it reached the model constraint of $h = -100{,}000$ cm at the surface.

Again, most impressive differences occurred between the grouped combinations NoCon and YesCon (Table 5). Under drainage conditions, the lower near-saturated hydraulic conductivity of NoCon lead to less cumulative drainage and a final water content—representing field capacity [55]—which was 15 percent higher than with YesCon. The infiltrating water volume in the infiltration experiment was very small for NoCon (Figure 3c). During the drying period, transpiration was higher at NoCon soils, after 45 days the surplus summed up to 22 percent (Table 5). Consequently, the mean water head in the root zone (z = 0–50 cm) was also considerably lower (NoCon) at the end of the drying experiment. Nevertheless, the temporal course of root zone water head was less negative during the first 14 days and decreased faster in the second half of the experiment (Figure 4).

Including dewpoint potentiometry measurements did not change simulation results significantly (difference between EM and EM + DP, and between EM + FH + HI and ALL). A difference between hood infiltrometry (HI) and falling head method (FH) occurred only in the drainage experiment where cumulative drainage based only on FH was nearly 10 percent lower.

Table 6 points out which HSP-parameters influenced simulated water balance quantities. All results were significantly correlated with K_s and α_1. On average, K_s, θ_s, and τ had higher influence (means of absolute correlation coefficients were 0.34, 0.32, and 0.32, respectively) than the parameters describing the finer pore fraction (α_2, n_2, w_2) and n_1 which were hardly correlated with the resulting water balance quantities.

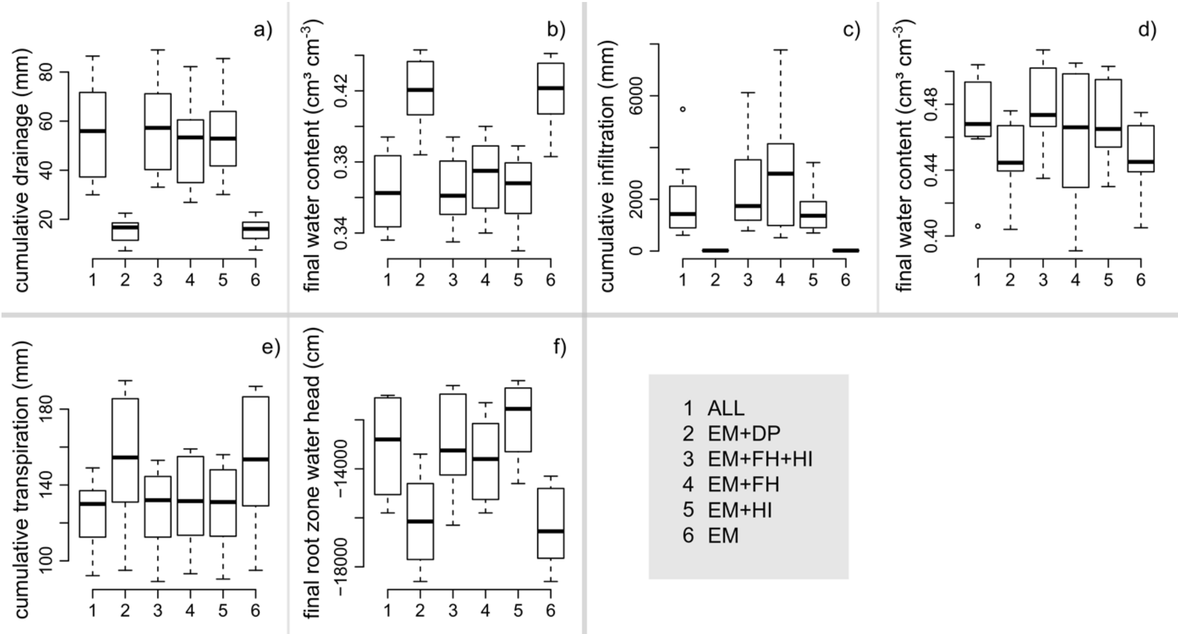

Figure 3. Modelling results. (**a**) cumulative drainage in mm; (**b**) final water volume in mm, both from drainage experiment; (**c**) cumulative infiltration in mm; (**d**) final water volume in mm, both from infiltration experiment; site-based simulations: (**e**) transpiration in mm day^{-1}; (**f**) mean water head in the root zone in cm. Values of (**b**,**d**) refer to a soil column of 200 cm depth. Formal statistical analysis is not validly applicable as site and tillage treatment are present in the results as disturbance factors—graph only for visual expression.

Table 5. Relative comparison of modelling result; absolute model results were normalized by the corresponding result for ALL within data units of the same site and tillage treatment. Here presented is the mean of normalized values. Letters aside indicate corresponding groups identified by ANOVA and a post-hoc Tukey HSD-Test, α = 0.05. FRZWH is final root zone water head, Cum. means cumulative.

	Drainage Experiment				**Infiltration Experiment**				**Drying Period**			
	Cum. Drainage		**Water Storage**		**Cum. Infiltration**		**Water Storage**		**Transpiration**		**FRZWH**	
ALL	1.000	a	1.000	a	1.000	a	1.000	ab	1.000	a	1.000	a
EM + FH + HI	1.042	a	1.002	a	1.346	a	1.022	a	1.016	a	0.993	a
EM + HI	0.991	a	1.003	a	1.033	a	1.003	ab	1.026	a	0.927	a
EM + FH	0.915	b	1.023	a	1.572	a	0.980	bc	1.048	a	1.049	a
EM	0.297	c	1.157	b	0.013	b	0.955	b	1.215	b	1.266	b
EM + DP	0.293	c	1.157	b	0.013	b	0.955	b	1.222	b	1.245	b

Table 6. Pearson correlation coefficients (R) of simulation results with parameters for hydraulic soil properties functions. * indicates significant relationships, α = 0.05.

		K_s	θ_s	α_1	n_1	τ	α_2	n_2	w_2
Drainage exp.	cumulative drainage	0.41 *	0.66 *	0.27 *	0.03	0.32 *	0.05	0.08	0.17 *
	final water content	−0.36 *	0.01	−0.17 *	0.04	−0.41 *	−0.09 *	0.06	−0.08
Infiltration exp.	cumulative infiltration	0.71 *	0.32 *	0.19 *	0.07	0.30 *	0.07	−0.09 *	0.15 *
	final water content	0.17 *	0.75 *	0.15 *	0.09 *	0.03	0.00	0.00	0.11 *
Drying period	transpiration	−0.27 *	0.17 *	−0.16 *	0.10 *	−0.24 *	−0.16 *	0.03	−0.06
	root zone water head	0.14 *	0.02	0.10 *	−0.08	0.61 *	0.17 *	−0.37 *	0.07
	mean of absolute values	0.34	0.32	0.17	0.07	0.32	0.09	0.10	0.11

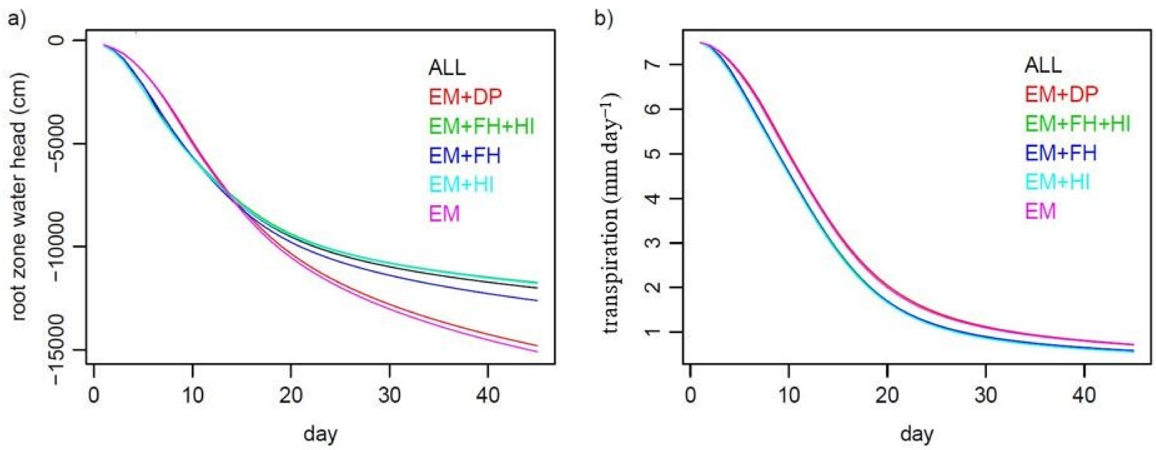

Figure 4. Development of water head in the root zone (**a**) and transpiration rate (**b**) during drying period. Daily values, diurnal variations neglected.

4. Discussion

For the water retention curve, data were derived by two methods: EM and DP. Figure 1 shows smooth transition between these methods which was observed for all samples. This was also reported by Schelle et al. [56]. Higher discrepancy occurred in the conductivity curve. Three methods surveyed unsaturated and saturated conductivity: FH, HI, EM. The backbone of the applied measurement procedure was EM as it yielded data for retention and conductivity curve. Nevertheless, by EM only matric flow was observed as no gravity-driven macropore flow occurred in the bottom-sealed experiment. In contrast, macropore flow was the dominant flow process in FH and HI experiments and measured values were two to four orders of magnitude higher then maximum conductivity values of EM (Figure 1). Applying a functional approach [31], we could also quantify the effects of these differences. Especially the results for experimental field capacity, infiltration rates, and actual transpiration in a dry period were remarkable and caused by the better representation of macro-pore system with YesCon methods. In contrast, drying simulations did not include drier conditions than $h = -15{,}000$ cm. The importance of DP-measurements was supposed to rise during more intensive drying.

The herein applied evaluation procedure was designed on a basic level to keep the focus on the comparison of measurement methods and their combination. Hence, phenomena like hysteresis or shrinking were neglected and arise potential for further research. The sampled soils were silt-dominated, hydrophilic and affected by agricultural management. Consequently, the results are not representative for clay or sand soils, water repellent soils and differing land use systems like forests or fallows.

In a considerable number of fits, the parameters reached their predefined constraints. In concrete studies, this behaviour should be examined in more detail. Especially τ was highly variable together with high correlation to simulation results. This emphasized a need for further investigation, especially considering the habit to set this parameter to a fixed value in fitting applications (e.g., [57]). Accordingly, Dettmann et al. [58] yielded improved HSP-fits with τ as free fitting parameter and suggested further modifications of fitting procedures. Additionally, it was surprising that w_2, the weighing parameter accounting for bimodality, did not differ between method combinations. Bimodality was expected to be better observable with YesCon but the result might lead to the interpretation that the retention curve includes enough information for determination of bimodality. Nevertheless, the lower variability for w_2 in YesCon measurements pointed out more accurate determination of bimodality.

All measurements implied physical impacts on soil structure which might have caused bias in observations of hydraulic soil properties or soil structure. During infiltration measurements in the field, only a small part at the surface of the treated soil volume was exposed to considerable forces. In contrast, undisturbed samples for lab measurements (FH and EM) underwent multiple steps of sample handling also in saturated state where structural stability is lowest. Moreover, the variability of replicated FH measurements was considerably higher than that of HI. This was most likely a result of different sampling volumes—the cross-sectional area of the flow domain for HI (483 cm^2 at soil surface) was more than nine times larger than that of FH (55 cm^2)—and the higher number of measured data pairs (1 for FH, 2–3 for HI). In the small cores, the probability for a continuous macro-pore to control saturated hydraulic conductivity was high, which partly explained the higher variability in FH-measurements.

5. Conclusions

The intention of this study was to quali- and quantitatively evaluate different combinations of measurement methods for the parametrization of hydraulic soil properties functions. Analysing the results and practical considerations, we emphasized the importance of measurements of hydraulic conductivity near saturation as the basis for soil water modelling in silt-dominated, structured, arable soils. We suggested applying infiltration experiments in the field—in our case using hood infiltrometer—additionally to the evaporation method. Compared to lab measurement with falling head method, higher sampling volume and lower error-proneness increased representativeness of parametrization, at least at profile scale. Nevertheless, we still saw a need to extend the measurement range of infiltration experiments to account also for the transition range between macro- and mesopore flow at $h = -2.5$ to -6.0 cm. Additionally, further research should concentrate on the evaluation of combined measurement procedures for a wider range of land use and soil management systems.

Author Contributions: Conceptualization, T.W., G.B., S.J., A.S. and K.S.; Formal Analysis, K.-H.F.; Writing—Original Draft Preparation, T.W.; Writing—Review & Editing, T.W., J.K., P.C.; Funding Acquisition, A.S., K.S., K.-H.F.

Funding: This research was funded by Austrian Science Fund (I2122-B16) and Deutsche Forschungsgemeinschaft (SCHW 1448/6-1, FE 504/11-1.)

Acknowledgments: We are thankful to the administration of agricultural schools in the province Lower Austria for supporting our field experiments and providing meteorological data. Special elevation deserves Christoph Häusler for collaboration in field and lab work. Four anonymous reviewers helped to improve the manuscript significantly.

Conflicts of Interest: The authors declare no conflict of interest.

Abbreviations

The following abbreviations are used in this manuscript:

HSP	hydraulic soil properties, includes $\theta(h)$ and $K(h)$
h	soil water head (cm)
θ	volumetric water content ($cm^3\ cm^{-3}$)
$\theta(h)$	water retention function
K	soil hydraulic conductivity (cm day^{-1})
i	index for data pair of $\theta(h)$- or $K(h)$-series
z	soil depth (cm, positive downwards)
PTF	pedotransfer function(s)
pF	decadic logarithm of absolute soil water head (pF = $\log_{10}\|h\|$)
EM	evaporation method
DP	dewpoint potentiometry
FH	falling head method
HI	hood infiltrometer
ALL	combination of all methods (4 lines above)
YesCon	combinations of measurement methods with separate conductivity measurements
NoCon	combinations of measurement methods without separate conductivity measurements
VGM	van Genuchten-Mualem model for HSP

j index for subcurves in bimodal VGM
K_s saturated hydraulic conductivity (cm day^{-1})
θ_s saturated soil water content (cm^3 cm^{-3})
θ_r residual soil water content (cm^3 cm^{-3})
S_e degree of saturation, θ/θ_s
α parameter in VGM, representing air-entry point (cm^{-1})
n parameter in VGM, representing slope of $\theta(h)$ (dimensionless)
m parameter in VGM, here simplified to $m = 1 - 1/n$
τ parameter in VGM, representing tortuosity (dimensionless)
w_2 weighing factor for subcurve i = 2 in VGM (dimensionless)
Φ evaluation criterion of objective function in parameter optimization (Equation 4)
r number of data pairs of $\theta(h)$
k number of data pairs of $K(h)$
$\boldsymbol{b}$ parameter vector in parameter optimization

Reference

1. Assouline, S.; Or, D. Conceptual and Parametric Representation of Soil Hydraulic Properties: A Review. *Vadose Zone J.* **2013**, *12*, 108–112. [CrossRef]
2. Vereecken, H.; Schnepf, A.; Hopmans, J.; Javaux, M.; Or, D.; Roose, T.; Vanderborght, J.; Young, M.; Amelung, W.; Aitkenhead, M.; et al. Modeling Soil Processes: Review, Key challenges and New Perspectives. *Vadose Zone J.* **2016**, *15*, 1–57. [CrossRef]
3. Kutilek, M. Soil hydraulic properties as related to soil structure. *Soil Tillage Res.* **2004**, *79*, 175–184. [CrossRef]
4. Wösten, J.H.M.; Pachepsky, Y.A.; Rawls, W.J. Pedotransfer functions: Bridging the gap between available basic soil data and missing soil hydraulic characteristics. *J. Hydrol.* **2001**, *251*, 123–150. [CrossRef]
5. Vereecken, H.; Weynants, M.; Javaux, M.; Pachepsky, Y.; Schaap, M.G.; van Genuchten, M. Using Pedotransfer Functions to Estimate the van Genuchten–Mualem Soil Hydraulic Properties: A Review. *Vadose Zone J.* **2010**, *9*, 795–820. [CrossRef]
6. Dane, J.H.; Topp, G.C.; Campbell, G.S.; Al-Amoodi, L.; Dick, W.A. *Methods of Soil Analysis: Physical Methods*; Soil Science Society of America: Madison, WI, USA, 2002; p. 1692.
7. Gribb, M.M.; Kodesova, R.; Ordway, S.E. Comparison of Soil Hydraulic Property Measurement Methods. *J. Geotech. Geoenviron. Eng.* **2004**, *130*, 1084–1095. [CrossRef]
8. Nasta, P.; Assouline, S.; Gates, J.B.; Hopmans, J.W.; Romano, N. Prediction of Unsaturated Relative Hydraulic Conductivity from Kosugi's Water Retention Function. *Procedia Environ. Sci.* **2013**, *19*, 609–617. [CrossRef]
9. Gribb, M.M.; Forkutsa, I.; Hansen, A.; Chandler, D.G.; McNamara, J.P. The Effect of Various Soil Hydraulic Property Estimates on Soil Moisture Simulations. *Vadose Zone J.* **2009**, *8*, 321–331. [CrossRef]
10. Nimmo, J.R.; Rubin, J.; Hammermeister, D.P. Unsaturated flow in a centrifugal field: Measurement of hydraulic conductivity and testing of Darcy's Law. *Water Resour. Res.* **1987**, *23*, 124–134. [CrossRef]
11. Malengier, B.; Di Emidio, G.; Peiffer, H.; Ciocci, M.C.; Kišon, P. Unsaturated permeability and retention curve determination from in-flight weight measurements in a bench-scale centrifuge. *Geotech. Test. J.* **2015**, *38*, 243–254. [CrossRef]
12. Fu, X.; Shao, M.; Lu, D.; Wang, H. Soil water characteristic curve measurement without bulk density changes and its implications in the estimation of soil hydraulic properties. *Geoderma* **2011**, *167–168*, 1–8. [CrossRef]
13. Wind, G. Capillary conductivity data estimated by a simple method. In Proceedings of the UNESCO/IASH Symposion 'Water in the Unsaturated Zone', Wageningen, The Netherlands, June 1966; pp. 181–191.
14. Schindler, U.; Durner, W.; von Unold, G.; Mueller, L.; Wieland, R. The evaporation method: Extending the measurement range of soil hydraulic properties using the air-entry pressure of the ceramic cup. *J. Plant Nutr. Soil Sci.* **2010**, *173*, 563–572. [CrossRef]
15. Vachaud, G.; Dane, J.H. Instantaneous Profile. In *Methods of Soil Analysis. Part 4—Physical Methods*; Soil Science Society of America: Madison, WI, USA, 2002; pp. 937–945.
16. Mubarak, I.; Mailhol, J.C.; Angulo-Jaramillo, R.; Ruelle, P.; Boivin, P.; Khaledian, M. Temporal variability in soil hydraulic properties under drip irrigation. *Geoderma* **2009**, *150*, 158–165. [CrossRef]

17. Hardie, M.A.; Lisson, S.; Doyle, R.B.; Cotching, W.E. Evaluation of rapid approaches for determining the soil water retention function and saturated hydraulic conductivity in a hydrologically complex soil. *Soil Tillage Res.* **2013**, *130*, 99–108. [CrossRef]
18. Van Dam, J.C.; Stricker, J.N.M.; Droogers, P. Inverse Method to Determine Soil Hydraulic Functions from Multistep Outflow Experiments. *Soil Sci. Soc. Am. J.* **1994**, *58*, 647–652. [CrossRef]
19. Durner, W.; Iden, S.C. Extended multistep outflow method for the accurate determination of soil hydraulic properties near water saturation. *Water Resour. Res.* **2011**, *47*, 427–438. [CrossRef]
20. Minasny, B.; Field, D.J. Estimating soil hydraulic properties and their uncertainty: The use of stochastic simulation in the inverse modelling of the evaporation method. *Geoderma* **2005**, *126*, 277–290. [CrossRef]
21. Angulo-Jaramillo, R.; Vandervaere, J.P.; Roulier, S.; Thony, J.L.; Gaudet, J.P.; Vauclin, M. Field measurement of soil surface hydraulic properties by disc and ring infiltrometers. *Soil Tillage Res.* **2000**, *55*, 1–29. [CrossRef]
22. Latorre, B.; Peña, C.; Lassabatere, L.; Angulo-Jaramillo, R.; Moret-Fernández, D. Estimate of soil hydraulic properties from disc infiltrometer three-dimensional infiltration curve: Numerical analysis and field application. *J. Hydrol.* **2015**, *527*, 1–12. [CrossRef]
23. Richard, G.; Sillon, J.; Marloie, O. Comparison of Inverse and Direct Evaporation Methods for Estimating Soil Hydraulic Properties under Different Tillage Practices. *Soil Sci. Soc. Am. J.* **2001**, *65*, 215–224. [CrossRef]
24. Zhang, K.; Burns, I.G.; Greenwood, D.J.; Hammond, J.P.; White, P.J. Developing a reliable strategy to infer the effective soil hydraulic properties from field evaporation experiments for agro-hydrological models. *Agric. Water Manag.* **2010**, *97*, 399–409. [CrossRef]
25. Kumahor, S.K.; De Rooij, G.H.; Schlüter, S.; Vogel, H.J. Water Flow and Solute Transport in Unsaturated Sand—A Comprehensive Experimental Approach The investigation of solute transport during unsaturated water flow in soil. *Vadose Zone J.* **2015**, *1*, 14. [CrossRef]
26. Zhuang, L.; Bezerra Coelho, C.; Hassanizadeh, S.; van Genuchten, M. Analysis of the Hysteretic Hydraulic Properties of Unsaturated Soil. *Vadose Zone J.* **2017**, *16*, 1–9. [CrossRef]
27. Peters, A.; Durner, W. Simplified evaporation method for determining soil hydraulic properties. *J. Hydrol.* **2008**, *356*, 147–162. [CrossRef]
28. Mermoud, A.; Xu, D. Comparative analysis of three methods to generate soil hydraulic functions. *Soil Tillage Res.* **2006**, *87*, 89–100. [CrossRef]
29. Siltecho, S.; Hammecker, C.; Sriboonlue, V.; Clermont-Dauphin, C.; Trelo-Ges, V.; Antonino, A.C.D.; Angulo-Jaramillo, R. Use of field and laboratory methods for estimating unsaturated hydraulic properties under different land uses. *Hydrol. Earth Syst. Sci.* **2015**, *19*, 1193–1207. [CrossRef]
30. Bennett, N.D.; Croke, B.F.; Guariso, G.; Guillaume, J.H.; Hamilton, S.H.; Jakeman, A.J.; Marsili-Libelli, S.; Newham, L.T.; Norton, J.P.; Perrin, C.; et al. Characterising performance of environmental models. *Environ. Model. Softw.* **2013**, *40*, 1–20. [CrossRef]
31. Romano, N.; Nasta, P. How effective is bimodal soil hydraulic characterization? Functional evaluations for predictions of soil water balance. *Eur. J. Soil Sci.* **2016**, *67*, 523–535. [CrossRef]
32. Madi, R.; Huibert De Rooij, G.; Mielenz, H.; Mai, J. Parametric soil water retention models: A critical evaluation of expressions for the full moisture range. *Hydrol. Earth Syst. Sci.* **2018**, *22*, 1193–1219. [CrossRef]
33. Stumpp, C.; Engelhardt, S.; Hofmann, M.; Huwe, B. Evaluation of pedotransfer functions for estimating soil hydraulic properties of prevalent soils in a catchment of the Bavarian Alps. *Eur. J. For. Res.* **2009**, *128*, 609–620. [CrossRef]
34. Campbell, E.C.; Campbell, G.S.; Barlow, W.K. A dewpoint hygrometer for water potential measurement. *Agric. Meteorol.* **1973**, *12*, 113–121. [CrossRef]
35. Klute, A.; Dirksen, C. Hydraulic conductivity and diffusivity: Laboratory methods. In *Methods of Soil Analysis. Part 1. Physical and Mineralogical Methods*, 2nd ed.; Klute, A., Ed.; American Society of Agronomy: Madison, WI, USA, 1986; pp. 687–734.
36. Schwärzel, K.; Punzel, J. Hood Infiltrometer—A New Type of Tension Infiltrometer. *Soil Sci. Soc. Am. J.* **2007**, *71*, 1438–1447. [CrossRef]
37. Priesack, E.; Durner, W. Closed-Form Expression for the Multi-Modal Unsaturated Conductivity Function. *Vadose Zone J.* **2006**, *5*, 121–124. [CrossRef]
38. van Genuchten, M.T. A Closed-form Equation for Predicting the Hydraulic Conductivity of Unsaturated Soils. *Soil Sci. Soc. Am. J.* **1980**, *44*, 892. [CrossRef]

39. Mualem, Y. A new model for predicting the hydraulic conductivity of unsaturated porous media. *Water Resour. Res.* **1976**, *12*, 513–522. [CrossRef]
40. Kemper, W.D.; Koch, E.J. *Aggregate Stability of Soils from Western United States and Canada. Measurement Procedure, Correlation With Soil Constituents*; United State Department of Agriculture: Washington, DC, USA, 1966; pp. 1–57.
41. ÖNORM EN ISO 14688-1:2018-06-15. *Geotechnical Investigation and Testing, Identification and Classification of Soil, Part 1: Identification and Description*; Austrian Standards: Vienna, Austria, 2018; p. 22.
42. Bagarello, V.; Castellini, M.; Iovino, M. Influence of the Pressure Head Sequence on the Soil Hydraulic Conductivity Determined With Tension Infiltrometer. *Appl. Eng. Agric.* **2005**, *21*, 383–391. [CrossRef]
43. Matula, S.; Miháliková, M.; Lufinková, J.; Bát'ková, K. The role of the initial soil water content in the determination of unsaturated soil hydraulic conductivity using a tension infiltrometer. *Plant Soil Environ.* **2016**, *61*, 515–521. [CrossRef]
44. ÖNORM L 1065:2006-12-01. *Physikalische Bodenuntersuchungen—Bestimmung der hydraulischen Leitfähigkeit in gesättigten Zylinderproben*; Austrian Standards: Vienna, Austria, 2006.
45. METER Group Inc. *WP4C Dew Point PotentiaMeter*, version ju ed.; METER Group Inc.: Pullman, WA, USA, 2017.
46. Simunek, J.; Sejna, M.; Saito, H.; Sakai, M.; van Genuchten, M. *The HYDRUS-1D Software Package for Simulating the One-Dimensional Movement of Water, Heat, and Multiple Solutes in Variably-Saturated Media*, version 4.08; HYDRUS Software Series 3; Department of Environmental Science, University of California: Riverside, CA, USA, 2009; p. 332.
47. Karaboga, D. *An Idea Based on Honey Bee Swarm for Numerical Optimization*; Technical Report TR06; Erciyes University: Melikgazi/Kayseri, Turkey, 2005; p. 10,
48. Vega Yon, G.; Munoz, E. ABCoptim: An Implementation of the Artificial Bee Colony (ABC) Algorithm. Technical Report. 2017. Available online: https://cran.r-project.org/web/packages/ABCoptim/ABCoptim.pdf (accessed on 2 August 2018) .
49. Peters, A.; Durner, W. *SHYPFIT 2.0 User's Manual*; Technical Report June; Institut für Ökologie, Technische Universität Berlin: Berlin, Germany, 2015.
50. Bezerra-Coelho, C.R.; Zhuang, L.; Barbosa, M.C.; Soto, M.A.; Genuchten, M.T.V. Further tests of the HYPROP evaporation method for estimating the unsaturated soil hydraulic properties. *J. Hydrol. Hydromech.* **2017**, *66*, 161–169. [CrossRef]
51. Feddes, R.; Kowalik, P.; Zaradny, H. *Simulation of Field Water Use and Crop Yield*; Pudoc: Wageningen, The Netherlands, 1978.
52. R Core Team. *R: A Language and Environment for Statistical Computing*; R Foundation for Statistical Computing: Vienna, Austria, 2016.
53. Tukey, J.W. Comparing Individual Means in the Analysis of Variance. *Biometrics* **1949**, *5*, 99. [CrossRef] [PubMed]
54. De Mendiburu, F. Agricolae: Statistical Procedures for Agricultural Research. R Package Version 1.2-4. 2016. Available online: https://lair.ownr.io/ui/cran/p/agricolae/src (accessed on 2 August 2018) .
55. Soil Science Society of America. In *Glossary of Soil Science Terms*; SSSA: Madison, WI, USA, 2008.
56. Schelle, H.; Heise, L.; Jänicke, K.; Durner, W. Water retention characteristics of soils over the whole moisture range: A comparison of laboratory methods. *Eur. J. Soil Sci.* **2013**, *64*, 814–821. [CrossRef]
57. Werisch, S.; Grundmann, J.; Al-Dhuhli, H.; Algharibi, E.; Lennartz, F. Multiobjective parameter estimation of hydraulic properties for a sandy soil in Oman. *Environ. Earth Sci.* **2014**, *72*, 4935–4956. [CrossRef]
58. Dettmann, U.; Bechtold, M.; Frahm, E.; Tiemeyer, B. On the applicability of unimodal and bimodal van Genuchten-Mualem based models to peat and other organic soils under evaporation conditions. *J. Hydrol.* **2014**, *515*, 103–115. [CrossRef]

CSIRO PUBLISHING

Soil Research, 2019, **57**, 703–711
https://doi.org/10.1071/SR18347

Effects of tillage intensity on pore system and physical quality of silt-textured soils detected by multiple methods

Thomas Weninger[A,E], *Janis Kreiselmeier*[B,C], *Parvathy Chandrasekhar*[B,C], *Stefan Julich*[C], *Karl-Heinz Feger*[C], *Kai Schwärzel*[B], *Gernot Bodner*[D], and *Andreas Schwen*[A]

[A]Institute for Soil Physics and Rural Water Management, University of Natural Resources and Life Sciences, Muthgasse 18, 1190 Vienna, Austria.
[B]UNU Institute for Integrated Management of Material Fluxes and of Resources (UNU-FLORES), United Nations University, 01067 Dresden, Germany.
[C]Institute of Soil Science and Site Ecology, Faculty of Environmental Sciences, TU Dresden, 01737 Tharandt, Germany.
[D]Division of Agronomy, Department of Crop Sciences, University of Natural Resources and Life Sciences, Vienna, Konrad Lorenz-Straße 24, 3430 Tulln, Austria.
[E]Corresponding author. Email: thomas.weninger@boku.ac.at

Abstract. Understanding the effects of agricultural management practices on soil functionality is an ongoing challenge in environmental science and agricultural practice. In the present study we quantified the effects of changes in tillage intensity on soil physical quality and pore size distribution after 6, 10 and 23 years. At three long-term tillage experimental sites in central Europe we analysed soils under four different soil management systems: conventional mouldboard tillage; chiselling + rotary harrow; rotary harrow; and no till. These treatments differed in mechanical intensity and depth. Pore size distributions were calculated from soil water retention curves based on high-resolution measurements. Subsequently, fractions of functional pore size classes and indicators of soil physical quality were determined and compared between the treatments. In addition, we evaluated the performance of two calculation approaches for pore size distribution: (1) fitting of a smoothing cubic spline; and (2) a bimodal van Genuchten function. The parametric function yielded a higher proportion of storage pores by approximately 3–5%. The combination of multiple measurement and evaluation methods enabled detailed comparison of soil physical characteristics between different tillage treatments. No-till soils showed a distinct lack of transmissive pores and higher bulk density, but similar plant-available water capacity, compared with the other treatments. Under all soil management systems, aeration deficits were observed, emphasising the high vulnerability for compaction of silt-dominated arable soils with a low organic matter content. Hence, the design of agricultural soil management strategies on such soils needs to consider the risks of compaction as thoroughly as erosion or chemical degradation.

Additional keywords: high-resolution measurements, hydraulic soil properties, pore size distribution, soil degradation, soil management.

Received 23 November 2018, accepted 29 April 2019, published online 1 July 2019

Introduction

Pores, with their considerable different sizes and shapes, are the reaction zone of soil (Gupta *et al*. 2008). The soil pore size distribution (PSD), which is the fraction of distinct pore sizes in the whole pore system, determines the functionality of soil. This functionality is essential for civilisation and ensures the production of food, the cleaning of waste water or the storage of water and carbon. Especially valuable in times of changing climate and increasing demands on soil and water resources is the ability of soil to store water. Consequently, the loss of functional soil pore space, more generally physical soil degradation, is an actual global threat (Lal 2000; Eswaran *et al*. 2001; Commission of the European Communities 2006). Agriculturally used soils are most vulnerable and need to be protected and regenerated by adapted soil management strategies (FAO 2017).

The soil pore system is a combination of textural and structural pores (Lal and Shukla 2004). The former are generic voids between primary soil particles, whereas the latter originate from secondary soil formation processes, like aggregation, shrinking–swelling, freezing–thawing or biological activity. Of these two subsystems, only structure can be changed by soil management in order to improve the functionality of the soil, especially with a focus on water (Rabot *et al*. 2018). In arable land, optimisation of the tillage regime is thought of as means of improving soil structure. Hydrological and physical soil properties that are affected by tillage include water storage capacity, hydraulic conductivity or aggregate stability. However, for a meaningful evaluation of the advantages and restrictions of different tillage intensities, appropriate methods are needed that allow detailed analysis of the soil pore system and its functionality. Commonly used methods are either direct measurements from images, obtained from computed tomography (Grevers *et al*. 1989; Anderson and Hopmans 2013) or thin sections (Kubiena 1938; Elliot and Heck 2007), or indirect derivation from the soil water retention curve (SWRC; the relationship between soil water head h and volumetric water content θ) via the law of capillarity (e.g. Lal and Shukla 2004). The direct methods allow only analysis of the macropore system on reasonably sized samples due to limits in resolution (Schlüter *et al*. 2018). Nevertheless, a broad understanding of processes can be derived from such images, including the shapes of pores, organic particles and similar characteristics. The informative value of quantitative image analysis is highly dependent on methodological aspects such as resolution and image analysis algorithms (Anderson and Hopmans 2013). Conversely, indirect methods are based on model simplifications, which may imply uncertainty in the outcomes of soil physical studies (Kutilek 2004; Tuller and Or 2004). Indirect methods are commonly used at larger scales because they do not require expensive instruments and are less time consuming than direct methods. The results of such measurements provide valuable quantitative information about the effects of certain processes on linked soil functions and can be used directly for soil physical modelling.

The effects of different soil and land management strategies on soil pore characteristics and soil hydraulic properties have been the subject of extensive research (Horel *et al*. 2015; Schjønning *et al*. 2017; Blanco-Canqui and Ruis 2018). Different results have been reported as a consequence of tremendous variability in climate, soil texture and differences in soil management systems. Pires *et al*. (2017) characterised changes in the pore system of no-till (NT) and conventionally tilled (CT) soils using three-dimensional microscale computed tomography, micromorphological analyses of thin sections of impregnated blocks and indirect determination of PSD via the SWRC and fitting of a cubic spline. On clay soil in subtropical climate, Pires *et al*. (2017) found a larger, more complex pore system after 26 years of NT, supposedly caused by higher biological activity than under CT. In another study, only minor beneficial effects of NT were shown by Wairiu and Lal (2006), who used mercury porosimetry to detect PSD in two 38-year-old tillage experiments on silt loam. In contrast, Peña-Sancho *et al*. (2017) found lower porosity and a lack of macropores under NT as well as considerable seasonal variability in PSD under CT and reduced tillage (RT) on loam soil (23-year tillage experiment; SWRC derived from pressure plate apparatus). Kodesova *et al*. (2011) characterised macropore structure ($h > -70$ cm) under CT and 30 years grass coverage by inverse simulation of a multistep outflow experiment and micromorphological images of thin sections. Grassland soils, as an extreme case of NT, had more capillary pores and matrix pores than soils under CT. Similarly, Schwen *et al*. (2011) analysed the macroporosity of a silt loam in eastern Austria by inversely simulated tension infiltrometer experiments, finding found higher conductivity after 11 years of NT due to highly connective and less tortuous macropores compared with CT and RT, whereas CT and RT showed high seasonal variability in soil physical properties.

More generally, the review by Horel *et al*. (2015) summarised changes in soil hydraulic properties after a change in land use or soil management. As a main outcome, Horel *et al*. (2015) stated that negative effects, such as a decrease in plant-available water, increased bulk density and loss of soil organic matter, may be expected with intensifications in soil disturbance. The transformation of soil properties after a change in soil management strategies may last for several years or decades, especially on heavily textured soils. Nevertheless, Horel *et al*. (2015) also concluded that robust statements about the effects of distinct management strategies on the physical properties of soils are hampered by inconsistencies in scientific and agricultural methodology or the heterogeneity of soil.

Similarly, the analytical methodology used in the studies cited above is often not consistent. To achieve continuous results over the whole soil moisture range, a mathematical function needs to be approximated to measurements on the SWRC. To this end, two different approaches are primarily used: (1) a parametric function with the aim of condensing the information into a preferably small number of parameters; or (2) an interpolation via more complex functions, like a cubic spline defined by a vast number of parameters (Othmer *et al*. 1991). The latter method has the advantage of yielding approximations closer to measurements, and consequently allows a more precise interpretation of the resulting PSD. In contrast, parametric functions are the standard way to input soil physical properties into simulation models for soil water dynamics. Commonly, simple S- or C-shaped functions are fitted to the data. However, most soils show a more complex PSD, and the lack of flexibility in the function used may cause low goodness of fit and hamper the interpretation of differences between certain treatments (Durner 1994; Lozano *et al*. 2016). Hence, bi- or multimodal parametric functions are increasingly being used (Romano and Nasta 2016; Reynolds 2017). In this study we compared the two approaches using data measured by the evaporation method (Schindler *et al*. 2010) combined with dewpoint hygrometry (Campbell *et al.* 1973). We examined whether the choice of approximation scheme affects statements about soil physical quality (SPQ; Reynolds *et al*. 2009) and fractions of functional pore sizes (Lal and Shukla 2004), both of which were derived from the PSD.

The main objective of the present study was to quantify the changes in PSD in arable fields after a conversion from mouldboard ploughing to conservation tillage or NT. Consequently, the findings of the study would add information to the incomplete picture about the implications of different-intensity tillage strategies on the physical constitution of soil. The experimental locations were representative of silt-dominated arable soils under a temperate climate, which account for the biggest part of crop production in central Europe. To obtain highly informative and valuable results we applied a unique combination of different high-resolution measurement methods and evaluation approaches.

Materials and methods

Sampling sites and procedure

Soil sampling and experiments took place at three long-term tillage trials in north-eastern Austria and Saxony, Germany (Table 1). Four different tillage treatments had been established on the fields for 6, 10 and 23 years: (1) CT with a mouldboard plough and rotary harrow; (2) RT with a chisel plough and rotary harrow; (3) minimal tillage (MT) using only a rotary harrow; and (4) NT with a direct seeder. Intensive tillage operations (mouldboard and chisel plough) were conducted after harvest; before seeding of the subsequent cash crop, only the rotary harrow or direct seeder were used. Undisturbed soil samples were collected in steel cores (250 cm^3; inner diameter 8.4 cm, height 5 cm) at the soil surface, as were disturbed samples adjacent to the cores. Sampling was conducted between three and five times at the three sites throughout the vegetation period in 2016 (Table 2). Volumetric water content, θ, before sampling was between 0.20 and 0.35 cm^3 cm^{-3}; hence, the soil was neither near saturation nor were drying cracks present on the soil surface, and the sampling points were placed in inter-row spaces to avoid machine tracks.

Measurement methods

The data for the retention curves (data pairs of θ and *h*) were obtained using the evaporation method and a HYPROP device (METER Group, Munich, Germany; Schindler *et al*. 2010) and a dew point hygrometer (WP4C PotentiaMeter; METER Group). In addition, hood infiltrometer (Schwärzel and Punzel 2007) experiments were conducted to measure hydraulic conductivity in the near-saturated range, bulk density was measured by oven drying (105°C, 24 h) of 250-cm^3 core samples and saturated hydraulic conductivity was measured in the laboratory using the falling head method (Reynolds and Elrick 2002). The sampling and measurement procedures have been described in detail elsewhere (Weninger *et al*. 2018). Failure in one of the methods used was inevitable in single cases, and in such cases data from the whole respective dataset (i.e. sampling point) had to be excluded from further analyses. This explains the discrepancy between maximum possible data extent calculated from Table 2 and actual data extent in Table 3.

Data processing and statistics

Retention curves for each experimental plot were approximated to measured data using two different approaches: a cubic spline and a bimodal van Genuchten (bVG) function (Othmer *et al*. 1991). First, values for soil water head *h* were transformed to pF values (pF = $\log_{10}(h)$). The density of data points over the pF range was very heterogeneous, hence data were classified with a class width of 0.2 pF to balance weights of measurements. The means of all data inside the respective classes were used as nodes for the fitting. The high flexibility of the cubic spline led to implausible oscillations in the resulting curve in the transition zone between the measurement ranges of the two combined methods. Consequently, we used a smoothing cubic spline (sCUB) to balance these irregularities (R Core Team 2016; smoothing parameter = 0.5). The fitting yielded two continuous functions (sCUB and bVG) for each sampled point, which were used to predict θ for the centres of pF classes (width 0.2, as above). Subsequently, the predicted class centre

Table 1. Descriptions of study sites

Texture classification was as follows: 2 mm > sand ≥ 0.063 mm > silt ≥ 0.002 mm > clay (British Standards Institution 2018). WRB, World Reference Base

	Site A	Site B	Site C
Location name	Lüttewitz (Germany)	Hollabrunn (Austria)	Obersiebenbrunn (Austria)
Crop	Winter wheat	Winter wheat	Sunflower
Soil texture (sand/silt/clay; g g^{-1})	0.03/0.78/0.19	0.24/0.55/0.21	0.34/0.50/0.16
Soil type (WRB)	Luvisol	Chernozem	Chernozem
Mean annual precipitation (mm)	650	520	520
Mean annual temperature (°C)	8.5	9.0	9.4
Altitude (m above sea level)	270	235	150
Soil organic carbon[A] (g kg^{-1})	10–20	10–20	10–20
Year tillage experiment established	1993	2006	2010

[A]Values for soil organic carbon were derived in several campaigns over recent years (Bodner G, Weninger T, unpubl. data); thus, the values are not results of the present study and a range is given.

Table 2. Data composition

Treatments, in order of decreasing tillage intensity, are conventional tillage (CT), reduced tillage (RT), minimal tillage (MT) and no tillage with direct seeding (NT). Site A is in Lüttewitz (Germany), Site B is in Hollabrunn (Austria) and Site C is in Obersiebenbrunn (Austria)

	Site A	Site B	Site C
Treatments	CT, RT, MT, NT	CT, RT, MT, NT	CT, RT, MT, NT
No. measurement campaigns	5	3	4
No. treatment replicates per campaign	5 for all	3, 11, 3	11, 3, 3, 3

Table 3. Selected soil physical properties measured at three long-term tillage trials in Lüttewitz, Germany (Site A), Hollabrunn, Austria (Site B) and Obersiebenbrunn, Austria (Site C)

Within each site, different letters in the 'Group' column indicate significant differences among treatments (Tukey's HSD test, $P = 0.05$). For a detailed description of each of the sites, see Table 1. n, number of observations; $K_{s(FH)}$, saturated hydraulic conductivity (cm day^{-1}) measured by the falling head laboratory method; $K_{s(HI)}$, is saturated conductivity (cm day^{-1}) measured by a hood infiltrometer; CT, conventional tillage; RT, reduced tillage; MT, minimal tillage; NT, no tillage and direct seeding

Site	Treatment	n	$\log_{10}(K_{s(FH)})$			$\log_{10}(K_{s(HI)})$			Bulk density (g cm^{-3})			Porosity (cm^3 cm^{-3})		
			Mean	CV	Group	Mean	CV	Group	Mean	CV	Group	Mean	CV	Group
A	CT	25	2.55	0.30	a	2.81	0.15	a	1.30	0.06	a	0.509	0.06	a
	RT	16	3.45	0.04	b	3.03	0.11	b	1.14	0.08	b	0.570	0.06	b
	MT	19	2.61	0.25	a	3.02	0.15	ab	1.29	0.06	a	0.514	0.06	a
	NT	19	2.63	0.26	a	2.64	0.11	a	1.34	0.05	a	0.494	0.05	a
B	CT	17	3.11	0.27	a	2.78	0.18	a	1.27	0.07	a	0.520	0.07	a
	RT	14	3.39	0.24	a	2.73	0.13	a	1.27	0.08	a	0.520	0.07	a
	MT	18	2.52	0.41	a	2.61	0.13	a	1.34	0.06	a	0.494	0.06	a
	NT	16	2.58	0.45	a	2.49	0.18	a	1.51	0.04	b	0.429	0.05	b
C	CT	20	2.85	0.26	ab	2.27	0.18	ab	1.30	0.07	a	0.510	0.06	a
	RT	11	3.18	0.20	a	2.42	0.11	a	1.26	0.05	a	0.526	0.05	a
	MT	20	2.90	0.24	ab	2.52	0.10	a	1.25	0.06	a	0.529	0.05	a
	NT	20	2.37	0.36	b	2.05	0.16	b	1.40	0.04	b	0.471	0.04	b

Table 4. Soil physical parameters and indicators for soil physical quality evaluated

Abbreviation	Description
$K_{s(FH)}$	Saturated hydraulic conductivity, measured by the falling head laboratory method (units used herein: cm day^{-1})
$K_{s(HI)}$	Field-saturated hydraulic conductivity measured by a hood infiltrometer (cm day^{-1})
ρ_d	Bulk density from oven drying of soil core samples of a defined volume (g cm^{-3})
P	Porosity; volume of pores divided by the total, undisturbed volume (cm^3 cm^{-3}), calculated as follows: $1 - \rho_d/2.65$
PAWC	Plant-available water capacity (cm^3 cm^{-3}); water volume stored between h = 100 cm and h = 15 000 cm
AC	Air capacity (cm^3 cm^{-3}); air-filled pore volume at h = –100 cm
RFC	Relative field capacity (cm^3 cm^{-3}), calculated as 1 – (AC/P)

values of all corresponding replicates (same site and treatment) were pooled (the sample size at this point is given in Table 3, column n) and the mean, s.d. and CV were calculated and analysed.

Three different outcomes were used to evaluate the results: (1) graphical interpretation of curves; (2) classification into functional pore size classes after Greenland (1981); and (3) capacity-based indicators for soil physical quality (Reynolds *et al*. 2009). For the graphical interpretation of curves, water content data (predicted as described above) was normalised by the maximum observed water content, θ_{max} (approximation for saturated water content, θ_s), yielding effective saturation, $S_e(h)$. Results for the same site and treatment were averaged and plotted together with the first derivative of $S_e(h)$, which corresponds to the PSD.

For the second and third outcomes, absolute values for θ were used and the conversion between soil water head h on the retention curve and the corresponding pore diameter was made using the simplified capillary equation $h = 1490r^{-1}$ (where h is soil water head (cm) and r is the equivalent pore radius (μm)). Following Greenland (1981), pores with a calculated diameter >500 μm were classified as fissures, those with diameters between 50 and 500 μm were classified as transmissive pores, those with diameters between 0.5 and 50 μm were classified as storage pores, those with diameters between 0.005 and 0.5 μm were classified as residual pore, and those with a diameter <0.005 μm were classified as bonding pores. The predicted values for the borders of classes were interpolated, the fractions of pore volume in the different pore classes were calculated and the results for the same site and treatment were averaged and analysed statistically for differences between treatments. For the third evaluation approach, soil physical parameters and capacity-based indicators for SPQ (Reynolds *et al*. 2009) were calculated according to Table 4. The selected indicators are widely used for interpretation of SPQ and ensure comparability to similar studies.

All data was processed using R version 3.3.1 (R Core Team 2016). Normality or log-normality of selected results for comparison of treatment effects was tested by visual interpretation of Q–Q plots. Saturated hydraulic conductivity values derived by falling head laboratory method ($K_{s(FH)}$) and in the field by hood infiltrometer experiments ($K_{s(HI)}$) were represented best by a log-normal distribution; other metrics followed a normal distribution. The significance of differences between treatments was analysed by analysis of variance (ANOVA), with Tukey's honestly significant difference (HSD) test used as post hoc test to define coherent groups (de Mendiburu 2016). A paired t-test was used to detect significant differences between results derived by the two approximation approaches.

Results and Discussion

Effects of tillage intensity on physical soil conditions

Results of measured soil physical properties are given in Table 3, and SPQ indicators calculated from the retention curve are given in Table 5. $K_{s(FH)}$ and $K_{s(HI)}$ enable inference of the presence of connective macropores (fissures and transmission pores according to the classification used) because the water flow measured predominantly occurs through these pores. No consistent differences between treatments were found, but most of the lowest conductivities were found under NT systems and highest conductivities under the RT and MT systems (Table 3). These findings are in agreement with the review of Blanco-Canqui and Ruis (2018), who did not find systematic effects of tillage on saturated hydraulic conductivity. Nevertheless, Blanco-Canqui and Ruis (2018) identified more distinct differences for infiltration capacity, which was highest under NT. Furthermore, NT soils showed higher values of bulk density, ρ_d, than other treatments at two of the three sites (Table 3), which is in accordance with 24 of 62 available studies reviewed by Blanco-Canqui and Ruis (2018). However, in medium-textured soils (the term used in comparison with sandy and clayey or fine-textured soil by Blanco-Canqui and Ruis 2018, hence comparable to the soils sampled herein), 18 of 24 studies reviewed by Blanco-Canqui and Ruis (2018) found significantly higher ρ_d under NT. This agreed with the fact that medium-textured or silt-dominated soils are especially vulnerable to compaction by clogging of pores (Horn *et al*. 1995). In the present study results, air capacity (AC) was also distinctly lower under NT, whereas plant-available water capacity (PAWC) was in the same range as for all other treatments. In contrast, no systematic limitations in AC under NT were found by Reynolds *et al*. (2009), who analysed 13 soils containing less silt, and Lozano *et al*. (2016) on an Argentinian loam with soil organic carbon (SOC) content of 40–56 g kg^{-1}. Consequently, higher SOC content could decrease the vulnerability of the sampled soils to compaction, and an improvement may be expected after a longer period of NT management (Murphy 2015; Blanco-Canqui and Ruis 2018).

Classifying SPQ indicators in terms of their agricultural usability (Reynolds *et al*. 2009) showed that, regardless of treatment, all soils sampled except one (ρ_d = 1.14 g cm^{-3}) had too-high ρ_d, with values ranging from 1.25 to 1.51 g cm^{-3} (Table 3; the optimal ρ_d range for loamy soils is between 0.9 and 1.2 g cm^{-3}; Reynolds *et al*. 2009). Similarly, results for relative field capacity (RFC) were between 0.724 and 0.900 cm^3 cm^{-3} (except for one soil, in which RFC was 0.673 cm^3 cm^{-3}), indicating potential yield losses due to a lack of aeration (Table 5; the optimal RFC range is between 0.6 and 0.7 cm^3 cm^{-3}). Results for AC followed the same trend even though the variability between treatments and sites was higher, and certain soils could be denoted as optimal (>0.14 m^3 m^{-3}), whereas in others aeration was poor (<0.10 m^3 m^{-3}). The PAWC was at least 0.203 m^3 m^{-3}, hence ideal in all soils (optimal range >0.20 m^3 m^{-3}). This may also be explained by the high fraction of silt together with low organic matter content (e.g. Horn *et al*. 1995).

Pore size distribution

All SWRCs and their derived PSDs are compared in Figs 1 and 2. Interpretations were based on sCUB (Fig. 1) because it represented measured data better than bVG. The most intensive treatment CT showed a distinct bimodal character for PSD at all sites. In all three tillage experiments there was an obvious difference between NT and all other treatments, which showed a mode (peak) in the range of transmissive or course

Table 5. Soil physical quality indicators calculated from retention curves for the three sites in Lüttewitz, Germany (Site A), Hollabrunn, Austria (Site B) and Obersiebenbrunn, Austria (Site C)

Within each site, different letters in the 'Group' column indicate significant differences among treatments (Tukey's HSD test, P = 0.05). For a detailed description of each of the sites, see Table 1. AC, air capacity; PAWC, plant-available water capacity; RFC, relative field capacity; VG, bimodal van Genuchten model; CT, conventional tillage, RT, reduced tillage; MT, minimal tillage; NT, no tillage and direct seeding

	PAWC (cm^3 cm^{-3})						AC (cm^3 cm^{-3})						RFC (cm^3 cm^{-3})						Relative difference of means (VG – spline)		
	Cubic spline			VG			Cubic spline			VG			Cubic spline			VG					
	Mean	CV	Group	Mean	CV	Group	Mean	CV	Group	Mean	CV	Group	Mean	CV	Group	Mean	CV	Group	PAWC	AC	RFC
Site A																					
CT	0.286	0.09	a	0.299	0.12	ab	0.089	0.43	a	0.079	0.59	a	0.827	0.08	a	0.847	0.10	a	0.013	–0.010	0.020
RT	0.320	0.12	b	0.339	0.16	c	0.126	0.41	b	0.114	0.58	a	0.780	0.11	a	0.802	0.13	a	0.019	–0.012	0.022
MT	0.259	0.16	c	0.276	0.18	a	0.104	0.43	ab	0.095	0.62	a	0.801	0.10	a	0.820	0.13	a	0.017	–0.009	0.019
NT	0.298	0.08	ab	0.325	0.07	bc	0.052	0.43	c	0.031	0.62	b	0.897	0.05	b	0.938	0.04	b	0.027	–0.020	0.041
Site B																					
CT	0.223	0.15	ab	0.238	0.17	ab	0.174	0.38	a	0.162	0.43	a	0.673	0.16	a	0.695	0.17	a	0.015	–0.011	0.022
RT	0.243	0.14	a	0.259	0.18	a	0.132	0.35	ab	0.121	0.43	ab	0.750	0.10	b	0.770	0.12	ab	0.016	–0.011	0.020
MT	0.244	0.06	a	0.254	0.07	a	0.103	0.32	b	0.099	0.34	b	0.793	0.07	b	0.803	0.07	b	0.009	–0.005	0.009
NT	0.203	0.13	b	0.219	0.17	b	0.054	0.46	c	0.046	0.66	c	0.876	0.07	c	0.893	0.08	c	0.015	–0.008	0.018
Site C																					
CT	0.246	0.09	a	0.270	0.13	ab	0.143	0.33	a	0.118	0.49	a	0.724	0.11	a	0.773	0.13	a	0.023	–0.024	0.049
RT	0.263	0.06	ab	0.298	0.10	a	0.134	0.25	a	0.099	0.44	a	0.748	0.08	a	0.814	0.09	a	0.035	–0.035	0.066
MT	0.271	0.06	b	0.263	0.15	b	0.134	0.35	a	0.115	0.52	a	0.750	0.11	a	0.786	0.13	a	–0.008	–0.019	0.036
NT	0.255	0.08	ab	0.287	0.10	ab	0.074	0.32	b	0.044	0.63	b	0.843	0.06	b	0.908	0.06	b	0.032	–0.031	0.065
																		Mean	0.017	–0.016	0.032

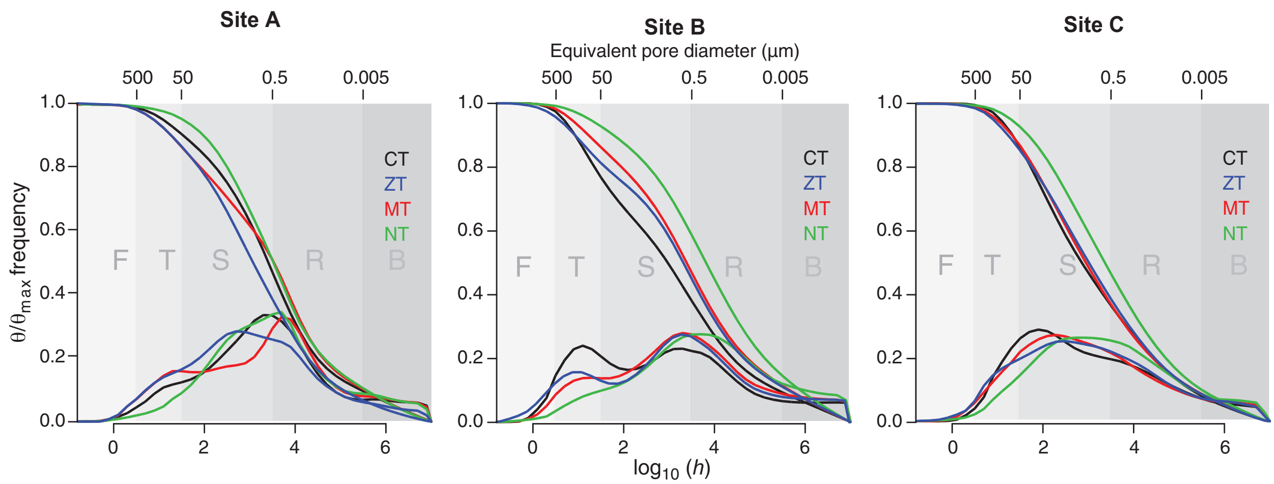

Fig. 1. Relative soil water retention curves (lines starting from 1.0) and deviated pore size distributions (lines starting at 0.0) derived by fitting a smoothing cubic spline for different treatments (CT, conventional tillage; RT, reduced tillage; MT, minimal tillage; NT, no tillage and direct seeding) at Site A (Lüttewitz, Germany), Site B (Hollabrunn, Austria) and Site C (Obersiebenbrunn, Austria). Different shades of grey indicate functional pore size classes (Greenland 1981), as follows: F, >500 µm (fissures); T, 50–500 µm (transmission pores; important for water movement and gas exchange); S, 0.5–50 µm (storage pores; retention against percolation); R, 0.005–0.5 µm (residual pores; retention and diffusion of ions in solution); B, <0.005 µm (bonding pores). Soil water head, *h*, was measured in centimetres. θ, volumetric water content; θ_{max}, maximum observed water content.

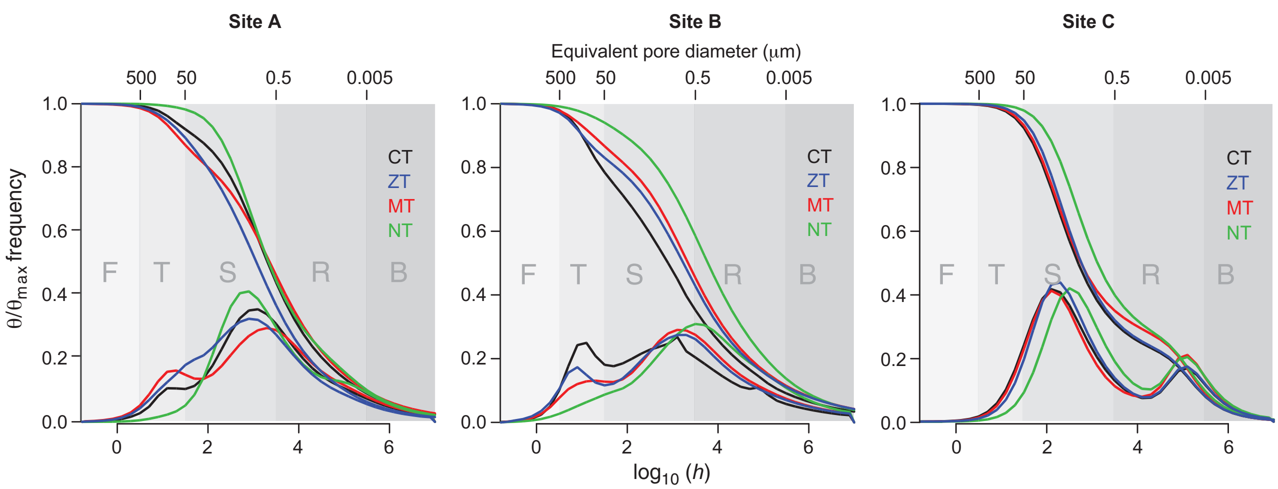

Fig. 2. Relative soil water retention curves (lines starting from 1.0) and deviated pore size distributions (lines starting at 0.0) derived by fitting of a bimodal van Genuchten function for different treatments (CT, conventional tillage; RT, reduced tillage; MT, minimal tillage; NT, no tillage and direct seeding) at Site A (Lüttewitz, Germany), Site B (Hollabrunn, Austria) and Site C (Obersiebenbrunn, Austria). Different shades of grey indicate functional pore size classes (Greenland 1981), as follows: F, >500 µm (fissures); T, 50–500 µm (transmission pores; important for water movement and gas exchange); S, 0.5–50 µm (storage pores; retention against percolation); R, 0.005–0.5 µm (residual pores; retention and diffusion of ions in solution); B, <0.005 µm (bonding pores). Soil water head, *h*, was measured in centimetres. θ, volumetric water content; θ_{max}, maximum observed water content.

storage pores. This mode was not present in the NT treatment, which was surprising because NT was expected to have more biologically built macropore, such as earthworm burrows or decayed roots (e.g. Wairiu and Lal 2006; Schwen *et al.* 2011; Alvarez *et al.* 2014). Fig. 3 shows quantitative comparison of pore volume belonging to functional pore size categories. On average, NT soils had 0.082 m^3 m^{-3} less transmission pores than the other treatments (referring to total pore volume; s.d. = 0.095). In contrast, the NT treatment was richer in residual pores. Results from comparable studies using a coarser, size-based classification were variable without a uniform trend (Blanco-Canqui and Ruis 2018). In contrast with the present study, significantly lower fractions of storage and transmission pores were found in CT than in several types of conservation tillage by Pagliai *et al.* (2004) and Abdollahi and Munkholm (2017).

The variability between PSD curves of the same treatment was exceptionally low, as evidenced by the resulting indicators for SPQ (Table 5) and functional pore size classification (Fig. 3). Especially for CT, we expected comparably higher temporal variability due to seasonal changes (e.g. Tebrügge and Düring 1999; Kargas *et al.* 2016; Soracco *et al.* 2018). Most

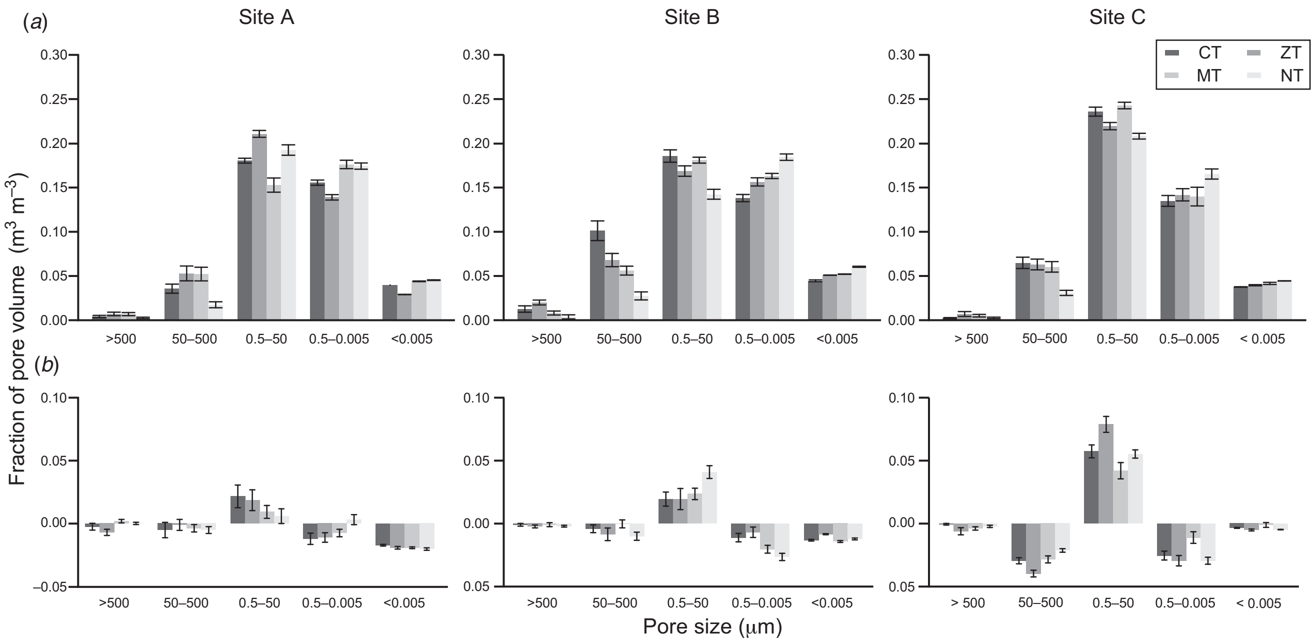

Fig. 3. (*a*) Pore size volume fractions in functional pore size classes relative to total bulk volume for different treatments (CT, conventional tillage; RT, reduced tillage; MT, minimal tillage; NT, no tillage and direct seeding) at Site A (Lüttewitz, Germany), Site B (Hollabrunn, Austria) and Site C (Obersiebenbrunn, Austria). Class boundaries were detected by interpolation using smoothing cubic splines. (*b*) Corresponding differences between pore size volume fractions obtained using cubic spline fitting and the bimodal van Genuchten model for soil water retention curves (positive results indicate a higher value obtained using cubic spline fitting). Functional pore sizes were classified as follows: >500 μm, fissures; 50–500 μm, transmission pores (important for water movement and gas exchange); 0.5–50 μm, storage pores (retention against percolation); 0.005–0.5 μm, residual pores (retention and diffusion of ions in solution); <0.005 μm, bonding pores. Data show the mean ± s.d.

likely the low variability between single samples within the same treatment resulted from the normalisation with θ_{max}. Consequently, in future studies measurements will be adapted and extended to analyse the seasonal variability of the characteristics examined for multiple vegetation periods. The focus of the present study was on long- and mid-term changes (6, 10, 23 years) of soil physical conditions due to different tillage intensity, and the low variability during the sampled period strengthens the results and interpretations.

Effects of fitting procedure

Soil physical parameters derived from retention curves can be affected by the type of fitting procedure applied to the measured $\theta(h)$ data points. We tested two different approaches to derive continuous retention curves and quantified the differences in the evaluation metrics (Table 5). The differences were significant for all indicators, as analysed by paired *t*-tests ($\alpha = 0.05$). Using bVG rather than sCUB resulted in an overestimation of PAWC and an underestimation of AC of <2%, whereas RFC was overestimated by approximately 3%. This resulted in a higher proportion of samples where AC was classified as poor. In contrast, the resulting classification of PAWC (ideal) and RFC (potentially lacking aeration) did not differ between the two approaches. The fitting of the bVG function yielded a higher variability in SPQ metrics that was the result of lower goodness of fits compared with the more flexible and data-driven sCUB (Othmer *et al*. 1991; Kastanek and Nielsen 2001). Nevertheless, the effective differences between the two approaches after pooling replicate data were distinctively smaller than on single measurements as reported by Othmer *et al*. (1991). Hence, appropriate replication increases the possibility of detecting differences in PSD or SPQ between certain soil management regimes also using the less flexible parametric function (bVG). Bimodal functions should be used, because the lack of flexibility in unimodal functions may hamper the detection of such differences in certain soils (Lozano *et al*. 2016).

The most distinct differences between retention curves derived by the two different functions were visible at Site C (Obersiebenbrunn, Austria). There, bVG exhibited clear bimodality with a second mode in the range of residual pores (Fig. 2). The sCUB at Site C followed an irregular unimodal shape, whereas other sites were more similar to bimodality (Fig. 1). This may be interpreted as tendency of bVG to yield poor fits to irregularly shaped retention data because there is a certain probability that a second mode is detected even if it is not fully supported by measurements. This is in contrast with the results of Romano and Nasta (2016), who found benefits in using bimodal functions even for weakly bimodal PSD. Fig. 3*b* again shows that using the parametric bVG function overestimated storage pores, which determine PAWC, compared with sCUB. However, considerable differences regarding larger pores responsible for aeration were only found at Site C, where the overall pattern showed least bimodality in pore size distribution.

Conclusions and relevance

The use of a cubic spline function was found to be preferable to the parametric bVG model due to higher flexibility, especially for irregularly shaped data. We also found significant differences between the two approaches when used as a basis for a functional classification of the soil pore system.

The soils analysed were silt dominated and showed a lack of aeration, whereas water capacity was optimal. The higher bulk density of the NT system compared with the other tillage treatments was primarily related to a lower fraction of large, aerated pores. Graphical representation of PSD revealed this lack of transmissive pores in NT soils, whereas NT soils had higher PAWC. Additional analysis of indicators for SPQ confirmed these interpretations, and low organic matter content increased the vulnerability of the soil to compaction. Although silt-dominated soils are most endangered by erosion and thus target sites for RT systems, a loss of aeration has to be controlled to avoid adverse conditions for root aeration, plant growth and consequently yield. The results presented herein are representative of a significant portion of the agricultural soils in central Europe, and the methodology allows sound and detailed interpretations. Future advances in modelling of changes in soil pore systems based on such results will improve the opportunities for the development of sophisticated agricultural management strategies.

Conflicts of interests

The authors declare no conflicts of interest.

Acknowledgements

The authors thank the administration of agricultural schools in the province of Lower Austria for supporting the field experiments and providing meteorological data. The Austrian part of this project was funded by the Austrian Science Fund (FWF; I2122-B16) and the German part of the study was funded by the Deutsche Forschungsgemeinschaft DFG (SCHW 1448/6-1, FE 504/11-1).

References

Abdollahi L, Munkholm LJ (2017) Eleven years' effect of conservation practices for temperate sandy loams: II. Soil pore characteristics. *Soil Science Society of America Journal* **81**, 392–403. doi:10.2136/sssaj2016.07.0221

Alvarez CR, Taboada MA, Perelman S, Morrás HJM (2014) Topsoil structure in no-tilled soils in the Rolling Pampa, Argentina. *Soil Research* **52**, 533–542. doi:10.1071/SR13281

Anderson SH, Hopmans JW (2013) 'Soil–Water–Root Processes: Advances in Tomography and Imaging.' SSSA Special Publication 61. (Soil Science Society of America (SSSA): Madison, WI) https://doi.org/10.2136/sssaspecpub61

Blanco-Canqui H, Ruis SJ (2018) No-tillage and soil physical environment. *Geoderma* **326**, 164–200. doi:10.1016/j.geoderma.2018.03.011

Campbell EC, Campbell GS, Barlow WK (1973) A dewpoint hygrometer for water potential measurement. *Agricultural Meteorology* **12**, 113–121. doi:10.1016/0002-1571(73)90012-5

Commission of the European Communities (2006) Communication from the Commission to the Council, the European Parliament, the European Economic and Social Committee and the Committee of the Regions: thematic strategy for soil protection. Technical report. Available at https://eur-lex.europa.eu/legal-content/EN/TXT/?uri=CELEX:52006DC0231 [verified 8 November 2018].

de Mendiburu F (2016) agricolae: statistical procedures for agricultural research. R package version 1.2–4. Available at https://cran.r-project.org/web/packages/agricolae/index.html [verified 13 June 2019].

Durner W (1994) Hydraulic conductivity estimation for soils with heterogeneous pore structure. *Water Resources Research* **30**, 211–223. doi:10.1029/93WR02676

Elliot TR, Heck RJ (2007) A comparison of optical and X-ray CT technique for void analysis in soil thin section. *Geoderma* **141**, 60–70. doi:10.1016/j.geoderma.2007.05.001

British Standards Institution (2018) BS EN ISO 14688–1:2018. Geotechnical investigation and testing – identification and classification of soil, Part 1 – identification and description.(BSI: London)

Eswaran H, Lal R, Reich PF (2001) Land degradation: an overview. In 'Responses to land degradation. Proceedings of the Second International Conference on Land Degradation and Desertification', Khon Kaen, Thailand. (Eds EM Bridges, ID Hannam, LR Oldeman, FWT Pening de Vries, SJ Scherr, S Sompatpanit) (Oxford Press: New Delhi, India)

FAO (2017) Voluntary guidelines for sustainable soil management. Available at http://www.fao.org/3/a-bl813e.pdf [verified 6 June 2019].

Greenland DJ (1981) Soil management and soil degradation. *Journal of Soil Science* **32**, 301–322. doi:10.1111/j.1365-2389.1981.tb01708.x

Grevers MCJ, de Jong E, Arnaud RJS (1989) The characterization of soil macroporosity with CT scanning. *Canadian Journal of Soil Science* **69**, 629–637. doi:10.4141/cjss89-062

Gupta RK, Abrol I, Finkl CW, Kirkham MB, Arbestain MC, Macías F, Chesworth W, Germida JJ, Loeppert RH, Cook MG, Schwag GO, Konstankiewicz K, Pytka J, Oertli JJ, Singer A, Edmonds WJ, Feng Y, Feldman SB, Shang C, Zalazny LW, Ford PW, Clothier BE (2008) Soil pores. In 'Encyclopedia of Soil Science'. (Ed. W Chesworth) pp. 693–698. (Springer: Dordrecht, Netherlands)

Horel Á, Tóth E, Gelybó G, Kása I, Bakacsi Z, Farkas C (2015) Effects of land use and management on soil hydraulic properties. *Open Geosciences* **7**, 1442–1454. doi:10.1515/geo-2015-0053

Horn R, Domzzał H, Słowinská-Jurkiewicz A, van Ouwerkerk C (1995) Soil compaction processes and their effects on the structure of arable soils and the environment. *Soil & Tillage Research* **35**, 23–36. doi:10.1016/0167-1987(95)00479-C

Kargas G, Kerkides P, Sotirakoglou K, Poulovassilis A (2016) Temporal variability of surface soil hydraulic properties under various tillage systems. *Soil & Tillage Research* **158**, 22–31. doi:10.1016/j.still.2015.11.011

Kastanek FJ, Nielsen DR (2001) Description of soil water characteristics using cubic spline interpolation. *Soil Science Society of America Journal* **65**, 279–283. doi:10.2136/sssaj2001.652279x

Kodesova R, Jirku V, Kodes V, Muhlhanselova M, Nikodem A, Žigová A (2011) Soil structure and soil hydraulic properties of Haplic Luvisol used as arable land and grassland. *Soil & Tillage Research* **111**, 154–161. doi:10.1016/j.still.2010.09.007

Kubiena W (1938) 'Micropedology.' (Collegiate Press: Ames, IA)

Kutilek M (2004) Soil hydraulic properties as related to soil structure. *Soil & Tillage Research* **79**, 175–184. doi:10.1016/j.still.2004.07.006

Lal R (2000) Physical management of soils of the tropics: priorities for the 21st century. *Soil Science* **165**, 191–207. doi:10.1097/00010694-200003000-00002

Lal R, Shukla MK (2004) 'Principles of Soil Physics.' (Marcel Dekker: New York, NY)

Lozano LA, Soracco CG, Villarreal R, Ressia JM, Sarli GO, Filgueira RR (2016) Soil physical quality and soybean yield as affected by chiseling and subsoiling of a no-till soil. *Revista Brasileira de Ciência do Solo* **40**, 1–12. doi:10.1590/18069657rbcs20150160

Murphy BW (2015) Impact of soil organic matter on soil properties – a review with emphasis on Australian soils. *Soil Research* **53**, 605–635. doi:10.1071/SR14246

Othmer H, Diekkrüger B, Kutilek M (1991) Bimodal porosity and unsaturated hydraulic conductivity. *Soil Science* **152**, 139–150. doi:10.1097/00010694-199109000-00001

Pagliai M, Vignozzi N, Pellegrini S (2004) Soil structure and the effect of management practices. *Soil & Tillage Research* **79**, 131–143. doi:10.1016/j.still.2004.07.002

Peña-Sancho C, López M, Gracia R, Moret-Fernández D (2017) Effects of tillage on the soil water retention curve during a fallow period of a semiarid dryland. *Soil Research* **55**, 114–123. doi:10.1071/SR15305

Pires LF, Borges JA, Rosa JA, Cooper M, Heck RJ, Passoni S, Roque WL (2017) Soil structure changes induced by tillage systems. *Soil & Tillage Research* **165**, 66–79. doi:10.1016/j.still.2016.07.010

R Core Team (2016) R: A language and environment for statistical computing. (R Foundation for Statistical Computing: Vienna, Austria.) Available at https://www.r-project.org/ [verified 13 June 2019].

Rabot E, Wiesmeier M, Schlüter S, Vogel HJ (2018) Soil structure as an indicator of soil functions: a review. *Geoderma* **314**, 122–137. doi:10.1016/j.geoderma.2017.11.009

Reynolds WD (2017) Use of bimodal hydraulic property relationships to characterize soil physical quality. *Geoderma* **294**, 38–49. doi:10.1016/j.geoderma.2017.01.035

Reynolds WD, Elrick DE (2002) Falling head soil core (tank) method. In 'Methods of Soil Analysis, Part 4, Physical Methods'. (Eds JH Dane, GC Topp) pp. 809–812 (Soil Science Society of America: Madison, WI)

Reynolds WD, Drury CF, Tan CS, Fox CA, Yang XM (2009) Use of indicators and pore volume–function characteristics to quantify soil physical quality. *Geoderma* **152**, 252–263. doi:10.1016/j.geoderma.2009.06.009

Romano N, Nasta P (2016) How effective is bimodal soil hydraulic characterization? Functional evaluations for predictions of soil water balance. *European Journal of Soil Science* **67**, 523–535. doi:10.1111/ejss.12354

Schindler U, Durner W, von Unold G, Mueller L, Wieland R (2010) The evaporation method: extending the measurement range of soil hydraulic properties using the air-entry pressure of the ceramic cup. *Journal of Plant Nutrition and Soil Science* **173**, 563–572. doi:10.1002/jpln.200900201

Schjønning P, Lamandé M, Crétin V, Nielsen JA (2017) Upper subsoil pore characteristics and functions as affected by field traffic and freeze–thaw and dry–wet treatments. *Soil Research* **55**, 234–244. doi:10.1071/SR16149

Schlüter S, Großmann C, Diel J, Wu GM, Tischer S, Deubel A, Rücknagel J (2018) Long-term effects of conventional and reduced tillage on soil structure, soil ecological and soil hydraulic properties. *Geoderma* **332**, 10–19. doi:10.1016/j.geoderma.2018.07.001

Schwärzel K, Punzel J (2007) Hood infiltrometer – a new type of tension infiltrometer. *Soil Science Society of America Journal* **71**, 1438–1447. doi:10.2136/sssaj2006.0104

Schwen A, Bodner G, Scholl P, Buchan GD, Loiskandl W (2011) Temporal dynamics of soil hydraulic properties and the water-conducting porosity under different tillage. *Soil & Tillage Research* **113**, 89–98. doi:10.1016/j.still.2011.02.005

Soracco CG, Lozano LA, Villarreal R, Melani E, Sarli GO (2018) Temporal variation of soil physical quality under conventional and no-till systems. *Revista Brasileira de Ciência do Solo* **42**, e0170408. doi:10.1590/18069657rbcs20170408

Tebrügge F, Düring R-A (1999) Reducing tillage intensity – a review of results from a long-term study in Germany. *Soil & Tillage Research* **53**, 15–28. doi:10.1016/S0167-1987(99)00073-2

Tuller M, Or D (2004) Retention of water in soil and the soil water characteristic curve. In 'Encyclopedia of Soils in the Environment'. (Ed. D Hillel) pp. 278–289. (Elsevier: Amsterdam, Netherlands)

Wairiu M, Lal R (2006) Tillage and land use effects on soil microporosity in Ohio, USA and Kolombangara, Solomon Islands. *Soil & Tillage Research* **88**, 80–84. doi:10.1016/j.still.2005.04.013

Weninger T, Bodner G, Kreiselmeier J, Chandrasekhar P, Julich S, Feger K-H, Schwärzel K, Schwen A (2018) Combination of measurement methods for a wide-range description of hydraulic soil properties. *Water (Basel)* **10**, 1021. doi:10.3390/w10081021

Handling Editor: Stephen Anderson

Soil & Tillage Research 192 (2019) 222–232

Contents lists available at ScienceDirect

Soil & Tillage Research

journal homepage: www.elsevier.com/locate/still

Quantification of soil pore dynamics during a winter wheat cropping cycle under different tillage regimes

Janis Kreiselmeier[a,b,*], Parvathy Chandrasekhar[a,b], Thomas Weninger[c], Andreas Schwen[c], Stefan Julich[b], Karl-Heinz Feger[b], Kai Schwärzel[a,d]

[a] United Nations University, Institute for Integrated Management of Material Fluxes and of Resources (UNU-FLORES), Ammonstraße 74, 01067 Dresden, Germany
[b] Technische Universität Dresden, Institute of Soil Science and Site Ecology, Pienner Straße 19, 01737 Tharandt, Germany
[c] University of Natural Resources and Life Sciences (BOKU), Institute for Soil Physics and Rural Water Management (IHLW), Muthgasse 18, 1190 Vienna, Austria
[d] Thünen Institute of Forest Ecosystems, Alfred-Möller-Straße 1, 16225 Eberswalde, Germany

ARTICLE INFO

Keywords:
Conservation agriculture
Soil hydraulic properties
Temporal variation

ABSTRACT

The water retention characteristic (WRC) and the hydraulic conductivity characteristic (HCC) vary in time due to tillage system, weather conditions and biological activity. These changes in WRC and HCC are a result of varying pore size distributions (PSD). Considering these alterations in soil hydrological models has been shown to improve simulations of water dynamics. An important prerequisite for such an approach is the periodic quantification of WRC and HCC, e.g., over a cropping cycle. Therefore, our study frequently quantified WRC and HCC together with other soil physical and chemical properties on a long-term (23 years) tillage experiment with a silt loam soil. The aim was to identify differences between the three treatments conventional tillage (CT) with a moldboard plow, reduced mulch tillage (RT) with a cultivator and no tillage (NT) with direct seeding. WRC and HCC were parameterized using the bimodal version of the well-known Kosugi retention model together with the Mualem conductivity model to account explicitly for both textural and structural pores. Consequently, bimodal PSD were inferred using the Kosugi parameters. The structural part of the bimodal Kosugi model clearly showed a shift in the PSD on CT and RT from larger to smaller pores throughout the winter wheat growing season with a recovery later in the season on RT. Saturated hydraulic conductivity was positively correlated with the abundance of transmission pores (diameter 50–500 μm) which has implications for infiltration processes under the influence of seasonal PSD changes. Overall, a frequent experimental quantification of PSD may be warranted for modeling soil water on short time scales, e.g., during a cropping cycle, while for longer time frames one to two measurement campaigns per year may be sufficient to describe soil hydraulic behaviour.

1. Introduction

Turnover inversion tillage with a moldboard plow or conventional tillage (CT) has long been the method of choice for soil cultivation. In the past century, reduced forms of tillage (RT) such as mulching using no-turnover chisel cultivators and no tillage (NT) have emerged (Lal et al., 2007). These systems have been established, among others, to prevent and reduce soil erosion and carbon loss, preserve soil moisture and reduce production costs (Holland, 2004). With conservation agriculture on the rise the use of these tillage techniques has increased worldwide in the past decades (Kassam et al., 2015). The choice of tillage system together with other management practices affects water retention characteristic (WRC) and hydraulic conductivity characteristic (HCC) (Blanco-Canqui and Ruis, 2018). In a study by Kargas and Londra (2015) on a loamy soil, water retention and porosity were higher about two months after roto-tillage compared to that on an NT plot. A comparison of CT- and NT-plots on a sandy clay revealed higher water retention close to saturation under CT. At more negative pressure heads, the trend was reversed with higher retention on NT (Martínez et al., 2008), indicating the establishment of distinctly different pore size distributions (PSD) between treatments with more macropores under CT and greater microporosity under NT. Reichert et al. (2016) found that under NT relatively small pores draining at pressure heads (h) < -60 cm may form at the expense of larger pores improving water availability for plants and reducing rapid drainage of soil water. This change in PSD was attributed to initial soil compaction in the absence of annual soil loosening and the following re-arrangement of particles as a consequence of shrinking-swelling as well as biological processes.

* Corresponding author.
E-mail address: kreiselmeier@unu.edu (J. Kreiselmeier).

https://doi.org/10.1016/j.still.2019.05.014
Received 11 December 2018; Received in revised form 24 April 2019; Accepted 16 May 2019
Available online 23 May 2019

Table 1
Soil texture as determined by the combined sieve and sedimentation method for the three tillage treatments conventional tillage (CT), reduced mulch tillage (RT) and no tillage (NT). Values presented are arithmetic means (n = 5) with the standard deviation in brackets.

Treatment	Depth	Clay	Silt	Sand	WRB soil texture classification
		< 2 µm	2-63 µm	63-2000 µm	
	(m)	% (w/w)			
CT	0.00-0.05	18.6 (0.8)	78.0 (1.4)	3.4 (0.2)	SiL, Silt Loam
	0.25-0.30	17.3 (0.8)	78.9 (1.0)	3.8 (0.2)	
RT	0.00-0.05	20.5 (1.2)	76.6 (0.8)	2.9 (0.4)	
	0.25-0.30	21.3 (2.2)	75.2 (1.8)	3.5 (0.7)	
NT	0.00-0.05	20.7 (0.9)	76.0 (1.6)	3.2 (0.1)	
	0.25-0.30	18.4 (1.4)	78.0 (1.2)	3.6 (0.2)	

These ongoing changes in soil structure within an NT-system have been observed up to 14 years after its establishment (Reichert et al., 2016). As opposed to the previous studies, Blanco-Canqui et al. (2017) found no differences in WRC on a silty clay loam between long-term NT (35 years), disk, chisel and moldboard plowing systems.

Results presented in the literature are usually subject to site- and experiment-specific conditions (Blanco-Canqui et al., 2017; Kargas and Londra, 2015) such as climate, soil type, measurement methods, sampling strategies as well as rather broad and unclear definitions of the tillage techniques applied (Derpsch et al., 2014; Horel et al., 2015). Therefore, the effects of these systems on soil physical (SPP) and soil hydraulic (SHP) properties can hardly be generalized (Blanco-Canqui and Ruis, 2018). Further, many studies only take mere 'snapshots' of the state of SPP and SHP at one or few points during the cropping seasons when in fact, soil structure varies with time. This may contribute to the previously described conflictive results (Strudley et al., 2008). Processes behind temporal variations in soil structure and SHP can be aggregate disintegration through freeze-thaw cycles (Li and Fan, 2014; Oztas and Fayetorbay, 2003) as well as slaking and mechanical breakdown of larger aggregates caused by heavy rainfall (Xiao et al., 2018). Wetting-drying cycles may either increase macroporosity when occurring at high intensities or decrease mean soil pore radius while increasing pore heterogeneity during longer phases of soil drying (Bodner et al., 2013a, 2013b). The amount of organic residue has been shown to be directly related to aggregate formation (De Gryze et al., 2005). Tillage systems such as CT, RT and NT cause a different vertical stratification of these residues. This has implications for the abundance of water-stable aggregates in such systems on the soil surface (Andruschkewitsch et al., 2014) and with that their resilience towards impacts of temperature and precipitation (Blanco-Canqui and Ruis, 2018). Other drivers of changes in SPP and SHP are (decaying) root systems (Rasse et al., 2000; Swinnen et al., 1995) and biological activity where the choice of tillage system influences stabilization of aggregates (Green et al., 2007). Further factors are roots of taprooting crop species and earthworms that both create and colonize macroscopic biopores with diameters (∅) > 2 mm (Han et al., 2015; Kautz et al., 2014). For biopores (∅ > 5 mm), roots have been shown to enhance soil structure while along pore walls earthworms may homogenize aggregates on a microscale (µm to mm) (Haas and Horn, 2018).

In recent years, temporal changes in the WRC and HCC have been identified and quantified more and more (e.g. Kargas et al., 2016; Pena-Sancho et al., 2017; Schwen et al., 2011b). Considering the variations in soil structure and SHP in hydrological models may allow for better quantification of water fluxes from and into the soil (Alletto et al., 2015; Schwen et al., 2011a). This may ultimately lead to improved management of the natural resource soil and the ecosystem services it provides (Vereecken et al., 2016). One such improved management option may be the adjustment of irrigation schedules according to simulation results considering time-variable SHP (Feki et al., 2018). Previously discussed approaches usually quantify SHP at few occasions throughout one or more cropping cycles and implement the obtained parameters in a stepwise manner into models such as HYDRUS 2D/3D (Alletto et al., 2015; Schwen et al., 2011a) or FEST-WB (Feki et al., 2018). Another approach is modeling the evolution of PSD post-tillage (Or et al., 2000) or as a result of a change in agricultural management, e.g., CT to NT or CT to pasture (Schwärzel et al., 2011). However, data availability has been identified as a limiting factor for an efficient calibration of this model (Chandrasekhar et al., 2018).

In this study, we aimed at frequently recording the WRC and HCC throughout an entire winter wheat cropping cycle to quantify the evolution of PSD under different tillage treatments. Experiments were conducted on a long-term tillage trial established 23 years ago on a silt loam soil in eastern Germany. Treatments included plots under CT, RT and NT. Following the conceptual framework of Reichert et al. (2016), we hypothesize that the long-term NT system established 23 years ago has reached a 'quasi steady-state' of soil structure with comparably little temporal variation. Therefore, we expected more temporal variability of the PSD under CT and RT due to the physical disturbance of annual tillage and greater exposure of these treatments to environmental factors such as precipitation and temperature.

2. Material and methods

2.1. Field site

Sampling took place between December 2015 and August 2016 on an agricultural experimental field in the Loess Hill Region of Saxony, eastern Germany (51°7′6 N, 13°13′43E, 275 m.a.s.l.). The tillage trial was established in 1992/93. Prevalent soil type is a Haplic Luvisol (IUSS Working Group WRB, 2015; Koch et al., 2009) with a silt loam texture in the topsoil from 0.00 m to 0.05 m and at 0.25 m to 0.30 m depth on all tillage plots (Table 1). The mean annual temperature is 8.7 °C and the mean annual precipitation is 753 mm.

2.2. Tillage and crop rotation

Since 1992/93 four different tillage practices have been applied to the field with plots laid out in large parallel strips with sizes varying between 5.4 and 7.8 ha. In our study, we covered three practices, namely CT, RT and NT. On all variants, organic residue from the winter wheat harvest was chopped and left on the field after harvest. Residue management after harvest with a cultivator mixed the residue into the upper soil layer 5 to 8 cm deep on CT and RT. On NT, straw remained on the surface. CT represented the tillage system with the highest energy input into the soil. Here, annual tillage was done with a turnover moldboard plow up to a depth of 0.30 m. RT was a treatment with comparably less mechanical disturbance. Here, annual tillage was done with a no-turnover cultivator to a depth of 0.15 m. The least intensive technique applied to the study site was NT where the crop was sown with a direct drill without previous seedbed preparation. Only before sugar beet sowing (*Beta vulgaris*), a shallow seedbed (0.03 – 0.05 m) was prepared with a disc harrow to ensure optimal starting conditions for the seedlings (Koch et al., 2009).

Crop rotation encompassed two years of winter wheat followed by

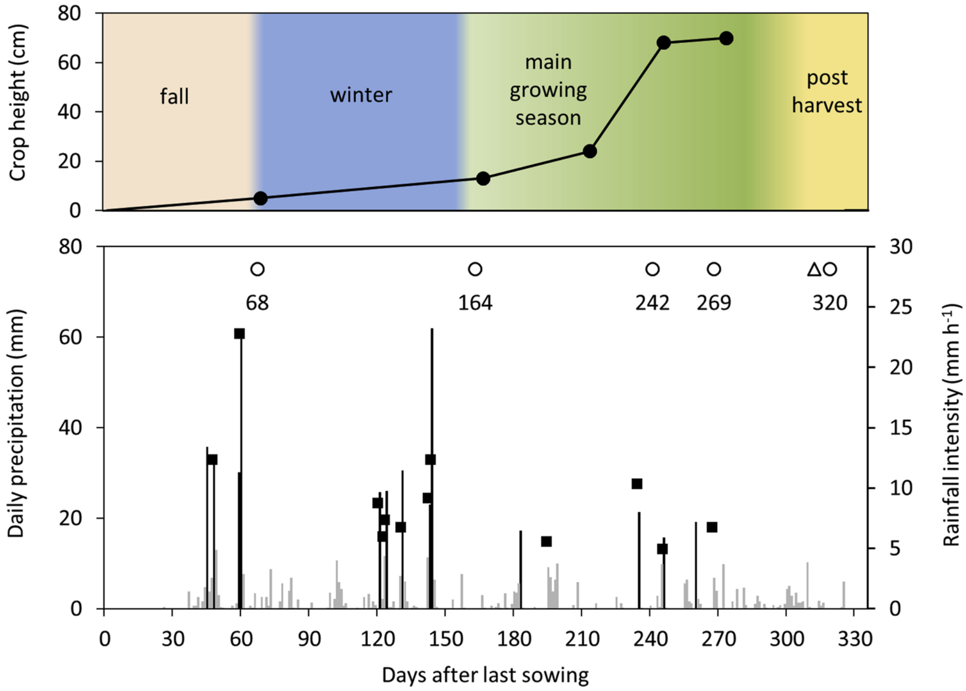

Fig. 1. Daily precipitation (bottom diagram) since the time of last sowing (2 October 2015). Effective rainfall (> 10 mm d^{-1}) as defined by Moret and Arrúe (2007) is highlighted in black. Largest rainfall intensities on any given day exceeding 5 mm h^{-1} are displayed as squares. Times of sampling are marked by circles where labels show days since sowing of winter wheat on 2 October 2015 and the triangle marks harvest. The top diagram shows the measured crop height at time of sampling. The backdrop indicates the main seasons.

sugar beet. In 2015 and during the main study period in 2016, the field was cultivated with winter wheat (*Triticum aestivum;* Variety: *Kerubino*), which had been sown on all plots on 2 October 2015, ten and two days after annual tillage on CT and RT, respectively. Hereafter, we refer to sampling times in terms of days passed since that last sowing or the month in which we sampled. Crop harvest was on 9 August 2016. Fig. 1 gives an overview on times of sowing, harvest and sampling as well as crop growth status and rainfall events during the observation period. Moret and Arrúe (2007) defined an effective rainfall at > 10 mm d^{-1}. However, even at that magnitude precipitation can theoretically be distributed over 24 h with moderate intensities of only 0.4 mm h^{-1}. Mechanical breakdown of aggregates is dependent on the kinetic energy of rainfall (Bissonnais, 1996). Therefore, rainfall intensities in Fig. 1 were calculated based on half-hourly records from a weather station on-site and only intensities ≥ 5 mm h^{-1} are displayed. In the first couple of weeks after sowing, the station was not recording any rainfall which was probably due to a malfunction. During the remainder of the study, precipitation records are valid when compared to data from surrounding meteorological stations.

2.3. Sampling

While changes in soil structure likely also occur deeper down the profile we expected most of its variation close to the surface with precipitation and temperature having a direct impact here. Therefore, sampling was only done for the topsoil from 0 to 5 cm depth. Field work started in December 2015 and continued with four campaigns throughout 2016 (Fig. 1). One of the campaigns was done after harvest while the other three were done during the main winter wheat growing period from March to June 2016. Generally, we tried to avoid visible disturbances of the soil surface such as wheel tracks.

In each campaign five undisturbed soil cores (250 cm^3) from each tillage plot were carefully taken and stored at 4 °C until further processing. Further, we collected disturbed samples in paper bags at each location (n = 5). Samples were air-dried at room temperature and gently passed through a 2 mm-sieve. Part of the sieved material was further ground for CN analysis.

2.4. Saturated hydraulic conductivity

Considering (near-) saturated hydraulic conductivity in the parametrization of WRC and HCC improves soil water modeling outcomes due to a better representation of the soil macroporous system (Weninger et al., 2018). Therefore, the collected undisturbed soil cores (250 cm^3) were analyzed for their saturated hydraulic conductivity (K_S) in the laboratory. Samples were saturated with degassed tap water for 24 h. Water levels during this time were gradually raised to avoid trapping air inside the pores. Falling head method was then applied using the commercial KSAT™ device (METER Environment, Munich). Originally, this method was only recommended for K_S-values < 86 cm d^{-1} (Klute and Dirksen, 1986). On our site, we found values that were more than one order of magnitude larger. However, the KSAT™ device is very precise in measuring water level decline with time when applying the falling head method (METER Environment, 2019). Therefore, it can even be used for a K_S-range, where traditionally the constant head method was preferred (K_S > 86 cm d^{-1}). The (ideally exponential) water level decline with time was fitted with an exponential function. Only those measurements with a coefficient of determination (R^2) > 0.999 were considered valid measurements and consequently used for K_S calculations.

2.5. Water retention and hydraulic conductivity characteristic

Subsequent to the K_S-measurements, the cores were analyzed for their drying WRC and HCC using the simplified evaporation method based on Wind's approach (Wind, 1969). Saturated cores were directly transferred to the commercial HYPROP™ system (METER Environment, Munich, Germany). Thereby two tensiometers were inserted vertically at depths of 1.25 and 3.75 cm into the 5 cm high soil core. The sample was then left to dry under laboratory conditions with temperatures between 19 and 24 °C while a scale continuously measured the weight change as a result of evaporating water. At the dry end, we additionally used data points obtained from dewpoint hygrometer measurements in the $|h|$ range 4 to 6 $\log_{10}$[cm]. With texture as a determining factor for water retention in this range they were not expected to vary much with time (Blume et al., 2016). Therefore, sieved (< 2 mm) and mixed samples from two occasions (164 and 320 days after last sowing) per treatment were measured and averaged.

With an agriculturally used silt loam we expected a bimodality of the soil structure to some degree with textural and structural pore domains. When ignoring bimodality in the characterization of the measured WRC and HCC by using unimodal models (e.g., Kosugi, 1996; van Genuchten, 1980) large errors in the numerical simulation of infiltration processes may occur (Romano and Nasta, 2016). Therefore, we fitted the bimodal version (Romano et al., 2011) of the Kosugi (1996) and Mualem (1976) model based on the assumption of a lognormal PSD to our data. The WRC is given by

$$S_e(h) = \frac{\theta - \theta_r}{\theta_s - \theta_r} = \sum_{i=1}^{k} w_i \left\{ \frac{1}{2} erfc \left[\frac{\ln\left(\frac{h}{h_{mi}}\right)}{\sqrt{2}\,\sigma_i} \right] \right\} \tag{1}$$

where S_e (-) is the effective saturation at pressure head h (cm), θ (cm^3 cm^{-3}) the volumetric water content, θ_s and θ_r (cm^3 cm^{-3}) are the saturated and residual water content, respectively. Bimodality of the WRC is expressed by k = 2 defining a structural (i = 1) and textural (i = 2) domain, w_i (-) is a factor assigning weights to both domains with $0 \leq w_i \leq 1$ and $\Sigma w_i = 1$, *erfc* is the complementary error function, h_{mi} (cm) is the median pressure head at which the effective saturation of the respective subcurve $S_{ei}(h_{mi}) = 0.5$ and σ_i (-) is the standard deviation of the lognormal soil pore radius defining the width of the PSD. The HCC is given by

$$K(h) = K_s \frac{S_e^{0.5}}{4\left[\sum_{i=1}^{k} \frac{w_i}{h_{mi}} exp\left(\frac{\sigma_i^2}{2}\right)\right]^2} \left\{ \sum_{i=1}^{k} \frac{w_i}{h_{mi}} exp\left(\frac{\sigma_i^2}{2}\right) erfc\left[\frac{\sigma_i}{\sqrt{2}} erfc^{-1}(2\,S_{ei})\right] \right\}^2 \tag{2}$$

The PSD corresponding to the WRC can be calculated according to

$$g(r) = \sum_{i=1}^{k} w_i \left(\frac{\Phi}{\sqrt{2\pi}\,\sigma_i r}\right) exp\left[-\frac{\ln\left(\frac{r}{r_{mi}}\right)^2}{2\sigma_i^2}\right] \tag{3}$$

where Φ is the porosity here defined as θ_s- θ_r, r_{mi} is the median pore radius calculated from h_{mi} using the Young-Laplace equation that relates pore radii to h through $r_{mi} = 0.149$ cm^2 / h_{mi} (Seki, 2007). In its normalized form Eq. (3) becomes

$$f(r) = \sum_{i=1}^{k} w_i \left(\frac{1}{\sqrt{2\pi}\,\sigma_i}\right) exp\left[-\frac{\ln\left(\frac{r}{r_{mi}}\right)^2}{2\sigma_i^2}\right] \tag{4}$$

Measured HYPROP data were fitted in R (R Development Core Team, 2017) with a local polynomial regression with a low degree of smoothing to obtain θ-h and K-h pairs from $|h|$ 0 to 3 $\log_{10}$[cm] at intervals of 0.1. For that, the loess function contained in the stats package (R Development Core Team, 2017) was used where fitting at individual data points is weighted towards the surrounding data points. The weighting, or degree of smoothing, is controlled by the 'span' parameter. We chose a span of 0.28 which was low enough to conserve local data variations and high enough to retain enough data for an accurate smoothing fit without too much random variation. The obtained values were averaged for treatment and campaign groups. The Kosugi and Mualem models were then fitted simultaneously to the averaged θ-h and K-h pairs by applying nonlinear least-square regression. Fitted parameters were σ_i, h_{mi}, θ_s, θ_r and w_i. Most results of the evaporation measurements displayed a relatively smooth change in θ close to saturation which is why θ_s was relatively constrained to just below porosity. The additional data points from dewpoint hygrometer measurements from $|h|$ 4 to 6 $\log_{10}$[cm] constrained the possible range for θ_r such that there was no need to fix it. The K_S parameter was fixed to the group geometric mean K_S obtained from the previously described lab falling head measurements. As measured $K(h)$ values were only available in a relatively limited range of about $|h|$ 2 to 3 $\log_{10}$[cm], more weight ($\times 10^3$) was put on the $\theta(h)$ data in the objective function.

We calculated the volume fraction taken up by different pore size classes as defined by Greenland (1981) from the area under the curve of the bimodal PSD (Eq. 3) resulting in fissures (∅ > 500 µm), transmission (∅ 50–500 µm), storage (∅ 0.5–50 µm), residual (∅ 0.005 - 0.5 µm) and bonding (∅ < 0.005 µm) pores. These pore size classes are arbitrarily defined but nevertheless reflect the main 'tasks' of those classes such as water movement (transmission pores) and retention (storage pores).

2.6. Basic soil properties

Following the evaporation method soil cores were oven-dried at 105 °C for 24 h to determine their dry bulk density (ρ_B). Air-dried disturbed samples were used to determine the texture as well as carbon (C) and nitrogen (N) contents. Soil texture was obtained from the combined sieving and sedimentation analysis. This was done for all treatments only for one occasion (March 2016) as texture was not expected to vary much between the closely spaced sample points of different campaigns. Prior to the analysis, organic substance was removed adding hydrogen peroxide and 2-Octanol to prevent foam formation. Dispersion of particles was achieved adding a sodium diphosphate solution. C and N concentrations were measured from the air-dried ground material with the Vario TOC™ cube (Elementar, Hanau, Germany). As the soil on our site was devoid of carbonates, the concentration of total C can be assumed to represent organic C (OC). From this we calculated OC and total N stocks for the investigated surface layer of 5 cm using the respective ρ_B (Ellert and Bettany, 1995).

2.7. Statistical analysis

All statistical analyses were performed in R 3.4.2. (R Development Core Team, 2017). K_S was log-normally transformed for analysis. For calculation of coefficients of variation (CV) we used CV = 100 (exp(s^2) - 1)$^{0.5}$ where s^2 is the variance of the lognormal data (Lee et al., 1985). Geometric means (GM) of untransformed K_S values were calculated.

One-way analyses of variance (ANOVA) were performed on the quantities ln K_S, ρ_B, as well as OC and N stocks to evaluate the influence of tillage and sampling occasion. If ANOVA was significant, multiple comparisons were done using the least significant differences (LSD) test (Webster, 2007) using the emmeans package in R (Lenth et al., 2018). Further, the temporal variation of θ at $|h|$ 0–3 $\log_{10}$[cm] was compared at intervals of 0.5 for each treatment using one-way ANOVA followed by LSD. The significance level was $p < 0.05$ for all tests.

3. Results

3.1. Rainfall patterns prior to each sampling

In the 68 days after last sowing and prior to our first sampling, a total of 171 mm effective rainfall (> 10 mm d^{-1}) was recorded (Fig. 1). Several days had comparably high effective rainfall (35.8, 32.6, 30.2 and 59.8 mm d^{-1}). The event closest to our sampling date happened eight days before with a maximum intensity of 22.8 mm h^{-1}. After 164 days, 201 mm of effective rainfall had accumulated with the most intense event 20 days before sampling at a maximum intensity of 12.4 mm h^{-1}. During the growing season 242 and 269 days after sowing 39 and 35 mm effective rainfall were recorded, respectively. Highest intensities were 10.4 and 4.2 mm h^{-1} seven and nine days before sampling, respectively. An example of a heavy rainfall event with a significant surface runoff on the field during the 242-day-campaign is shown in Fig. 2a). That day a total of 15.8 mm was recorded with a maximum intensity of 5 mm h^{-1}. After harvest, little effective rainfall was observed (10.2 mm) with a low maximum intensity of 0.8 mm h^{-1} eleven days before the field campaign.

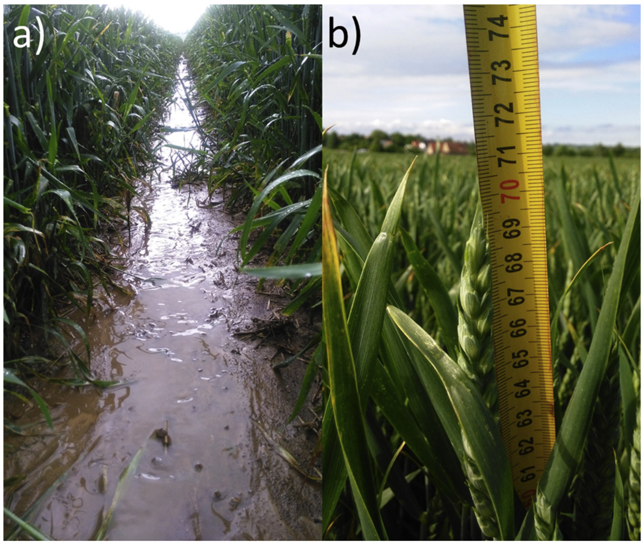

Fig. 2. a) Water running down wheel tracks on 3 June 2016 after a heavy rainfall event. Measurements on all treatments were already completed shortly before. b) Winter wheat around the flowering phase end of May 2016.

3.2. Basic soil properties

Overall ρ_B was in the order NT (1.32 g cm^{-3}) > CT (1.30 g cm^{-3}) > RT (1.28 g cm^{-3}) (not significant at $p < 0.05$). Significant temporal variation was only observed for CT and RT (Fig. 3). In December 2015, ρ_B was lower under RT ($p < 0.05$) and CT compared to NT. Over the winter, soil consolidated in tilled plots with significantly increased ρ_B values while under NT there was a slight decrease. During the main growing period from March to June, ρ_B decreased again while in NT there was an increase until May followed by a decrease in June. Throughout the cropping season, CT revealed the lowest standard deviations.

Soil OC and N stocks for the surface soil layer down to 5 cm depth were always higher under untilled soil (Fig. 4). The same was true for N stocks. Tillage distributed organic residue up to 15 (RT) and 30 cm (CT) depth on an annual basis while under NT it remained on the surface. Turnover moldboard plowing resulted in the lowest OC stocks in the surface layer (0–5 cm) while RT had only slightly more. Measurements at 25 to 30 cm in March 2016 (not shown here) revealed highest OC stocks under CT (0.93 kg m^{-2}), followed by NT (0.65 kg m^{-2}) and RT (0.43 kg m^{-2}). Jacobs et al. (2015) evaluated OC stocks at the same site. We recalculated their OC stocks from 20 to 30 cm to a 5 cm layer which resulted in the same sequence with CT (0.90 kg m^{-2}), followed by NT (0.76 kg m^{-2}) and RT (0.64 kg m^{-2}) 12 years after the establishment of the tillage trial. At the time of our study, 11 years later, our data therefore points to a potential further reduction in OC stocks from 25 to 30 cm under RT and NT. This may be explained by the lack of new organic matter supply to this layer under those treatments and an accumulation closer to the surface.

3.3. Saturated hydraulic conductivity

K_S obtained from the 250 cm^3 soil cores was highly variable within groups (Fig. 5). Variation was largest for NT during the summer months in May and June. CVs ranged from 35 to 601% (CT), 75 to 1808% (RT) and 27 to 1354% (NT) between sampling occasions. Overall treatment GMs were in the order CT (461 cm d^{-1}) > RT (323 cm d^{-1}) > NT (287 cm d^{-1}) (not significant at $p < 0.05$). In December, K_S was by almost one order of magnitude lower on NT compared to tilled plots (Fig. 5; significant at $p < 0.05$). By spring and throughout summer values of all treatments were around the same magnitude with decreases shortly before harvest and sharp increases in August after harvest. Statistically significant temporal variation was only observed on RT with decreases from December to March and an increase from June to August.

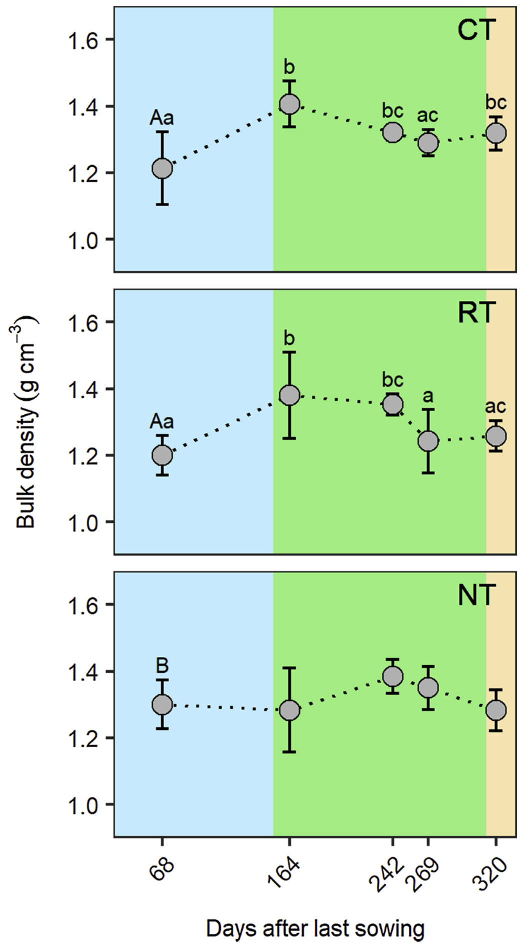

Fig. 3. Bulk density changes with time under conventional tillage (CT), reduced mulch tillage (RT) and no tillage (NT). Blue background indicates winter period including the first sampling in December 2015, 68 days after last sowing, green background indicates main cropping season starting March 2016 and yellow background indicates time after harvest. Error bars denote standard deviation ($n = 5$). Same upper- and lowercase letters indicate no significant differences in bulk density at $p < 0.05$ (LSD) among treatments and within treatments, respectively.

3.4. Water retention

Table 2 shows the change of θ within treatments over the measured h-range. The evolution of θ over time was similar for all treatments in relative terms. Close to saturation a decrease in water contents relative to the December measurements (68 days) could be observed. Between $|h|$ 1.5 and 2 $\log_{10}$[cm] there was a point from which on θ increased for tilled plots. These results point to a shift of abundance of larger pores (r > 50 µm) towards smaller pores (r < 50 µm) during the winter period. Later in the growing season these effects reversed to some extent after 269 days and more so after 320 days.

The parameters of the reference water retention curves obtained from fitting Kosugi's and Mualem's bimodal model to averaged θ-h and K-h pairs from HYPROP evaporation experiments are displayed in Table 3. The overall fit was very good for both the WRC and the HCC with relatively low RMSE values. Previous tests with unimodal fits produced almost one order of magnitude larger RMSE values for θ (not shown here) while $\log_{10} K(h)$ RMSE were similar. Residual water contents were constraint to below 0.04 cm^3 cm^{-3} by the provided

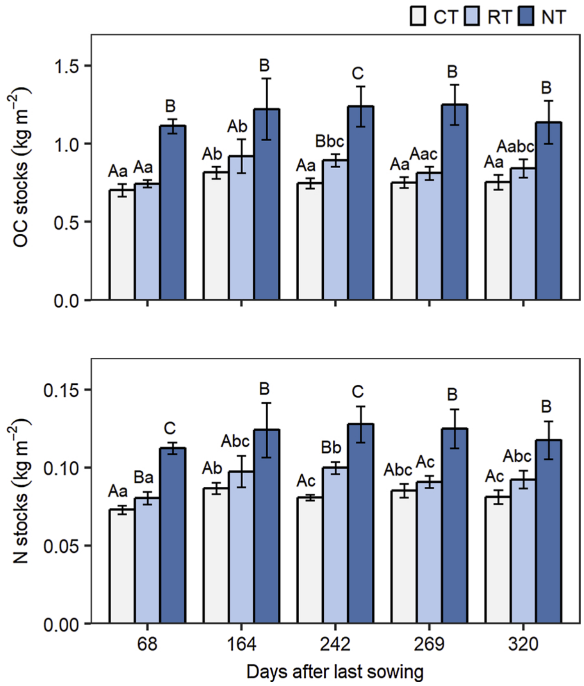

Fig. 4. Soil organic carbon (OC) and total nitrogen stocks (N) as calculated for the top 5 cm using the respective bulk density (ρ_B) under conventional tillage (CT), reduced mulch tillage (RT) and no tillage (NT). Error bars denote standard deviation ($n = 5$). Same upper- and lowercase letters indicate no significant differences at $p < 0.05$ (LSD) among treatments and within treatments, respectively.

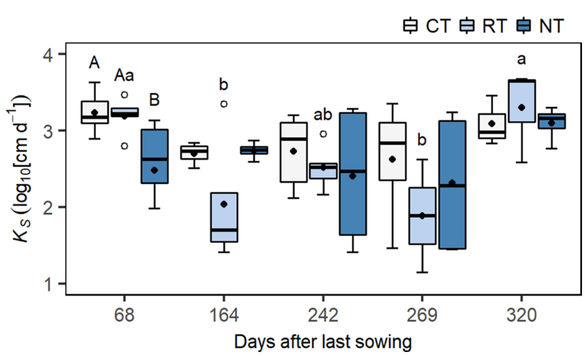

Fig. 5. Saturated hydraulic conductivity (K_S) from laboratory falling head measurements under conventional tillage (CT), reduced mulch tillage (RT) and no tillage (NT). Outliers are marked by empty circles while black circles mark the arithmetic mean of $\log_{10}$-transformed values. Same upper-and lowercase letters indicate no significant differences at $p < 0.05$ (LSD) among treatments and within treatments, respectively.

dewpoint hygrometer measurements. On all treatments, θ_s followed the same trend over the winter wheat growing season. From December to June values declined up to shortly before the harvest in August. For most occasions θ_s was highest under RT. Median pressure heads of the structural domain (h_{m1}) differed by up to two orders of magnitude between campaigns for all treatments. Corresponding r_{m1} were comparably large in December and increased until March 2016. By May r_{m1} was in the same order of magnitude as its textural counterpart r_{m2}. While on NT r_{m1} then remained at similar values to r_{m2} for the rest of the observed period, it decreased back to previous values under CT and RT in June and after harvest in August. While the median pressure heads of the textural domain (h_{m2}) differed with time their values always remained within the same order of magnitude except for NT in May where h_{m2} reached the defined upper boundary of 10,000 cm.

3.5. Pore size distribution

As outlined in section 3.4, there is a trend in the temporal evolution of WRC and PSD parameters over the winter 2015/16 and during the growing season 2016 especially evident in the change of Kosugi parameter h_{m1} and the derived r_{m1} (Table 3). These trends are also statistically backed by measured θ showing significant changes with time over the whole measured h-range (Table 2). This section focusses on the change in shape and position of the PSD after last tillage and sowing in September and October 2015. Bimodal PSDs are displayed in the form of normalized curves (Eq. 4; Fig. 6) because they were more effective in highlighting structural and textural differences. For bimodal PSDs considering Φ (Eq. 3) the textural domain tended to overshadow the structural domain as it took up more of the total pore volume fraction, i.e., Φ, making it impractical to visualize the evolution of the structural mode. Additionally, Fig. 7 displays the volumetric frequency of only the structural domain as calculated by Eq. 3.

For CT and RT two distinct modes in the normalized PSD can be identified (Fig. 6). Under RT the structural distribution mode had a higher frequency than its textural counterpart while the distribution of this subcurve was much narrower ($\sigma_1 < \sigma_2$) which was also true for CT. Under NT the bimodality was less pronounced with more emphasis on the textural mode. The boundary of both modes was at pore radii between 30 and 40 µm. In March (164 days after the last sowing) the two distinct modes could still be identified. However, the frequency of the textural distribution had increased at the expense of structural frequency. By May (242 days after last sowing), bimodality had almost vanished and the WRC approximated the unimodal form of the Kosugi model. Only on RT and to some extent on CT a recovery of larger pores could be seen in June (269 days after last sowing) and after harvest in August (320 days after last sowing). At the same time the peak of the textural distribution of NT shifted towards larger pores while the distribution became narrower covering a smaller range of pore sizes.

Considering the total pore volume, the disappearance of macropores after 164 and 242 days on CT and RT is clearly visible with a shift towards smaller pores and growing heterogeneity (increasing σ_1; Table 3) together with an increase in frequency (Fig. 7). On NT, only the frequency had decreased after 164 days but no shift towards smaller pores was observed. After 242 days the structural domain on all treatments was practically not existent anymore or had rather merged with the textural domain on all treatments. Only on RT this development reversed after 269 and 320 days.

Fig. 8 shows the pore volume fraction for fissures (∅ > 500 µm), transmission (∅ 50–500 µm), storage (∅ 0.5–50 µm), residual (∅ 0.005 - 0.5 µm) and bonding (∅ < 0.005 µm) pores (Greenland, 1981) obtained from the area under PSD curves considering Φ (Eq. 3). As already indicated by the bimodal PSD, transmission pores (and to some extent fissures) decreased until May and increased again for the last two dates on CT and RT. On NT the abundance in transmission pores was comparably lower but showed similar temporal variations. Overall volume fraction taken up by storage pores was greater under NT which points to improved water retention at the absence of annual tillage. The porosity of fissures and transmission pores showed a moderate positive linear relationship with pooled group GMs of K_S with $n = 15$ ($R^2 = 0.30$, $p < 0.05$ and $R^2 = 0.53$, $p < 0.01$, respectively) highlighting their importance in infiltration processes and explaining some of the variation in K_S. This relationship of K_S with transmission pore volume fraction was especially pronounced under CT with $n = 5$ ($R^2 = 0.87$, $p < 0.05$). Porosities of other size classes did not show any significant correlation with K_S.

Table 2
Changes in volumetric water contents (θ) over the measured pressure head (h) range under conventional tillage (CT), reduced mulch tillage (RT) and no tillage (NT). Same lowercase letters are not significantly different at $p < 0.05$ (LSD) among h steps. Time since last sowing refers to days passed since 2 October 2015.

		θ ($cm^3\,cm^{-3}$) at |h| (log_{10}[cm])													
	Time since last sowing (d)	**0.0**		**0.5**		**1.0**		**1.5**		**2.0**		**2.5**		**3.0**	
CT	68	0.452	a	0.448	a	0.421	a	0.379	ab	0.336	a	0.290	a	0.221	a
	164	0.439	b	0.434	ab	0.410	ab	0.385	ab	0.366	b	0.334	b	0.271	b
	242	0.408	c	0.405	c	0.401	bc	0.387	a	0.360	b	0.318	bc	0.250	c
	269	0.409	d	0.404	c	0.390	c	0.366	bc	0.339	a	0.300	a	0.235	d
	320	0.432	cd	0.427	b	0.401	bc	0.361	c	0.332	a	0.302	ac	0.246	cd
		0.0		**0.5**		**1.0**		**1.5**		**2.0**		**2.5**		**3.0**	
RT	68	0.484	a	0.467	a	0.424	a	0.369	ab	0.333	ab	0.297	a	0.241	a
	164	0.444	b	0.436	b	0.407	b	0.378	abc	0.358	ac	0.326	b	0.274	b
	242	0.424	b	0.419	b	0.408	b	0.387	a	0.358	c	0.325	b	0.266	b
	269	0.426	b	0.421	b	0.403	b	0.367	bc	0.337	ab	0.304	a	0.253	a
	320	0.452	b	0.445	b	0.410	b	0.362	c	0.328	b	0.294	a	0.243	a
		0.0		**0.5**		**1.0**		**1.5**		**2.0**		**2.5**		**3.0**	
NT	68	0.454	a	0.449	a	0.431	a	0.411	ab	0.393	ab	0.360	a	0.287	a
	164	0.443	b	0.434	b	0.421	b	0.404	abc	0.388	ac	0.359	b	0.295	b
	242	0.421	b	0.419	b	0.417	b	0.411	a	0.394	c	0.356	b	0.283	b
	269	0.437	b	0.435	b	0.429	b	0.414	bc	0.392	ab	0.352	a	0.268	a
	320	0.444	b	0.440	b	0.429	b	0.409	c	0.383	b	0.343	a	0.267	a

n = 5 except for 68 days after sowing: CT (n = 9), RT (n = 6), NT (n = 7).

4. Discussion

4.1. Influence of tillage and weather on the pore size distribution

Despite the long time that had passed since last annual tillage its effects on the WRC and its corresponding PSD persisted even 164 days after the last sowing activity. Distinct structural and textural domains could clearly be identified in tilled plots (Fig. 6) with abundant fissures and transmission pores (Fig. 8) despite large amounts of received effective rainfall (Fig. 1). Prior to our first sampling bimodality may have been more pronounced. However, intense precipitation events (maximum intensity eight days prior: 22.8 mm h^{-1}) on the bare field leading to aggregate disintegration as a consequence of slaking and mechanical breakdown (Xiao et al., 2018) likely caused a substantial amount of interaggregate porosity to degrade. Further, pore loss directly following tillage, defined as complete closure of interaggregate pores due to gravity and rainfall, may have added to a decline in structural pores (Alletto and Coquet, 2009; Or et al., 2000) and increases in ρ_B (Pena-Sancho et al., 2017). In December, the structural domain was more pronounced under RT compared to CT (Fig. 7) which is probably related to the different mechanical impacts of both techniques. While inversion tillage with a moldboard plow creates large clods of soil with little physical aggregate disruption (Andruschkewitsch et al., 2014) tillage with a cultivator creates a more heterogeneous structure as expressed in the distinct modes of PSD (Fig. 6). Further, more abundant water-stable macroaggregates (> 250 μm) with higher OC contents have been found on RT (and NT) compared to CT on the same field (Andruschkewitsch et al., 2014) thus making RT (and NT) soil structure more resilient towards precipitation impacts. Andruschkewitsch et al. (2014) attributed these findings to higher organic matter incorporation into the first 15 cm under RT as opposed to moldboard plowing on CT that transported organic material down to 30 cm depth. Our observations of OC stocks and those of Jacobs et al. (2015) confirmed the organic matter distribution as influenced by the tillage system (Fig. 4) which may also favor root development in the topsoil of RT and NT as a result of greater soil structural stability (Martínez et al., 2008).

Despite the intense rainfalls and assumed loss in porosity since tillage K_S was comparably high on tilled plots (Table 3; Fig. 5). Abundant fissures and transmission pores under CT and RT together with comparably low ρ_B (Fig. 3) and high Φ favored rapid infiltration on these

Table 3
Reference curve parameters residual (θ_r) and saturated (θ_s) water content, pressure heads at effective saturation $S_{ei}(h_{mi}) = 0.5$ for both the structural (h_{m1}) and textural (h_{m2}) domains, their respective standard deviations of the lognormal pore radii σ_1 and σ_2, and the weighting factor for the structural domain (w_1). The weighting factor of textural domain (w_2) can be obtained by 1-w_1. Saturated hydraulic conductivity (K_S) is presented as geometric mean of laboratory falling head measurements. Goodness of fit between observed and modeled values is expressed by the root mean square error (RMSE) for both the water retention and hydraulic conductivity characteristic. Time since last sowing refers to days passed since 2 October 2015.

	Time since last sowing d	θ_r $cm^3\,cm^{-3}$	θ_s	h_{m1} cm	h_{m2}	r_{m1} μm	r_{m2}	σ_1 –	σ_2 –	w_1 –	K_S cm d^{-1}	RMSE θ $cm^3\,cm^{-3}$	RMSE K log_{10}[cm d^{-1}]
CT	68	0.0241	0.4582	14	1068	107.8	1.4	0.68	3.08	0.07	1708	0.0025	0.0012
	164	0.0326	0.4487	8	2866	180.5	0.5	1.47	2.00	0.17	505	0.0033	0.0078
	242	0.0118	0.4078	1304	8732	1.1	0.2	2.13	3.80	0.65	535	0.0018	0.0164
	269	0.0273	0.4094	384	6826	3.9	0.2	2.68	2.16	0.56	420	0.0034	0.0337
	320	0.0317	0.4444	19	4098	79.5	0.4	1.89	1.95	0.31	1236	0.0042	0.0084
RT	68	0.0174	0.4842	9	1938	156.9	0.8	0.87	3.18	0.18	1557	0.0033	0.0127
	164	0.0345	0.4449	9	2905	166.2	0.5	0.91	2.15	0.16	109	0.0025	0.0023
	242	0.0076	0.4253	2434	2654	0.6	0.6	3.12	3.29	0.83	330	0.0061	0.0131
	269	0.0329	0.4289	17	3225	87.2	0.5	1.27	2.26	0.20	77	0.0025	0.0032
	320	0.0108	0.4569	11	2085	137.9	0.7	0.67	3.38	0.12	2021	0.0035	0.0051
NT	68	0.0368	0.4605	10	2948	150.4	0.5	1.69	2.02	0.13	302	0.0039	0.0038
	164	0.0390	0.4490	8	3218	180.4	0.5	1.72	1.93	0.13	549	0.0034	0.0039
	242	0.0057	0.4235	1469	10000	1.0	0.1	1.46	3.76	0.48	256	0.0018	0.0065
	269	0.0146	0.4403	927	3333	1.6	0.4	0.88	3.33	0.25	205	0.0016	0.0036
	320	0.0146	0.4495	1015	2236	1.5	0.7	0.76	3.44	0.16	1248	0.0014	0.0061

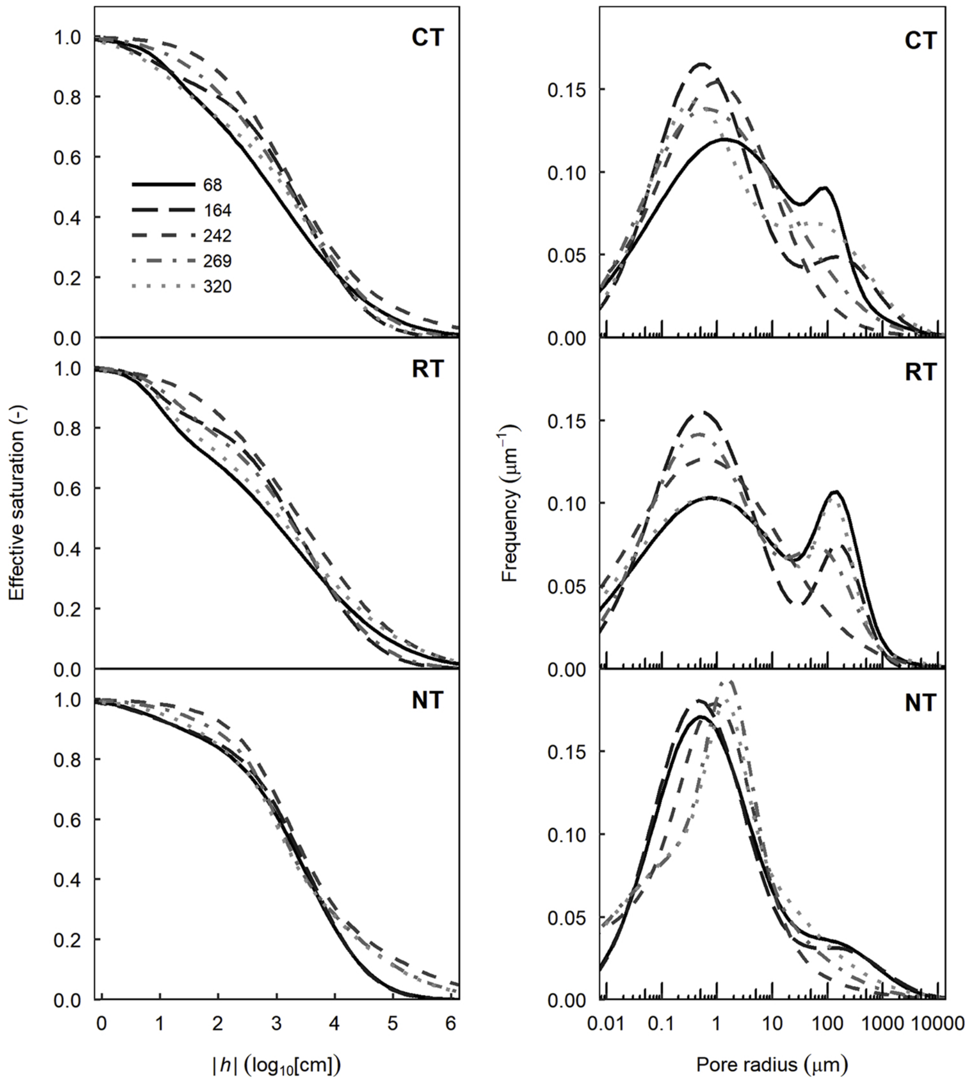

Fig. 6. Evolution of normalized water retention curves (left; Eq. 1) and their respective bimodal pore size distributions (right; Eq. 4) under all three treatments conventional tillage (CT), reduced mulch tillage (RT) and no tillage (NT). Different lines represent days passed since last sowing of winter wheat on 2 October 2015.

plots. Additionally, on RT more plant residues were mixed into the top soil after the previous harvest providing additional flow paths. Therefore, a factor explaining the large variability in K_S throughout the season are the relatively short soil cores (height = 5 cm) used for measurements where individual large biopores such as earthworm burrows and root channels reaching from top to bottom dominated flow processes in few of the cores (Mallants et al., 1997; Reynolds et al., 2000).

By March (164 days after last sowing), the significant increase in ρ_B points to the continuing post-tillage compaction (Fig. 3) of the soil due to effective rainfall (201 mm; Fig. 1) as observed by other authors (Moret and Arrúe, 2007; Pena-Sancho et al., 2017; Schwen et al., 2011b). K_S was further reduced (Fig. 5; significant only for RT) following the loss in transmission pores on CT and RT that were almost halved in volume fraction. As for the PSD, intraaggregate pores were created at the expense of interaggregate pores (Figs. 6, 7). Freeze-thaw cycles may have disintegrated larger aggregates (1000–5000 μm) favoring the formation of smaller aggregates (250–1000 μm) (Li and Fan, 2014) thereby homogenizing the soil structure towards a more unimodal PSD. Again, lower macroaggregate stability on CT might explain the shift of the structural domain towards smaller pores while on RT only a decrease in volumetric frequency was observed. On NT there was barely any change in the PSD by that time indicating persistence of the prevalent soil structure against freeze-thaw cycles. Chopped straw residues and remaining stubbles from the last winter wheat harvest possibly moderated extremes in moisture and temperature in addition to the positive effects of organic matter incorporation on aggregate stability and the absence of mechanical disturbance (Blanco-Canqui and Ruis, 2018). Nevertheless, r_{m1} increased slightly during winter on all treatments. Bodner et al. (2013a) found an increase in Kosugi parameter r_m and a decrease of σ connected to increasing wetting-drying cycle intensities. With frequent precipitation events prior to the March sampling this may explain the larger r_{m1} values despite aggregate disintegration through freeze-thaw cycles. Converse to Bodner et al. (2013a) our corresponding σ_1 increased which might be due to the bimodal parameterization we used where the additional width in the structural curve could be to some extent balanced by a decline in the textural heterogeneity σ_2 (Table 3).

By the end of May (242 days after last sowing), the structural mode on all plots had practically disappeared with hardly any difference between r_{m1} and r_{m2} (Table 3) leading to a unimodal homogeneous PSD. Transmission pore volume fraction was also at a minimum on all treatments (Fig. 8). As pointed out in the previous paragraph, r_{m1} has been found to be positively correlated to the intensity of wetting-drying cycles. However, during a phase of water deficit r_m was found to decrease together with slight increases in σ due to aggregate coalescence

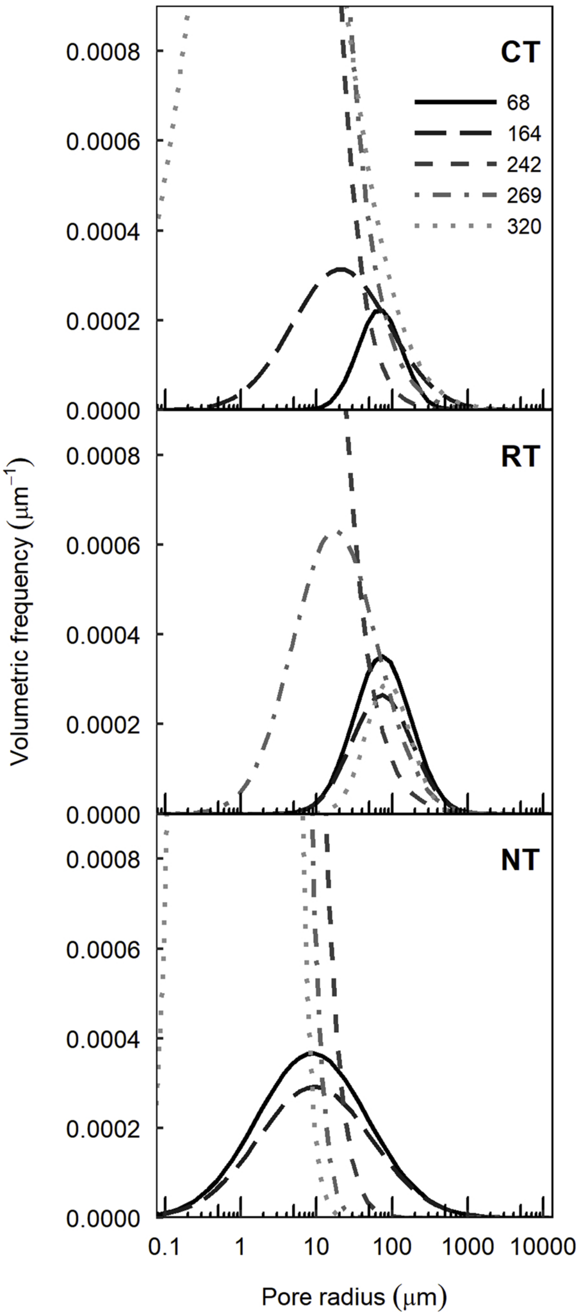

Fig. 7. Evolution of the soil structural domain of the PSD considering porosity (Φ) defined as the difference between saturated (θ_s) and residual (θ_r) water content (Eq. 3) under all three treatments conventional tillage (CT), reduced mulch tillage (RT) and no tillage (NT). Different lines represent days passed since last sowing of winter wheat on 2 October 2015.

in favor of smaller pore size classes (Bodner et al., 2013a) as also seen in a slight increase of storage pores on all plots. On all treatments such a decrease in r_{m1} together with an increase of σ_1 (only on CT and RT) was observed. Since the last sampling 78 days prior comparably little effective rainfall (39 mm) had accumulated. In addition to the lack of effective rainfall crop growth (Fig. 1) tends to increase evapotranspiration throughout the season especially in the flowering phase of winter wheat (Kang et al., 2003). This potentially aggravated water availability and lead to the observed reduction in interaggregate pores. While the structural domain disappeared the overall pore volume increased as indicated by a reduction in ρ_B under CT and RT resulting in a unimodal but wider PSD.

By the end of June (269 days after last sowing), some of the structural PSD domain was restored on RT. Here, continued decay of abundant organic matter mixed into the upper soil layer may have contributed to the regeneration of the structural domain. In addition to decaying organic matter, weather conditions could have played a role again. Within about 27 days since the last sampling, 35 mm effective rainfall had accumulated together with increased evapotranspiration which could have intensified wetting-drying cycles again compared to the previous period leading to an increase in r_{m1} or macroporosity (Bodner et al., 2013a, 2013b). This would also explain the continuing decrease in ρ_B on CT and RT while on NT wetting-drying cycles were moderated through straw residue covering the surface. Despite a distinctly higher transmission pore volume fraction K_S-values did not increase which points to a poor connectivity of the newly developed macropores.

In the 51 days to the next sampling after harvest, only 10.2 mm h^{-1} effective rainfall was observed with weak intensities (maximum intensity: 0.8 mm h^{-1}). Larger K_S-values despite higher ρ_B in August suggest that fissures or biopores, i.e., earthworm burrows, decaying stalks and especially root channels (Blanco-Canqui and Ruis, 2018; Strudley et al., 2008) together with newly formed transmission pores governed the percolation process. Up to 43 and 36% of winter wheat roots grown at tillering and ear emergence stages, respectively, have been shown to already have decayed by the end of the growing season shortly before harvest (Swinnen et al., 1995). This underlines their potential to provide root channels for infiltration but also their contribution to a more heterogeneous and stable soil structure at this stage of our measurements as observed in the PSDs (Figs. 6, 7) and increases in pore size classes with $\varnothing > 50\,\mu m$ on all treatments (Fig. 8).

Overall, temporal variability in PSD was more pronounced on tilled plots. This was also true for ρ_B which showed significant changes over time confirming the hypothesis of a comparably inert soil structure on NT. Nevertheless, PSD under NT showed changes in its structural domain. Seasonal averages in ρ_B and K_S were not significantly different between treatments which raises the question when and how often SHP and SPP need to be quantified for modeling applications. In case of modeling e.g. irrigation schedules (Feki et al., 2018) a seasonal quantification may be warranted while for studies covering a larger time span beyond a cropping season, i.e., more than one year, a less detailed description with one or two observations per year may be sufficient. Our results can be summarized to four distinct phases of a winter wheat cropping cycle on a silt loam soil that should be observed especially on tilled plots such as CT and RT:

(1) Some weeks after (annual) tillage (here 68 days) with the newly created loose macropore-rich structure as the initial phase of the cycle when instantaneous pore loss (Or et al., 2000) has already closed the larger instable void spaces. Volume fraction taken up by transmission pores is still high (RT > CT) at that time highlighting the difference to the untilled system (NT) (Fig. 8).
(2) After winter (164 days) when environmental conditions (mostly temperature and moisture) have led to a continued settling of the structural domain as built up by tillage. The tillage effect is still visible in abundant fissures and transmission pores but a tendency to a shift towards the textural domain with a decline in overall Φ can be observed. Pore volumes under NT hardly experienced any changes by that time (Fig. 8).
(3) Mid to end of the growing season before harvest (242 days) when bimodality has disappeared (Figs. 6, 7) because of rainfall impact and intensified soil drying through increased evapotranspiration. Volume fractions taken up by fissures and transmission pores are at a seasonal minimum (Fig. 8).
(4) Shortly before and after harvest (269 and 320 days, respectively) when effects of root growth and organic matter decay come to show

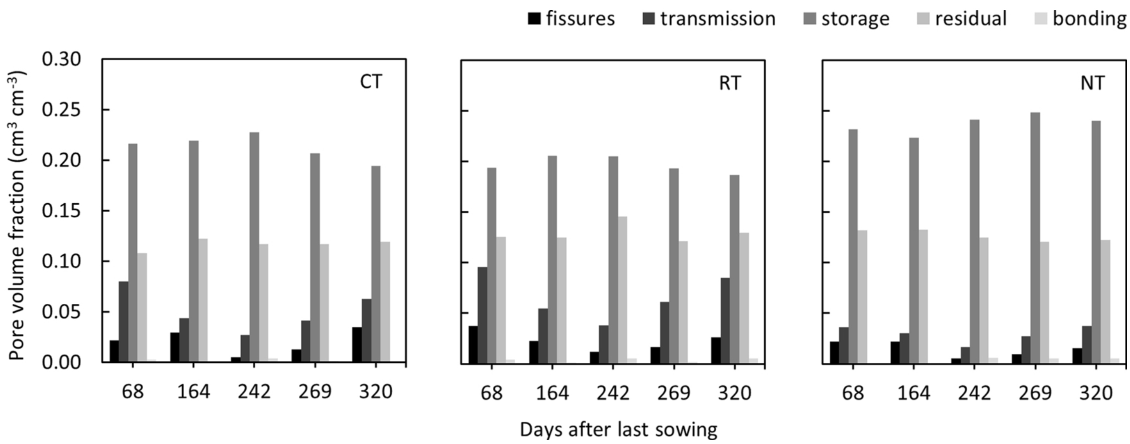

Fig. 8. Volume fraction of different pore size classes (Greenland, 1981) obtained from the area under bimodal pore size distribution (Eq. 3). Classes were fissures (diameter (∅) > 500 µm), transmission (∅ 50–500 µm), storage (∅ 0.5–50 µm), residual (∅ 0.005 - 0.5 µm) and bonding (∅ < 0.005 µm) pores.

with a restoration of the soil structural domain as seen in increases in fissures and transmission pores as well as a general loosening process with lower ρ_B and increasing K_S.

It needs to be stressed that these results are site specific and restricted to the top soil layer. For other tillage/cropping systems, soil types and depths soil structure may respond differently towards the influence of environmental conditions. In our case, RT for example was more resilient against environmental conditions degrading soil structure compared to CT due to higher OC stocks incorporated into the top soil layer. On the other hand, the CT system in our study may be more resilient towards aggregate disintegration and compaction in greater depths due to a more balanced organic matter distribution. In systems, where organic residue is removed overall soil structure may be more vulnerable.

5. Conclusions

The frequent observation of soil structural changes within a winter wheat cropping season showed distinct temporal variations in the derived soil pore size distribution of tilled plots CT and RT. Here, changes in soil pore space occurred mostly in pore classes with ∅ > 50 µm which are associated with water transport. Saturated hydraulic conductivity varied together with abundances of transmission pores highlighting the susceptibility of infiltration processes at saturation towards changes in PSD. Soil structure under NT was temporally more stable with its comparably lower transmission but more storage pores.

These results highlight the need to explicitly consider the evolution of the structural domain of tilled soils in modeling frameworks. This may especially be relevant when simulating soil water fluxes over a short time period e.g. a cropping season. Going one step further than a mere stepwise implementation of SHP into hydrological models as outlined in the introduction section would be to predict the evolution of soil pore space using an existing model (cf. Chandrasekhar et al., 2018). This study with its data provides a basis for that. In the long run, predicting such soil pore space changes would ideally replace the majority of costly and time-consuming field and laboratory measurements. Remaining challenges are spatial heterogeneity of soil structure as well as site- and management-specific conditions that hamper comparison and generalization of quantified soil structural changes.

Acknowledgements

The research was supported by the German Research Foundation (DFG) [grant numbers SCHW 1448/6-1 and FE 504/11-1]; and the Austrian Science Fund (FWF) [grant number I-2122-B16]. We would like to thank D. Kunzendorf for giving us the opportunity to work on the tillage trials Lüttewitz of Südzucker AG and supporting us in our field work. We are also deeply indebted to G. Fontenla Razzetto and G. Ciesielski who helped with field and/or laboratory measurements.

Appendix A. Supplementary data

Supplementary material related to this article can be found, in the online version, at doi:https://doi.org/10.1016/j.still.2019.05.014.

References

Alletto, L., Coquet, Y., 2009. Temporal and spatial variability of soil bulk density and near-saturated hydraulic conductivity under two contrasted tillage management systems. Geoderma 152, 85–94. https://doi.org/10.1016/j.geoderma.2009.05.023.
Alletto, L., Pot, V., Giuliano, S., Costes, M., Perdrieux, F., Justes, E., 2015. Temporal variation in soil physical properties improves the water dynamics modeling in a conventionally-tilled soil. Geoderma 243–244, 18–28. https://doi.org/10.1016/j.geoderma.2014.12.006.
Andruschkewitsch, R., Koch, H.-J., Ludwig, B., 2014. Effect of long-term tillage treatments on the temporal dynamics of water-stable aggregates and on macro-aggregate turnover at three German sites. Geoderma 217–218, 57–64. https://doi.org/10.1016/j.geoderma.2013.10.022.
Bissonnais, Y., 1996. Aggregate stability and assessment of soil crustability and erodibility: I. Theory and methodology. Eur. J. Soil Sci. 47, 425–437. https://doi.org/10.1111/j.1365-2389.1996.tb01843.x.
Blanco-Canqui, H., Ruis, S.J., 2018. No-tillage and soil physical environment. Geoderma 326, 164–200. https://doi.org/10.1016/j.geoderma.2018.03.011.
Blanco-Canqui, H., Wienhold, B.J., Jin, V.L., Schmer, M.R., Kibet, L.C., 2017. Long-term tillage impact on soil hydraulic properties. Soil Tillage Res. 170, 38–42. https://doi.org/10.1016/j.still.2017.03.001.
Blume, H.-P., Brümmer, G.W., Fleige, H., Horn, R., Kandeler, E., Kögel-Knabner, I., Kretzschmar, R., Stahr, K., Wilke, B.-M., 2016. Physical properties and processes. Scheffer/Schachtschabel Soil Science. Springer, Berlin Heidelberg, Berlin, Heidelberg, pp. 175–283. https://doi.org/10.1007/978-3-642-30942-7_6.
Bodner, G., Scholl, P., Kaul, H.-P., 2013a. Field quantification of wetting–drying cycles to predict temporal changes of soil pore size distribution. Soil Tillage Res. 133, 1–9. https://doi.org/10.1016/j.still.2013.05.006.
Bodner, G., Scholl, P., Loiskandl, W., Kaul, H.-P., 2013b. Environmental and management influences on temporal variability of near saturated soil hydraulic properties. Geoderma 204–205, 120–129. https://doi.org/10.1016/j.geoderma.2013.04.015.
Chandrasekhar, P., Kreiselmeier, J., Schwen, A., Weninger, T., Julich, S., Feger, K.-H., Schwärzel, K., 2018. Why we should include soil structural dynamics of agricultural soils in hydrological models. Water 10, 1862. https://doi.org/10.3390/w10121862.
De Gryze, S., Six, J., Brits, C., Merckx, R., 2005. A quantification of short-term macro-aggregate dynamics: influences of wheat residue input and texture. Soil Biol. Biochem. 37, 55–66. https://doi.org/10.1016/j.soilbio.2004.07.024.
Derpsch, R., Franzluebbers, A.J., Duiker, S.W., Reicosky, D.C., Koeller, K., Friedrich, T., Sturny, W.G., Sá, J.C.M., Weiss, K., 2014. Why do we need to standardize no-tillage research? Soil Tillage Res. 137, 16–22. https://doi.org/10.1016/j.still.2013.10.002.
Ellert, B.H., Bettany, J.R., 1995. Calculation of organic matter and nutrients stored in soils under contrasting management regimes. Can. J. Soil Sci. 75, 529–538. https://doi.org/10.4141/cjss95-075.
Feki, M., Ravazzani, G., Ceppi, A., Mancini, M., 2018. Influence of soil hydraulic variability on soil moisture simulations and irrigation scheduling in a maize field. Agric. Water Manag. 202, 183–194. https://doi.org/10.1016/j.agwat.2018.02.024.
Green, V., Stott, D., Cruz, J., Curi, N., 2007. Tillage impacts on soil biological activity and

aggregation in a Brazilian Cerrado Oxisol. Soil Tillage Res. 92, 114–121. https://doi.org/10.1016/j.still.2006.01.004.
Greenland, D.J., 1981. Soil management and soil degradation. J. Soil Sci. 32, 301–322. https://doi.org/10.1111/j.1365-2389.1981.tb01708.x.
Haas, C., Horn, R., 2018. Impact of small-scaled differences in micro-aggregation on physico-chemical parameters of macroscopic biopore walls. Front. Environ. Sci. 6. https://doi.org/10.3389/fenvs.2018.00090.
Han, E., Kautz, T., Perkons, U., Uteau, D., Peth, S., Huang, N., Horn, R., Köpke, U., 2015. Root growth dynamics inside and outside of soil biopores as affected by crop sequence determined with the profile wall method. Biol. Fertil. Soils 51, 847–856. https://doi.org/10.1007/s00374-015-1032-1.
Holland, J.M., 2004. The environmental consequences of adopting conservation tillage in Europe: reviewing the evidence. Agric. Ecosyst. Environ. 103, 1–25. https://doi.org/10.1016/j.agee.2003.12.018.
Horel, Á., Tóth, E., Gelybó, G., Kása, I., Bakacsi, Z., Farkas, C., 2015. Effects of land use and management on soil hydraulic properties. Open Geosci. 7. https://doi.org/10.1515/geo-2015-0053.
IUSS Working Group WRB, 2015. World Reference Base for Soil Resources 2014, Update 2015 International Soil Classification System for Naming Soils and Creating Legends for Soil Maps (No.106). World Soil Resources Reports. FAO, Rome.
Jacobs, A., Jungert, S., Koch, H.-J., 2015. Soil organic carbon as affected by direct drilling and mulching in sugar beet – wheat rotations. Arch. Agron. Soil Sci. 61, 1079–1087. https://doi.org/10.1080/03650340.2014.981669.
Kang, S., Gu, B., Du, T., Zhang, J., 2003. Crop coefficient and ratio of transpiration to evapotranspiration of winter wheat and maize in a semi-humid region. Agric. Water Manag. 59, 239–254. https://doi.org/10.1016/S0378-3774(02)00150-6.
Kargas, G., Kerkides, P., Sotirakoglou, K., Poulovassilis, A., 2016. Temporal variability of surface soil hydraulic properties under various tillage systems. Soil Tillage Res. 158, 22–31. https://doi.org/10.1016/j.still.2015.11.011.
Kargas, G., Londra, P.A., 2015. Effect of tillage practices on the hydraulic properties of a loamy soil. Desalin. Water Treat. 54, 2138–2146. https://doi.org/10.1080/19443994.2014.934110.
Kassam, A., Friedrich, T., Derpsch, R., Kienzle, J., 2015. Overview of the worldwide spread of conservation agriculture. Field Actions Sci. Rep. 8, 1–11.
Kautz, T., Lüsebrink, M., Pätzold, S., Vetterlein, D., Pude, R., Athmann, M., Küpper, P.M., Perkons, U., Köpke, U., 2014. Contribution of anecic earthworms to biopore formation during cultivation of perennial ley crops. Pedobiologia 57, 47–52. https://doi.org/10.1016/j.pedobi.2013.09.008.
Klute, A., Dirksen, C., 1986. Hydraulic conductivity and diffusivity: laboratory methods. In: Klute, A. (Ed.), Methods of Soil Analysis. Part 1. Physical and Mineralogical Methods. ASA and SSSA, Madison, WI, pp. 687–734.
Koch, H.-J., Dieckmann, J., Büchse, A., Märländer, B., 2009. Yield decrease in sugar beet caused by reduced tillage and direct drilling. Eur. J. Agron. 30, 101–109. https://doi.org/10.1016/j.eja.2008.08.001.
Kosugi, K., 1996. Lognormal distribution model for unsaturated soil hydraulic properties. Water Resour. Res. 32, 2697–2703. https://doi.org/10.1029/96WR01776.
Lal, R., Reicosky, D.C., Hanson, J.D., 2007. Evolution of the plow over 10,000 years and the rationale for no-till farming. Soil Tillage Res. 93, 1–12. https://doi.org/10.1016/j.still.2006.11.004.
Lee, D.M., Elrick, D.E., Reynolds, W.D., Clothier, B.E., 1985. A comparison of three field methods for measuring saturated hydraulic conductivity. Can. J. Soil Sci. 65, 563–573. https://doi.org/10.4141/cjss85-060.
Lenth, R., Singmann, H., Love, J., Buerkner, P., Herve, M., 2018. Emmeans: Estimated Marginal Means, aka Least-squares Means. R package version 1.2.3. .
Li, G.-Y., Fan, H.-M., 2014. Effect of freeze-thaw on water stability of aggregates in a black soil of Northeast China. Pedosphere 24, 285–290. https://doi.org/10.1016/S1002-0160(14)60015-1.
Mallants, D., Mohanty, B.P., Vervoort, A., Feyen, J., 1997. Spatial analysis of saturated hydraulic conductivity in a soil with macropores. Soil Technol. 10, 115–131. https://doi.org/10.1016/S0933-3630(96)00093-1.
Martínez, E., Fuentes, J.-P., Silva, P., Valle, S., Acevedo, E., 2008. Soil physical properties and wheat root growth as affected by no-tillage and conventional tillage systems in a Mediterranean environment of Chile. Soil Tillage Res. 99, 232–244. https://doi.org/10.1016/j.still.2008.02.001.
METER Environment, 2019. KSAT Operation Manual. https://metergroup-83d0.kxcdn.com/app/uploads/2018/12/KSAT_Manual.042019.pdf.
Moret, D., Arrúe, J.L., 2007. Dynamics of soil hydraulic properties during fallow as affected by tillage. Soil Tillage Res. 96, 103–113. https://doi.org/10.1016/j.still.2007.04.003.
Mualem, Y., 1976. A new model for predicting the hydraulic conductivity of unsaturated porous media. Water Resour. Res. 12, 513–522.
Or, D., Leij, F.J., Snyder, V., Ghezzehei, T.A., 2000. Stochastic model for posttillage soil pore space evolution. Water Resour. Res. 36, 1641–1652. https://doi.org/10.1029/2000WR900092.
Oztas, T., Fayetorbay, F., 2003. Effect of freezing and thawing processes on soil aggregate stability. Catena 52, 1–8. https://doi.org/10.1016/S0341-8162(02)00177-7.
Pena-Sancho, C., Lopez, M.V., Gracia, R., Moret-Fernandez, D., 2017. Effects of tillage on the soil water retention curve during a fallow period of a semiarid dryland. Soil Res. 55, 114. https://doi.org/10.1071/SR15305.
R Development Core Team, 2017. R: A Language and Environment for Statistical Computing. R Foundation for Statistical Computing.
Rasse, D.P., Smucker, A.J.M., Santos, D., 2000. Alfalfa root and shoot mulching effects on soil hydraulic properties and aggregation. Soil Sci. Soc. Am. J. 64, 725. https://doi.org/10.2136/sssaj2000.642725x.
Reichert, J.M., da Rosa, V.T., Vogelmann, E.S., da Rosa, D.P., Horn, R., Reinert, D.J., Sattler, A., Denardin, J.E., 2016. Conceptual framework for capacity and intensity physical soil properties affected by short and long-term (14 years) continuous no-tillage and controlled traffic. Soil Tillage Res. 158, 123–136. https://doi.org/10.1016/j.still.2015.11.010.
Reynolds, W.D., Bowman, B.T., Brunke, R.R., Drury, C.F., Tan, C.S., 2000. Comparison of tension infiltrometer, pressure infiltrometer, and soil core estimates of saturated hydraulic conductivity. Soil Sci. Soc. Am. J. 64, 478. https://doi.org/10.2136/sssaj2000.642478x.
Romano, N., Nasta, P., 2016. How effective is bimodal soil hydraulic characterization? Functional evaluations for predictions of soil water balance: functional evaluations for bimodal soil. Eur. J. Soil Sci. 67, 523–535. https://doi.org/10.1111/ejss.12354.
Romano, N., Nasta, P., Severino, G., Hopmans, J.W., 2011. Using bimodal lognormal functions to describe soil hydraulic properties. Soil Sci. Soc. Am. J. 75, 468. https://doi.org/10.2136/sssaj2010.0084.
Schwärzel, K., Carrick, S., Wahren, A., Feger, K.-H., Bodner, G., Buchan, G., 2011. Soil hydraulic properties of recently tilled soil under cropping rotation compared with two-year pasture. Vadose Zone J. 10, 354. https://doi.org/10.2136/vzj2010.0035.
Schwen, A., Bodner, G., Loiskandl, W., 2011a. Time-variable soil hydraulic properties in near-surface soil water simulations for different tillage methods. Agric. Water Manag. 99, 42–50. https://doi.org/10.1016/j.agwat.2011.07.020.
Schwen, A., Bodner, G., Scholl, P., Buchan, G.D., Loiskandl, W., 2011b. Temporal dynamics of soil hydraulic properties and the water-conducting porosity under different tillage. Soil Tillage Res. 113, 89–98. https://doi.org/10.1016/j.still.2011.02.005.
Seki, K., 2007. SWRC fit - a nonlinear fitting program with a water retention curve for soils having unimodal and bimodal pore structure. Hydrol. Earth Syst. Sci. Discuss. 4, 407–437. https://doi.org/10.5194/hessd-4-407-2007.
Strudley, M., Green, T., Ascoughii, J., 2008. Tillage effects on soil hydraulic properties in space and time: state of the science. Soil Tillage Res. 99, 4–48. https://doi.org/10.1016/j.still.2008.01.007.
Swinnen, J., Van Veen, J.A., Merckx, R., 1995. Root decay and turnover of rhizodeposits in field-grown winter wheat and spring barley estimated by 14C pulse-labelling. Soil Biol. Biochem. 27, 211–217. https://doi.org/10.1016/0038-0717(94)00161-S.
van Genuchten, M.T., 1980. A closed-form equation for predicting the hydraulic conductivity of unsaturated soils. Soil Sci. Soc. Am. J. 44, 892. https://doi.org/10.2136/sssaj1980.03615995004400050002x.
Vereecken, H., Schnepf, A., Hopmans, J.W., Javaux, M., Or, D., Roose, T., Vanderborght, J., Young, M.H., Amelung, W., Aitkenhead, M., Allison, S.D., Assouline, S., Baveye, P., Berli, M., Brüggemann, N., Finke, P., Flury, M., Gaiser, T., Govers, G., Ghezzehei, T., Hallett, P., Hendricks Franssen, H.J., Heppell, J., Horn, R., Huisman, J.A., Jacques, D., Jonard, F., Kollet, S., Lafolie, F., Lamorski, K., Leitner, D., McBratney, A., Minasny, B., Montzka, C., Nowak, W., Pachepsky, Y., Padarian, J., Romano, N., Roth, K., Rothfuss, Y., Rowe, E.C., Schwen, A., Šimůnek, J., Tiktak, A., Van Dam, J., van der Zee, S.E.A.T.M., Vogel, H.J., Vrugt, J.A., Wöhling, T., Young, I.M., 2016. Modeling soil processes: review, key challenges, and new perspectives. Vadose Zone J. 15. https://doi.org/10.2136/vzj2015.09.0131.
Webster, R., 2007. Analysis of variance, inference, multiple comparisons and sampling effects in soil research. Eur. J. Soil Sci. 58, 74–82. https://doi.org/10.1111/j.1365-2389.2006.00801.x.
Weninger, T., Bodner, G., Kreiselmeier, J., Chandrasekhar, P., Julich, S., Feger, K.-H., Schwärzel, K., Schwen, A., 2018. Combination of measurement methods for a wide-range description of hydraulic soil properties. Water 10, 1021. https://doi.org/10.3390/w10081021.
Wind, G.P., 1969. Capillary conductivity data estimated by a simple method. Proceedings of the Wageningen Symposium - June 1966 - Water in the Unsaturated Zone. Presented at the UNESCO/IASH, International Association of Scientific Hydrology.
Xiao, H., Liu, G., Zhang, Q., Fenli, Z., Zhang, X., Liu, P., Zhang, J., Hu, F., Elbasit, M.A.M.A., 2018. Quantifying contributions of slaking and mechanical breakdown of soil aggregates to splash erosion for different soils from the Loess plateau of China. Soil Tillage Res. 178, 150–158. https://doi.org/10.1016/j.still.2017.12.026.

Geoderma 338 (2019) 187–196

Contents lists available at ScienceDirect

Geoderma

journal homepage: www.elsevier.com/locate/geoderma

Estimating the extent of fire induced soil water repellency in Mediterranean environment

Thomas Weninger[a], Vilim Filipović[b,*], Mirel Mešić[b], Brent Clothier[c], Lana Filipović[b]

[a] University of Natural Resources and Life Sciences Vienna (BOKU), Institute of Hydraulics and Rural Water Management, Muthgasse 18, 1190 Vienna, Austria
[b] University of Zagreb, Faculty of Agriculture, Department of Soil Amelioration, Svetošimunska 25, 10000 Zagreb, Croatia
[c] Plant & Food Research, Fitzherbert Science Centre, Palmerston North, New Zealand

ARTICLE INFO

Handling Editor: Michael Vepraskas

Keywords:
Burnt soil
Forest fire
Soil water repellency estimation
Infiltration
Sub-critical SWR

ABSTRACT

The fire occurrence in Mediterranean climate regions and the area affected by fire in general are rising due to prolonged drought periods and redistribution of rainfall. This can have effect on soil properties and local scale hydrology by increasing fire induced soil water repellency (SWR). The main objective of our research was to assess the degree of fire induced SWR in the Mediterranean karst area using multiple easy-to-perform field and laboratory methods. The field infiltration measurements were performed with a tension disc infiltrometer (TI) and a minidisc tension infiltrometer (MD) using water and ethanol as an infiltrating liquid on two locations: burnt (B) and control (C, unaffected by fire). Additionally, water drop penetration time test (WDPT), and molarity of ethanol droplet time test (MED) were applied at the laboratory on disturbed and undisturbed soil samples at various depths. All measurements revealed significant differences between burnt and control plots. Infiltration and hydraulic conductivity were reduced and repellency index (RI) was increased at the fire affected sites. The SWR decreased with depth which can be associated with decreasing organic matter and fire burning effect. The WDPT and MED methods in combination with mini disc tension infiltrometer measurements were found useful for the determination of sub-critical SWR. Further research is needed to develop a framework for the quantitative SWR classification, as well as subsequent estimation of the relevance of SWR on critical hydrological processes such as infiltration, runoff, and preferential flow.

1. Introduction

In the near future, an increasing number of wildfires of various extents and severities is expected to occur in the Northern Hemisphere due to changing climate (Giannakopoulos et al., 2009; Santer et al., 2018). Soil surface conditions change after a fire, amongst others resulting in soil water repellency (SWR). Post-fire SWR is usually caused by facultatively hydrophobic organic compounds resulting from litter and soil organic matter combustion (Doerr et al., 2000; DeBano, 2000; Jordán et al., 2013; Zheng et al., 2016). During a fire, organic substances in the soil become volatilized with a proportion travelling downward following the temperature gradient in the litter and soil until they condense in a concentrated form (DeBano and Krammes, 1966; DeBano et al., 1970; Savage, 1974). It is known that heating of hydrophilic soil containing > 2–3% organic matter induces a certain level of SWR (DeBano, 1991). Mataix-Solera et al. (2014) moreover stated that soil texture, namely sand content which is positively correlated to SWR, is the main soil property controlling fire-induced SWR along with quality of organic matter. The SWR impacts the soil water balance by reducing infiltration capacity (Filipović et al., 2018), increased overland flow and soil erosion (Doerr et al., 2000), development of fingered flow in preferential flow paths (Deurer and Bachmann, 2007), and the creation of unstable, irregular wetting fronts (Bughici and Wallach, 2016). On the other hand, SWR may stabilize soil organic matter against dilution or erosion by water and increase aggregate stability (Bachmann et al., 2008; Zheng et al., 2016).

The physical metric representing SWR is the contact angle between soil and water (Hallett, 2007) which may be directly measured in the laboratory using high-speed cameras (Bachmann et al., 2000). More practical are the indirect methods like the water drop penetration time test (WDPT), the measurement of infiltration rate using infiltrometers, or the molarity of ethanol droplet test (MED) (Doerr, 1998, Table 1; Hallett, 2007). These methods are easily applied but have certain shortcomings. The WDPT and MED only account for critical SWR, where the contact angle is > 90°. In infiltration experiments to determine SWR, usually mini disc (MD) infiltrometers are used. They

* Corresponding author.
E-mail address: vfilipovic@agr.hr (V. Filipović).

https://doi.org/10.1016/j.geoderma.2018.12.008
Received 29 August 2018; Received in revised form 19 November 2018; Accepted 3 December 2018

Table 1
Classification of soil water repellency results (modified after Doerr, 1998).

SWR, verbal rating	None	Slight			Strong			Severe		Extreme
WDPT class	0	1	2	3	4	5	6	7	8	9
WDPT (s)	< 5	6–10	11–30	31–60	61–180	181–300	301–600	601–900	901–3600	> 3600
MED class	1,2	3,4			5			6		7
% Ethanol	0,3	5,8.5			13			24		36

measure SWR via the suppressed water sorptivity of water repellent soil (Tillman et al., 1989). Advances of methodology, especially the ongoing development of appropriate repellency indices from tension infiltrometer measurements, enable a reliable estimation of SWR even though manifold options in the experimental setup (e.g. applied water head, infiltration area, used fluids) or evaluation approaches diminish comparability with older results (Beatty and Smith, 2014; Pekárová et al., 2015; Schwen et al., 2015; Sepehrnia et al., 2016). Nevertheless, sub-critical SWR (contact angle < 90°) may be analyzed using tension infiltrometers which is important as its widespread relevance for soil hydrology is still under-recognized (Hallett et al., 2001; Lichner et al., 2007; Müller et al., 2016). Additionally, measurements of SWR are not trivial, because of the variable state of soil, and because several factors affect SWR, especially fire-induced SWR. These are for example soil texture, soil moisture, vegetation type and time since burning (DeBano, 2000; MacDonald and Huffman, 2004; Liu et al., 2012; Jordán et al., 2013; Plaza-Álvarez et al., 2018). Besides, there is also need for further research about the difference in the degree of SWR detected by undisturbed or disturbed samples (Graber et al., 2006).

An opportunity for a more direct and representative assessment of SWR is the combination of different methods. Sepehrnia et al. (2016) calculated SWR from WDPT and MD experiments on a wettable and a water repellent soil (depth 0–60 cm) in Iran. Mean results of actual (on field-moist samples) and potential (samples dried at 65 to 70 °C for 24 h) WDPT for water repellent soil (n = 540 for both) were 438 and 106 times greater than those for wettable soil, respectively. The MD experiments were carried out to calculate the repellency index from water and ethanol sorptivity (RI_c), as well as the proposal of water repellency cessation time and a modified repellency index (RI_m) which were derived by relating to each other the initial (hydrophobic soil) and the final stage (wettable) of a single infiltration run with water. The water repellency cessation times, RI_c, and RI_m were about eight, seven, and two times greater than those in wettable soil, respectively. Additionally, higher content of organic matter was stated to be significantly related to SWR. Alagna et al. (2017) applied the same methodology on two managed pine woodlands of the coastal Mediterranean region (Spain and Italy). Generally, the WDPT test and MD experiment results yielded consistent SWR estimations and were correlated one to another. It was confirmed that WDPT could discriminate between wettable and hydrophobic conditions but could not account for sub-critical SWR. In this state, infiltration is reduced but not eliminated and hydrological processes may subsequently be affected. By MD experiments, sub-critical conditions were disclosed and information about spatial variability could have been added by the combination of methods which represent different soil volumes.

Most studies where SWR has been investigated on burnt and unburnt soil showed that fire can either induce (Zavala et al., 2009; Varela et al., 2010; Stoof et al., 2011; Granged et al., 2011; Plaza-Álvarez et al., 2018) or destroy SWR, and that it can develop it in the deeper soil layers (Jordán et al., 2010). Tessler et al. (2008) assessed in situ SWR by > 3400 WDPT tests on 31 burnt and 15 control sites. Measurements were conducted monthly over a period of seven months and in three depths (0, 5, and 10 cm) to observe the temporal evolution of SWR after fire. Immediately after the fire, the SWR was highest on the surface of burnt sites and decreased significantly with time and depth. In contrast, Capra et al. (2018) did not find any SWR by lab experiments on air-dried samples from two recently burnt and two unburnt sites at Sardinia (Italy), as did White et al. (2017) in situ at Australian coastal sand soils. Both used the WDPT method to estimate SWR.

MacDonald and Huffman (2004) used repeated sampling to quantify changes in SWR over time (in one-year period) and identified soil moisture thresholds for the loss of SWR. The SWR was assessed with critical surface tension (CST) at 36 sites stratified by burn severity and 9 unburnt sites over depth from 0 to 18 cm. The SWR was strongest in sites burnt at high and moderate severity, decreased with depth, and was spatially highly variable. The fire-induced SWR weakened with time and disappeared one year after burning. The soil moisture thresholds above which water repellent soils became hydrophilic were approximately 0.10 g g^{-1} of unburnt sites, 0.13 g g^{-1} for sites burnt under low severity and 0.26 g g^{-1} for sites burnt at moderate and high severity.

The importance of SWR for soil hydrology is increasingly recognized and changes in climate will certainly increase it. The main objective of our research was to assess the degree of fire induced soil water repellency using a combination of easy-to-perform field and laboratory methods. The experiments were performed in Mediterranean karst area at the Croatian coast after a wildfire. The aim was also to focus our research on sub-critical SWR range, which is highly interesting and often under-recognized in environmental studies.

2. Materials and methods

2.1. Field site and infiltration measurements

The field site was located at the Croatian coast near the city of Trogir (43° 31′ 48″ N, 16° 15′ 0″ E). The selection of the site was performed following the forest fire that spread during July 2017. The exact location for infiltration measurements and undisturbed soil sampling were divided into three burnt plots (B_1, B_2, B_3), and two control plots (C_1, C_2) which were unaffected by fire (30 m apart). Small elevation

Table 2
Summary of selected soil characteristics, measured on samples from 0 to 5 cm depth (n = 3). Soil hydraulic conductivity value (K) was calculated according to Dohnal et al. (2010); subscript MD stands for mini disc infiltrometer, TI for glass tension infiltrometer, h denotes the applied experimental water head. Textural classes are: 2 mm ≥ sand > 0.063 mm ≥ silt > 0.002 mm ≥ clay. Abbreviations used for chemical metrics: C_{inorg} is inorganic carbon content, EC is electrical conductivity. Both pH and EC were measured in soil-H_2O-solution.

Treatment	Bulk density /g cm^{-3}	$K_{MD,\ h=-2\ cm}$ /cm day^{-1}	$K_{TI,\ h=-1\ cm}$ /cm day^{-1}	Texture % sand/silt/clay	C_{inorg} /g g^{-1}	pH_{H2O} /−	EC /μS cm^{-1}
Burnt	1.03 (0.03)	25.7 (0.09)	66.7 (0.80)	26/61/13	0.058	7.8	253
Control	1.09 (−)	164.8 (0.59)	61.2 (0.19)	37/48/15	0.058	7.9	184

differences were noticed between the plots (smaller than 0.5 m altitude) and in the soil texture (Table 2), however the selected control plots were chosen mainly due to their proximity to the burnt area. The soil type can be classified as Cambisol with silt loam (B plots) and loam texture (C plots, Table 2; IUSS Working Group, 2015). The site has a mild Mediterranean climate with an annual precipitation of 810 mm and average annual air temperature of 16.3 °C (meteorological station Split, Marjan).

In the field, infiltration experiments were conducted using two instruments: a glass tension disc infiltrometer (TI) and a minidisc tension infiltrometer (MD). Although MD is the standard method for in situ water repellency assessments, we used a second instrument with larger infiltration area to gain additional data supporting our results and to be able to have measurements at multiple applied pressures. General information on tension disc infiltrometry can be found in Clothier and White (1981), Perroux and White (1988) or Angulo-Jaramillo et al. (2016). Infiltration experiments were performed on 20th July. Initial soil water content was measured from the soil surface (instrument penetration depth was 5 cm) using a handheld TDR (Spectrum technologies, USA) and ranged from 0.07 to 0.10 $m^3\,m^{-3}$. A self-constructed TI was also used, where the liquid reservoir was made from glass and directly assembled to the disc (Fig. 1, ii). The infiltrometer disc consisted of porous glass (pore diameter = 40 μm) and had a disc radius of 5.8 cm (Lamparter et al., 2010). This type of infiltrometer allows for the use of both water and ethanol for infiltration measurements (Schwen et al., 2015). Before each infiltration measurement a thin layer of uniform very-fine glass powder was used at the soil surface to ensure good contact between soil and the porous disc (Dragonite, Jaygo Inc.; diameter: 0.45 mm). Infiltration measurements with water and ethanol were conducted on three burnt (B) and two control (C) plots. Three different pressure heads ($h = -5, -3, -1$ cm) were applied sequentially and the time for the first 5 air bubbles rising in the tension supply tube was recorded (Beatty and Smith, 2014). At the same time, infiltration measurements with water and ethanol were also performed using a MD infiltrometer (Meter, metergroup.com) at pressure head $h_0 = -2$ cm in nine repetitions on burnt (B) and three repetitions on control (C) plots.

Differences in the dynamic viscosity (η) of water (η = 1.0 mPa) and ethanol (η = 1.2 mPa) result in different liquid infiltration rates, even at identical liquid contents. For that reason, the infiltration rates of ethanol were corrected for the difference in viscosity between water and ethanol using a factor of 1.2 (Jarvis et al., 2008). In order to consider the different physicochemical properties of the infiltrating liquids, the ethanol pressure head values were additionally scaled based on the capillary rise equation which considers the difference between surface tension and density of two liquids:

$$h_i = \frac{2\sigma_i \cos\gamma}{r\rho_i g} \quad (1)$$

where σ is the surface tension (mN m^{-1}), γ is the contact angle (°), r is the equivalent capillary radius (m), ρ is the density of the liquid (g cm^{-3}), and g is the acceleration due to gravity (m s^{-2}). The subscript i refers to water (w) or ethanol (e). With the water and ethanol surface tension at 20 °C of 72.7 mN m^{-1} and 22.4 mN m^{-1}, and a density of 0.998 g cm^{-3} and 0.789 g cm^{-3}, respectively, a correction factor between h_e and h_w of 2.5 was assumed (Diamantopoulos and Durner, 2013; Lamparter et al., 2010; Filipović et al., 2018). Multiplying h_e with 2.5 results in the effective supply pressure ($h_{e,\,eff}$) giving the applied ethanol pressure heads of −12.5, −7.5, and − 2.5 cm. The correction factor assumes that the contact angles of water/ethanol and the soil surface are identical ($\gamma_e = \gamma_w$), even though water contact angle in the field was changing with time.

For both infiltration methods, the index of water repellency *RI* was calculated from the relation of sorptivity of water $S_w(h_0)$ and the sorptivity of 96.5% ethanol $S_e\,(h_0)$ (Tillman et al., 1989; Hallett et al., 2001). The sorptivities were estimated from the slope of a linear approximation of the cumulative infiltration vs. the square root of time (Eq. (2), Clothier et al., 2000). Due to the non-linear shape of this relation, the early-time cumulative infiltration was used in the analysis which is recorded during the first two time steps with observable infiltration (Hunter et al., 2011; Pekárová et al., 2015). For MD, early-time was defined as the first minute, for the glass infiltrometer 6 min of observation were needed for two valid observation time steps as the changing rate of water level in the reservoir was very low. Experiments using different liquids had to be conducted on different, adjacent soil spots, at a distance of 20 to 50 cm to each other. To extend the data base in comparison to the traditional calculation of *RI* from the sorptivity results of the corresponding pairs, a representative *RI* value was calculated using a permutation approach where every measured S_w was combined with every S_e (Pekárová et al., 2015). By analyzing TI measurements, the *RI* was calculated for each pressure step (with early-time and permutation approaches) and the three resulting *RI* values with their coefficients of variance (CV) were averaged. For MD, results of both approaches to calculate *RI*, permutation and paired, were presented.

$$I = S\,t^{0.5} \quad (2)$$

$$RI = 1.95\,S_e(h_0)/S_w(h_0) \quad (3)$$

2.2. Laboratory estimation of soil water repellency in undisturbed and disturbed soil

Undisturbed soil samples (250 cm^3 cylinder) were taken from burnt (3×) and control plots (3×), air-dried and analyzed in the laboratory at BOKU (Vienna, Austria). To estimate the persistence of SWR, the water drop penetration time (WDPT) test was used as well as the molarity of ethanol droplet (MED) test to obtain the degree of SWR. Ten drops of water for WDPT and different aqueous - ethanol solutions (i.e., 3%, 5%, 8.5%, 13%, 24% and 36% for MED test), each of 200 μl, were applied to the soil layer using a hypodermic syringe. Between the

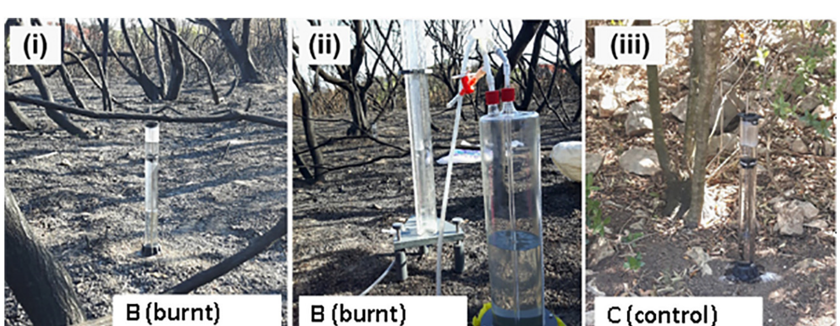

Fig. 1. Site location (Trogir, Croatia) and infiltration measurements (20th July 2017) with water and ethanol on: (i) burnt plot using mini disc infiltrometer (ii) burnt plot using large glass tension disk infiltrometer and (iii) control plot using mini disc infiltrometer.

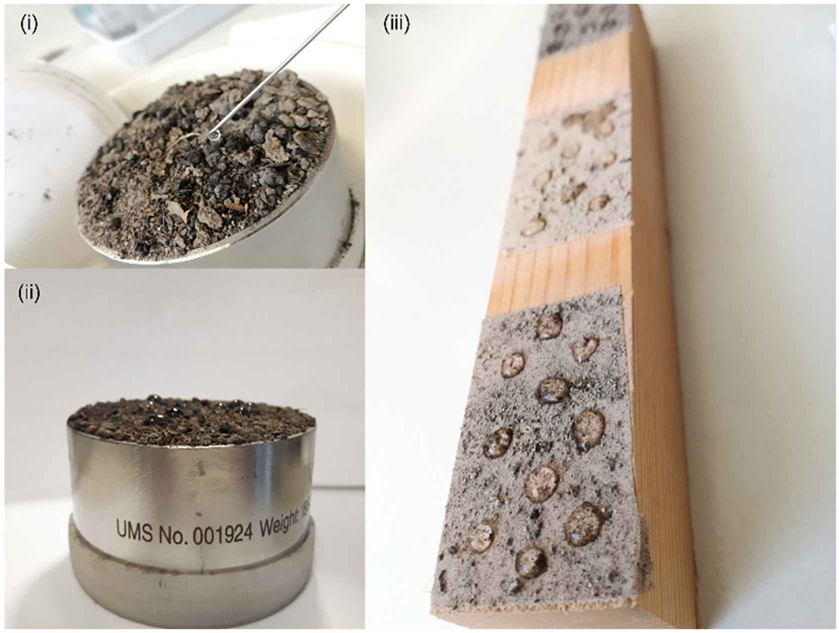

Fig. 2. Preforming the WDPT/MED tests on undisturbed (i, ii) and disturbed single-grain layer (iii) soil samples to estimate the extent on SWR from burnt site located at the Mediterranean coast (Croatia, Trogir).

placement of each drop, a delay of 5 s was used. This delay was to simplify the procedure for the observer. With delay it was easier and more precise to follow the droplet penetration and to record the time. Firstly, the WDPT of soil surface in undisturbed soil samples was recorded (Fig. 2, i and ii). Although the soil moisture/water repellency relationship is complex, generally SWR disappears when soils become wet (Doerr et al., 2000). Hence, samples were air-dried again after each step of WDPT and subsequent MED testing. The penetration time of each drop was recorded, and the average time taken as representative of the WDPT/MED for each sample. Because the SWR layer is frequently found below the soil surface (DeBano et al., 1979) the test was conducted at 4 depths: on the soil surface, at depths of 1, 2 and 3 cm. To allow measurements on deeper layers, soil was pressed out of the core from the bottom by use of a plastic plug and the upper layer was removed with a knife.

For disturbed WDPT/MED tests soil was separated in layers 0–1 cm, 1–3 cm and 4–5 cm, crushed and sieved (< 2 mm). We filled the soil into dishes with a diameter of 50 mm to a height of 10 mm, the surface was flattened and slightly compacted with a small glass cup (Doerr, 1998). Here, no repellency was detected on any samples (WDPT < 5 s). For that reason, the sample preparation for the modified sessile drop method was used, as proposed by Bachmann et al. (2000). A single-grain (SG) layer of soil material was arranged on a double-sided adhesive tape (TWIN TAPE, Schuller Eh'klar, St. Florian, Austria) fixed on a plain piece of wood and WDPT and MED tests were carried out for each soil layer respectively (Fig. 2, iii).

Additional lab experiments were carried out for soil characterization on three separately taken samples at burnt and control plots at 0 to 5 cm depth. We measured the soil bulk density gravimetrically using core samples (250 cm^{-3}), the grain size distribution by a combination of fine sieving and the sedimentation method as well as soil pH and electrical conductivity in H_2O solution. Soil organic carbon content was obtained by subtracting inorganic carbon content (Scheibler method) from total carbon content (Vario MAX CN Analyzer, Elementar Analysensysteme GmbH, Germany).

2.3. Data processing and statistics

The data series were tested for normality and log-normality using the Anderson-Darling test (Anderson and Darling, 1954) which failed in half of the cases of WDPT and MED test series on undisturbed samples (n = 10 drops). The main reason for these results, together with small sample size, is the low resolution of data in hydrophilic spots. It is neither possible, nor meaningful, to measure very short penetration times, usually even a duration below 5 s is assigned to be non-repellent (Table 1). Consequently, a visual interpretation via Q-Q-plots (not presented) was supposed to yield a more robust basis for an estimation of normality and showed that patterns of not-transformed data are sufficiently comparable to normal distribution. On the disturbed SG-layer all units in both original and logarithmic form passed the test for normality. The results from field determination of *RI*, and extended by permutation, matched normality clearly better when logarithmically transformed (Fig. 3). Hence, logarithmic values were used for *RI* and the presented results were re-transformed to original scale. In contrast, for the evaluation of laboratory methods the original data was processed.

A comparison of results derived by the different methods can only be done by qualitative interpretation as the different methods measure different characteristics, or in different scales. Quantitative differences were analyzed between control and fire-affected samples and between different soils depths, and always comparing results from the same method. Therefore, ANOVA with a subsequent post-hoc Tukey HSD-test were conducted with Statistical Analysis Software (SAS Institute, 2001).

3. Results and discussion

3.1. Characterization of soil water repellency

Commonly, WDPT is considered to account for persistence and MED for the severity of SWR. The special characteristic of tension infiltrometer measurement is its sensitivity for subcritical SWR. Our results showed fire-induced presence of SWR in all its forms (Table 3). This statement was justified by the comparison of burnt area with the control plot, as well as classifications according to Table 1. In MD results (Fig. 4), the infiltration rate of water was distinctively reduced at burnt plots compared to the control, while ethanol infiltration was similar at both soils. Also, the measurements with the TI showed a clear difference between water and ethanol infiltration rates (Fig. 5). Water

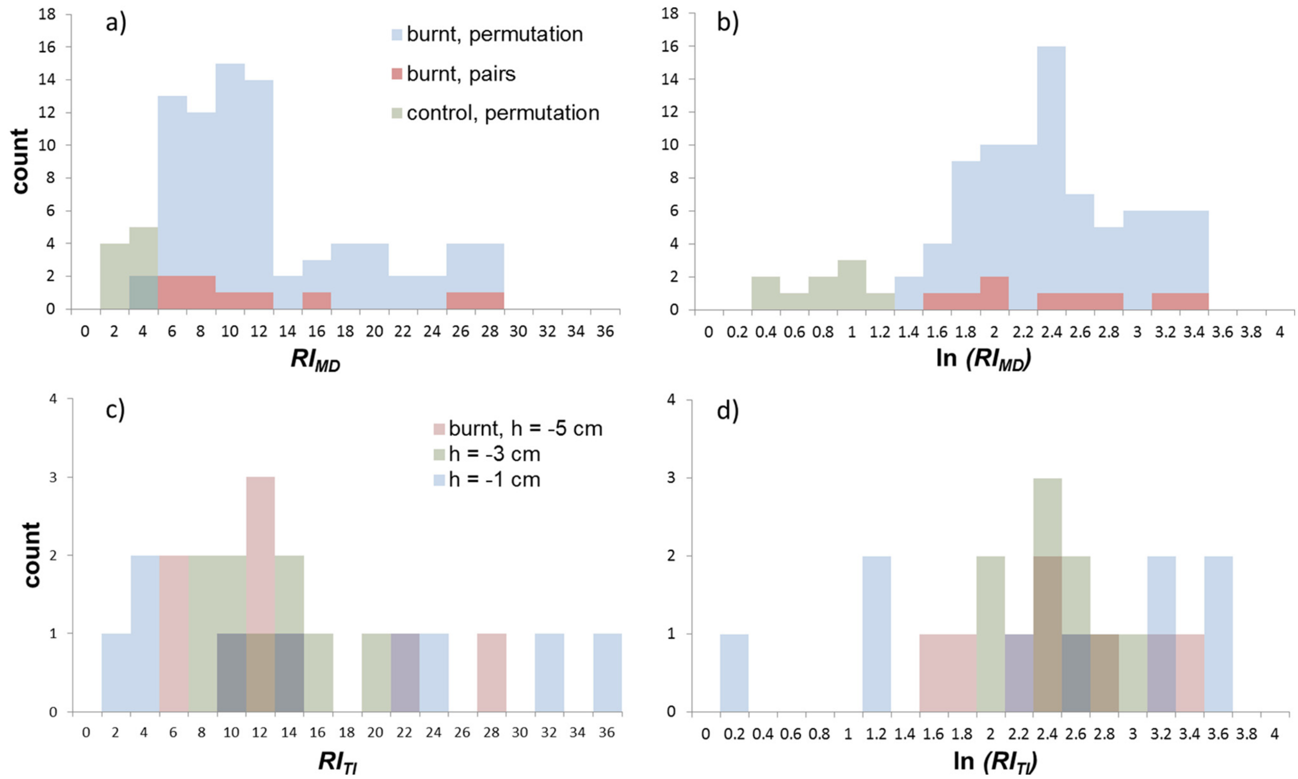

Fig. 3. Histograms of measurement results for RI of mini disc infiltrometer (a, b) and glass tension infiltrometer (c, d). Original (a, c) and logarithmic (b, d) values are presented. Tension infiltrometer measurements were derived by permutation, mini disc by both permutation and analysis of original paired measurements for comparison.

infiltration was again more limited on burnt soil than on control, even though the difference was less distinguished and restricted to measurements at lower matric potential heads (−3 cm and − 5 cm). Moreover, both infiltration methods identified baseline SWR in the control soil, even though $RI_{MD} = 2.09$, hence marginally higher than the threshold of 1.95 (Tillman et al., 1989). This difference between TI and MD was also visible by a comparison of Figs. 4 and 5 where the difference between water infiltration at burnt and control areas was greater at MD (difference between the final slopes of blue lines in Fig. 4, B and C) than at TI (four lines for water measurements). For burnt soils, both MD and TI results were nearly equal at approximately $RI = 12$, which means that initial water sorptivity was decreased by SWR to around 2/12 of its original value. These values could be placed in the medium degree compared with mean results from studies using similar methodology (e.g. Lichner et al., 2017: 1.22 to 13.09, Alagna et al., 2017: 2.1 to 29.7).

An interpretation of quantitative results using classification systems (Doerr, 1998; Table 1) showed few relevant differences in severity and persistence of SWR. The severity at the surface was extreme (MED class, Table 3) while the persistence was two ordinal levels lower, hence strong. Considering the impact of SWR on local hydrology, this indicated the high importance of conditions at the beginning of rainfall events which may lead to surface runoff peaks, but which decreases rather quickly. Moreover, the tests on a single grain layer (SG) yielded quantitative results for samples where no critical SWR was detected with traditional approaches (Table 3 and trials with 10 mm layer of disturbed sample where WDPT was zero in all cases). Hence, this methodology indicated a finer resolution of water repellency observations of sub-critical SWR. Further information about sub-critical SWR might arise from a classification or correlation of SG results and *RI*

Table 3
Results of water repellency measurements with different methods at different depths, mean values given, coefficients of variation in brackets. Classifications are made according to Table 1. Letters (a, b, c) beside selected numbers indicate significant differences between results for depth layers; control was always significantly different from burnt samples (α = 0.05). WDPT is water drop penetration time, MED is molarity of ethanol droplet test (indicating the used method), RI is repellency index. Usage of subscripts: ud means test was conducted on undisturbed sample, d on disturbed sample (single grain layer), 24% stands for 24% EtOH solution used, TI is tension infiltrometer and MD mini disc infiltrometer, SOM is soil organic matter content. RI_{TI} was calculated from measurements at h = −5 cm as this was the first applied water head in the experiment.

Depth /cm	$WDPT_{ud}$ class	$WDPT_{ud}$ /s	$WDPT_d$ /s	$MED_{ud,24\%}$ class	$MED_{ud,24\%}$ /s	$MED_{d,24\%}$ /s	RI_{TI} /−	RI_{MD} /-	SOM /g g^{-1}
0	5	268 (1.1) - a	7762 - a	7	27.6 (1.2) - a	4050 - a	12.40	11.77 (0.56)	0.108
1	3	42.8 (1.2) - b	(0.2)	7	8.0 (1.6) - a	(0.3)	(0.59)		
2	0	< 5 (−) - c	5459 - b	3	< 5 (−) - b	3588 - a			0.070
3	0	< 5 (−) - c	(0.3)	1	< 5 (−) - b	(0.2)			
4	–	–	1022 - c	–	–	471 - b			0.058
5	–	–	(0.6)	–	–	(0.7)			
Control	0	< 5	< 5	1	< 5	< 5	3.53 (0.56)	2.09 (0.25)	–
n	10/3	10 drops/ 3 replications	10/3	10/3	10/3	10/3	3 replications	9 rep.	3 rep.

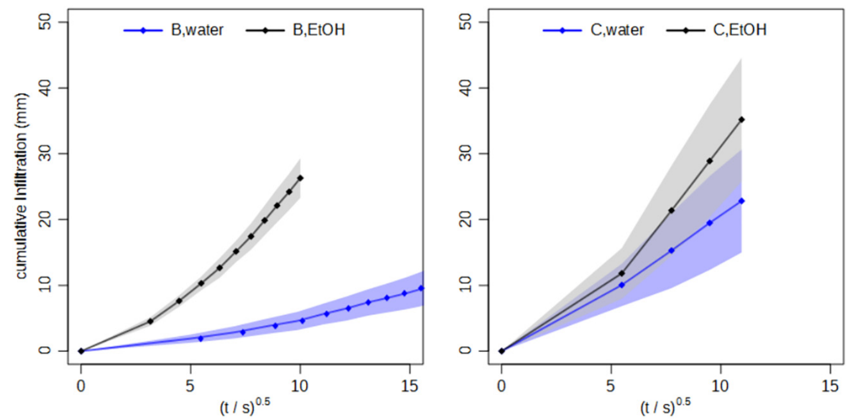

Fig. 4. Cumulative infiltration (mm) vs. square root of time ($s^{0.5}$) for mini disc infiltration measurements performed on 20th July 2017 in Trogir on burnt soil (B) and Control plot (C) performed with water and ethanol (EtOH) as infiltrating liquids. Shaded areas are the 95%-confidence intervals, sample size for B is 9, for C is 6.

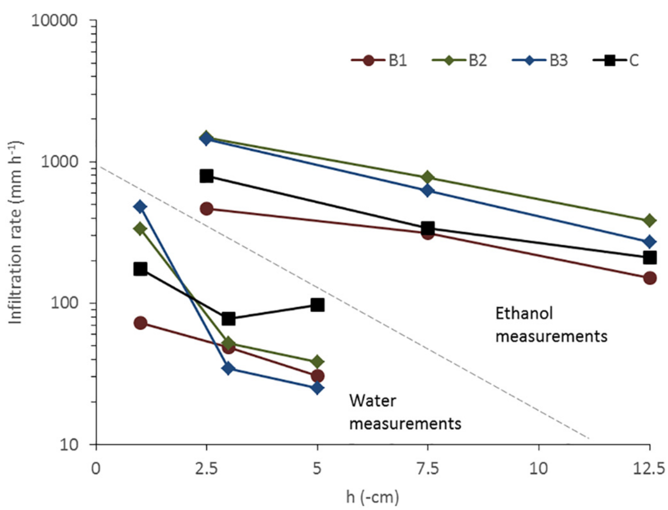

Fig. 5. Steady state infiltration of water and ethanol measured with glass tension infiltrometer at different pressure heads for burnt (B1, B2, and B3) plots and control (C). The infiltration rates obtained with ethanol have been corrected due to difference in viscosity (by a factor of 1.2) and due to differences in surface tension and density ethanol pressure heads were multiplied with 2.5 to obtain actual effective pressure head.

values. As data from the SG approach was, to our knowledge, not yet presented in literature, no direct classification was available. However, the wider range in comparison to results of the traditional WDPT and MED setup will allow a finer classification, especially for sub-critical SWR. For *RI*, large data sets are available, but a classification has not yet been considered. The results were hampered by methodological inconsistencies even though the MD technique provides opportunities for a standardization of *RI* determination (Lewis et al., 2006). Both methods have great potential to advance the evaluation of practical relevance of sub-critical SWR, which is still considered to be underestimated (Hallett et al., 2001; Müller et al., 2016).

The time for first five air bubbles (TFFB) rising in the tension supply tube of the TI was recorded and analyzed in addition to traditional readings (Fig. 6). The time measurement started immediately after placing the TI on the soil, and on burnt sites a distinct delay of infiltration start was observed (Fig. 6a). This was also mentioned by Beatty and Smith (2014) who questioned representativity of this period due to initial calibration processes of the experimental system. Nevertheless, the TFFB infiltration was slightly slower on burnt sites (slopes in Fig. 6a) which indicated presence of SWR. In our study, one bubble represented an infiltrating volume of 1 ml, corresponding to approximately 0.1 mm. Beatty and Smith (2014) postulated strong correlation between infiltration rates measured via TFFB and traditional early-time readings which means that measurements could be conducted much faster when only the time for five rising bubbles would be needed. Here, we found a certain agreement (Fig. 6b) but the limited number of samples did not allow a valid statement. Furthermore, the TI in the herein used form was not useful for detection of temporally variable, but still small infiltration rates due to the large diameter of the water reservoir caused only minor changes in water level during the experiment.

3.2. Water repellency depending on soil depth

The laboratory methods of WDPT and MED, both on undisturbed and SG-disturbed samples, were done on subsamples from different soil depths (as described above). The SWR was found only down to 1 cm soil depth with WDPT and to 2 cm with MED on undisturbed samples (Table 3, Fig. 7). In contrast, the SG-setup gave values also on deeper samples with a greater measuring range (Fig. 8). All methods showed a considerable deviation relative to control measurements, where drops infiltrated almost immediately for all tested depths (Table 3). Moreover, Fig. 9 showed a good relationship between soil organic carbon (SOC) content and WDPT on the SG samples. The small sample size (n = 3) does not allow sound regression analysis but the tendency went along with established knowledge about organic components generally causing SWR, even though the actual composition of SOC significantly influences the extent of SWR (Zheng et al., 2016). Moreover, the development of fire-induced SWR in deeper soil layers depends mainly on temperature and is determined by the duration and intensity of the wildfire (DeBano, 2000). Badia-Villas et al. (2014) presented results from a comparable soil horizon where an artificial fire over 220 min with 500 °C maximal surface temperature did not induce critical SWR below 2 cm of soil depth. Accordingly, Robichaud et al. (2008) analyzed a large dataset of SWR measurements after wildfires and reported a maximum of SWR in depths from 1 to 3 cm.

3.3. Variability of different methods for SWR estimation

Four different laboratory and two different field methods were used for SWR estimation. Great differences were observed between the values (Table 3) and also the variability, expressed as CV, was different depending on the method. As classifications for WDPT and MED (Table 1) did not account for measurements on SG layer, we additionally presented the results in seconds for the WDPT and MED-measurements with 24% ethanol solution (Table 3). Especially WDPT and *RI* were reported to be highly variable (e.g. Di Prima et al., 2017; Lichner et al., 2017; White et al., 2017). In this study, we found highest variability in the results of WDPT and the drop penetration time of a

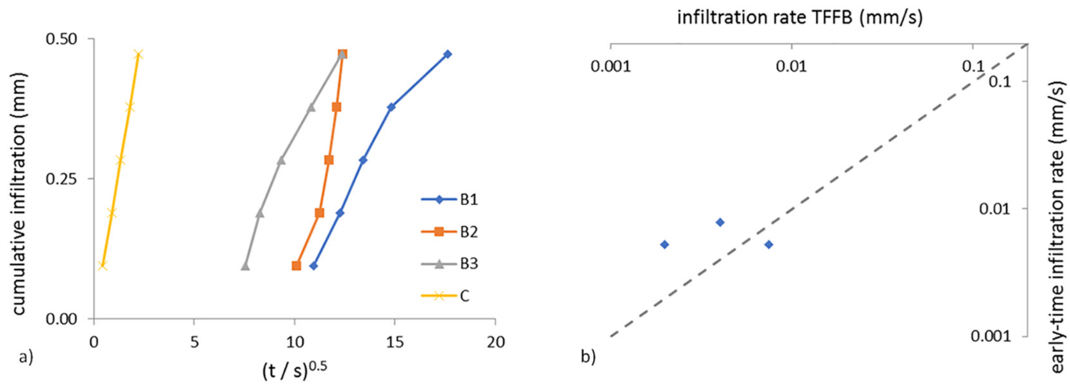

Fig. 6. Time of first five bubbles (TFFB) arising in the tension infiltrometer experiments; a) cumulative infiltration vs. square root of time, with B1, B2, B3 representing burnt plots, while C is control; b) comparison of infiltration rates measured by TFFB and traditional reading, dashed is 1:1-line.

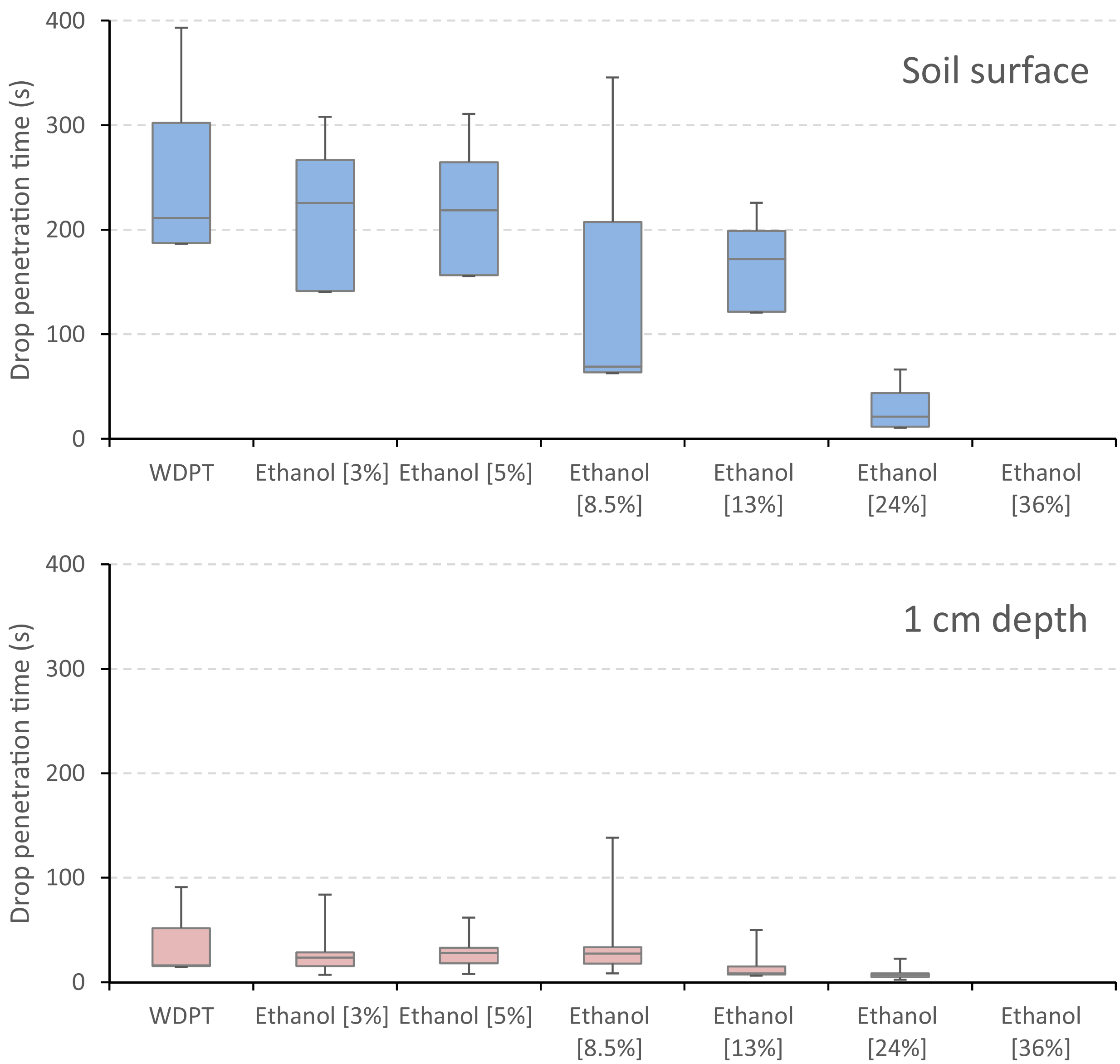

Fig. 7. A Box plot of water drop penetration time (WDPT) and penetration time of solutions with 3 to 24% ethanol performed on undisturbed soil samples (250 cm^3 cylinders) at soil surface (upper graph) and at 1 cm depth (lower graph) in burnt plots. Box boundaries indicate 25th and 75th percentiles, the line in the middle represent median values and top and bottom whiskers represent minimum and maximum values (n = 30).

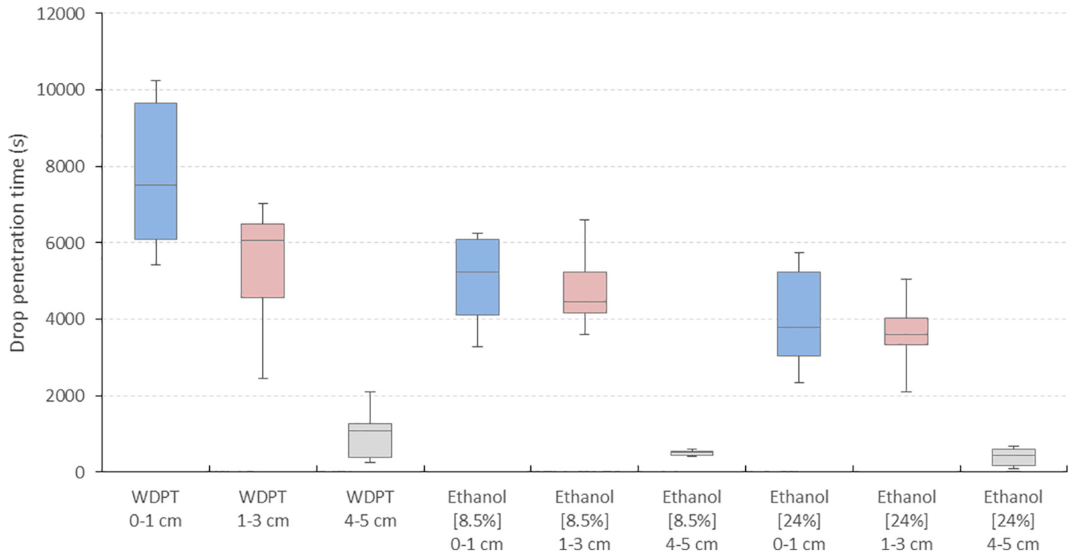

Fig. 8. A Box plot of water drop penetration time (WDPT) and penetration time of solutions with 3 to 24% ethanol performed on disturbed single-grain layer soil samples at different depth (0–1, 1–3, and 4–5 cm) in burnt plots. The Box boundaries indicate 25th and 75th percentiles, the line in the middle represent median values and top and bottom whiskers represent minimum and maximum values (n = 30).

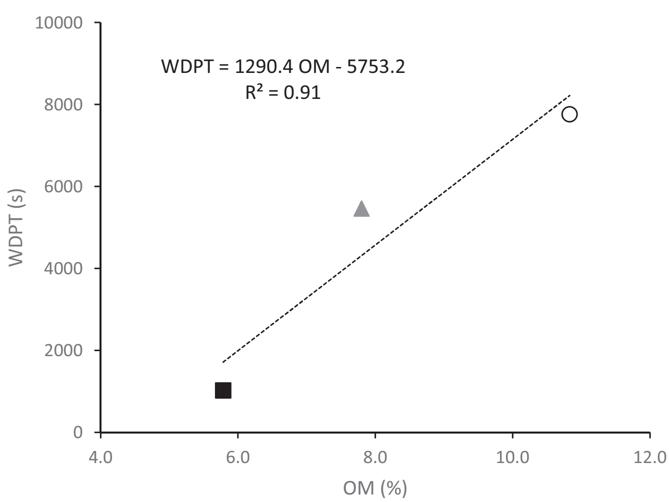

Fig. 9. Relationship between organic matter (OM) content and water drop penetration time on a single-grain layer (WDPT) at different depth: 0–1 cm (open circle), 1–3 cm (triangle), and 4–5 cm (square) for burnt plots (B1, B2 and B3). OM values from double measurement on mixed samples, WDPT is the average of 30 measurements.

24% ethanol solution. Absolute values from SG were much higher than for undisturbed samples but CVs were significantly lower. Hence, the precision of measurements was increased by modifying the WDPT method. Using a SG-layer, the distorting effects of surface capillarity or roughness were omitted. As the liquid drops were orders of magnitude larger than the soil grains, only the grain surface properties were the determinant for the spreading of drops. In previous studies (King, 1981; Graber et al., 2006) possible reasons were found why SWR between undisturbed and disturbed soil may be different which include: surface roughness, pore size distribution, pore connectivity, and soil bulk density and a change in the distribution and orientation of materials responsible for repellency (e.g., organic matter, fungal filaments, biofilms, leaf litter). On SG-layers of wettable soils the drops still spread immediately what showed that the wetting process on soil grain surfaces was not affected or hindered by the glue of the tape. Hence, no restrictions on the applicability of this modification are to be expected due to interactions of water and the tape. Nevertheless, we still saw potential for improvement especially in the design of drop application. On the other hand, sample disturbance alters SWR (Graber et al., 2006), hence an additional determination on undisturbed soil, preferably in the field, is advisable. The variability in the results of the two field infiltration measurements were comparable and both were considerably lower than with the WDPT and MED on undisturbed samples (Table 3). By using the permutation approach for the analysis of infiltration experiments the CV was decreased in comparison to the paired approach (values not presented), hence an estimation of SWR for the actual area was more representative.

4. Conclusion

Our quantitative results extended the available studies about fire-induced SWR to the calcareous East-Mediterranean coastal area. Four different measurement methods were applied and distinct SWR, at least in the top layer of 0 to 2 cm depth, was found with both field and lab methods. The selected burnt plots showed large SWR effect and differences to a control plot (unaffected by fire). The field infiltration measurements using TI and MD performed with water and ethanol showed large differences in infiltration volumes, sorptivities, and finally the calculated *RI*. The SWR was found to decrease with increasing depth and correlate with organic matter content, as found in previous studies. The effect of fire induced SWR was clearly detected with all applied methods. The study also resulted in pointing out the necessity in unique repellency index classification system and more defined methodological approach. Comparing our quantitative and ordinal results with other studies, SWR at the soil surface was moderate to strong. As a further outcome, we altered the setup of the traditional lab methods WDPT and MED which were considered to be used exclusively for critical repellency (contact angle > 90°) and evaluated the applicability of this modification to enable measurements also in sub-critical ranges. Despite limited sample extent, a finer resolution of the water repellency status was observed for samples which were assessed as fully wettable by traditional methods. Further research is needed to develop a framework for the quantitative evaluation and classification of SWR, especially sub-critical SWR, as well as subsequent estimation of the relevance of SWR on local scale hydrology.

Acknowledgement

We acknowledge travel funding from the bilateral agreement project HR20/2016 funded by the Austrian Agency for International Cooperation in Education and Research (OeAD) and the Ministry of Science and Education of the Republic of Croatia. Special thanks go to Viet Son Dinh and Filip Kranjčec for assistance during field and lab work.

References

Alagna, V., Iovino, M., Bagarello, V., Mataix-Solera, J., Lichner, L., 2017. Application of minidisk infiltrometer to estimate water repellency in Mediterranean pine forest soils. J. Hydrol. Hydromech. 65, 254–263. https://doi.org/10.1515/johh-2017-0009.

Anderson, T.W., Darling, D.A., 1954. A test of goodness of fit. J. Am. Stat. Assoc. 49 (268), 765–769. https://doi.org/10.1080/01621459.1954.10501232.

Angulo-Jaramillo, R., Bagarello, V., Iovino, M., Lassabatere, L., 2016. Infiltration Measurements for Soil Hydraulic Characterization. Springer International Publishing, Switzerland, pp. 386. https://doi.org/10.1007/978-3-319-31788-5.

Bachmann, J., Ellies, A., Hartge, K.H., 2000. Development and application of a new sessile drop contact angle method to assess soil water repellency. J. Hydrol. 231–232, 66–75. https://doi.org/10.1016/s0022-1694(00)00184-0.

Bachmann, J., Guggenberger, G., Baumgartl, T., Ellerbrock, R.H., Urbanek, E., Goebel, M.O., Kaiser, K., Horn, R., Fischer, W.R., 2008. Physical carbon sequestration mechanisms under special consideration of soil wettability. J. Plant Nutr. Soil Sci. 171, 14–26. https://doi.org/10.1002/jpln.200700054.

Badia-Villas, D., Gonzalez-Perez, J.A., Aznar, J.M., Arjona-Gracia, B., Marti-Dalmau, C., 2014. Changes in water repellency, aggregation and organic matter of a mollic horizon burned in laboratory: soil depth affected by fire. Geoderma 213, 400–407. https://doi.org/10.1016/j.geoderma.2013.08.038.

Beatty, S.M., Smith, J.E., 2014. Infiltration of water and ethanol solutions in water repellent post wildfire soils. J. Hydrol. 514, 233–248. https://doi.org/10.1016/j.jhydrol.2014.04.024.

Bughici, T., Wallach, R., 2016. Formation of soil–water repellency in olive orchards and its influence on infiltration pattern. Geoderma 262, 1–11. https://doi.org/10.1016/j.geoderma.2015.08.002.

Capra, G.F., Tidu, S., Lovreglio, R., Certini, G., Salis, M., Bacciu, V., Ganga, A., Filzmoser, P., 2018. The impact of wildland fires on calcareous Mediterranean pedosystems (Sardinia, Italy) – an integrated multiple approach. Sci. Total Environ. 624, 1152–1162. https://doi.org/10.1016/j.scitotenv.2017.12.099.

Clothier, B.E., White, I., 1981. Measurement of sorptivity and soil-water diffusivity in the field. Soil Sci. Soc. Am. J. 45, 241–245. https://doi.org/10.2136/sssaj1981.03615995004500020003x.

Clothier, B.E., Vogeler, I., Magesan, G.N., 2000. The breakdown of water repellency and solute transport through a hydrophobic soil. J. Hydrol. 231-232, 255–264. https://doi.org/10.1016/s0022-1694(00)00199-2.

DeBano, L.F., 1991. The effect of fire on soil properties. USDA For. Serv. Gen. Tech. Rep. INT-280, 151–156.

DeBano, L.F., 2000. The role of fire and soil heating on water repellency in wildland environments: a review. J. Hydrol. 231–232, 195–206. https://doi.org/10.1016/s0022-1694(00)00194-3.

DeBano, L.F., Krammes, J.S., 1966. Water repellent soils and their relation to wildfire temperatures. Int. Assoc. Sci. Hydrol. Bull. 2, 14–19. https://doi.org/10.1080/02626666609493457.

DeBano, L.F., Mann, L.D., Hamilton, D.A., 1970. Translocation of hydrophobic substances into soil by burning organic litter. Soil Sci. Soc. Am. Proc. 34, 130–133. https://doi.org/10.2136/sssaj1970.03615995003400010035x.

DeBano, L.F., Rice, R.M., Conrad, C.E., 1979. Soil Heating in Chaparral Fires: Effects on Soil Properties, Plant Nutrients, Erosion and Runoff. United States Department of Agriculture, Forest Service, Research Paper PSW-145. Pacific Southwest Forest and Range Experimental Station, Berkeley, California (21 pp).

Deurer, M., Bachmann, J., 2007. Modeling water movement in heterogeneous water-repellent soil: 2. A conceptual numerical simulation. Vadose Zone J. 6, 446–457. https://doi.org/10.2136/vzj2006.0061.

Di Prima, S., Bagarello, V., Angulo-Jaramillo, R., Bautista, I., Cerdà, A., del Campo, A., González-Sanchis, M., Iovino, M., Lassabatere, L., Maetzke, F., 2017. Impacts of thinning of a Mediterranean oak forest on soil properties influencing water infiltration. J. Hydrol. Hydromech. 65 (3), 276–286. https://doi.org/10.1515/johh-2017-0016.

Diamantopoulos, E., Durner, W., 2013. Physically-based model of soil hydraulic properties accounting for variable contact angle and its effect on hysteresis. Adv. Water Resour. 59, 169–180. https://doi.org/10.1016/j.advwatres.2013.06.005.

Doerr, S.H., 1998. On standardizing the 'water drop penetration time' and the 'molarity of ethanol droplet' techniques to classify soil hydrophobicity: a case study using medium textured soils. Earth Surf. Process. Landf. 23, 663–668. https://doi.org/10.1002/(sici)1096-9837(199807)23:7 < 663::aid-esp909 > 3.0.co;2-6.

Doerr, S.H., Shakesby, R.A., Walsh, R.P.D., 2000. Soil water repellency: its causes, characteristics and hydro-geomorphological significance. Earth Sci. Rev. 51, 33–65. https://doi.org/10.1016/s0012-8252(00)00011-8.

Dohnal, M., Dusek, J., Vogel, T., 2010. Improving hydraulic conductivity estimates from minidisk Infiltrometer measurements for soils with wide pore-size distributions. Soil Sci. Soc. Am. J. 74, 804–811. https://doi.org/10.2136/sssaj2009.0099.

Filipović, V., Weninger, T., Filipović, L., Schwen, A., Bristow, K.L., Zechmeister-Boltenstern, S., Leitner, S., 2018. Inverse estimation of soil hydraulic properties and water repellency following artificially induced drought stress. J. Hydrol. Hydromech. 66, 170–180. https://doi.org/10.2478/johh-2018-0002.

Giannakopoulos, C., Le Sager, P., Bindi, M., Moriondo, M., Kostopoulou, E., Goodess, C.M., 2009. Climatic changes and associated impacts in the Mediterranean resulting from a 2 °C global warming. Glob. Planet. Chang. 68, 209–224. https://doi.org/10.1016/j.gloplacha.2009.06.001.

Graber, E.R., Ben-Arie, O., Wallach, R., 2006. Effect of sample disturbance on soil water repellency determination in sandy soils. Geoderma 136, 11–19. https://doi.org/10.1016/j.geoderma.2006.01.007.

Granged, A.J.P., Jordán, A., Zavala, L.M., Bárcenas, G., 2011. Fire-induced changes in soil water repellency increased fingered flow and runoff rates following the 2004 Huelva wildfire. Hydrol. Process. 25, 1614–1629. https://doi.org/10.1002/hyp.7923.

Hallett, P.D., 2007. An introduction to soil water repellency. In: Proceedings of the 8th International Symposiom on Adjuvents for Agrochemicals (ISAA2007), 6–9 August, 2007, Columbus, Ohio, USA, (13pp).

Hallett, P.D., Baumgartl, T., Young, I.M., 2001. Subcritical water repellency of aggregates from a range of soil management practices. Soil Sci. Soc. Am. J. 65, 184–190. https://doi.org/10.2136/sssaj2001.651184x.

Hunter, A.E., Chau, H.W., Si, B.C., 2011. Impact of tension infiltrometer disc size on measured soil water repellency index. Can. J. Soil Sci. 91, 77–81. https://doi.org/10.4141/cjss10033.

IUSS Working Group WRB, 2015. World Reference Base for Soil Resources 2014, Update 2015. International Soil Classification System for Naming Soils and Creating Legends for Soil Maps. World Soil Resources Reports No. 106. FAO, Rome.

Jarvis, N., Etana, A., Stagnitti, F., 2008. Water repellency, near-saturated infiltration and preferential solute transport in a macroporous clay soil. Geoderma 143, 223–230. https://doi.org/10.1016/j.geoderma.2007.11.015.

Jordán, A., Gonzalez, A.F., Zavala, L.M., 2010. Re-establishment of soil water repellency after destruction by intense burning in a Mediterranean heathland (SW Spain). Hydrol. Process. 24, 736–748. https://doi.org/10.1002/hyp.7519.

Jordán, A., Zavala, L.M., Mataix-Solera, J., Doerr, S.H., 2013. Soil water repellency: origin, assessment and geomorphological consequences. Catena 108, 1–5. https://doi.org/10.1016/j.catena.2013.05.005.

King, P.M., 1981. Comparison of methods for measuring severity of water repellence of sandy soils and assessment of some factors that affect its measurement. Aust. J. Soil Res. 19, 275–285. https://doi.org/10.1071/sr9810275.

Lamparter, A., Bachmann, J., Deurer, M., Woche, S.K., 2010. Applicability of ethanol for measuring intrinsic hydraulic properties of sand with various water repellency levels. Vadose Zone J. 9, 445–450. https://doi.org/10.2136/vzj2009.0079.

Lewis, S.A., Wu, J.Q., Robichaud, P.R., 2006. Assessing burn severity and comparing soil water repellency, Hayman Fire, Colorado. Hydrol. Process. 20, 1–16. https://doi.org/10.1002/hyp.5880.

Lichner, L., Hallett, P.D., Feeney, D., Dugova, O., Sir, M., Tesar, M., 2007. Field measurement of soil water repellency and its impact on water flow under different vegetation. Biologia 62, 537–541. https://doi.org/10.2478/s11756-007-0106-4.

Lichner, L., Rodný, M., Marschner, B., Chen, Y., Nadav, I., Tarchitzky, J., Schacht, K., 2017. Comparison of various techniques to estimate the extent and persistence of soil water repellency. Biologia 72 (9), 982–987. https://doi.org/10.1515/biolog-2017-0112.

Liu, H., Ju, Z., Bachmann, J., Horton, R., Ren, T., 2012. Moisture-dependent wettability of artificial hydrophobic soils and its relevance for soil water desorption curves. Soil Sci. Soc. Am. J. 76, 342–349. https://doi.org/10.2136/sssaj2011.0081.

MacDonald, L.H., Huffman, E.L., 2004. Post-fire soil water repellency: persistence and soil moisture thresholds. Soil Sci. Soc. Am. J. 68, 1729–1734. https://doi.org/10.2136/sssaj2004.1729.

Mataix-Solera, J., Arcenegui, V., Zavala, L.M., Perez-Bejarano, A., Jordán, A., Morugan-Coronado, A., Barcenas-Moreno, G., Jimenez-Pinilla, P., Lozano, E., Granged, A.J.P., Gil-Torres, J., 2014. Small variations in soil properties control fire-induced water repellency. Span. J. Soil Sci. 4, 51–60. https://doi.org/10.3232/SJSS.2014.V4.N1.03.

Müller, K., Carrick, S., Meenken, E., Clemens, G., Hunter, D., Rhodes, P., Thomas, S., 2016. Is subcritical water repellency an issue for efficient irrigation in arable soils? Soil Tillage Res. 161, 53–62.

Pekárová, P., Pekár, J., Lichner, L., 2015. A new method for estimating soil water repellency index. Biologia 70, 1450–1455. https://doi.org/10.1515/biolog-2015-0178.

Perroux, K.M., White, I., 1988. Designs for disc permeameters. Soil Sci. Soc. Am. J. 52, 1205–1215. https://doi.org/10.2136/sssaj1988.03615995005200050001x.

Plaza-Álvarez, P.A., Lucas-Borja, M.E., Sagra, J., Moya, D., Alfaro-Sánchez, R., González-Romero, J., De las Heras, J., 2018. Changes in soil water repellency after prescribed burnings in three different Mediterranean forest ecosystems. Sci. Total Environ. 644, 247–255. https://doi.org/10.1016/j.scitotenv.2018.06.364.

Robichaud, P.R., Lewis, S.A., Ashmun, L.E., 2008. New Procedure for Sampling Infiltration to Assess Post-fire Soil Water Repellency. Res. Note RMRS-RN-33. U.S. For. Serv. Rocky Mtn. Res. Stn, Fort Collins, CO.

Santer, B.D., Po-Chedley, S., Zelenika, D.M., Cvijanovic, I., Bonflis, C., Durack, P.J., Fu, Q., Kiehl, J., Mears, C., Painter, J., Pallota, G., Solomon, S., Wentz, J.F., Zou, Z.-C., 2018. Human influence on the seasonal cycle of tropospheric temperature. Science 361 (6399), eaas8806.

SAS Institute, 2001. SAS/STAT User's Guide, Version 8–1. SAS Institute Inc, Cary North Carolina.

Savage, S.M., 1974. Mechanism of fire-induced water repellency in soils. Soil Sci. Soc. Am. J. 38, 652–657. https://doi.org/10.2136/sssaj1974.03615995003800040033x.

Schwen, A., Zimmermann, M., Leitner, S., Woche, S.K., 2015. Soil water repellency and its impact on hydraulic characteristics in a beech forest under simulated climate change. Vadose Zone J. 14, 1–11. https://doi.org/10.2136/vzj2015.06.0089.

Sepehrnia, N., Hajabbasi, M.A., Afyuni, M., Lichner, L., 2016. Extent and persistence of water repellency in two Iranian soils. Biologia 71, 1137–1143. https://doi.org/10.1515/biolog-2016-0135.

Stoof, C.R., Moore, D., Ritsema, C.J., Dekker, L.W., 2011. Natural and fire-induced soil water repellency in a Portuguese Shrubland. Soil Sci. Soc. Am. J. 75, 2283–2295. https://doi.org/10.2136/sssaj2011.0046.

Tessler, N., Wittenberg, L., Malkinson, D., Greenbaum, N., 2008. Fire effects and short-term changes in soil water repellency. Catena 74, 185–191. https://doi.org/10.1016/j.catena.2008.03.002.

Tillman, R.W., Scotter, D.R., Wallis, M.G., Clothier, B.E., 1989. Water-repellency and its measurement by using intrinsic sorptivity. Aust. J. Soil Tes. 27, 637–644. https://doi.org/10.1071/sr9890637.

Varela, M.E., Benito, E., Keizer, J.J., 2010. Wildfire effects on soil erodibility of woodlands in NW Spain. Land Degrad. Dev. 21, 75–82. https://doi.org/10.1002/ldr.896.

White, A.M., Lockington, D.A., Gibbes, B., 2017. Does fire alter soil water repellency in subtropical coastal sandy environments? Hydrol. Process. 31, 341–348. https://doi.org/10.1002/hyp.11000.

Zavala, L.M., Gonzalez, F.A., Jordán, A., 2009. Fire-induced soil water repellency under different vegetation types along the Atlantic dune coast-line in SW Spain. Catena 79, 153–162. https://doi.org/10.1016/j.catena.2009.07.002.

Zheng, W., Morris, E.K., Lehmann, A., Rillig, M.C., 2016. Interplay of soil water repellency, soil aggregation and organic carbon. A meta-analysis. Geoderma 283, 39–47. https://doi.org/10.1016/j.geoderma.2016.07.025.

J. Hydrol. Hydromech., 66, 2018, 2, 170–180
DOI: 10.2478/johh-2018-0002

Inverse estimation of soil hydraulic properties and water repellency following artificially induced drought stress

Vilim Filipović[1*], Thomas Weninger[2], Lana Filipović[1], Andreas Schwen[3], Keith L. Bristow[4], Sophie Zechmeister-Boltenstern[5], Sonja Leitner[5]

[1] University of Zagreb, Faculty of Agriculture, Department of Soil Amelioration, Svetošimunska 25, 10000 Zagreb, Croatia.
[2] University of Natural Resources and Life Sciences Vienna (BOKU), Institute of Hydraulics and Rural Water Management, Muthgasse 18, 1190 Vienna, Austria.
[3] Austrian Agency for Health and Food Safety (AGES), Institute for Plant Protection Products, Spargelfeldstraße 191, 1220 Vienna, Austria.
[4] CSIRO Agriculture & Food, PMB Aitkenvale, Townsville, QLD 4814, Australia.
[5] University of Natural Resources and Life Sciences Vienna (BOKU), Institute of Soil Research, Peter-Jordan-Straße 82, 1190 Vienna, Austria.
[*] Corresponding author. Tel.: 00385 1 2393711. E-mail: vfilipovic@agr.hr

Abstract: Global climate change is projected to continue and result in prolonged and more intense droughts, which can increase soil water repellency (SWR). To be able to estimate the consequences of SWR on vadose zone hydrology, it is important to determine soil hydraulic properties (SHP). Sequential modeling using HYDRUS (2D/3D) was performed on an experimental field site with artificially imposed drought scenarios (moderately M and severely S stressed) and a control plot. First, inverse modeling was performed for SHP estimation based on water and ethanol infiltration experimental data, followed by model validation on one selected irrigation event. Finally, hillslope modeling was performed to assess water balance for 2014. Results suggest that prolonged dry periods can increase soil water repellency. Inverse modeling was successfully performed for infiltrating liquids, water and ethanol, with R^2 and model efficiency (E) values both > 0.9. SHP derived from the ethanol measurements showed large differences in van Genuchten-Mualem (VGM) parameters for the M and S plots compared to water infiltration experiments. SWR resulted in large saturated hydraulic conductivity (K_s) decrease on the M and S scenarios. After validation of SHP on water content measurements during a selected irrigation event, one year simulations (2014) showed that water repellency increases surface runoff in non-structured soils at hillslopes.

Keywords: Inverse modeling; Water and ethanol infiltration; SHP estimation; Water dynamics; HYDRUS (2D/3D).

INTRODUCTION

Soil water repellency (SWR) is a reduction in the rate of wetting and retention of water in soil caused by drying and the presence of various hydrophobic coatings on soil particles. The physical background is not yet fully understood, but it is widely accepted that this phenomenon is most likely caused by water-repellent compounds that can coat soil mineral particles or be present as interstitial matter in soil pores (Doerr et al., 2000). SWR can increase substantially due to seasonal events, e.g. drought periods and/or wildfires (Jordan et al., 2013; Schwen et al., 2015). With the projected continuation of climate change, frequency and severity of drought events will intensify in most regions of the globe and the relevance of SWR effect on soil water dynamics is expected to increase in the future (Fischer and Knutt, 2014; Stocker et al., 2013).

SWR is not a stationary soil property but highly variable over time, depending on soil water content. Generally, SWR increases with decreasing water content (Jordan et al., 2013). Furthermore, although dry soils may be very water repellent initially, the repellency effect can disappear after prolonged contact with water. The duration of this process is described as repellency persistence. Besides persistence, SWR is also defined by severity of repellency, both of which can be expressed quantitatively (Chau et al., 2014). The intensity of SWR is characterized by the contact angle between soil surface and infiltrating water (Subedi et al., 2013). Hydrophobic conditions are present if contact angle above 90° is present, however even the contact angle in between 0° and 90° can affect water infiltration (Hallett et al., 2001). The SWR cannot be measured directly as physical value in the field, but has to be obtained indirectly, e.g. by observing the difference in flow behavior between water and fully-wetting fluid. Due to specific physico-chemical properties of ethanol (i.e. lower surface tension), ethanol is considered to be complete wetting fluid which is commonly used in SWR estimation (i.e. zero repellency; Lamparter et al., 2010; Watson and Letey, 1970). Further established methods (laboratory) are based on the influence which SWR has on other soil physical parameters, e.g. contact angle between water and soil surface, water drop penetration time, or capillary effect (Letey et al., 2000; Shang et al., 2008).

In comparison to non-repellent soils, water repellent soils have different infiltration patterns (initially postponed infiltration which increases after contact angle between water and soil particles decreases e.g. Bughici and Wallach, 2016; Debano, 1975) and increased fractions of preferential flow (e.g. Ritsema et al., 1993; 2000) or surface runoff (Lemmnitz et al., 2008). Soil infiltration experiments with a KBr tracer performed by Clothier et al. (2000) demonstrated (i) transient behavior of fingered preferential flow during the breakdown of hydrophobicity as a result of increasing soil water content, and (ii) solute penetration of the whole soil pore space after complete wetting. Hence, SWR appears to be reversible and very dynamic in time and space, thus making it difficult to predict. In a review by Jordan et al. (2013) the authors show that the majority of previous SWR studies are focused on the relationship between SWR and different soil properties (texture, organic matter content, soil chemical characteristics) or microbiological activity as a response to soil management. However, SWR dynamics under different climatic scenarios and how it can affect soil moisture in the long term remains unclear.

To assess the water dynamics under various field conditions as well as for predictions of future scenarios, modeling has proven to be an appropriate tool (Šimůnek et al., 2016; Vereecken et al., 2016). However, in available modeling software applications for plot or profile scale SWR is not accounted for as a separate parameter, but may be preferably expressed during the procedure of soil hydraulic properties (SHP) estimation. Several studies highlight that the influence of SWR on SHP is evident in the hysteresis effect (Bauters et al., 1998; Czachor et al., 2010). Generally, the hysteresis is highly related to SWR, and the SWR effect is primarily detectable on the wetting curve (Hardie et al., 2013; Stoffregen and Wessolek, 2014). In a laboratory study focusing on SWR-influenced SHP, Diamantopoulos et al. (2013) performed multistep inflow/outflow experiments with water and ethanol on four substrates, where they gradually induced water repellency by adding water repellent material (hydrophobic sand) in different ratios to soil. The experiments were performed with initially dry or initially saturated conditions to account for hysteresis, and inverse parameter estimation was performed to obtain SHP. Their results showed that SWR affects SHP on the wetting curve, contributing to the hysteresis effect, and that the artificial mixtures with a higher fraction of water repellent substances had a larger effect of SWR on SHP compared to naturally repellent soils. Therefore, during SHP estimation in water repellent soils, it is important to account for the most severe SWR effects expected during the initial soil wetting process (infiltration).

Hysteretic forms of SHP are sometimes implemented in modeling applications to account for SWR, e.g. Nieber et al. (2000) simulated infiltration in wettable and water repellent sand with a 2D finite-element model where SWR was taken into account by including hysteresis in the water retention curve and two slightly different equations for the unsaturated hydraulic conductivity function. Ganz et al. (2014) modeled water infiltration patterns in water repellent soils as well, but using a 3D-simulation in HYDRUS (2D/3D). They emphasized a strong need for the inclusion of hysteresis (model implemented in HYDRUS by Lenhard and Parker, 1992) and a scaling procedure based on independently measured contact angle data (method by Bachmann et al., 2007).

To investigate the impact of different rainfall distribution patterns on soil water dynamics, modeling using data from an artificially induced drought stress field experiment was performed in order to investigate the full effect of SWR on the hysteretic wetting curve. The objective of this study was (i) to estimate SHP from disc infiltrometer experiments with water and ethanol using inverse modeling approach and (ii) to further assess the impact of different artificially induced drought scenarios on SWR and consequently on local vadose zone hydrology using HYDRUS (2D/3D).

MATERIALS AND METHODS

Field site description

The experimental field was set up at the iLTER-site (International Long Term Ecological Research) in the Rosalian Mountains, Austria (47°42′26.33″ N, 16°17′54.5″ E, 600 m a.s.l.; Leitner et al., 2017). The mean annual temperature is 6.5°C and the mean annual precipitation is 796 mm at this location. The experimental site was situated in a forested hillslope with mature beech trees (*Fagus silvatica* L.) and no understory on a plateau with a sloping angle of 16°. The soil type was classified as Podsolic Cambisol according to the WRB (World reference base for soil resources, IUSS, 2014) covering impermeable granitic bedrock at 75–80 cm below the soil surface following the hillslope curvature. The soil profile was covered with an organic matter O horizon (0–7 cm), followed by an eluvial humus Aeh-horizon (7–25 cm), a cambic, slightly humusosesquioxidic Bhs-horizon (25–50 cm) over weathered granitic rock debris (C-horizon 50–75 cm) (Schwen et al., 2014). To assess the impact of changed rainfall distribution patterns on various soil properties, this experimental trial was established in 2013 (Leitner et al., 2017). Briefly, two artificially induced drought stress scenarios were applied during the vegetation period (May-October): a moderately (M) stressed scenario which had six consecutive cycles of four weeks drying followed by an intensive 75 mm irrigation, and a severely (S) stressed scenario which had three cycles of eight weeks drying followed by a larger irrigation event with 150 mm of irrigation. Stressed plots were protected from natural rainfall during vegetation periods by a plastic roof 1.20 m above the soil surface (each treatment having 4 plots, 2 m × 2 m, Fig. 1). Plots were irrigated with sprinkler irrigation systems with axial-flow full cone nozzles (Series 460, Lechler GmbH) installed under the roofs using descaled tap water from a nearby field station. The duration of the irrigation events were 2h each. To be able to compare the results with natural conditions, four control plots (C) received only natural rainfall. Drought plots had additional trenches (20 cm deep) at the upper end of the plot to avoid any lateral flow and/or surface runoff from elevated ground to enter the plots. In each plot, soil volumetric water content was measured at 10 cm depth in the Aeh horizon (VWC, TDR theta ML2x probes, UMS, Germany), with measurement intervals of 30 minutes. Climatic data were collected from a meteorological station located 500 m from the field site and used to calculate evapotranspiration according to Penman-Monteith (Monteith, 1981).

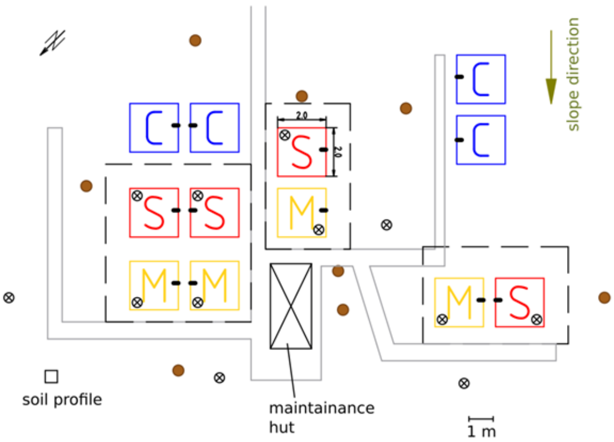

Fig. 1. iLTER experimental site scheme with bold lines as bridge pathways, dashed lines as plot roofs, colored squares as experimental units (2 × 2 m), black bold dashes as TDR-probes, X-ed circles as locations of performed infiltration experiments and brown points as trees. C stands for control, M for moderate, and S for severe stress. Infiltration experiments for control areas in Schwen et al. (2015) were conducted outside of the equipped squares to minimize influences to the soil system, especially to soil biology by ethanol.

Measurements of soil hydraulic parameters

Infiltration experiments were performed during September 2014 in all three scenarios (M, S, and C) in four repetitions as described elsewhere (Schwen et al., 2014, 2015) using a self-

Table 1. Basic soil physical properties at the iLTER experimental site (Austria) for Podsolic Cambisol soil profile: clay, silt and sand fraction, total porosity φ, bulk density ρb, and soil organic carbon (OC) content, Values were derived from a soil profile where samples were taken from incremental 5-cm-layers (uppermost sample from depth = 0–5cm), averaged for soil horizons (standard deviation in brackets). More detailed in Schwen et al., 2014, Fig. 1(b).

Horizon	Depth	Clay	Silt	Sand	OC	Porosity, φ	Bulk density, ρ_b
	cm	g g^{-1}	g g^{-1}	g g^{-1}	g g^{-1}	cm^3 cm^{-3}	g cm^{-3}
O	0–7	0.120 (–)	0.520 (–)	0.360 (–)	0.051 (–)	0.630 (–)	0.980 (–)
Aeh	7–25	0.090 (0.0125)	0.252 (0.0343)	0.659 (0.0438)	0.016 (0.0095)	0.510 (0.0326)	1.300 (0.0941)
Bhs	25–50	0.088 (0.0092)	0.240 (0.0524)	0.673 (0.0611)	0.002 (0.0027)	0.428 (0.0268)	1.516 (0.0712)
C	50–75	0.083 (0.0382)	0.191 (0.0204)	0.726 (0.0565)	0.000 (–)	0.378 (0.0164)	1.644 (0.0391)

constructed tension disc glass infiltrometer which allowed using both water and ethanol as infiltrating liquids (Schwen et al., 2015). These data served as an input for SHP estimation using inverse modeling (the procedure is explained in the next section). Before the infiltration measurements were made, the organic litter was removed to ensure that the measurements were performed at the top of the mineral Aeh horizon. Additionally, a thin layer of uniform glass beads was used at the soil surface to ensure good contact between soil and the porous disc (Dragonite, Jaygo Inc.; diameter: 0.45 mm). Infiltration measurements (water and ethanol) were conducted using different pressure heads (e.g., –10, –5, –3, –1 cm), in four replicates (one per plot) with each liquid. At the end of the water infiltration, the soil was covered to prevent any physical disturbance. Two days later, infiltration experiments were performed at the same specific spots using ethanol as the infiltration liquid with the glass beads layer replaced where necessary. Differences in the dynamic viscosity (η) of water (η = 1.0 mPa) and ethanol (η = 1.2 mPa) results in different liquid infiltration rates, even at identical liquid contents. To be able to compare the two infiltration experiments, the infiltration rates of ethanol were corrected for the difference in viscosity between water and ethanol using a factor of 1.2 (Jarvis et al., 2008). Considering different physicochemical properties of water and ethanol, the ethanol pressure head values were scaled based on the capillary rise equation which takes into account the difference between surface tension and density of particular liquids:

$$h_i = \frac{2\sigma_i cos\gamma}{r\rho_i g} \tag{1}$$

where σ is the surface tension (mN m^{-1}), γ is the contact angle (°), r is the equivalent capillary radius (m), ρ is the density of the liquid (g cm^{-3}), and g is the acceleration due to gravity (m s^{-2}). The subscript i refers to water (w) or ethanol (e). With the water and ethanol surface tension at 20°C of 72.7 mN m^{-1} and 22.4 mN m^{-1}, and a density of 0.998 g cm^{-3} and 0.789 g cm^{-3}, respectively, a correction factor between h_e and h_w of 2.5 was assumed (Diamantopoulos et al., 2013; Lamparter et al., 2010). Multiplying h_e with 2.5 results in the effective supply pressure ($h_{e,\ eff}$) giving the applied ethanol pressure heads of –25, –12.5, –7.5, and –2.5 cm. The correction factor assumes that the contact angles of water/ethanol and soil surface are identical ($\gamma_e = \gamma_w$), despite the fact that water contact angle in the field was oscillating in time. However, the differences in the contact angle reflect SWR through the different infiltration volumes for each liquid and consequently inversely estimated SHP. Initial water content was determined using the gravimetric method on undisturbed soil cores of 250 cm^3 volume (n = 4 per treatment). Average initial water content values were 0.17, 0.19, and 0.31 cm^3 cm^{-3} for M, S and C treatments prior to the water infiltration experiments. The same water contents were assumed to be present prior to ethanol infiltration experiments (no additional sampling/measurements were done in order to prevent disruption of the infiltration spots). Using the same soil core samples, SHP were estimated using the evaporation method (Schindler et al., 2010; device: HYPROP, UMS GmbH, Munich, Germany). Although SHP was measured by the evaporation method, only part of the measured data was used to obtain certain hydraulic parameters (porosity, θ_s) while the rest of the curve fitting was performed using inverse modeling based on the data from the infiltration experiments. SWR tend to be more expressed in drier soils and decreases with increased soil moisture (Dekker and Ritsema, 1994; Diamantopoloulos et al., 2013; Liu et al., 2012), thus starting with initially dried soil and performing infiltration experiments to investigate SWR in different treatments seemed appropriate. Particle size distribution was determined by a combination of sieving and sedimentation experiments according to Gee and Or (2002). Basic soil physical properties for the iLTER experimental site are given in Table 1.

Numerical modeling

Numerical modeling was performed with the HYDRUS (2D/3D) model (Šimůnek et al., 2016) using a three-step simulation process:

1. Inverse modeling based on water and ethanol field infiltration data – to obtain SHP;
2. Simulation of a particular irrigation event using obtained SHP – to validate the model using field TDR measurements;
3. Seasonal simulation (2014) – to assess the effect of SWR on water dynamics in hillslope areas.

This approach is explained in more detail in the following sections.

Inverse modeling to estimate soil hydraulic properties

Tension disc infiltration measurement data (average of four repetitions) with water and ethanol for the S, M, and C plots (Schwen et al., 2015) were used to obtain SHP using inverse modeling (Hopmans et al., 2002). A numerical solution of the Richards' equation coupled with the Levenberg-Marquardt nonlinear minimization method implemented in the HYDRUS (2D/3D) model was used. The program solves the equation numerically using a quasi-three-dimensional axisymmetric finite element code. The Richards' equation, which describes isothermal Darcian flow in a variably saturated rigid porous medium, is used in the model in its modified form (Šimůnek et al., 1998):

$$\frac{\partial\theta}{\partial t}=\frac{1}{r}\frac{\partial}{\partial r}\left(rK\frac{\partial h}{\partial r}\right)+\frac{\partial}{\partial z}\left(K\frac{\partial h}{\partial z}\right)+\frac{\partial K}{\partial z} \tag{2}$$

where θ is the volumetric water content [L^3 L^{-3}], h is the pressure head [L], K is the unsaturated hydraulic conductivity [L T^{-1}], r is a radial coordinate [L], z is vertical coordinate [L], positive upwards, and t is time [L]. Equation (2) was solved numerically for the following initial and boundary conditions which reflect the initial and boundary conditions of the tension disc infiltrometer experiment:

$$\theta(r,z,t)=\theta_i \quad t=0 \tag{3}$$

$$h(r,z,t)=h_0 \quad 0<r<r_0,\ z=0 \tag{4}$$

$$\frac{\partial h(r,z,t)}{\partial z}=-1 \quad r>r_0,\ z=0 \tag{5}$$

$$h(r,z,t)=h_i \quad r^2+z^2\to\infty \tag{6}$$

where θ_i is the initial soil water content [L^3 L^{-3}], h_0 is the time-variable supply pressure head imposed by the tension disc infiltrometer for water (–10, –5, –3, –1 cm) and ethanol (–25, –12.5, –7.5, –2.5 cm) [L], and r_0 is the disc radius (porous disc radius of 2.9 cm) [L]. The SHP, estimated from ethanol infiltration volumes (scaled to match water physicochemical properties), were assumed to reflect the water infiltration in hydrophilic soil.

Soil hydraulic functions $\theta(h)$ and $K(h)$ used in the inverse and direct simulations (next section) were described using the van Genuchten-Mualem model (VGM, van Genuchten, 1980) defined as follows:

$$\theta(h)=\theta_r+\frac{\theta_s-\theta_r}{\left(1+|\alpha h|^n\right)^m} \quad \text{for } h<0 \tag{7}$$

$$\theta(h)=\theta_s \text{ for } h\geq 0$$

$$K(h)=K_s S_e^l\left(1-\left(1-S_e^{\frac{1}{m}}\right)^m\right)^2 \tag{8}$$

$$S_e=\frac{\theta-\theta_r}{\theta_s-\theta_r} \tag{9}$$

$$m=1-\frac{1}{n};\quad n>1 \tag{10}$$

where θ_r and θ_s denote residual and saturated volumetric water content [L^3 L^{-3}], respectively, K_s is the saturated hydraulic conductivity [L T^{-1}], S_e is the effective saturation [–], α [L^{-1}] and n [–] are shape parameters, and l [–] is a pore connectivity parameter. Pore connectivity parameter (l) was fixed to 0.5 as recommended by Mualem et al., (1976) to avoid optimization of large number of parameters. Please note that the initial condition was given in terms of the soil water content (values presented in field site description chapter). Šimůnek and van Genuchten (1997) showed that, compared to the use of pressure head, providing initial condition in this form ensures a more stable and unique solution of the inverse problem. Soil surface boundary conditions below the disc infiltrometer and the remaining soil surface are represented by Eqs. 4 and 5, respectively. Eq. 6 assumes that all subsurface boundaries are distant from the supply source and do not influence the results in any way. The inverse solution was obtained using a combination of cumulative infiltration data and observed initial/final water content after minimization of the objective function. The simulated axisymmetrical domain was 15 cm wide and 20 cm long soil block with 2501 nodes and increased density along the upper boundary due to the tension disc infiltrometer placement. The soil hydraulic parameters (θ_r, α, n, and K_s) were initially derived from particle size distribution and bulk density data using the ROSETTA pedotransfer functions (Schaap et al., 2001) (See Table 2). The θ_r parameter was not modified, as Šimůnek et al. (1998) and González et al. (2015) found that this parameter had little effect on the simulated θ and h time series. The inverse modeling approach proposed by Šimůnek and van Genuchten (1996) was then used to calibrate α, n, and K_s in the top soil layer of each treatment starting with the initial Aeh horizon properties (Table 2).

Modeling water dynamics in the M, S and C scenarios

After performing inverse VGM parameters estimation, direct modeling was performed. Simulations included selected irrigation event (on June 24th 2014, starting 60 hours before and after irrigation was performed) in the M and S treatments during one year period (2014, on a daily time frame) in all three scenarios (M, S, and C). Simulations were performed for two-dimensional variably saturated porous media using Richards' equation:

$$\frac{\partial\theta}{\partial t}=\frac{\partial}{\partial x_i}\left[K\left(K_{ij}^A\frac{\partial h}{\partial x_j}+K_{iz}^A\right)\right]-S \tag{11}$$

where θ represents the soil volumetric water content [L^3 L^{-3}], h pressure head [L], x_i (i = 1, 2) the spatial coordinates [L], t time [T], K_{ij}^A is the components of the dimensionless hydraulic conductivity anisotropy tensor (K^A) in the two main spatial directions x_i, K is the unsaturated hydraulic conductivity [L T^{-1}], and S accounts for root water uptake [L^3 L^{-3} T^{-1}]. The root water uptake was calculated using the Feddes et al. (1978) equation. The potential root water uptake was calculated taking into account seasonal dynamics of LAI and interception of the canopy at the forest sites (beech trees). A constant rooting depth (75 cm) with a root distribution adapted from Huang et al. (2011) was assumed. Effective precipitation was further calculated by subtracting losses due to interception from gross precipitation. Seasonal variations in beech canopy were estimated using dynamic LAI with a maximum value of 5.8 and interception capacity of 2.0 mm (Armbruster et al., 2004; Breuer et al., 2003). Based on the assumptions stated above, potential root water uptake was calculated in the study of Schwen et al. (2014), performed on the same site.

The simulated domain in 2D vertical space (for specific irrigation event simulation and one year modeling) was 0.75 m deep and 2 m long (corresponding to one plot; see Figure 6 in the results section). Atmospheric boundary conditions were selected at the top and seepage conditions at the right side (down slope) to mimic the possible lateral subsurface movement as the soil profile was located on an impermeable sloped

Table 2. Van Genuchten-Mualem (VGM) soil hydraulic parameters derived from pedotranfer soil functions (PTFs, Rosetta) based on soil texture and bulk density (Table 1) with the measured saturated water content value θ_s based on evaporation experiments (Schwen et al., 2014).

Horizon	θ_r	θ_s	α	n	K_s	l
	$cm^3\ cm^{-3}$	$cm^3\ cm^{-3}$	cm^{-1}	–	$cm\ day^{-1}$	–
Aeh	0.0433	0.47	0.026	1.4554	88.37	0.5
Bhs	0.0404	0.35	0.0335	1.4563	44.22	0.5
C	0.0391	0.32	0.0427	1.4735	36.8	0.5

bedrock. The simulation domain had 14882 nodes with the increased density at the top boundary (with 29350 2D elements). The soil layering and hydraulic properties were selected according to the Table 2, with the Aeh horizon extended to the soil surface.

Although Richards' equation is not considered applicable for hydrophobic medium (e.g., Diamantopoulos and Durner, 2013), because SWR is a reversible process and not a constant state, some of the classical physical approaches are still suitable when critical water content is exceeded.

Numerical simulations (i.e., infiltration volumes and TDR measurements) were evaluated using the coefficient of determination (R^2), root mean square error ($RMSE$) and model efficiency coefficient (E) (Nash and Sutcliffe, 1970):

$$R^2 = \left(\frac{\sum_{i=1}^{n}(O_i - \bar{O})(S_i - \bar{S})}{\sqrt{\sum_{i=1}^{n}(O_i - \bar{O})}\sqrt{\sum_{i=1}^{n}(S_i - \bar{S})}} \right) \tag{12}$$

$$RMSE = \left[\frac{\sum_{i=1}^{n}(S_i - O_i)^2}{n} \right]^{0.5}$$

$$E = 1 - \frac{\sum_{i=1}^{n}(O_i - S_i)^2}{\sum_{i=1}^{n}(O_i - \bar{O})^2} \tag{13}$$

where O_i and S_i are observed and simulated values, respectively, $\bar{O}$ and $\bar{S}$ represent the averages of observed and simulated values, respectively, and n is the number of observed/simulated points.

RESULTS AND DISCUSSION

Inverse simulations of tension disc infiltrometer data

Tension disc infiltration data were used to estimate SHP by performing inverse modeling with HYDRUS (2D/3D). Modeled data is compared with field data in Fig. 2. Water infiltration for the M and S scenarios had a very steady slow inflow rate

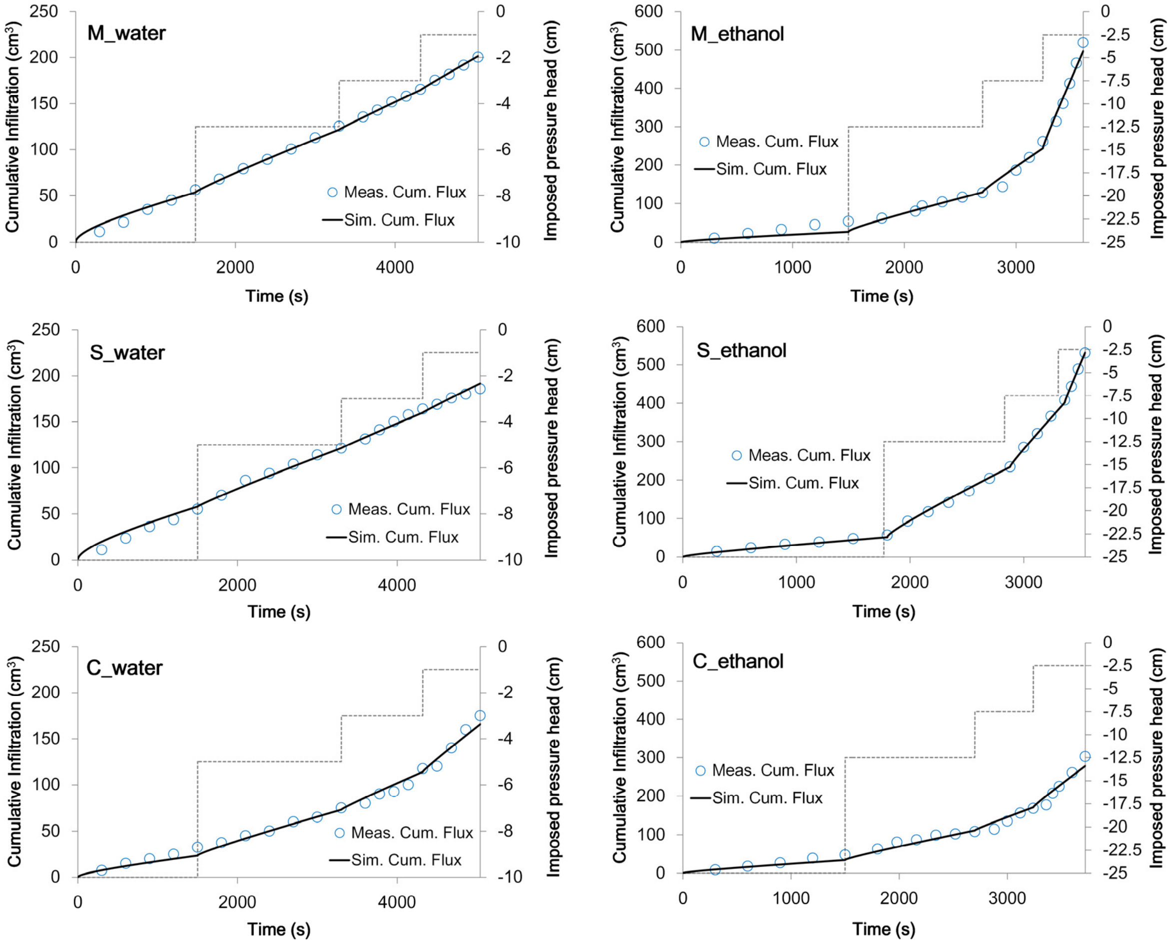

Fig. 2. Measured (circle) and simulated (solid line) infiltration cumulative fluxes for the M (moderately stressed), S (severe stressed) and C (control) scenarios with fitting performed using inverse optimization for water and ethanol liquids in HYDRUS (2D/3D) with an indication of the imposed pressure head and its duration (dotted line). Ethanol curves (_ethanol) are scaled in order to take account the different physicochemical properties and are directly comparable to water curves (_water).

Table 3. VGM parameters derived with inversion procedure using HYDRUS(2D/3D) from field infiltrometer data performed with water (_w) and ethanol (_e) liquids and statistical parameters (R^2, E, $RMSE$) describing goodness of model fitting for Aeh horizon.

Scenario	α	n	K_s	R^2	E	$RMSE$
	(cm^{-1})	(–)	cm day^{-1}			(cm^3)
M_w	0.036	1.717	23.45	0.998	0.998	2.77
M_e	0.100	1.713	1454.26	0.981	0.985	21.6
S_w	0.025	1.389	27	0.995	0.995	4.14
S_e	0.055	2.178	440	0.999	0.999	4.25
C_w	0.101	1.318	257.02	0.989	0.9910	5.11
C_e	0.056	1.393	460.8	0.982	0.981	11.03

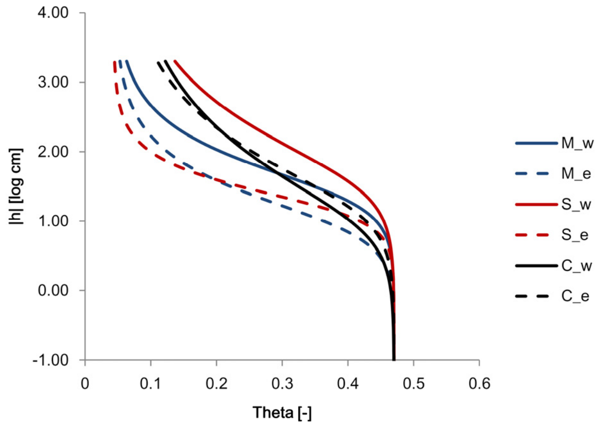

Fig. 3. Plotted retention curves for different VGM soil hydraulic parameter sets for various precipitation manipulation scenarios and different liquids (w, water vs. e, ethanol). Ethanol curves (_e) are scaled in order to take account the different physicochemical properties and are directly comparable to water curves (_w). M, moderately stressed scenario; S, severely stressed scenario; C, control scenario.

during the entire infiltration experiment and did not respond to the change in supply pressure. By contrast, a typical water infiltration curve found for non-repellent soils was observed in scenario C (although with reduced effect e.g. Šimůnek and van Genuchten, 1997), showing increased infiltration volumes at lower pressure heads (close to saturation). On the contrary, for M and S scenarios data showed reduced infiltration at lower pressure heads (h = –3 cm and –1 cm) and indicated that the larger pores were more hydrophobic than the smaller pores (Leue et al., 2015; Schwen et al., 2015). The final infiltration volumes were similar with 200.4, 185.7 and 175 ml for M, S and C scenarios, respectively. However, if these results are compared to the ethanol experimental data, it can be seen that the ethanol infiltration volumes are larger, with the final volumes of 519, 531 and 303 ml for M, S and C scenarios, respectively, indicating increased water repellency in the M and S scenarios. These data also show that the C scenario showed the smallest difference in total volume and infiltration curve behavior between water and ethanol. Similar results were observed by Jarvis et al. (2008) where they compared grassland to arable land with water and ethanol measurements and found that water repellency is smaller when water and ethanol infiltration volumes are similar (and *vice versa*).

The inverse optimization modeling worked well in both cases, showing a good fit for both infiltrating liquids, which can be observed visually and through statistical indicators (Fig. 2; Table 3). This shows that the VGM model describes soil hydraulic parameters well at this site. Observations through the profile indicate the presence of few macropores with a rather uniform structure (Schwen et al., 2014), suggesting that a single porosity model would be sufficient to describe the soil water dynamics (e.g. van Genuchten, 1980). Table 3 shows a large difference between soil hydraulic properties with water and ethanol for all optimized parameters. A large increase in K_s values in the M and S scenarios was found when ethanol as a complete wetting liquid was used (Table 3) compared to water infiltration where K_s was lower. Decreases of 98.3% and 93.8% in K_s values were noticed when comparing ethanol and water infiltration for M and S scenarios. In contrast, the control scenario shows a lower increase of 44.2% compared to the water infiltration measurements. This difference also indicates that

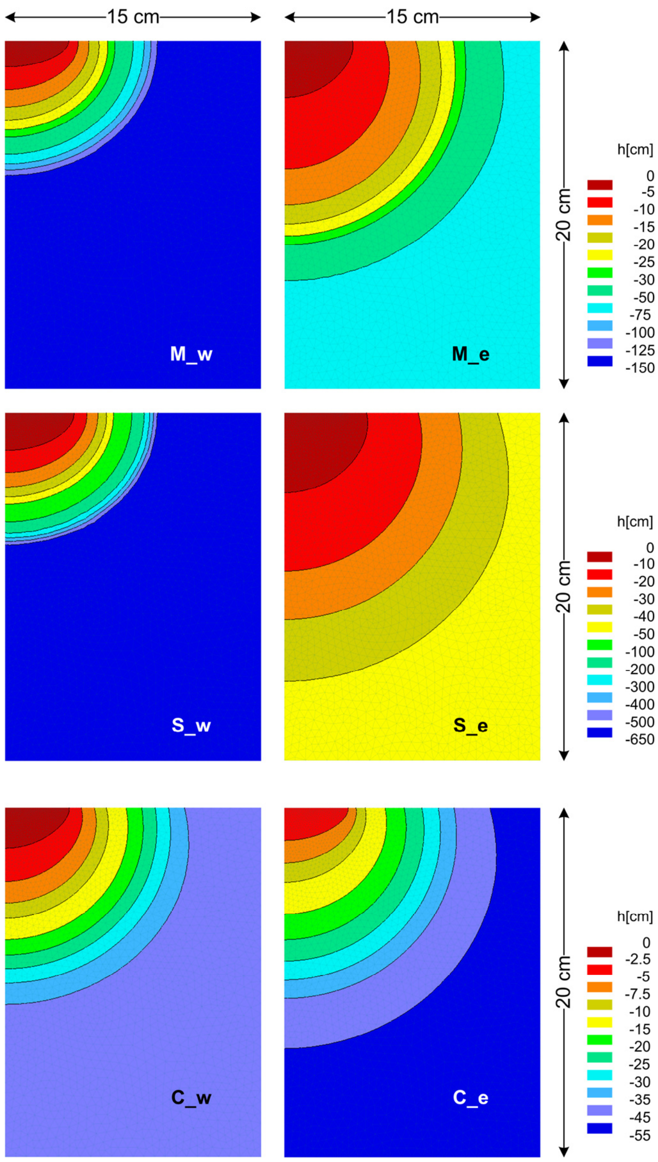

Fig. 4. Pressure head distribution for M (moderately stressed) S (severely stressed) and C (control) scenarios at the end of the tension infiltration field experiment using water (_w) and ethanol (_e).

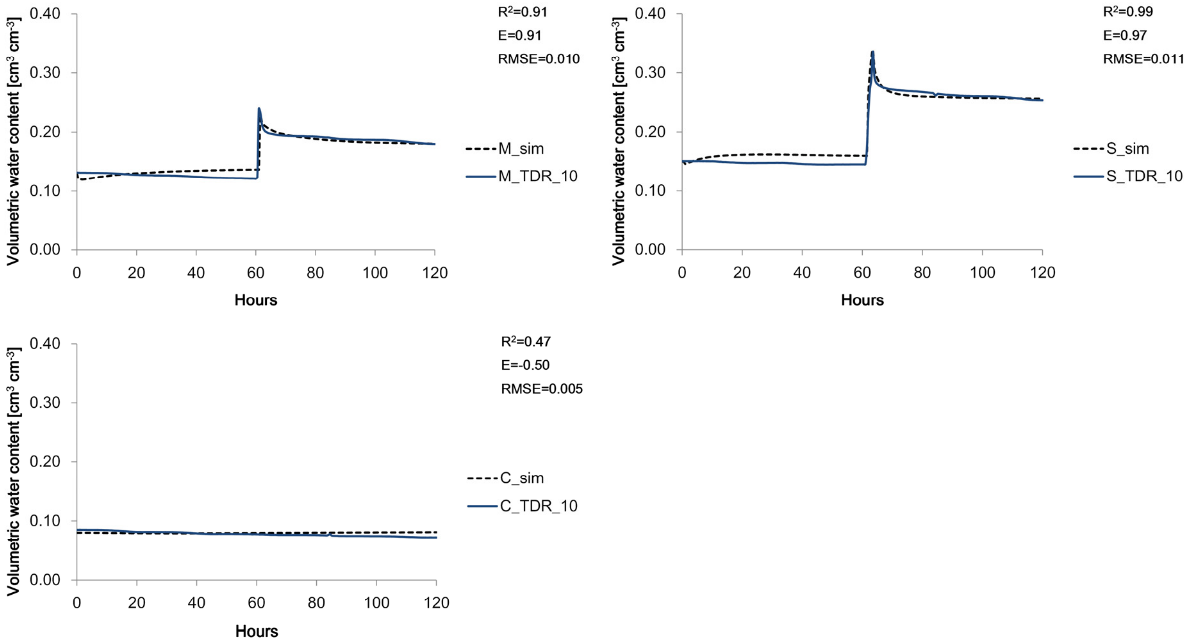

Fig. 5. Measured and simulated soil volumetric water content at 10 cm depth (Aeh horizon, TDR) using optimized parameters from water infiltration experiments from M (moderately stressed) S (severely stressed) and C (control) scenarios for the irrigation event at 24th of June 2014 (60 h before and after the event) with a 75 mm after 4 weeks of drought (M plots) and 150 mm irrigation after 8 weeks of drought (S plots) of irrigation for the event duration of 120 h.

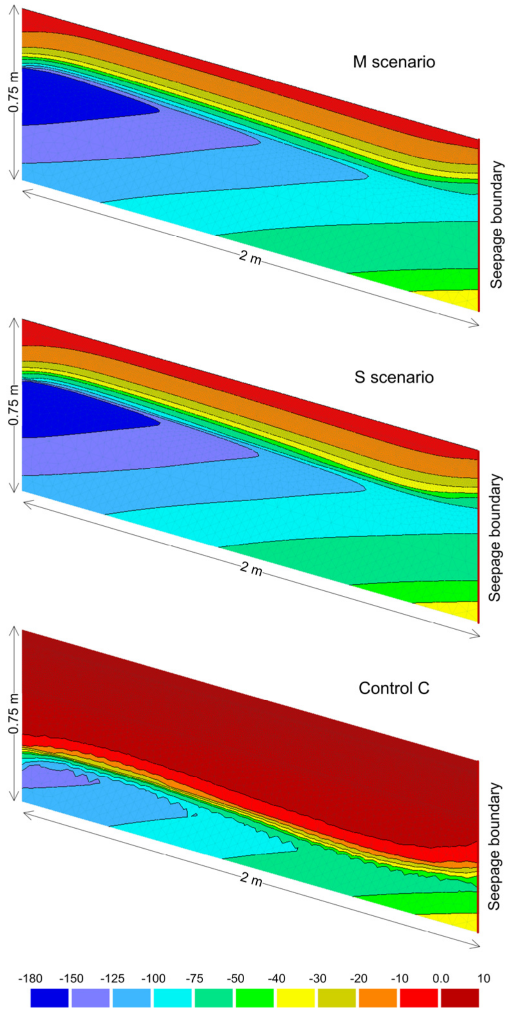

Fig. 6. Pressure head distribution for M (moderately stressed) S (severely stressed) and C (control) scenarios on the August 20th 2014 after 150 mm of the irrigation event on the previous day.

the control scenario had a certain degree of soil water repellency, which was most likely linked to the natural rainfall distribution e.g. critically low soil water content during longer periods with no rain (Schwen et al., 2015).

Fig. 3 shows fitted water retention curves based on the Table 2 parameter set for measurements derived from water (full lines) and ethanol infiltration (dotted lines). Again greater differences in the shape of the retention curve at the larger tension (dryer soil condition) were recorded between the artificially induced drought stress scenarios, while the control plot had a similar shape of the retention curve for both, water and ethanol obtained SHP. It should be noted that the small differences in water retention curves of control plot might be also connected to the fitting procedure in HYDRUS since more than one set of SHP can be realistic. In addition to changes in K_s values, α and n values were increased significantly during the optimization process for ethanol data (M and S plots), resulting in a different curve shape.

Pressure head snapshots were taken at the final time of the simulated disc tension infiltration field experiment performed in HYDRUS (2D/3D) (Fig. 4). These data show that the water infiltration plume in M and S scenarios is significantly reduced compared with the ethanol infiltration plume, resulting in a very dry bottom part of the soil block (20 cm depth) even after 1.5 hours of infiltration. This part of the soil block had a pressure head of approximately –150 and –650 cm for M and S scenarios, respectively, while the ethanol treated soil had a pressure head around –75 cm. The control plot also showed differences in final pressure head values, but the lowest pressure heads were –41.58 cm for water and –54.21 cm for ethanol infiltration, respectively. The differences in duration and infiltration volumes between the two applied liquids should also be taken into consideration. Occurrence of such extensive infiltration reduction increases the risk of preferential flow in structured soils (Jarvis et al., 2008) and the potential of surface runoff as well (Cerdà and Doerr, 2007), which is further evaluated through simulations of artificially induced drought stress scenarios in the next section.

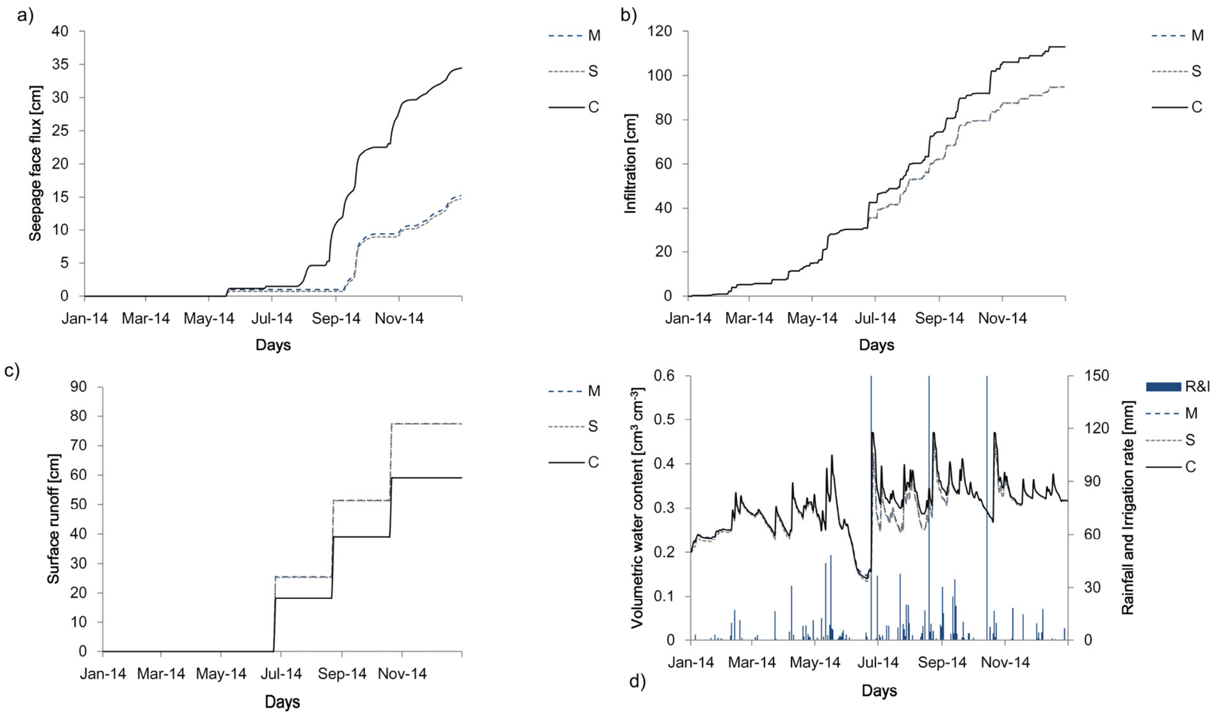

Fig. 7. Simulated cumulative seepage face flux (at the right side boundary, a), cumulative infiltration (b), cumulative runoff (c) and volumetric water content (d) at the M (moderately stressed) S (severely stressed) and C (control) scenarios during 2014 using natural rainfall and irrigation events.

Simulations of artificially induced drought stress scenarios

After the SHP were obtained by inverse modeling, a direct simulation of a particular irrigation event (on June 24th 2014) was performed for the M and S scenarios and also for the control scenario without any irrigation (Fig. 5). The selected event was simulated with a temporal resolution of 1h to provide detailed information regarding the model performance using the obtained SHP. The simulation was set to start and finish 60 hours before and after the irrigation event. Because the plots were covered during the rest of the season, simulating such shorter periods before and after the irrigation event in order to validate the model was assumed sufficient. The simulations were performed using the properties of the Aeh horizon derived from the water infiltration inverse modeling and compared to water contents measured by TDR probes at 10 cm depth (Aeh horizon) while the rest of the horizons had the same values for each layer as presented in the Table 2. Simulation of water content reproduced the field observation well with R^2 values above 0.9 and confident model efficiency values, while the model efficiency was low (–0.50) in the control scenario due to the absence of any variation during this limited period. Still, the RMSE of 0.005 indicated a good fit of the data of the control scenario. These model performance results for water content simulations are in line with previous studies using the HYDRUS model (e.g., Ajdary et al., 2007; Kandelous et al., 2011; Nakhaei and Šimůnek, 2014).

Fig. 5 clearly shows a dependence between soil water content and the amount of applied irrigation water for the M and S scenarios, e.g. an instant increase of soil water content in the M scenario from 0.12 to 0.29 $cm^3\ cm^{-3}$ at the time 60.5 hours is observed, and in S scenario from 0.15 to 0.34 $cm^3\ cm^{-3}$, both corresponding to the 75 and 150 mm of irrigation, respectively. The control scenario did not show any increase in soil water content due to the absence of natural rainfall and irrigation.

After obtaining hydraulic properties from the infiltration experiment and validating the model by comparing it to field water content measurements, one year simulations were performed for 2014 using a daily time step. The simulation included plant uptake and natural rainfall and irrigation events, in order to maximize the difference between the scenarios (in terms of water balance) and to reveal potential downsides of the water repellency (e.g., surface runoff, low water content). Fig. 6 shows the pressure head distribution on August 20th, 2014 (one day after irrigation events on both irrigated plots) in the three scenarios. The differences between the scenarios are seemingly negligible for the M and S scenarios. The low conductivity of the Aeh layer (23.45 cm day^{-1} and 27 cm day^{-1} for the M and S scenario, respectively) delayed the infiltration of the irrigation plume and induced surface runoff. On the contrary, due to its non-repellent state which was expressed in larger K_s values (257.02 cm day^{-1}), the irrigation plume saturated simulated profile till approximately 50 cm depth.

Our simulations suggest that in this particular case, the effect of hydrophobicity on large scale hydrology can have a substantial impact on water balance and its distribution between the infiltration and surface runoff. Fig. 7 shows differences in water balance (e.g., seepage face flux, infiltration rate and surface runoff) between artificially induced drought stress scenarios and the control plot. Due to similar SHP for the two imposed scenarios, the water balance and its distribution is almost identical. However, large seepage face flux (which in this case mimics subsurface lateral flow because of the impermeable bedrock at 75 cm) can be observed in the control plot (34.7 cm vs. 15 cm in the drought scenarios). Small K_s values in the M and S scenarios resulted in decreased infiltration and subsurface flow but increased surface runoff (77 cm in drought stress scenarios vs. 59 cm in control). The simulated water content (Fig. 7d) followed the rainfall and irrigation inputs very well and reflected the increased water levels at the top as well. The extent of the oscillations was linked directly to the estimated SHP, e.g. a quicker response of volumetric water content changes can be seen in a control plot with the applied irrigation (simulated). Our results are in accordance with previous studies (e.g. Lemmnitz et al., 2008) which indicate that the occurrence of soil water repellency on hillslopes is important when addressing larger scale soil hydrology on a seasonal basis.

CONCLUSIONS

The HYDRUS (2D/3D) model was used to estimate soil hydraulic properties from field tension disc infiltration experiments and to quantify soil water repellency effects using data from water and ethanol infiltration measurements. Additionally, simulations to fit the TDR field moisture measurements and to perform 2D water balance modeling on an artificially induced drought stress field experiment were conducted. The water and ethanol infiltration experiments showed a large variation among the treatments and control scenario, revealing the importance of prolonged soil drying on soil water repellency. The inverse modeling was performed successfully with R^2 and model efficiency (E) values above 0.9, indicating good fit with the field measured infiltration data for both liquids (water and ethanol). Soil hydraulic properties derived from the ethanol measurements showed significantly greater K_s values for the M and S scenarios, thus suggesting linkage between water repellency and reduced infiltration. Direct simulation of irrigation events showed good reliability of the model to fit water contents measured at 10 cm depth using TDR probes. One year simulations (2014) showed that the non-structured water repellent soils have a potential to produce increased surface runoff, as well as reduced subsurface lateral flow (if impermeable or low conductivity layer is present) or vertical drainage. Climatic change scenarios are predicting more intense and prolonged droughts, as well as more extreme rainfall events, which can lead to increased soil water repellency and result in changed water flow patterns at the plot scale. Further studies are needed to clarify the occurrence, non-linear nature and impact of SWR.

Acknowledgements. This project was partly funded by the Austrian Climate and Energy Fund (ACRP 6–DRAIN–KR13AC6K11008). Sonja Leitner received a PhD fellowship of the AXA Research Fund. We also acknowledge travel funding from the bilateral agreement project HR20/2016 funded by the Austrian Agency for International Cooperation in Education (OeAD) and the Ministry of the Science and Education of the Republic of Croatia.

REFERENCES

Ajdary, K., Singh, D.K., Singh, A.K., Khanna, M., 2007. Modelling of nitrogen leaching from experimental onion field under drip irrigation. Agr. Water Manage., 89, 15–28.

Armbruster, M., Seegert, J., Feger, K.H., 2004. Effects of changes in tree species composition on water flow dynamics – model applications and their limitations. Plant Soil, 264, 13–24.

Bachmann, J., Deurer, M., Arye, G., 2007. Modeling water movement in heterogeneous water-repellent soil: 1. Development of a contact angle–dependent water-retention model. Vadose Zone J., 6, 436–445.

Bauters, T.W.J., DiCarlo, D.A., Steenhuis, T.S., Parlange, J.-Y., 2000. Soil water content dependent wetting front characteristics in sands. J. Hydrology, 231–232, 244–254.

Breuer, L., Eckhardt, K., Frede, H.G., 2003. Plant parameter values for models in temperate climates. Ecol. Model., 169, 237–293.

Bughici, T., Wallach, R., 2016. Formation of soil-water repellency in olive orchards and its influence on infiltration pattern. Geoderma, 262, 1–11.

Cerdà, A., Doerr, S.H., 2007. Soil wettability, runoff and erodibility of major dry-Mediterranean land use types on calcareous soils. Hydrol. Process., 21, 17, 2325–2336.

Chau, H.W., Biswas, A., Vujanovic, V., Si, B.C., 2014. Relationship between the severity, persistence of soil water repellency and the critical soil water content in water repellent soils. Geoderma, 221–222, 113–120.

Clothier, B.E., Vogeler, I., Magesan, G.N., 2000. The breakdown of water repellency and solute transport through a hydrophobic soil. J. Hydrol., 231–232, 255–264.

Czachor, H., Doerr, S.H., Lichner, L., 2010.Water retention of repellent and subcritical repellent soils: new insights from model and experimental investigations. J. Hydrol., 380, 104–111.

Debano, L.F., 1975. Infiltration, evaporation, and water movement as related to water repellency 1. In: Gardner, W.R., Moldenhauer, W.C. (Eds.): Soil Conditioners. SSSA Spec. Publ. 7. SSSA, Madison, WI., pp. 155–164.

Dekker, L.W., Ritsema, C.J., 1994. How water moves in a water repellent sandy soil, 1. Potential and actual water repellency. Water Resour. Res., 30, 2507–2517.

Diamantopoulos, E., Durner, W., 2013. Physically-based model of soil hydraulic properties accounting for variable contact angle and its effect on hysteresis. Adv. Water Resour., 59, 169–180.

Diamantopoulos, E., Durner, W., Reszkowska, A., Bachmann, J., 2013. Effect of soil water repellency on soil hydraulic properties estimated under dynamic conditions J. Hydrol., 486, 175–186.

Doerr, S.H., Shakesby, R.A., Walsh, R.P.D., 2000. Soil water repellency: its causes, characteristics and hydrogeomorphological significance. Earth Sci. Rev., 51, 33–65.

Feddes, R.A., Kowalik, P.J., Zaradny, H., 1978. Simulation of Field Water Use and Crop Yield. John Wiley & Sons, New York.

Fischer, E.M., Knutti, R., 2014. Detection of spatially aggregated changes in temperature and precipitation extremes. Geophys. Res. Lett., 41, 2, 547–554.

Ganz, C., Bachmann, J., Noell, U., Diujnisveld, W.H.M., Lamparter, A., 2014. Hydraulic modeling and in situ electrical resistivity tomography to analyze ponded infiltration into a water repellent sand. Vadose Zone J., 13, 1, 1–14.

Gee, G.W., Or, D., 2002. Particle-size analysis. In: Dane, J.H., Topp, G.C. (Eds.): Methods of Soil Analysis. Part 4 – Physical Methods. SSSA Book Series, No. 5. SSSA, Madison, WI, USA, pp. 1381–1402.

González, M.G., Ramos, T.B., Carlesso, R., Paredes, P., Petry, M.T., Martins, J.D., Aires, N.P., Pereira, L.S., 2015. Modelling soil water dynamics of full and deficit drip irrigated maize cultivated under a rain shelter. Biosyst. Eng., 132, 1–18. DOI: 10.1016/j.biosystemseng.2015.02.001.

Hallett, P.D., Baumgartl, T., Young, I.M., 2001. Subcritical water repellency of aggregates from a range of soil management practices. Soil Sci. Soc. Am. J., 65, 184–190.

Hardie, A.H., Lisson, S., Doyle, R.B., Cothing, W.E., 2013. Evaluation of rapid approaches for determining the soil water retention function and saturated hydraulic conductivity in a hydrologically complex soil. Soil Till. Res., 130, 99–108.

Hopmans, J.W., Šimůnek, J., Romano, N., Durner, W., 2002. Inverse methods. In: Dane, J.H., Topp, G.C. (Eds.): Methods of Soil Analysis. Part 4. SSSA Book Series, No. 5. SSSA, Madison, WI, pp. 963–1008.

Huang, M., Barbour, S.L., Elshorbagy, A., Zettl, J.D., Si, B.C., 2011. Water availability and forest growth in coarse-textures soils. Canad. J. Soil Sci., 91, 199–210.

IUSS, 2014. World reference base for soil resources. FAO, Rome.

Jarvis, N., Etana, A., Stagnitti, F., 2008. Water repellency, near-saturated infiltration and preferential solute transport in a macroporous clay soil. Geoderma, 143, 223–230.

Jordán, A., Zavala, L.M., Mataix-Solera, J., Doerr, S.H., 2013. Soil water repellency: origin, assessment and geomorphological consequences. Catena, 108, 1–5.

Kandelous, M.M., Šimůnek, J., van Genuchten, M.Th, Malek, K., 2011. Soil water content distributions between two emitters of a subsurface drip irrigation system. Soil Soil Sci. Soc. Am. J., 75, 488–497.

Lamparter, A., Bachmann, J., Deurer, M., Woche, S.K., 2010. Applicability of ethanol for measuring intrinsic hydraulic properties of sand with various water repellency levels. Vadose Zone J., 9, 445–450.

Leitner, S., Minixhofer, P., Inselsbacher, E., Keiblinger, K.M., Zimmermann, M., Zechmeister-Boltenstern, S., 2017. Short-term soil mineral and organic nitrogen fluxes during moderate and severe drying-rewetting events. Appl. Soil Ecol., 114, 28–33.

Lemmnitz, C., Kuhnert, M., Bens, O., Güntner, A., Merz, B., Hüttl, R.F., 2008. Spatial and temporal variations of actual soil water repellency and their influence on surface runoff. Hydrol. Process., 22, 1976–1984.

Lenhard, R.J., Parker, J.C. 1992. Modeling multiphase fluid hysteresis and comparing results to laboratory investigations. In: Genuchten, M.Th., Leij, F.J., Lund, L.J. (Eds.); Proc. Intl. Workshop on Indirect Methods for Estimating the Hydraulic Properties of Unsaturated Soils. University of California, Riverside, CA.

Letey, J., Carrillo, M.L.K., Pang, X.P., 2000. Approaches to characterize the degree of water repellency. J. Hydrol., 231–232, 61–65.

Leue, M., H.H. Gerke, Godow, S.C., 2015. Droplet infiltration and organic matter composition of intact crack and biopore surfaces from clay-illuvial horizons. J. Plant Nutr. Soil Sci., 178, 250–260.

Liu, H., Ju, Z., Bachmann, J., Horton, R., Ren, T., 2012. Moisture-dependent wettability of artificial hydrophobic soils and its relevance for soil water desorption curves. Soil Sci. Soc. Am. J., 76, 342–349.

Monteith, J.L., 1981. Evaporation and surface temperature. Q. J. R. Meteorol. Soc., 107, 1–27.

Mualem, Y., 1976. A new model for predicting the hydraulic conductivity of unsaturated porous media. Water Resour. Res., 12, 3, 513–521.

Nakhaei, M., Šimůnek, J., 2014. Parameter estimation of soil hydraulic and thermal property functions for unsaturated porous media using the HYDRUS-2D code. J. Hydrol. Hydromech., 62, 7–15.

Nash, J.E., Sutcliffe, J.V., 1970. River flow forecasting through conceptual models. Part I. A discussion of principles. J. Hydrol., 10, 282–90.

Nieber, J., Bauters, T.W.J., Steenhuis, T.S., Parlange, J.Y., 2000. Numerical simulation of experimental gravity-driven unstable flow in water repellent sand. J. Hydrol., 231–232, 295–307.

Ritsema, C.J., Dekker, L.W., 2000. Preferential flow in water repellent sandy soils: principles and modeling implications. J. Hydrol., 231–232, 308–319.

Ritsema, C., Dekker, L.W., Hendrickx, J.M.H., Hamminga, W., 1993. Preferential flow mechanism in a water repellent sandy soil. Water Resour. Res., 29, 2183–2193.

Schaap, M.G., Leij, F.J., van Genuchten, M.T., 2001. ROSETTA: a computer program for estimating soil hydraulic parameters with hierarchical pedotransfer functions. J. Hydrol., 251, 163–176.

Schindler, U., Durner, W., von Unold, Georg., Müller, L., 2010. Evaporation method for measuring unsaturated hydraulic properties of soils: extending the measurement range. Soil Sci. Soc. Am. J., 74, 1071–1083.

Schwen, A., Zimmermann, M., Bodner, G., 2014. Vertical variations of soil hydraulic properties within two soil profiles and its relevance for soil water simulations. J. Hydrol., 516, 169–181.

Schwen, A., Zimmermann, M., Leitner, S., Woche, S.K., 2015. Soil Water Repellency and its Impact on Hydraulic Characteristics in a Beech Forest under Simulated Climate Change. Vadose Zone J., 14, 12, 1–11.

Shang, J., Flury, M., Harsh, J.B., Zollars, R.L., 2008. Comparison of different methods to measure contact angles of soil colloids. J. Colloid Interface Sci., 328, 299–307.

Šimůnek, J., van Genuchten, M.Th., 1996. Estimating unsaturated soil hydraulic properties from tension disc infiltrometer data by numerical inversion. Water Resour. Res., 32, 2683–2696.

Šimůnek, J., van Genuchten, M.Th., 1997. Parameter estimation of soil hydraulic properties from multiple tension disc infiltrometer data. Soil Sci., 162, 383–398.

Šimůnek, J., Angulo-Jaramillo, R., Schaap, M.G., Vandervaere, J.P., van Genuchten, M.T., 1998. Using an inverse method to estimate the hydraulic properties of crusted soils from tension disc infiltrometer data. Geoderma, 86, 61–81.

Šimůnek, J., van Genuchten, M.Th., Šejna, M., 2016. Recent developments and applications of the HYDRUS computer software packages. Vadose Zone J., 15, 7. DOI: 10.2136/vzj2016.04.0033

Stocker, T.F., Qin, D., Plattner, G.-K. Tignor, M.M.B., Allen, S.K., Boschung, J., Nauels, A., Xia, Y., Bex, V., Midgley, P.M. (Eds.), 2013. Climate Change. The Physical Science Basis. Summary for Policymakers. Working Group I Contribution to the Fifth Assessment Report of the Intergovernmental Panel on Climate Change. Cambridge Univ. Press, Cambridge and New York, pp. 1–30.

Stoffregen, H., Wessolek, G., 2014. Scaling the hydraulic functions of a water repellent sandy soil. Int. Agrophys., 28, 349–358.

Subedi, S., Kawamoto, K., Komatsu, T., Moldrup, P., Wollesen de Jonge, L., Müller, K., Clothier, B., 2013. Contact angles of water-repellent porous media inferred by tensiometer-TDR probe measurement under controlled wetting and drying cycles. Soil Sci. Soc. Am. J., 77, 1944–1954.

van Genuchten, M.Th., 1980. A closed-form equation for predicting the hydraulic conductivity of unsaturated soils. Soil Sci. Soc. Am. J., 44, 892–898.

Vereecken, H., Schnepf, A., Hopmans, J.W., Javaux, M., Or, D., Roose, T., Vanderborght, J., Young, M.H., Amelung, W., Aitkenhead, M., Allison, S.D., Assouline, S., Baveye, P., Berli, M., Brüggemann, N., Finke, P., Flury, M., Gaiser, T., Govers, G., Ghezzehei, T., Hallett, P., Hendricks Franssen, H.J., Heppell, J., Horn, R., Huisman, J.A., Jacques, D., Jonard, F., Kollet, S., Lafolie, F., Lamorski, K., Leitner, D., McBratney, A., Minasny, B., Montzka, C., Nowak, W., Pachepsky, Y., Padarian, J., Romano, N., Roth, K., Rothfuss, Y., Rowe, E.C., Schwen, A., Šimůnek, J., Tiktak, A., Van Dam, J., van der Zee, S.E.A.T.M., Vogel, H.J., Vrugt, J.A., Wöhling, T., Young, I.M., 2016. Modeling soil processes: Review, key challenges, and new perspectives. Vadose Zone J., 15, 5. DOI: 10.2136/vzj2015.09.0131.

Watson, C.L., Letey, J., 1970. Indices for characterizing soil-water repellency based upon contact angle-surface tension relationships. Soil Sci. Soc. Am. Proc., 34, 841–844.

Received 17 July 2017
Accepted 29 December 2017

Note: Colour version of Figures can be found in the web version of this article.